Geophysical investigation of the shallow aquifer and its vulnerability in the Cu Chi rural district, HoChiMinh city region, Vietnam

Quoc Thanh Truong

THÈSE

Pour obtenir le grade de

DOCTEUR DE L'UNIVERSITÉ GRENOBLE ALPES

École doctorale : STEP - Sciences de la Terre de l'Environnement et des Planètes
Spécialité : Sciences de la Terre et de l'Environnement
Unité de recherche : Institut des Géosciences de l'Environnement

Etude géophysique de l'aquifère peu profond du district rural de Cu Chi et de sa vulnérabilité, région de HoChiMinh City, Viet Nam

Geophysical investigation of the shallow aquifer and its vulnerability in the Cu Chi rural district, HoChiMinh city region, Vietnam

Présentée par :

Quoc Thanh TRUONG

Direction de thèse :

Marc DESCLOITRES INGENIEUR DE RECHERCHE, Université Grenoble Alpes	Directeur de thèse

Rapporteurs :

Colette SIRIEIX
PROFESSEURE DES UNIVERSITES, Université de Bordeaux
Konstantinos CHALIKAKIS
DOCTEUR EN SCIENCES HDR, Avignon Université
Quy Nham PHAM
ASSOCIATE PROFESSOR, Hanoï University

Thèse soutenue publiquement le **22 février 2024**, devant le jury composé de :

Laurent OXARANGO, PROFESSEUR DES UNIVERSITES, Université Grenoble Alpes	Président
Marc DESCLOITRES, INGENIEUR DE RECHERCHE HDR, IRD délégation Sud-Est	Directeur de thèse
Colette SIRIEIX, PROFESSEURE DES UNIVERSITES, Université de Bordeaux	Rapporteure
Konstantinos CHALIKAKIS, DOCTEUR EN SCIENCES HDR, Avignon Université	Rapporteur
Quy Nhan PHAM, ASSOCIATE PROFESSOR, Hanoi University of Natural Resources & Environment	Rapporteur
Dan Phuoc NGUYEN, ASSOCIATE PROFESSOR, Ho Chi Minh City University of Technology	Examinateur

Invités :

Phong Tan NGO
DOCTEUR EN SCIENCES, University of Technology Ho Chi Minh City

ACKNOWLEDGMENTS

Ph.D. extends its heartfelt gratitude to Dr. Marc Descloitres, my dedicated supervisor, whose unwavering support guided me through the research and implementation phases of this thesis. I also deeply appreciate the invaluable guidance provided by supervisors Dr. Ngo Tan Phong, Dr. Tran Anh Tu, and Assoc. Prof. Tran Van Xuan.

An acknowledgment goes to the members Institute of Environmental Geosciences (IGE), notably Dr. Anatoly Legchenko, Prof. Laurent Oxarango, Mr. Henri Mora, Hervé Denis, and Dr. Yvan Rossier. Their support in conducting experiments and analyzing results at IGE has been indispensable.

I am grateful to the CARE laboratory at Ho Chi Minh University of Technology (HCMUT), especially Dr. Nguyen Thi Minh Tam, Dr. Tran Thanh Long, for their continuous support throughout the research process.

My sincere thanks extend to my colleagues at the Faculty of Geology Petroleum Engineering, Ho Chi Minh City University of Technology, for fostering an environment conducive to my research and study. I also thank to my students whose assistance was crucial in collecting geophysical data in Cu Chi.

Furthermore, I sincerely thank the French National Research Institute for Sustainable Development (IRD) and the French Embassy for their financial support, which significantly contributed to the success of my study and research endeavors.

ABSTRACT

GEOPHYSICAL INVESTIGATION OF THE SHALLOW AQUIFER AND ITS VULNERABILITY IN THE CU CHI RURAL DISTRICT, HO CHI MINH CITY REGION, VIETNAM

Ho Chi Minh City (HCMC) region in the south of Vietnam faces significant challenges from climate change and subsidence, with more frequent flooding, and threat of saltwater intrusion. As a proactive measure for future mitigation and development, particular attention is being paid towards sustainable groundwater resources. The northwest, characterized by high terrain and identified as the regional recharge area, is earmarked as a potential crucial groundwater reserve for the future.

The primary objective of this research is to understand better shallow groundwater resources and their vulnerability to surface pollution due to human practices. The second objective is to evaluate several geophysical methods for hydrogeology in the sedimentary geological context of the Saigon River area. An extensive geophysical field investigation was conducted using Time-Domain Electromagnetic (TDEM), Frequency Electromagnetic (FEM), and Electrical Resistivity Tomography (ERT) methods, being evaluated for their sensitivity to clayey layer detection using numerical modeling prior to the survey. These methods proved effective in characterizing the geometry of the aquifer and aquitard system to a depth of 150 meters for TDEM method, very sensitive to electrically conductive clayey layers. The research revealed that the absence of a surface clay layer thus facilitates groundwater recharge, posing a risk of surface pollutants easily infiltrating the aquifer. Moreover, deeper clay layers are discontinuous, increasing the vulnerability to the downward spread of contaminants. The research also points towards a new conceptual model of the aquifer involving geological transgression-regressions scenarios to explain the spatial distribution of the clayey aquitards, showing meanders and floodplains of the ancient Saigon River at depth.

Innovatively, the Nuclear Magnetic Resonance (NMR) method was also employed at the laboratory scale to classify the aquifer using core extracted from boreholes tests. Coupled with grain size analysis, the results show that the shallow aquifer is fine-grained. As field-scale NMR was unsuccessfully applied due to high noise conditions, analyses with pumping and tracer tests gave additional data, leading to the conclusion that NMR results are still preliminary as several improvements have to be made regarding noise reduction and specific yield determination.

For the future, the research paves the way for constructing 3D hydrodynamic models for sustainable exploitation. Vadose zone models will also facilitate the evaluation of pollution in the water table. Finally, this research highlights the efficiency of resistivity-based geophysical methods for sedimentary shallow aquifers characterization in Saigon River and HCMC regions. Combined with hydrogeological methods, future geophysical studies will help to address future groundwater challenges and contribute to the south of Vietnam's resilience against climate change impacts.

ÉTUDE GÉOPHYSIQUE DE L'AQUIFÈRE PEU PROFOND DU DISTRICT RURAL DE CU CHI ET DE SA VULNÉRABILITÉ, RÉGION DE HO CHI MINH CITY, VIET NAM

La région de Ho Chi Minh Ville (HCMV), dans le sud du Viet Nam, est confrontée à des défis importants liés au changement climatique et à la subsidence, avec des inondations plus fréquentes et la menace d'une intrusion d'eau salée. En tant que mesure proactive pour l'atténuation et les développements futurs, on doit accorder une attention particulière à la durabilité des ressources en eaux souterraines. Le nord-ouest, caractérisé par un terrain élevé et identifié comme la zone de recharge régionale, est désigné comme une réserve d'eau souterraine potentielle cruciale pour l'avenir.

L'objectif premier de cette recherche est de mieux comprendre les ressources en eaux souterraines peu profondes et leur vulnérabilité aux pollutions produites par les. Le second objectif est d'évaluer plusieurs méthodes géophysiques pour l'hydrogéologie dans le contexte géologique sédimentaire de la région de la rivière Saigon. Une étude géophysique approfondie a été menée sur le terrain à l'aide de méthodes électromagnétiques dans le domaine temporel (TDEM) et le domaine fréquentiel (FEM) et de tomographie de résistivité électrique (ERT), méthodes dont la sensibilité à la détection des couches argileuses a été évaluée avant d'aller sur le terrain à l'aide d'une modélisation numérique. Ces méthodes se sont avérées efficaces pour caractériser la géométrie de l'aquifère et du système aquitard jusqu'à une profondeur de 150 mètres pour la méthode TDEM, très sensible à la présence de couches électriquement conductrices. La recherche a révélé que l'absence de couche d'argile en surface, ce qui facilite la recharge de la nappe phréatique, et cette situation présente un risque facilité d'infiltration des polluants de surface vers l'aquifère. En outre, les couches d'argile plus profondes sont discontinues, ce qui accroît la vulnérabilité à la propagation des contaminants vers le bas. Les recherches ont également abouti à un nouveau modèle conceptuel de l'aquifère impliquant des scénarios géologiques de transgression-régression pour expliquer la distribution spatiale des aquitards argileux, qui révèlent en profondeur les méandres et les plaines d'inondation de l'ancienne rivière Saigon.

De manière innovante, la méthode de Résonance Magnétique Nucléaire (RMN) a également été employée à l'échelle du laboratoire pour classifier l'aquifère à l'aide de carottes extraites d'essais de forage. Associés à l'analyse de la taille des grains, les résultats de RMN montrent que l'aquifère peu profond est à grains fins. Comme la RMN à l'échelle du terrain n'a pas pu être employée avec succès en raison de conditions de bruit élevées, les analyses avec des essais de pompage et de traçage ont fourni des données supplémentaires, ce qui permet de conclure que les résultats de la RMN sont encore préliminaires car plusieurs améliorations doivent être apportées en ce qui concerne la réduction du bruit et la détermination du coefficient d'emmagasinement spécifique (Sy).

Pour l'avenir, la recherche ouvre la voie à la construction de modèles hydrodynamiques en 3D pour planifier une exploitation durable. Les modèles de la zone vadose faciliteront également l'évaluation de la pollution dans la nappe phréatique. Enfin, cette recherche met en évidence l'efficacité des méthodes géophysiques basées sur la résistivité pour la caractérisation des aquifères sédimentaires peu profonds dans la région de la rivière Saigon et de Ho Chi Minh Ville. Combinées aux méthodes hydrogéologiques, les futures études géophysiques permettront de relever les défis futurs liés aux eaux souterraines et contribueront à la résilience du sud du Vietnam face aux effets du changement climatique.

TABLE OF CONTENTS

LIST OF FIGURES

LIST OF TABLES

CHAPTER 1. INTRODUCTION

This chapter presents the general context of the Ho Chi Minh City region and why the Cu Chi district is an important area to study. We outline the main lack of information and raise hydrogeological questions to explain the general objective of the geophysical work and the methodology used. At last, the organization of the manuscript is described.

In the vicinity of the Mekong Delta, Ho Chi Minh City, a coastal city, is most affected by climate change and sea level rise (Dahm, et al., 2013) (Ha, et al., 2019). By 2050, according to forecast scenarios, most of the Southeast and central areas of Ho Chi Minh City region will be regularly flooded and below sea level (Asian Development Bank, 2010) (Scussolini, et al., 2017). However, the Northwest area of Ho Chi Minh City region has higher topography (5-20 m above sea level) and will not be affected by future sea level rise (Wu, et al., 2021) (Asian Development Bank, 2010). This is the case of the Cu Chi district, located 40 km to the NW of the HCM city. Cu Chi could potentially become *a future development area for the HCMC region (Figure 1.1).* Indeed, it is expected that significant population migration will occur in 2050 towards this district. In addition, today, in those elevated areas of Cu Chi, there are pollution sources related to human activities such as agriculture (cattle farms, rubber trees, and intensive cultivation), industrial parks, and residential areas which threaten the groundwater sources of the area. Besides, previous studies indicate that this region will play a crucial role in climate change adaptation, making the study of its groundwater resources and vulnerabilities necessary. Today very few studies exist in the Cu Chi district regarding groundwater resources for the future. It is time to initiate additional studies to contribute to its future management. This is the purpose of this Ph.D. We contribute to the knowledge of this district focusing on shallow groundwater resources (0-150 m deep) because shallow groundwater resources are the easiest resources used by the inhabitants and the easiest to be contaminated by surface pollution. This PhD proposes to use mainly geophysics because it is one of the most efficient tools for aquifer characterization. We are testing a) resistivity methods particularly the well-known Time Domain Electromagnetic method (TDEM) that is newly considered in Vietnam, thus evaluating its efficiency in Vietnam conditions, and b) a novel geophysical method, the Nuclear Magnetic Resonance (NMR) for estimating groundwater resources. Their efficiency is evaluated using well-known hydrological methods.

1.1 Uses of freshwater in the South of Vietnam

Freshwater is a vital resource for the South of Vietnam, particularly in the Mekong Delta (MD) and Ho Chi Minh City (HCMC) regions. It has a range of uses that are essential for human survival and the region's economic growth. Ensuring that the region has access to sufficient fresh water is essential for the well-being of its people and the growth of its economy. This PhD is addressing some of the issues related to the groundwater in the region of HCMC. In Southern Vietnam, groundwater is a crucial water supply to more than 35 million people for irrigation and drinking purposes. Groundwater is the only freshwater source for basic human needs in some coastal provinces (Ha, et al., 2022).

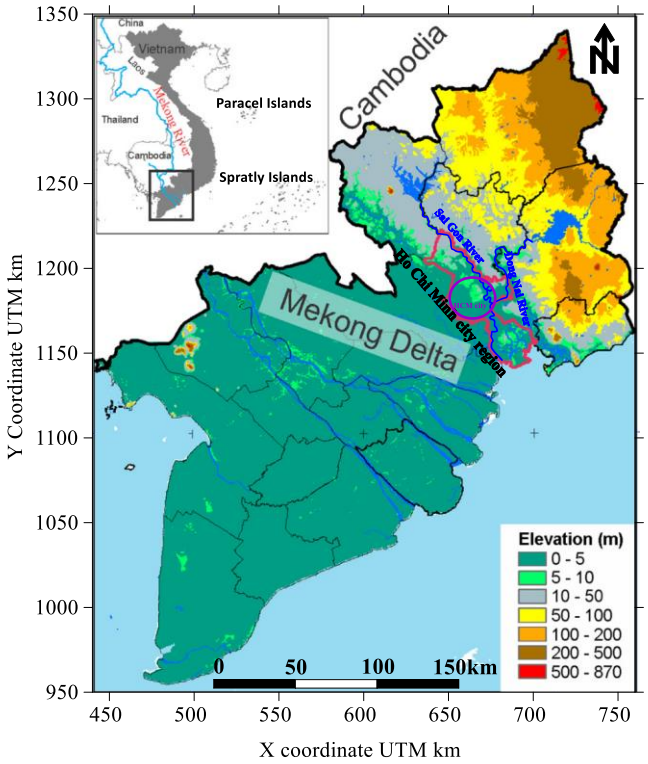

Figure 1.1 Mekong Delta and Ho Chi Minh City region.

The study area (delineated with a red line) encompasses the Cu Chi region, situated in the northwest of Ho Chi Minh City within the Saigon River basin (Ha, et al., 2022)

In the Mekong Delta, the origin of the freshwater uses is mainly the river water (and canals that are used to derive the main fluxes inland for irrigation). In addition to surface water tapping, groundwater extraction rates have also rapidly increased, from 140,000 m^3/day in 2001 2001 (Wagner, et al., 2012) to approximately 1.92 million m^3/day in 2010 (Vuong, et al., 2016) and as much as 2.8 million m^3/day in 2020 (Minderhoud, et al., 2020). Those values are quite old, and more recent values are available in the report on Water Resources Planning for Cuu Long River Basin in the Period 2022–2030 with Vision to 2050 (Government, 2023). However, those new data are related to the Mekong Delta only, not HCMC, therefore they are not useful in the frame of the present work. The Division for Water Resources Planning and Investigation for the South of Viet Nam (DWRPIS) reports that extraction rates have risen significantly in recent years, particularly in coastal areas and dense cities.

In the densely populated Ho Chi Minh City region, the major economic center of the country, the concentration of people living and working in the urban area has continuously increased over the years (General statistics office, 2021). This implies an increasing demand for clean water for daily life is a great pressure on the development of the city (Vuong, et al., 2016). Fresh water not only serves daily living needs but also serves the industrial and agricultural development of the city and surroundings (Vuong, et al., 2016). Currently, water supply in HCMC is provided by surface water of the Dong Nai River, and Saigon River, but also by groundwater. In 2012, the total water supply in HCMC was about 1.5 million m3/day, of which 44.7% was produced from groundwater (Vuong, et al., 2016). It is estimated that Ho Chi Minh City's domestic water demand will be 4.75 million m^3 in 2025 (Van Leeuwen, et al., 2016). To our knowledge, there is no more recent public study on HCMC water demand. Currently, surface water in Ho Chi Minh City is polluted due to industrial, agricultural, and household activities (Nguyen, et al., 2020) that have affected the treatment and operation of clean water supply plants. Therefore, the increased use of alternative groundwater sources is

increasing. Very recently, the HCMC city authorities released a policy limiting groundwater extraction: However, according to circular 27/2014/TT-BTNMT, small wells with extraction capacity < 10 m^3/day can be installed without any license or permission. Ministry of Natural Resources and Environment (MONRE) is responsible for all licenses for well fields > 3000 m^3/day, while provinces are responsible for licenses below that quantity. Within provinces, districts regulate groundwater licensing for extractions < 20 m^3/day. There is also no groundwater fee for small wells (< 20 m^3/day; Decree No 41/2021/NĐ-CP). Therefore, small wells < 10 m^3/day are not normally considered to be important in policy-making, although their influence in large numbers can be substantial. Installation of many wells in the MD could still negatively impact not only land subsidence but also fresh groundwater quantity due to salinization and contamination (Ha, et al., 2019) (Ha, et al., 2022) (Tu, et al., 2022) (Tran, et al., 2016). In short, groundwater is of major concern in the region of HCMC, as a precious resource that needs careful management.

1.2 Hazards in Ho Chi Minh City Region

1.2.1 The ground subsidence and the sea level rise (SLR)

Both are major challenges that are affecting the development of the Mekong Delta, Ho Chi Minh City urban area, and surrounding suburbs areas, as it can have devastating consequences on the region. The delta is one of the most important rice-growing regions in the world, and it is also home to millions of people who depend on the river for their livelihoods. As sea levels continue to rise, and as subsidence occurs, the delta is already at risk of being regularly partly flooded and damaged, including the erosion of the river banks and delta's coastline which can have a major impact on the local economy and the lives of the people who live there.

The main drivers of subsidence in southern Vietnam are natural processes and human activities, both of which contribute to the sinking of the land (Minderhoud, et al., 2018). As a consequence of SLR and subsidence, the relative sea level rises much faster because the land is sinking quickly (Boretti, 2020). In (Minderhoud, et al., 2018), as described in Figure 1.2, one can see that the HCMC region is strongly affected by the subsidence at the northeast of the MD

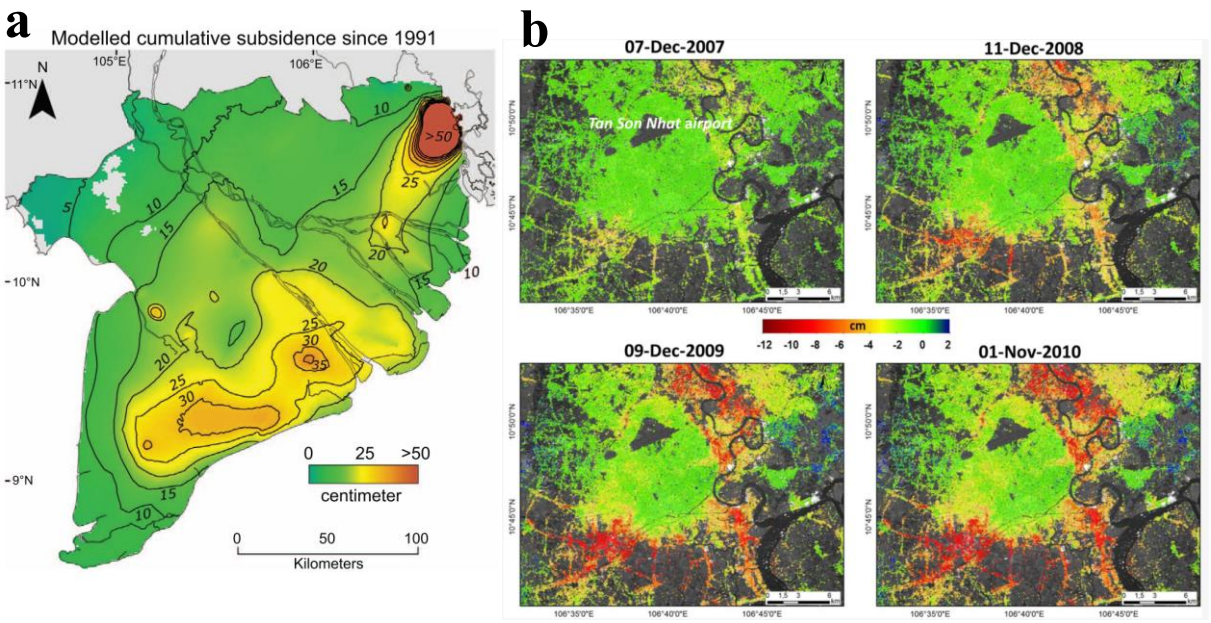

Figure 1.2 Illustration of the subsidence of the Mekong Delta and the city of Ho Chi Minh.

a) Modeled cumulative subsidence due to groundwater extraction induced during 25 years (Minderhoud, et al., 2017), b) Ho Chi Minh City area: measured vertical displacement trend spanning from 2006 to 2010. The subsidence's downward movement is indicated in red. (Dinh, et al., 2015)

In the urban area, the study of (Dinh, et al., 2015) presents different maps of the city center subsidence based on INSAR measurements (Figure 1.2 b). As an example, the Saigon River valley and southern suburbs have subsided by 10 cm in one year, between 2009 and 2010.

In MD and HCMC regions, overexploitation of groundwater resources is contributing as a contributing cause of a drop in the water table. Groundwater extraction reduces pore water pressure and leads to subsidence or settlement of the ground surface (Vuong, et al., 2016). Therefore, areas with agriculture, urban, and industrial development that are using a lot of groundwater resources will experience a higher rate of subsidence compared to areas that are not developed (Minderhoud, et al., 2018).

1.2.2 A high level of pollution

In HCMC urban centers, pollution sources come from industrial zones and people's domestic wastewater. Meanwhile, in rural areas, the main source of pollution comes from agricultural activities through the use of fertilizers and pesticides (Nguyen, et al., 2020)

Agricultural pollution

In the MD and the rural districts of the HCMC region (such as the Cu Chi district investigated in the present study), the use of pesticides and fertilizers has raised concerns over its impact on the environment and people's health (Pham, et al., 2013), (Chau, et al., 2015). The overuse of these chemicals could lead to the contamination of surface water and groundwater, posing a serious threat to the ecological balance and public health. When not used in moderation, these chemicals can seep into the soil and groundwater, affecting the quality of water and causing long-term harm to the ecosystem (Braun, et al., 2019). Regarding the northwest area of Ho Chi Minh City (our study area, described in part 1.3), it is a major agricultural area, and the use of fertilizers and pesticides in agriculture can have a significant

impact on groundwater resources (Wu, et al., 2021). This is an urgent issue because it not only affects the health of local residents but can also have long-term environmental impacts on the groundwater resources in the area.

The industrial and residential activities

In Ho Chi Minh City, water pollution due to wastewater from Industrial Parks and Export Processing Zones is very large. The main cause of water pollution was the discharge of untreated wastewater directly into surrounding canals by various industrial enterprises (Pham, et al., 2018). Industrial waste, chemicals, and other pollutants can leach into the groundwater, affecting its quality and making it unsafe for human consumption and other uses. Some common contaminants from industrial activities include heavy metals, volatile organic compounds, and salts (Phan, et al., 2019) (Nguyen, et al., 2020). In our study area, there are few Industrial Parks, but future developments may be planned to be implemented more in the future.

Residential activities can also contribute to groundwater pollution. There are many potential sources of contamination, including the improper disposal of household chemicals, septic systems, and the use of fertilizers and pesticides in landscaping and gardening. In addition, residential development can alter the natural drainage patterns and increase runoff, leading to increased infiltration of pollutants into the groundwater.

1.3 Consequences for HCMC region

As the Mekong Delta and the HCMC region are sinking, several environmental phenomena are occurring or will occur in the future with a much higher degree of intensity. As sea level rises, the region is at an increased risk of coastal and riverine flooding, which can have devastating impacts on communities and the local economy. The loss of agricultural land and infrastructure, along with the displacement of people, can lead to a decline in economic and social well-being.

1.3.1 Saline intrusion

Saline intrusion is a growing concern in coastal regions, particularly with the impact of climate change and rising sea levels. This phenomenon occurs when seawater infiltrates freshwater sources, leading to increased salinity levels in rivers, estuaries, and groundwater aquifers. Under the impact of climate change and sea level rise, saltwater intrusion is becoming more and more serious (Bergqvist, et al., 2012). Saline intrusion not only occurs in coastal agricultural areas but now the saline intrusion boundary in the Mekong Delta in the dry season has gone inland tens of kilometers (Nguyen, 2017). The rising salinity of the soil and water due to saltwater intrusion also affects food security in the region, reducing crop yields and threatening the livelihoods of farmers. When surface water has a high salt concentration it can have negative health effects and make it difficult for communities to access safe and clean water (Nguyen, et al., 2019). The HCMC region is not as strongly affected by saline intrusion but the city is facing regular saline intrusion into the Saigon River.

1.3.2 Flooding

The South of the HCMC region and the city itself, as well as huge surfaces in the MD, are regularly affected by flooding.

Flooding in urban areas

The city is located in a region where there are heavy rainfalls and flooding during the monsoon season, especially with high tide periods. Urbanization and growing population in the city have put pressure on the limited drainage system, causing frequent and severe flooding in many areas. Under the influence of subsidence and sea level rise, flooding is becoming more and more serious (Boretti, 2020) (Erban, et al., 2014). Governments and local authorities are working to improve drainage systems and develop flood management plans to minimize the impact of future floods.

Previous studies show that the impact of floods and inundation in Ho Chi Minh City is constantly increasing in the following years (Vachaud, et al., 2019). According to the forecast scenarios, by 2050 most of the southeast and central areas of Ho Chi Minh City will be regularly flooded and be below sea level (Asian Development Bank, 2010) (Scussolini, et al., 2017) Figure 1.3 and Figure 1.4. This not only affects the lives and economy of the people in the area but also poses a great challenge to the management of the local government (Vachaud, et al., 2019). Therefore, it is necessary to have an area that meets the needs of people's lives and is not affected by climate change and sea level rise as a future reserve for the city.

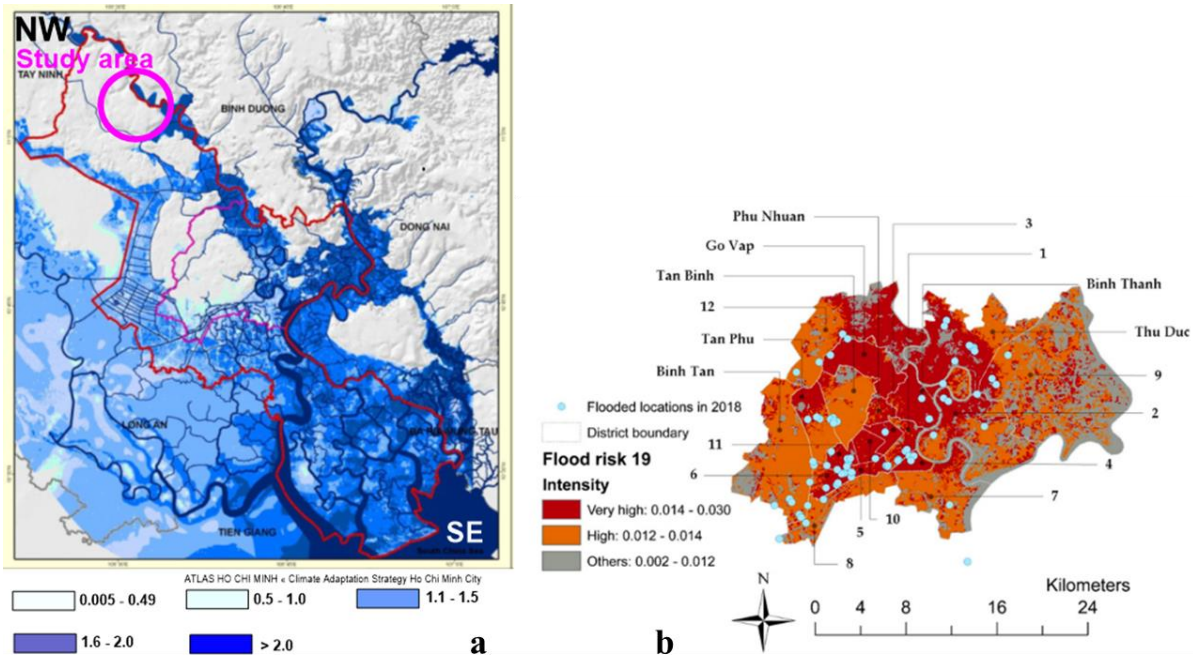

Figure 1.3 Flood in HCMC.

a) Ho Chi Minh City pessimistic scenario for Extreme floods in 2050, if no flood control systems are built (Asian Development Bank, 2010) and b) spatial arrangement of real flood-affected areas in Ho Chi Minh City in 2019, the high risk of flooding area concentrated in the center of Ho Chi Minh City (Wu, et al., 2021)

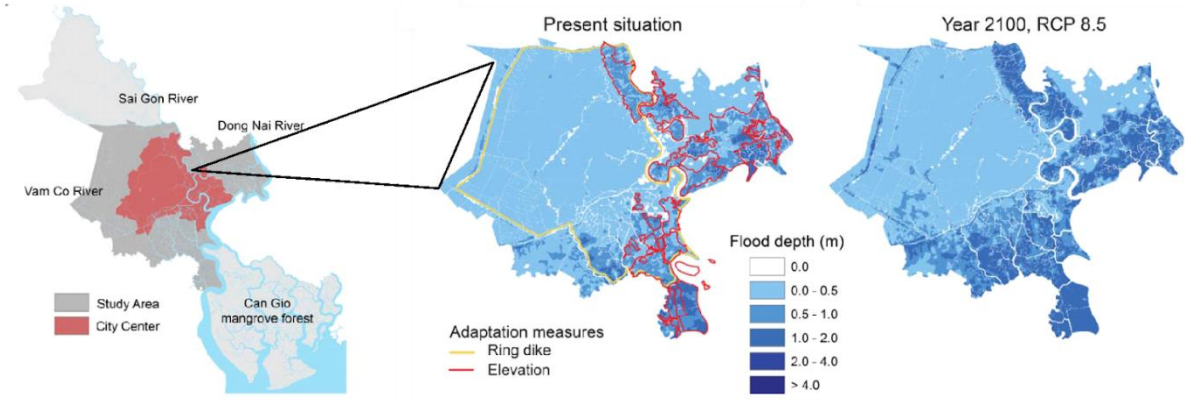

Figure 1.4 Ho Chi Minh City center, and flood depth of the 100-year flood forecast (Scussolini, et al., 2017)

The forecast outcomes indicate that the central region of Ho Chi Minh City is susceptible to flooding, with the forecast extending until the year 2100. Anticipated flood levels in the area range from 0.5 to 1 meter, with the riverbanks and southeast areas facing more severe impacts, experiencing flood depths of up to 4 meters.

1.3.3 Surface water and groundwater contamination

In urban areas, the combination of high tides and heavy rains can lead to flooding and thus to the flushing of pollutants on the surface towards the rivers due to the high runoff index. Previous studies show that surface water in Ho Chi Minh City is currently polluted due to agricultural, industrial, and domestic activities (Nguyen, et al., 2020). This has led to surface water in canals exceeding Vietnamese quality standards for food and domestic use (Wilbers, et al., 2014) making it necessary for people to rely on groundwater as a daily water source. In addition, very recent studies are focusing on Contaminants of Emerging Concern (CeCs). In the latest research published in 2022 by Caracciolo and colleagues (Caracciolo, et al., 2023), it was shown that the upstream area of the Saigon River corresponding to our research location, exhibits significant water pollution primarily attributed to insecticides, herbicides, and fungicides originating from agricultural activities. Pesticides, constituting 40–74% of the total concentration, dominate the chemical composition in the upstream sector. The majority of these identified pesticides are utilized in paddy fields and other crops, indicating substantial agricultural presence upstream.

In contrast, the downtown area of the Saigon River showcases a higher prevalence of pollutants stemming from pharmaceuticals, personal care products, and hormones. This disparity in pollutant types between upstream and downstream regions underscores the need for further investigations. Specifically, there is a call for studies to assess the capacity of pollutants to infiltrate the aquifer in the study area. Additionally, determining the sources responsible for discharging pollutants into the Saigon River is deemed essential. The research underscores the importance of understanding the complex dynamics of water pollution in different areas, particularly those influenced by distinct agricultural and urban activities.

In rural areas, the infiltration process is usually much higher and the pollutants can reach the groundwater more easily. River water can be contaminated if it is in connection with the aquifer, or receives local runoffs or wastewater from industrial zones. The spread of pollutants into the underground aquifer will lead to a decline in water quality, making it unsuitable for human consumption and agriculture (Figure 1.5).

Figure 1.5 Simplified view of hydrological processes showing the main difference between urban and rural catchments.

In rural areas, the surface runoff area is typically smaller compared to urban areas, resulting in a higher proportion of rainfall being transmitted to the aquifer. This is due to the presence of more permeable surfaces, such as natural soils and vegetation, which allow water to infiltrate into the ground rather than running off the surface. As a result, rural areas increased groundwater recharge, leading to higher water accumulation in the aquifer. (Halecki, et al., 2022)

We consider in our study the vulnerability of an aquifer to pollution as the degree to which it can be reached by soluble contaminants. In fact, the aquifer quality can be threatened from various way in agricultural, urban or industrial areas. Several vulnerability studies are often considering multiple factors contributing to assess various vulnerability index, such as land uses and land covers, aquifer type, geological context including clayey protective caps or barriers to underground fluxes, the degree of inter-connection with the adjacent river, among the most important. Nguyen at al., (2023) is considering the "DRASTIC" method applied to Ho Chi Minh City using seven parameters: depth to water table, net recharge, aquifer media, soil media, topography, impact of vadose zone and hydraulic conductivity. In the "refuge zones" defined previously, Nguyen at al., (2023) concludes that the aquifer is vulnerable to pollution due to shallow water table, loamy soils, high recharge and gentle slopes parameters. They also point out also that there is a need for further research in this area.

1.3.4 The importance of North-West zone of HCMC

As seen in Figure 1.7 below, the Northwest rural area of Ho Chi Minh city region has high topography and has been assessed as completely unaffected by climate change and future sea level rise (Wu, et al., 2021) (Asian Development Bank, 2010). Therefore, this area can become a reserve development for the city in the future. It can be also called a "refuge" area for human beings in the forthcoming decades. It can become a resettlement area for people in Ho Chi Minh when the city's center is below sea level and flooded by climate change, sea level rise, and subsidence in the future. In addition, the map of the boundary of saline intrusion in 2050 shows that the saline intrusion boundary with a concentration of 0.25% has a limited spreading towards the Hoa Phu area (approximate 10 km South of the elevated area), so the water quality in this area still meets the target for domestic demand daily living needs of the residents (Van Hong, et al., 2022).

In addition to being representative regarding its elevation, the selected Cu Chi area is an important zone of regional aquifer recharge. Therefore, it should be prioritized for protection, especially in areas where groundwater recharge occurs rapidly (Tu, et al., 2022). Actually, the area north and northwest of the city is the recharge zone for the entire aquifer system in the region, as well as for Mekong Delta aquifers according to (Vuong, et al., 2016) (Figure 1.6).

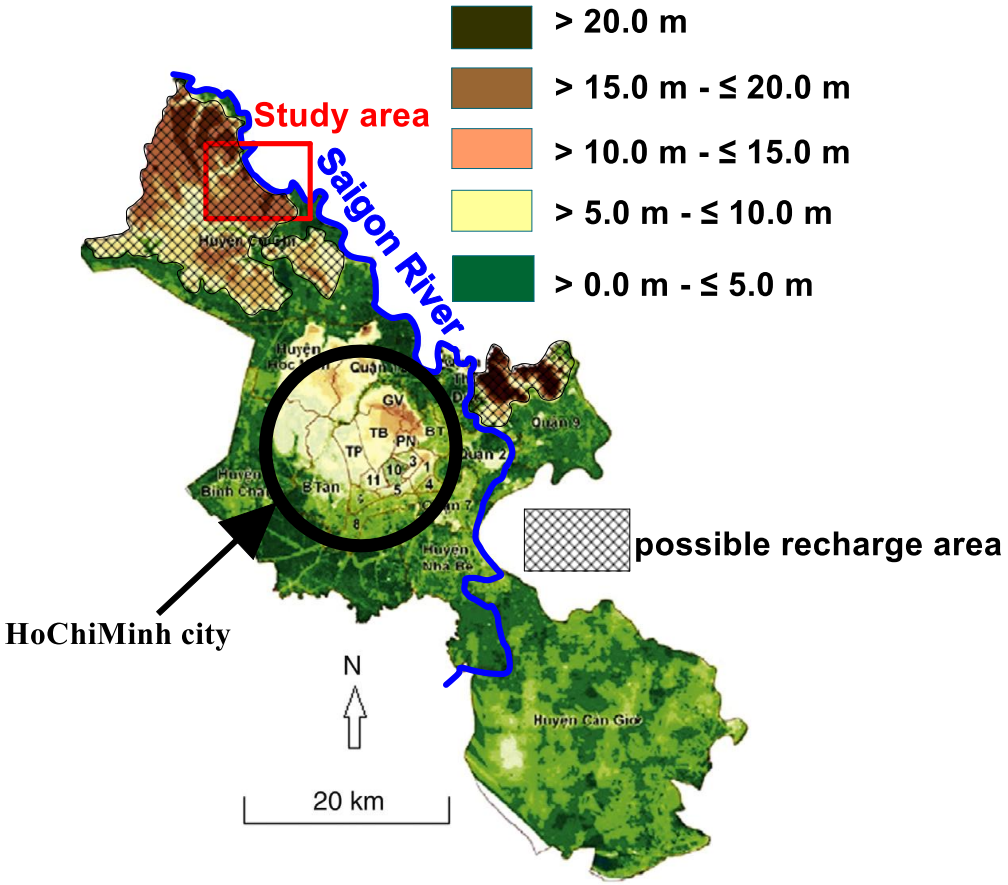

Figure 1.6 Ground surface elevation of HCMC in Vietnam.

Areas with high elevation are situated in the northwest and a smaller portion in the northeast, and these are represented by colors ranging from yellow to dark brown. The crossed area in the northwest signifies rechargeable areas, emphasizing high-altitude regions that are potential zones for recharging groundwater. This spatial distribution is crucial for understanding the topography and hydrological characteristics of HCMC. (Vuong, et al., 2016)

1.3.5 Motivation of the Ph.D. work

As the rural elevated areas will play a key role in the near future, it is necessary to conduct detailed studies to understand their groundwater systems: their geometry, their resources, their vulnerability to surface pollutants infiltration, and their interactions with surface river water. *This is the primary motivation for this PhD work.* Although there have been previous studies on the interactions between groundwater and the Saigon River, using a modeling approach (Long, et al., 2017) there has yet to be a detailed study of the hydrogeological system of the area. Indeed, large-scale studies based on geological information coming from sparse-space survey wells are difficult to assess the homogenous and continuity of the groundwater system accurately (Vuong, et al., 2016). Creating a conceptual model is an essential step in studying and managing groundwater resources because it helps to clarify the understanding of the aquifer

system and identify knowledge gaps and uncertainties. It also forms the basis for simulations of groundwater dynamics in the study area.

To achieve this objective, we propose to use geophysical techniques, as geophysics is known for giving valuable results in combination with hydrogeological methods. However, we need to have a clear understanding of the efficiency of geophysical tools that can be used in this geological context in order to be able to propose them (or not) for future work. *This is the second motivation for the PhD work.* To achieve a comprehensive study of the efficiency of those geophysical tools, we needed to select an area with a limited extension that combined several criteria making it as representative as possible of a larger region, the elevated sedimentary areas that are present in the border of the Mekong Delta. Therefore, the result of the PhD work could be applied to a larger regional scale.

1.3.6 The study area as a representative elevated area

Within the elevated "refuge" zones, we selected a smaller representative area, situated a few km to the North and Northeast of Cu Chi town Figure 1.7. This area is also a historical area where the National Liberation Front of South Vietnam was constructing shallow tunnels to conduct military operations. This area is crossed by the Saigon River. The area is approximately 70 km² and has a high elevation from 5 to 20 m above the mean sea level (MSL). It is not at risk of flooding (Duy, et al., 2018). The land use gathers all the main activities: agricultural zones (rubber tree plantations, high-tech agricultural zones, paddy fields, and some cattle farms), some small towns, and the industrial zones of Ben Cat.

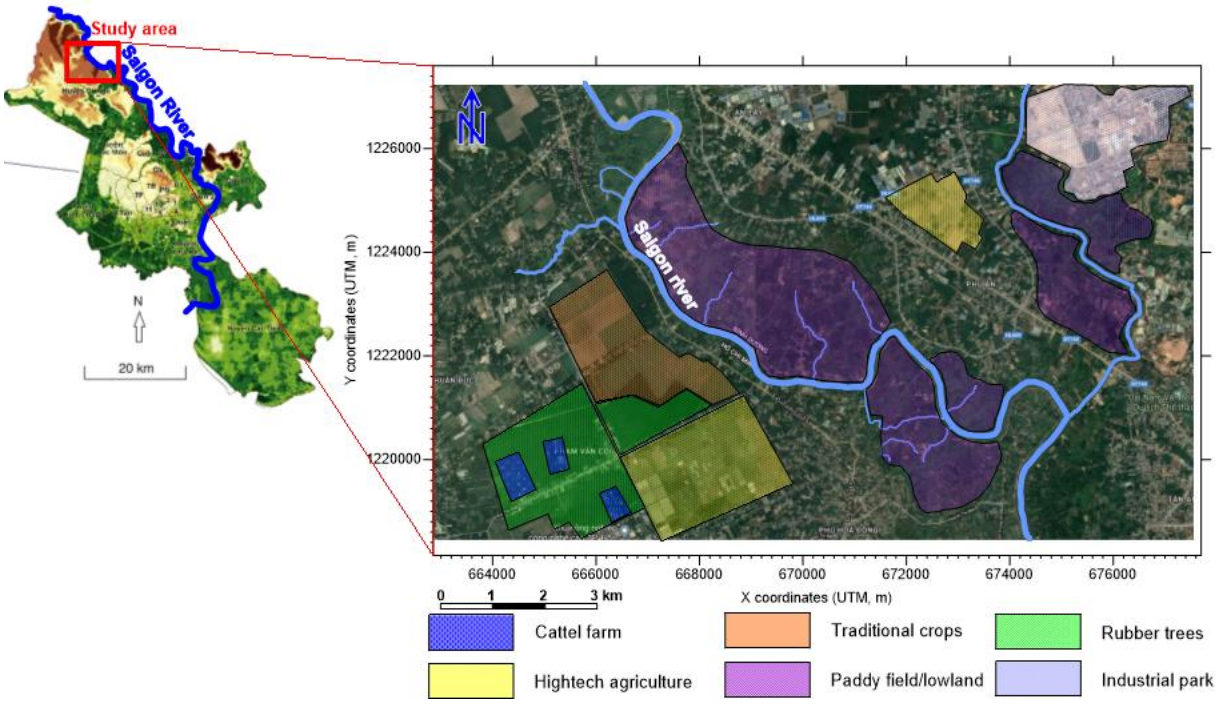

Figure 1.7 Study area, at the northwest of the Ho Chi Minh City region.

Various human activities within the study area are categorized by different colors. The blue regions denote areas designated for cattle farming, while yellow signifies zones allocated for high-tech agriculture. Orange represents areas dedicated to traditional crops, with cassava and sugarcane being the predominant crops. The purple shade characterizes paddy fields and lowland areas, predominantly situated along the Saigon River and concentrated in the Ben Cat area. Green is indicative of regions covered with rubber trees, and light purple highlights the operational zone of the industrial park.

This area was only partly surveyed with previous studies on geology and hydrogeology with maps and cross-sections having been carried out (Vuong, et al., 2016). Here, 90% of the population uses groundwater for daily living needs. Groundwater from residential wells has a greater risk of water quality degradation than concentrated water extraction stations (Tran, et al., 2016). The water used is concentrated in shallow aquifers susceptible to contamination. Previous studies made exactly in this area and using isotopes of $\delta^{18}O$ and $\delta^{2}H$ in surface water and groundwater samples have confirmed some interaction between groundwater and Saigon River (Tu, et al., 2022) as well as natural groundwater recharge from precipitation (Long, et al., 2017).

1.4 General scientific questions and methodology

1.4.1 Lack in previous studies

Recent hydrogeological studies (Tu, et al., 2022) (Long, et al., 2017) based on isotopes and hydrological modeling are precious to sketch the initial understanding of the processes linked with the recharge and groundwater-river interactions. Both studies are also pointing out the lack of information on hydraulic permeability from previous experimental pumping results, distributed discreetly in the study area. Hydrogeological maps and cross-sections of the Cu Chi area (presented in Chapter 2) indicate that a thick (5 m) clay layer is distributed from 0 to 5m deep on the surface and largely spread over the region. This layer can prevent the spread of pollutants from human activities to the underlying aquifer and can limit or even stop any infiltration and recharge. However, (Tu, et al., 2022) have shown that recharge can reach to the deep aquifer. This contradicts previous geological information and highlights the heterogeneity in the distribution of clayey sand in the area. Detailed geological studies are thus needed to determine the potential impact of human activities on the aquifer and assess the risk of vulnerability.

The regional study of the aquifer reserve was carried out by the Ministry of Natural Resources and Environment of Vietnam in 2016. The hydrogeological cross-section in the study area is only built from well information with long distances and lacks details. To summarize, aquifers are a priori separated by interbedded deep clay layers encountered in the boreholes (Van, et al., 2018) (Vuong, et al., 2016). However, due to relatively sparse borehole information (every 3 km), there is no proof of their lateral continuity at depth.

When studying the dynamic state of the aquifer system, according to the position of the river (upstream or downstream) the exchanges between the river and aquifer can be different (Van, et al., 2018). This direction of flux seems to depend on the depth at which the Saigon River is penetrating the aquifer and the thickness of the clay bed below the river. However, there are no studies that investigate how the river is penetrating the aquifer.

Regarding the resources, there is only scarce information on the water content of the aquifer, and only five pumping tests are available in the area, as described in the study by

(Vuong, et al., 2016) (Long, et al., 2017) and presented in chapter 2. To date, there is no existing hydrogeological model for managing future exploitation: there is a need to estimate the hydraulic parameters of aquifers to feed future models with spatialized information. In addition, no information on pollutant types, and how their transfer into the vadose zone. The hydrodynamic nature of the first 10 m (vadose zone) is unknown. There is a need to study the infiltration of pollutants into aquifers.

Regarding the previous geophysical studies (that will be described in Chapter 3) they are very rarely. They have investigated the use of magnetism and gravity and a combination of VES and MT methods (Pham, et al., 1994) to determine the depth of uplift and fault blocks and the characteristics of sediment layers in the area of Ho Chi Minh City. However, these studies had limitations such as sporadic results and large distances (a few km spacing) between measurement locations, making it difficult to detect heterogeneity in the geological formation. A regional vertical electrical sounding (VES) survey has also been conducted (Pham, et al., 2002) but this study has not detected the heterogeneous distribution of clayey sand in shallow sediments in the area which was suspected in a study of groundwater recharge (Tu, et al., 2022).

1.4.2 Hydrogeological questions

The lack of information regarding the aquifer in the selected Cu-Chi area helps in summarizing the general hydrogeological questions raised in the studied area. They can be classified into 3 categories. Those questions will also be detailed presented and explained in chapter 2.

- **Aquifer geometry characteristics**
  - How are organized aquifers in the first 150 m of the subsurface? Are the clayey layers extending laterally and separate aquifers, or are they continuous?
  - Is there a continuous clay layer at the surface (as displayed by hydrogeologists) that protects the first aquifer from surface pollution? Actually, if there is any discontinuity, there is a risk of vertical infiltration of pollutants through the vadose zone and between aquifers.
  - What are the types of sediments encountered?
  - What is the river sediment geometry in the vicinity of the river?
- **Groundwater resources characteristics**
  - What is the total resource available? What is the aquifer(s) effective porosity (specific yield, of its storativity in the case of confined aquifers)?
  - What are the types of sediments encountered that could give an indication of the aquifer quality?
- **Aquifer dynamic and vulnerability**
  - What is the velocity of infiltration in the vadose zone? What is the recharge rate in the area?
  - Are pollutants infiltrating down to the water table?
  - What could be the sustainable pumping flow rate of this aquifer for future needs?
  - What is the degree of connection between the Saigon River (SR) and the aquifer?

1.4.3 General objectives of the Ph.D.

This Ph.D. work intends to address the previous hydrogeological questions by contributing, using geophysical methods, to better evaluate the resources and vulnerability of shallow aquifers (0-150 m deep) in the refuge zone of Cu Chi. Indeed, geophysical methods are considered thanks to their ability to sound the ground to get information on the surface without drilling and because of their ability to get dense data compared to sparse boreholes. The expected outputs of the work are:

- Contribute to the construction of the detailed hydrogeological maps in the study area, including the presence of clay on the surface and the separation between aquifers at depth, if any.
- Achieve a better understanding of the sediment deposits and thus get improvement in the conceptual hydrogeological model of the area.
- Create new datasets required to construct hydrogeological models and simulate groundwater flows for understanding the interaction between shallow and deep aquifer, aquifer, and Saigon River. Such a 3D model (not done in this PhD work) could be used in the future to estimate the sustainable pumping flow to protect the aquifer.

A specific objective of this PhD, in addition to contributing to the general knowledge of the refuge zone aquifers, is to evaluate the efficiency of some geophysical methods in the context of a rural area in Vietnam, in order to be able to validate (or not) the use of these methods for future studies. To achieve this specific objective, we propose to compare the geophysical results to existing well-known methods of hydrogeology, geotechnics, and geology. The technical outputs expected of this approach are to:

- Confirm the efficiency of geophysical resistivity methods in delineating the aquifer geometry,
- Evaluate the contribution of a new geophysical method, the Magnetic Resonance Sounding (MRS) method, to estimate the aquifer parameters.

1.4.4 Methodology and geophysical methods

The main approach proposed is based on the application of classical and modern geophysical methods both at the field and laboratory scale, then comparing the results to well-known hydrological methods and experiments at laboratory scale. This back and forth between the laboratory and the field is made with the objective to validate (or not) geophysical methods in Vietnam conditions. The methodology involves several specific schemes that include the selection of appropriate geophysical methods, the execution of field surveys, the processing and interpretation of data, and the validation of results through comparison with other classical methods such as borehole information, well logs, and geological data. We aim to obtain reliable information about the subsurface and the groundwater resources. In this work, geophysics is mainly applied for the two first series of hydrogeological questions, i.e. a) the aquifer geometry configuration and b) the groundwater resources estimation. The questions on aquifer dynamics and its degree of pollution -and pollution migration in the vadose zone are not addressed in the frame of the manuscript but are currently (2023) addressed within the CARE laboratory research team in Vietnam using some data obtained in the Ph.D.

We propose to use mainly electrical resistivity methods. Electrical resistivity has been widely used for decades for hydrogeophysics. It allows discrimination of various geological formations, and this is well suited for our geological context (riverine and estuarine quaternary sediments). Electrical resistivity permits the delineation of the main soil types (McNeill, 1980) (Samouëlian, et al., 2005) so we made the hypothesis that detecting clay layers, saline intrusion (if any), and sandy or loamy aquifer would be possible in the first 100-150 m. In addition, the geological context of delta sedimentation usually leads to horizontally layered geometry well suited for many 1D interpretation geophysical algorithms. However, many distinct factors can influence an electrical resistivity value (porosity, groundwater conductivity, clay content, and saturation among others) and they can all act simultaneously, making the measurements more difficult to interpret. To measure resistivity at depth, there are several resistivity-based electrical and electromagnetic methods proposed, details as follow.

Geophysics for large-scale aquifer geometry characterization

For the large-scale (few km²) geometrical characterization of the Cu - Chi Aquifer, the Time Domain Electromagnetic (TDEM) method can be used for detecting shallow and deep groundwater aquifers (McNeill, 1994) (Fitterman, et al., 1986) from the surface down to 100-150 m deep with our instrument. This method can provide suitable survey productivity, has an excellent resolution of conductive layers, and allows 1D multi-layered earth calculation. This method is a must when dealing with the detection of electrically conductive terranes (resistivity below 50 Ω.m), such as saltwater intrusion and clayey layers. However, this method is not sensitive to resistive layers (i.e. above 300-500 Ω.m) and, therefore not adapted very well to the detailed investigation of sandy aquifers, usually more resistive. TDEM requires expensive equipment and must avoid electromagnetic noise coming from cultural and industrial noise and power lines. At last, TDEM is not very sensitive to shallow layers (0-5 m) due to the technical design of the instrument. We will discuss the aquifer geometry by comparing it with borehole information, well logs, other geological data as well as geotechnical analysis (grain size, clay estimate with methylene blue method). The total methodology for the large-scale characterization is summarized in Figure 1.8.

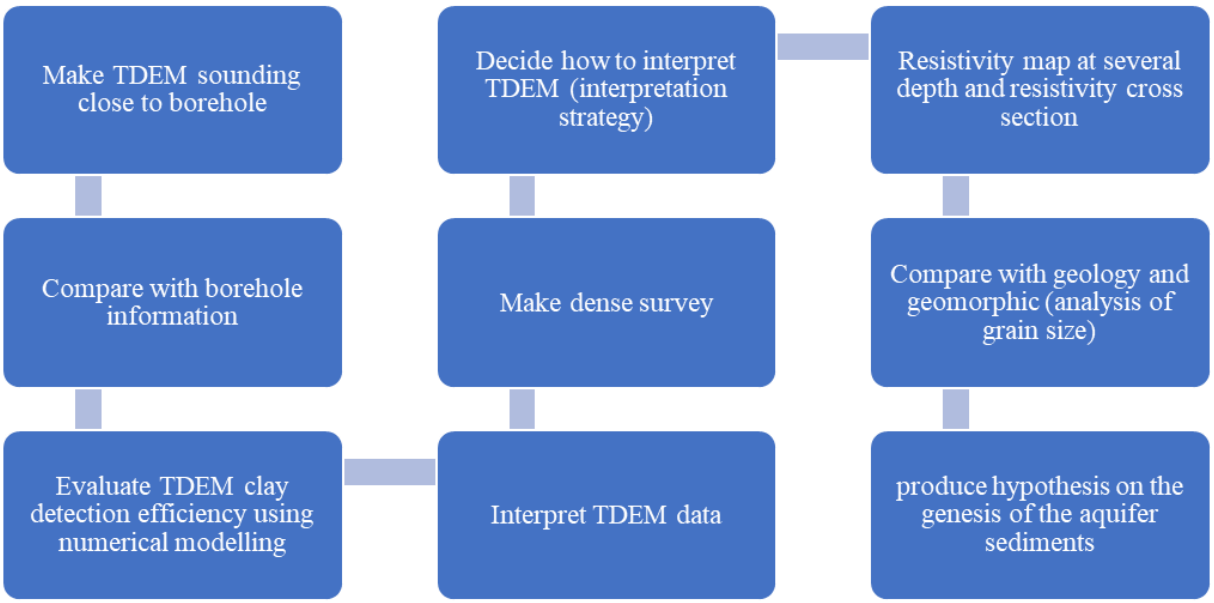

Figure 1.8 Overall methodology for applying Time-Domain Electromagnetic (TDEM) for aquifer geometry investigation.

This methodology is followed in the Ph.D. The outcome of this procedure should point out the efficiency of the Time-Domain Electromagnetic (TDEM) application in groundwater exploration within the southern region of Vietnam.

Geophysics for small-scale and shallow-depth aquifer geometry implementation

Second, for small-scale and shallow geological geometry characterization, we apply both Direct Current (DC) electrical methods and Frequency Electromagnetic (FEM) methods for shallow clayey detection. This allows to overcome the main limitation of TDEM for detecting shallow conductive layers due to its turn-off time. It is important to note that these methods are limited to depths not deeper 50 meters.

- DC electrical methods include many techniques and configurations (arrays), can be used in areas with electromagnetic noise, and are the most commonly used techniques for hydrogeological investigations. This method has also a good resolution for high resistivity layers (Kunetz, 1966) compared to TDEM. We used mainly the Electrical Resistivity Tomography (ERT) method for 2D detailed characterization (Loke, et al., 1996). Moreover, the lateral resolution of the method is excellent and will document the lateral continuity of shallow geological layers. This method is also costly and takes more time to operate.
- Frequency Electromagnetic method (FEM) (McNeill, 1980) has been used in “Slingram mode” to evaluate its ability to detect conductive clayey layers close to the surface and to quickly evaluate the lateral continuity of conductive clay (if any).

The methodology for the small-scale geometrical shallow characterization is summarized in Figure 1.9.

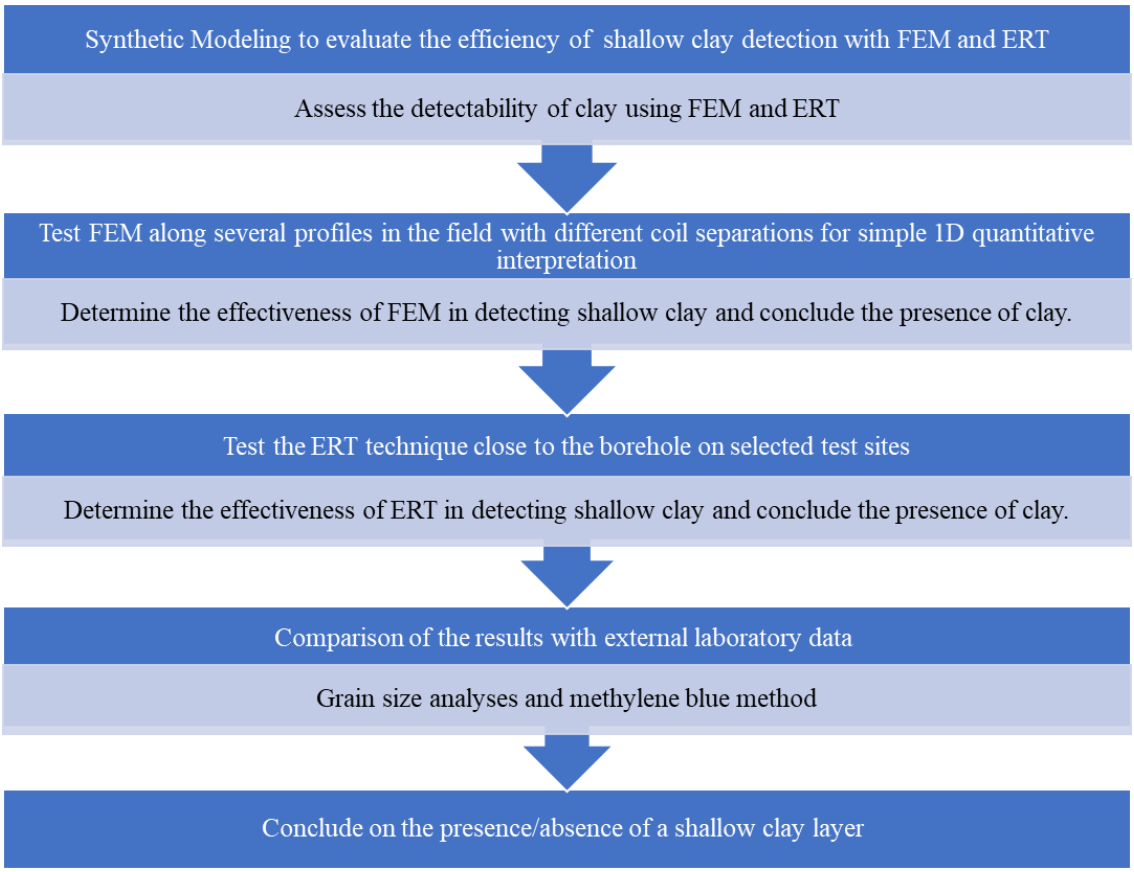

Figure 1.9 Methodology for investigating clay layers at a smaller scale.

As the shallow clay layer plays an important role in determining the vulnerability and natural recharge zone for the aquifer the FEM and ERT methods must be evaluated regarding the clay detection efficiency, then applied on test sites.

Geophysical methods for characterizing the groundwater resources

For this objective, we propose to use a relatively new geophysical method, the Nuclear Magnetic Resonance (NMR) method, that has been used only once in a sandy aquifer context in Vietnam (the coastal village of Mui Ne far from HCMC) and a karst region in the northwest (Giang, et al., 2012). Our work will be the first attempt to use this method in Vietnam for a major geological context, the sediment depositional environments of rivers. NMR has the unique ability to detect water content and classify the type of sediment, making it a valuable tool for resource exploration and could help in classifying the sediment type and thus the "aquifer quality". NMR is used to determine subsurface water content and hydraulic properties of the porous media based on the nuclear magnetic resonance (NMR) principle applied (Lubczynski, et al., 2004). This method reduces ambiguity in groundwater exploration compared with other classical geophysical methods. Therefore, the NMR approach may help evaluate the aquifer and establish the relationship between the NMR parameters and the water content of the reservoir, possibly getting an estimate of the aquifer's storage capacity. In addition, the relaxation time constants of MRS may help in qualifying the aquifer quality, i.e. grain size estimate that could be correlated with hydrogeological parameters (Legchenko, 2013). We attempt to use this method at two different scales.

- At the field scale, we used the Magnetic Resonance Sounding method (MRS). This sounding method has helped to determine the water reserve in many geological contexts in the world for two decades, giving estimates of the distribution of water content in the aquifer with depth (Behroozmand, et al., 2015). In addition, MRS is also a method to help determine the dynamic parameters of aquifers, building the relationship in hydrogeological parameters to assess the exploitability of aquifers and quality through the lithological distribution (Vouillamoz, et al., 2014). Preliminary tests (4 soundings) of MRS in our study zone have shown a high level of electromagnetic noise that severely limits the efficiency of the method in quantifying aquifers with a moderate amount of water. No quantification of the Cu Chi aquifer was possible using our equipment. Therefore, a second approach, at the core scale, has been foreseen for this PhD work.
- At the core scale, the use of NMR is the first attempt in Vietnam to get parameters on sedimentary aquifers, such as classifying the type of aquifer and estimating the water content in the aquifer.

The total methodology for the NMR core scale characterization is summarized in Figure 1.10.

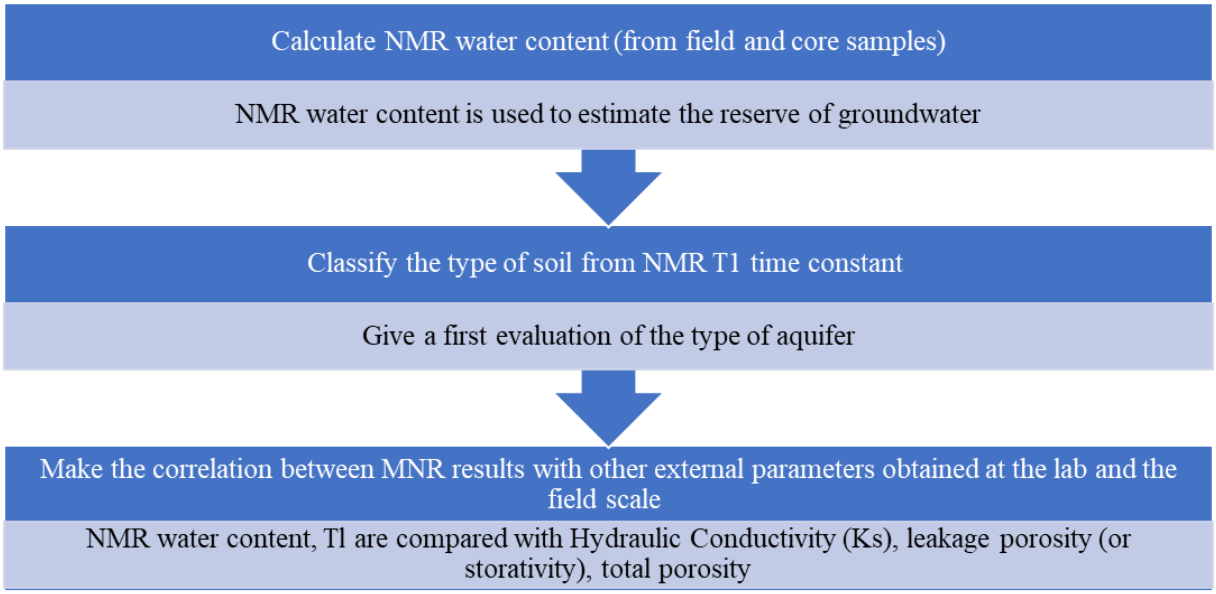

Figure 1.10 Methodology used for MRS/NMR.

The described procedure will be implemented in our study to analyze and understand the specific characteristics of the aquifers in the research area.

1.4.5 Other methods

To be able a) to evaluate the efficiency of the geophysical methods, and b) to provide valuable new information on aquifer characteristics, we needed external hydrogeological and geotechnical methods useful for determining effective porosity, specific yield Sy (or storativity), sediment types, soil type, hydrodynamic parameters at different scale.

- Geological and geotechnical methods

Geological observations are used to study the stratigraphic system in the study area, identifying aquifers and aquitards. In addition to field outcrop investigations, and classical sieve

methods to determine the particle composition curve distribution to classify sediment class. Besides, we use the methylene blue method (Arab, et al., 2015) (Gürses, et al., 2004) (Kahr, et al., 1995) to confirm (or not) the presence of mineralogical clay contained in the core sample with less than 2μm grain size (which is the domain of "granulometric clay" size), to assess the type of the aquifer (from fine to coarse sediments). We conduct experiments to determine saturated permeability values (Ks) on core samples and for soils in the field at shallow depths to compare with permeability results from pumping tests and to build correlations with geophysical parameters (NMR and resistivity).

- Hydrogeological methods

Two long-duration pumping tests (Kruseman, et al., 1990) have been conducted to determine permeability and storage coefficient, and specific yield of the aquifer. The results of the pumping test determine the flow capacity of the reservoir and compare it with the results from the lab test. In addition, a salt tracer test has been done to determine the effective porosity for the assessment groundwater reserve in the study area.

- Logging methods

Two common geophysical logging techniques, gamma-ray and resistivity, are used in five experimental boreholes drilled for the purpose of the Ph.D. The gamma-ray curve can differentiate between clay layers (high values) and sandstone layers (low values), while the resistivity curve shows low values for clayey layers and high values for sand layers. These curves form the basis for the logging method in determining the depth and thickness of aquifers. The logging results will be compared with surface geophysical data to gain a better understanding of the aquifer morphology and structure in the study area. Besides well log data are compared with NMR results measured in the core sample to detect the relationship between well log data and NMR water content, the T1 value to classify the category of the aquifer.

1.5 Organization of the manuscript

The manuscript is organized into five chapters

Chapter one is the present introduction.

Chapter two presents the background on the study area, with the necessary information regarding the groundwater but also on environmental data and context.

Chapter three presents the methods of the Ph.D., mainly the geophysical methods, as a necessary step for understanding, and evaluating, the geophysical results. This chapter presents also some results of synthetic modeling and detailed interpretation examples, in order to explain the main interpretation strategies and evaluate the uncertainty of the geophysical results

Chapter four presents the main results regarding the characteristics of the aquifer, first at a large scale using mainly the TDEM method, and data at a smaller scale using FEM and ERT. Analysis and discussion of the geophysical results are provided using mainly grain size analysis and literature review, to explain how the aquifer is organized and propose our hypothesis of genesis, providing a very new insight into the aquifer knowledge in the region. It is the major contribution of the Ph.D.

Chapter five explains the numerous attempts to use the new method of NMR, both at the scale of the field (MRS) and at the laboratory on borehole core samples (NMR). To understand and interpret the NMR results, several important and time-consuming external data have been acquired: boreholes, logging, long-duration pumping tests and tracer tests, several geotechnical analyses including grain size, hydraulic conductivity Ks, and more are also presented.

Finally, the conclusion presents general conclusion and questions that can be derived from our study and practical conclusions on the geophysical methods themselves to achieve the initial goals of the Ph.D. and their interest for future work in Vietnam, as well as proposals for future work.

CHAPTER 2. BACKGROUND AND HYDROGEOLOGICAL QUESTIONS

This chapter presents the main knowledge existing in the HCMC region and our selected area in the Cu Chi district useful for a) describing the main characteristics including geological and hydrogeological background, and b) presenting the detailed hydrogeological questions raised in the area, pointing those that are addressed by geophysics in the frame of the Ph.D.

2.1 Geographical context

2.1.1 Location of Ho Chi Minh City province, topography and hydrology

Ho Chi Minh City region, located in the south of Vietnam, occupies specific geographical coordinates between 10°10' to 10°38' latitude North and 106°02' to 106°54' longitude East (Figure 2.1). The region also has a 15km coastline along the East Sea (Thoang, et al., 2015) (Pham, et al., 2021). It is situated in the transitional region between the Southeast region and the Mekong Delta. It serves as a convergence point for major rivers such as the Dong Nai River, Saigon River, and Vam Co Dong River. This strategic location has made Ho Chi Minh City a significant economic center in the southern region and the country.

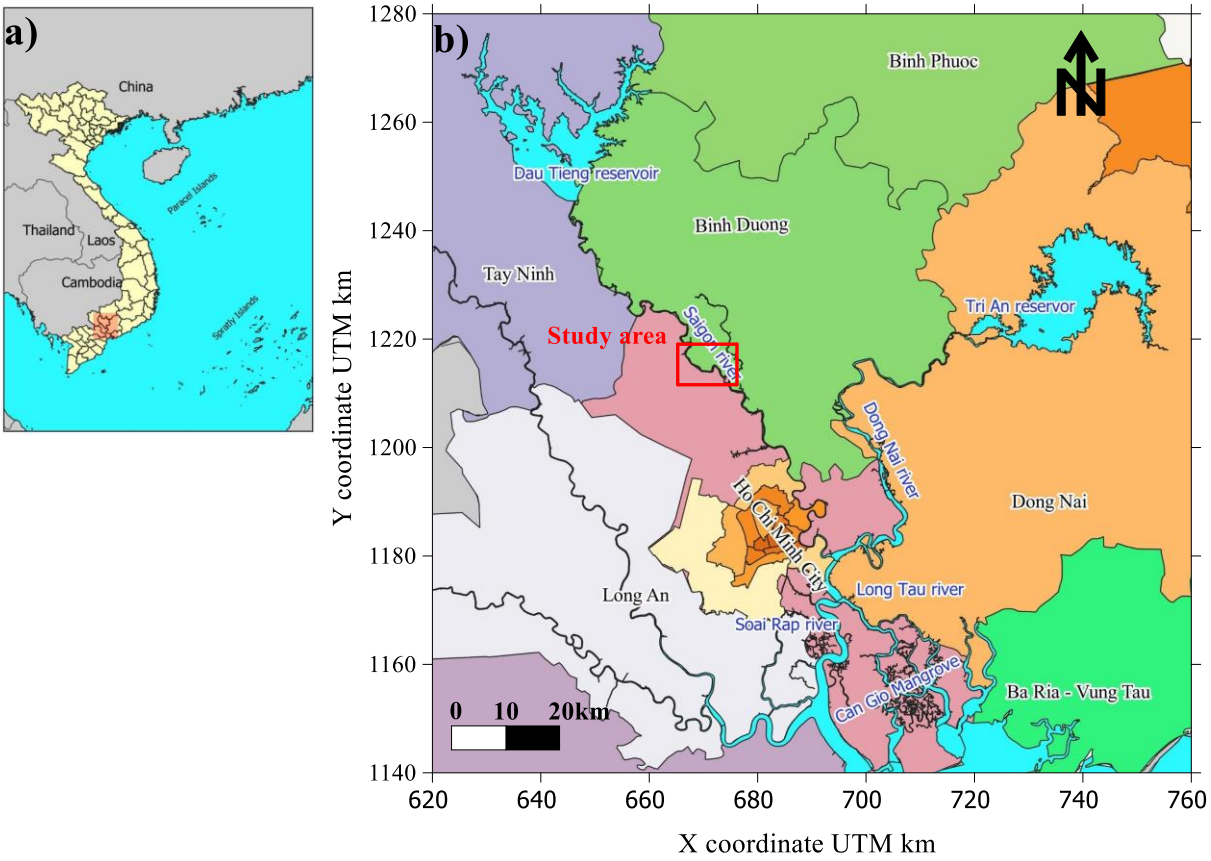

Figure 2.1 a) Location of Ho Chi Minh City region and b) administrative provinces in the South of Vietnam.

The city itself is mainly on the right bank of the Saigon River and has dense urban districts. Ho Chi Minh City is also characterized by a transition between the hilly terrain of the Central Highlands and the low-lying plains of the Mekong Delta. The topography can be divided into three sub-regions (NAWAPI, 2022). The highland region is located in the northern, northeastern, and part of the northwestern areas, including Cu Chi district (our study area), northeastern Thu Duc, and District 9. This region features undulating terrain with an average elevation ranging from 10 to 25 meters (Figure 2.2). Our research area, located northwest of

Ho Chi Minh City, is adjacent to the Saigon River in the northeast. The elevation varies, with the lowest point being approximately 1m in the riverside region. The highest elevation reaches around 15m in the central area, where agricultural activities and livestock farming are predominantly carried out. Besides, the study area is unaffected by flooding and rising sea levels.

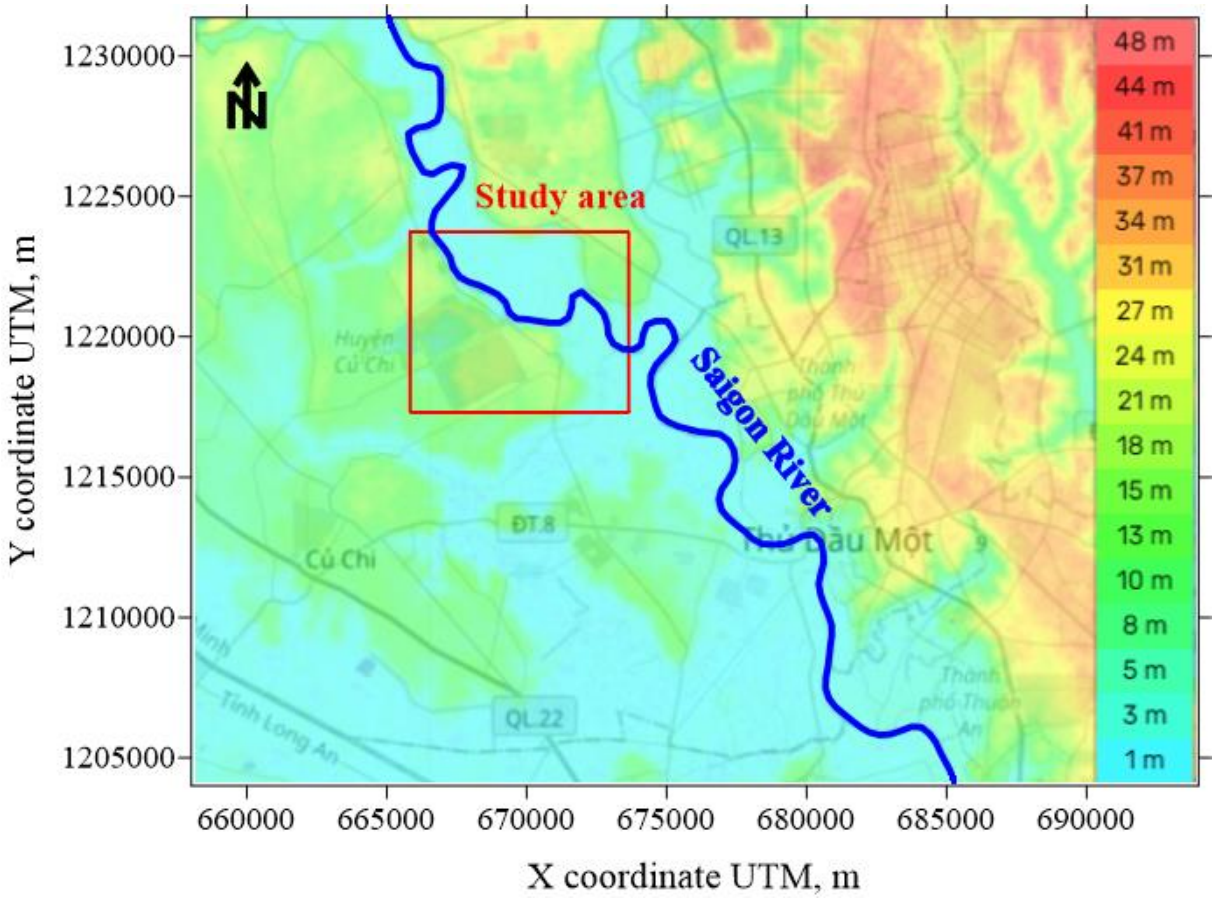

Figure 2.2 Topography in the Ho Chi Minh City area.

The study area of Cu Chi in the Northwest region of Ho Chi Minh City is shown with a red square, characterized in some parts by higher altitudes (+20 m) compared to the central and Southeast areas of the city. (Source of the topographic-map.com)

Ho Chi Minh City, situated in the downstream area of the Sai Gon-Dong Nai River basin, is heavily influenced by surface water flow in the region The city depends on two main rivers, the Sai Gon River and the Dong Nai River, for both water supply and drainage, including its downstream section known as the Nha Be River (NAWAPI, 2022) (Vuong, et al., 2016) (Phuoc Van, et al., 2013) (Figure 2.3).

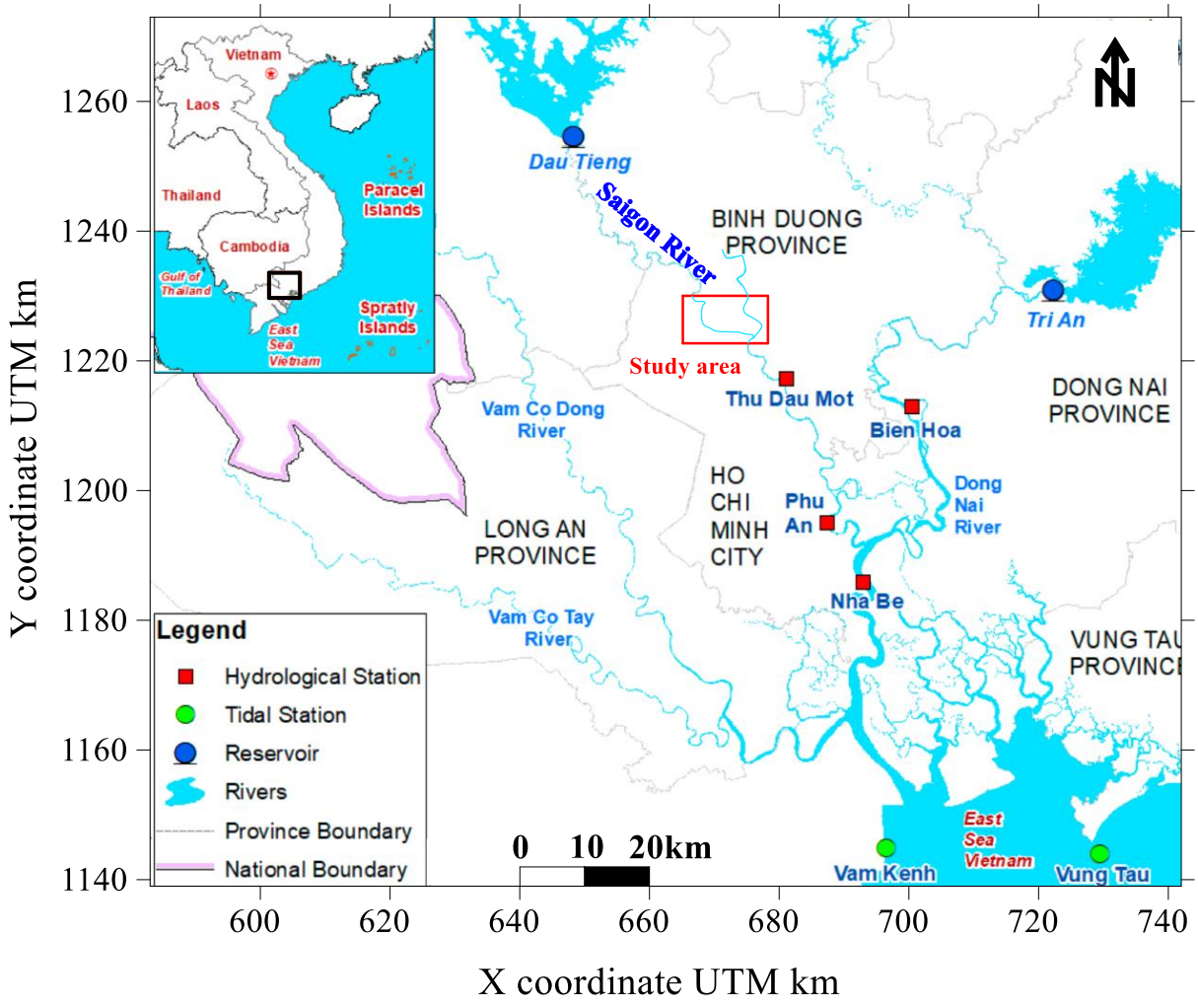

Figure 2.3 River system in Ho Chi Minh City region.

The study area within the Saigon River basin is constrained to the defined red square (Giang, et al., 2022)

The Saigon River experiences a semi-diurnal tidal regime, characterized by tidal amplitudes ranging from 1.5 to 3.1 meters. The Saigon River system governs a drainage area of 2,700 km². The highest recorded river flow occurred in 1986, reaching 84 m³/s, while the lowest flow was observed also in 1986 (Phuoc Van, et al., 2013). Water levels have also varied, with the highest recorded at 1.18 meters and the lowest at -0.34 meters on October 20, 1990.

2.1.2 Geomorphology, land use, population

Ho Chi Minh City's province is primarily segmented into five geomorphological main categories, formed by various geological processes and distinguished by unique surface characteristics and sediment compositions. These categories include River-formed Terrain, Sea-formed Terrain, River-sea Combined Terrain, Swamp-mixed Terrain, and Slope Processes Terrain. Our study area is situated mainly in the “river-formed terrain area”.

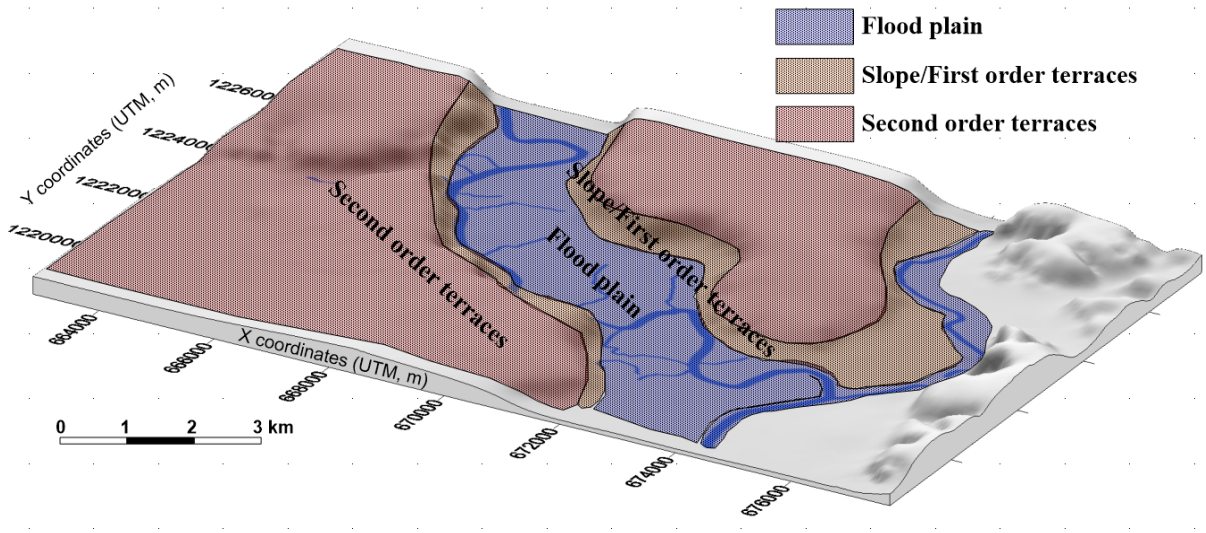

Figure 2.4 The typical geomorphological features in the study area.

Three geological structures have been suggested. These comprise the floodplain in low-lying riverine areas, denoted in blue; slope structures or First Order terraces, illustrated in orange; and Second Order terraces, indicated in red,

The main geomorphological features of our study area can be displayed in Figure 2.4 using the description made by (Khuc, 2000).

The classical features are the Low floodplains and High floodplains with relatively flat surfaces, at low elevations slightly sloping towards the river. The width of the floodplains varies from 30 to 1500 meters with heights ranging from 0.5 to 2 meters above sea level (asl). The composition of the floodplains includes sand, silt, clay, and occasionally organic matter. Currently, the low floodplains are still undergoing formation (Late Holocene age, Q_2^3). The high floodplains are only flooded during major floods, and they belong to the Middle-Late Holocene age (Q_2^{2-3}).

Then it is possible to observe in our study area First-order accumulation terraces: Concentrated in the Cu Chi district, appearing as remnants along the banks of the Saigon River or forming strips around second and third-order terraces. The first-order terraces have an average width of 100 to 500 meters and a height of 2 to 5 meters. They are composed of sand, silt, clay, etc., with an average thickness of 2 to 3 meters. The formation of the first-order terraces is influenced by the early-mid Holocene transgression (with the age of the first-order terraces being the early-mid Holocene, Q_2^{1-2}). Then the Second-order accumulation terraces have heights ranging from 5 to 15 meters and are composed of sand, scattered with gravel and lateritic pebbles on the upper part, transitioning to coarser sand containing quartz and pebbles (belonging to the Cu Chi Formation, Q_1^3cc). The sediment thickness ranges from a few meters to 28 meters.

The sedimentation system is a classical meandering river system. As seen in Figure 2.5, at the surface when in an arid climate, the tropical meandering rivers display a series of geomorphological systems such as oxbow lake, old flood plains, accretion crescents or prisms, and meander relics.

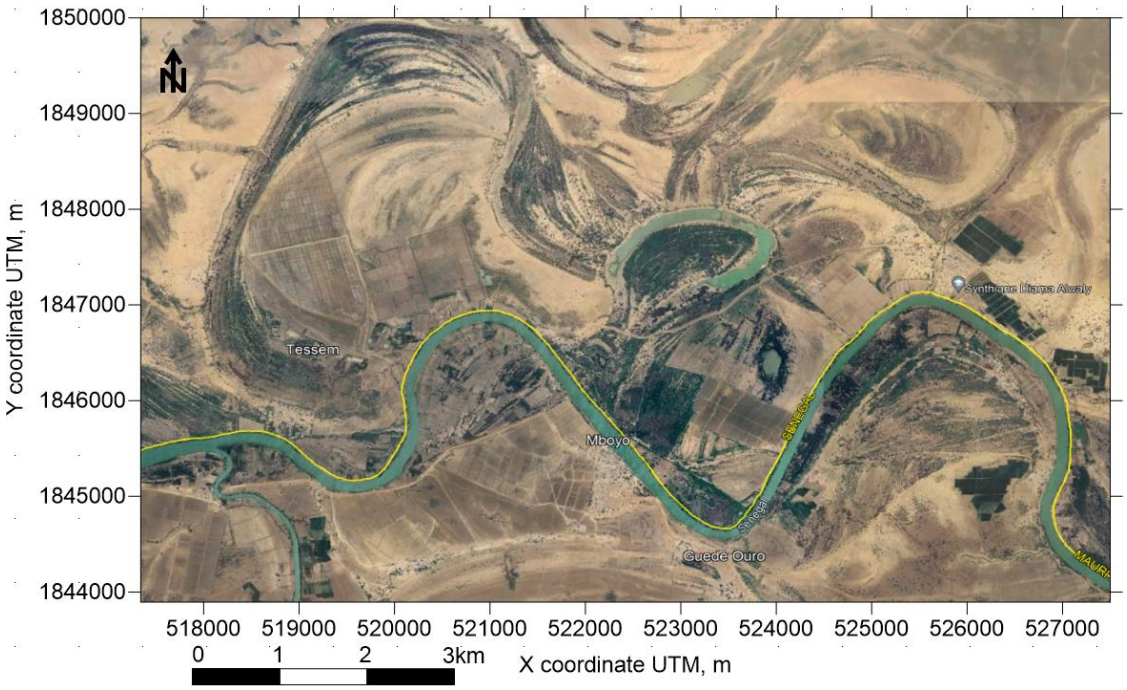

Figure 2.5 Meandering River system in the Senegal River (from Google Image, 2023).

In the absence of surface soils and vegetation, the shape and position of the former river bed, accompanied by distinct meandering horseshoe shapes, are revealed. Such geometries are expected to be present at depth also.

In tropical humid environments with dense human footprints, old hydrological features are no longer visible. The typical wavelength of the Saigon River meanders is 500 m to 1 km wide. The river itself is 100 m wide in our study area Figure 2.6. One could expect such geometries when exploring below the ground surface.

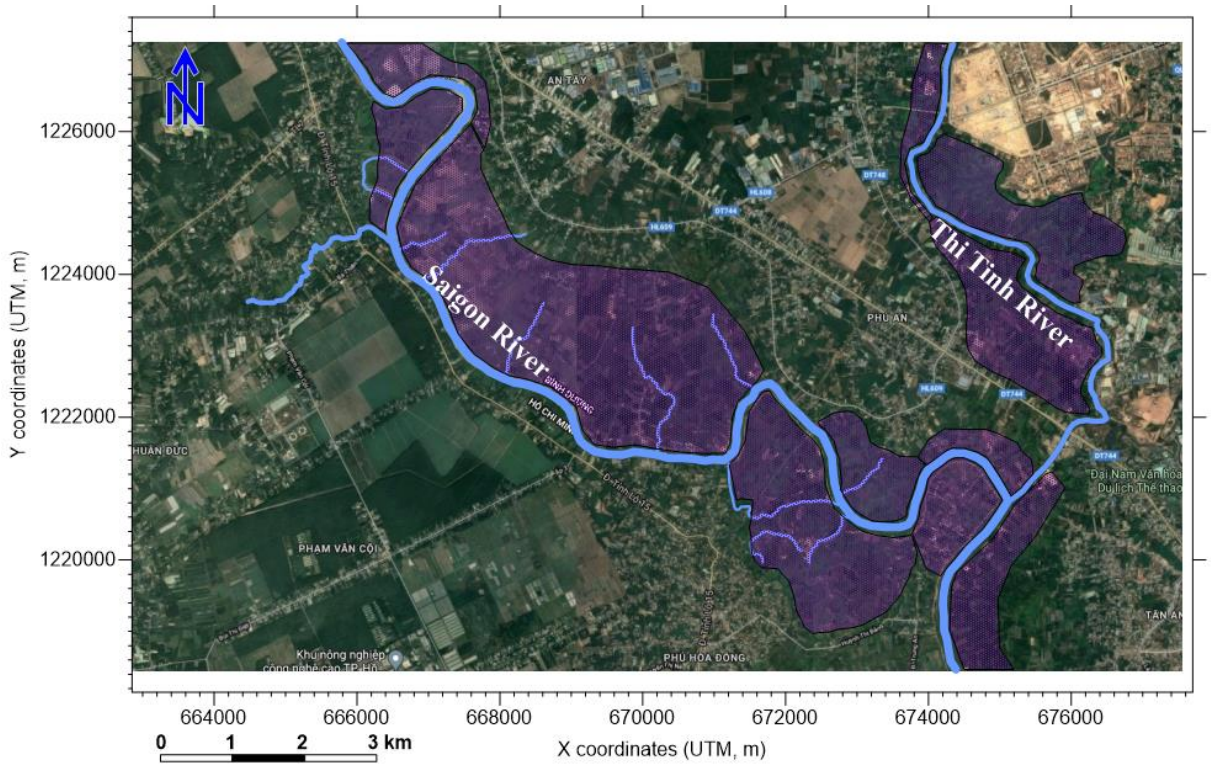

Figure 2.6 Shape of the river in the study area.

The main meandering is delineated using a blue curve. The topographical limit of the SR valley is delineated with a purple domain (From Google Image, 2023). Compared to the Senegal River, it is impossible to detect old river shapes due to vegetation, and human construction.

In Figure 2.7, typical depositional features are drawn as typical meandering river sedimentation at depth (Ghazi, et al., 2009). This drawing could be a guide for defining a sampling strategy for geophysics and interpreting the geophysical results if any of the features is characterized by resistivity contrast from others, and if the geophysical method has enough resolution to discriminate such geometries at depth.

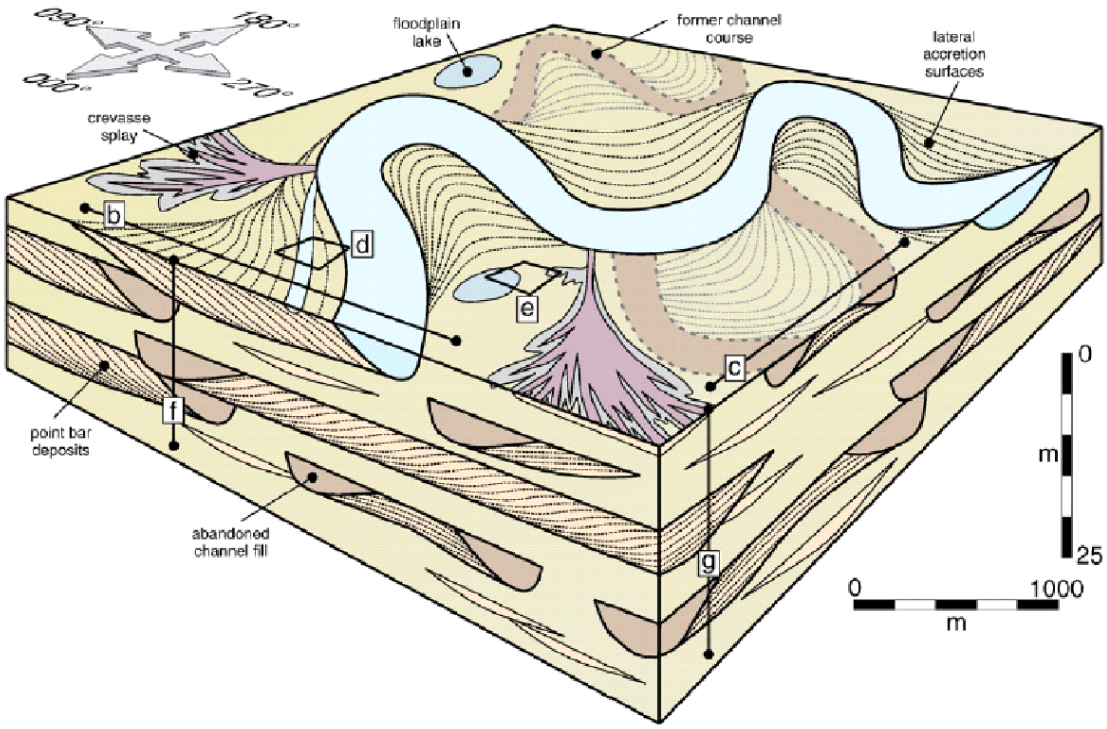

Figure 2.7 Sedimentary system fluvial described by (Ghazi, et al., 2009)

Different morphological units are drawn and could correspond to the surface and subsurface organization in our study area. a) Regional-scale facies model: Describing the overall distribution and characteristics of sedimentary facies across the region. b) Cross section through a laterally-accreting point bar: Illustrating the sedimentary features and depositional processes associated with a point bar that is accumulating laterally. c) Cross section through an abandoned meander loop: Depicting the geological features resulting from the abandonment of a meander loop in the river system. d) Architectural and facies complexity of a point bar succession: Highlighting the intricate structure and sedimentary facies variations within a point bar sequence. e) Architectural and facies complexity of a floodplain succession: Providing insight into the architectural and facies complexity observed in a floodplain setting. f) and g) Representative summary log sections through the succession: Offering concise representations of well logs through the sedimentary succession, capturing key lithological and stratigraphic information.

In addition, the study area is significant for its agricultural activities which have an impact on the underground recharge process. Agricultural activities favor rainfall infiltration. However, it also raises the risk of spreading pollutants into the groundwater caused by agricultural activities Figure 2.8.

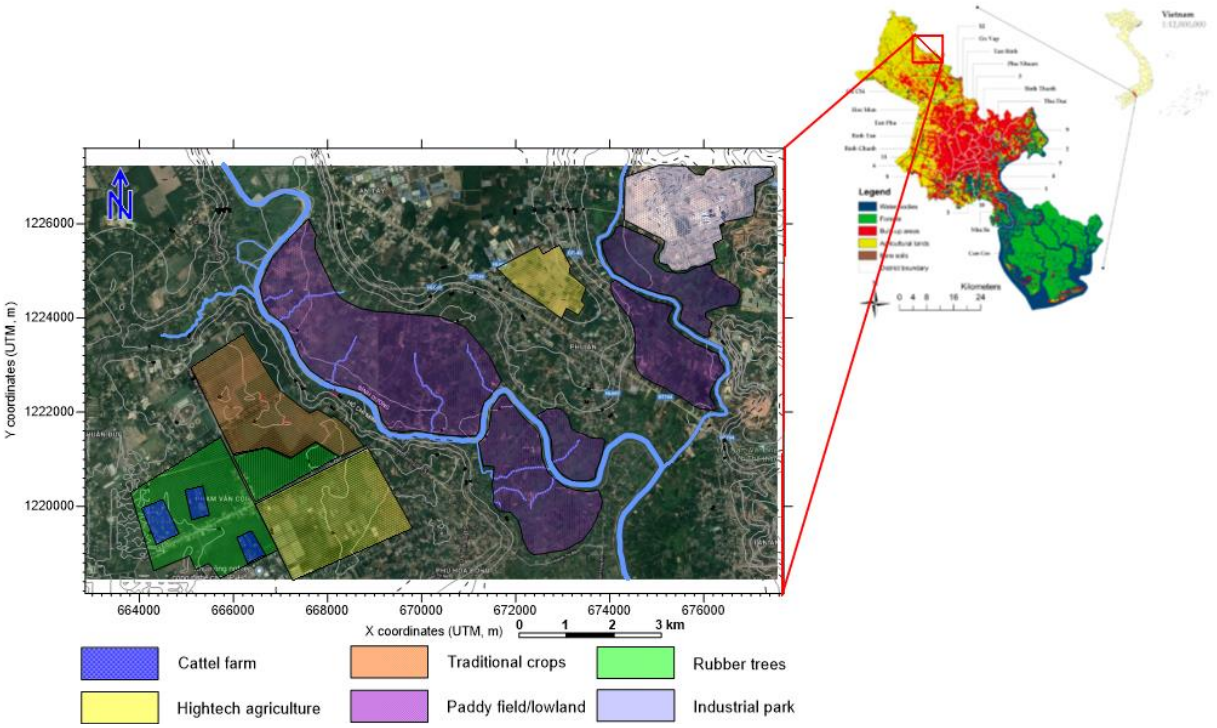

Figure 2.8 Land use map of Ho Chi Minh City region in 2018 (Wu, et al., 2021).

On the left, the land use map of the Cu Chi studied area reveals a predominantly agricultural landscape, with six distinct human activities influencing the underground water layer in the research zone. Cattle farming is denoted by the color blue, high-tech agriculture by yellow, traditional crops by orange, lowland or paddy fields by purple, rubber tree plantations by green, and the industrial park area is characterized by a light violet shade in the right corner of the study area.

Cu Chi district spans an area of 434.8 km² and has a population of 462,047 people in 2019, which translates to a population density of 1,063 people/km². Since 2009, the district's average annual population growth rate has been 3.02%, indicating rapid mechanical population growth and strong urbanization. As a result, the demand for water for domestic use, as well as agricultural and industrial activities, has rapidly increased, putting great pressure on the limited local water supply system. Groundwater serves as the main source of water for people's daily needs.

2.1.3 Climate

Ho Chi Minh City region is situated in the tropical monsoon zone, experiencing a year-round hot climate with distinct seasonal variations. The dry season typically spans from November to April, characterized by dry, hot weather and minimal rainfall. The rainy season occurs from May to October, featuring hot, humid conditions and abundant precipitation (Phuoc Van, et al., 2013). Ho Chi Minh City is influenced by two dominant wind directions: the Southwest-Monsoon and the Northeast-Northern Wind. The Southwest-Monsoon wind blows from the Indian Ocean during the rainy season, typically from June to October, The Northeast-Northern Wind blows from the East during the dry season, (Phuoc Van, et al., 2013). In the period 1997 to 2016, the average annual rainfall was 1943 mm. The northern region of the city, which receives a significant amount of rainfall over agricultural land, provides a larger water source for replenishing groundwater during the rainy season (DNRE, 2022). The temperature, from December to April, ranges from 26°C to 30°C. From May to November, the rainy season,

the temperature usually ranges from 27°C to 30°C (Phuoc Van, et al., 2013). The average relative humidity throughout the year is 79.5%, with a seasonal average of 80% and reaching absolute highs of 100%. During the dry season, the average humidity is 74.5%, with absolute lows dropping to around 20%.

2.2 Geology

2.2.1 General description

The subsurface of HCM City can be divided into two main layers: The Mesozoic basement rocks and the overlying Cenozoic sediments (Figure 2.9). The Mesozoic basement rocks comprise Jurassic sedimentary rocks and Cretaceous igneous rocks, which can be found at depths ranging from 50 to 70 meters in the northeast to over 300 meters in the southwest in HCMC region. Those formations outcrop 10 to 40 km to the east of our study area.

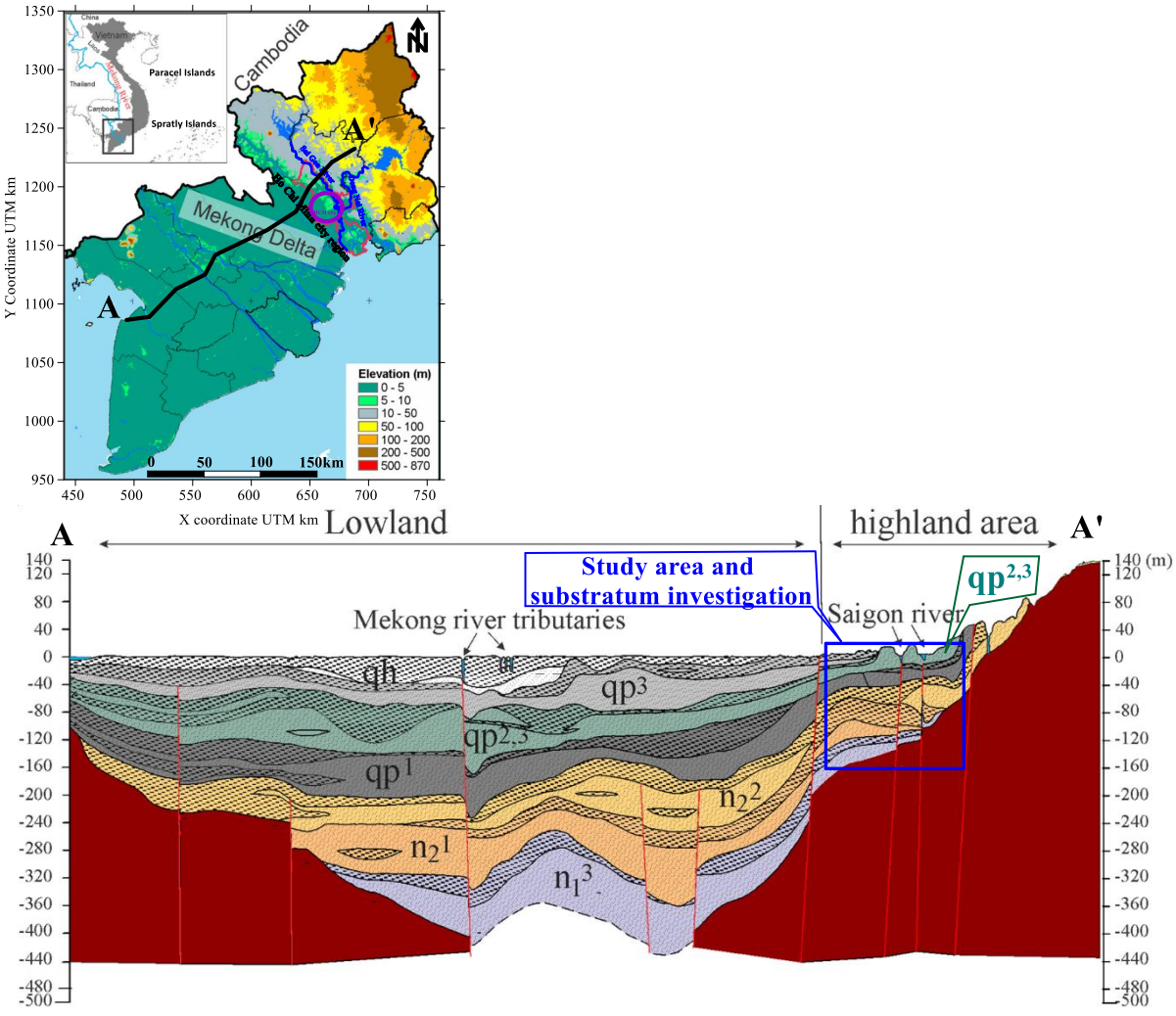

Figure 2.9 Hydrogeological cross-section from the Mekong Delta (Lowland) to the South East (highland area) (Ha, et al., 2022)

The research area is located in the Saigon River basin, which is the transition area from highland to lowland. Below is our research area, the substratum is expected at 150-170m deep

On top of the basement rocks lie the Cenozoic sediments, consisting of deltaic sediments that formed during the Miocene to Holocene periods, influenced by local tectonic activity and sea level changes. The lower portion of the Cenozoic sediments comprises the Miocene and

Pliocene formations. The Miocene formation consists of alluvial and marine sediments, with thicknesses varying from 17.5 meters to 40 meters. The Pliocene formation is inclined from the northeast to the southwest, with thicknesses ranging from 0 to 155 meters.

The Cenozoic sediments also include Quaternary formations, formed in five sedimentary cycles corresponding to five phases of marine transgression alternating with marine regression. These cycles, numbered from 1 to 5 in Figure 2.10, are well recognized in the deltas of Vietnam, including the HCM City area (Nghi, et al., 1991).

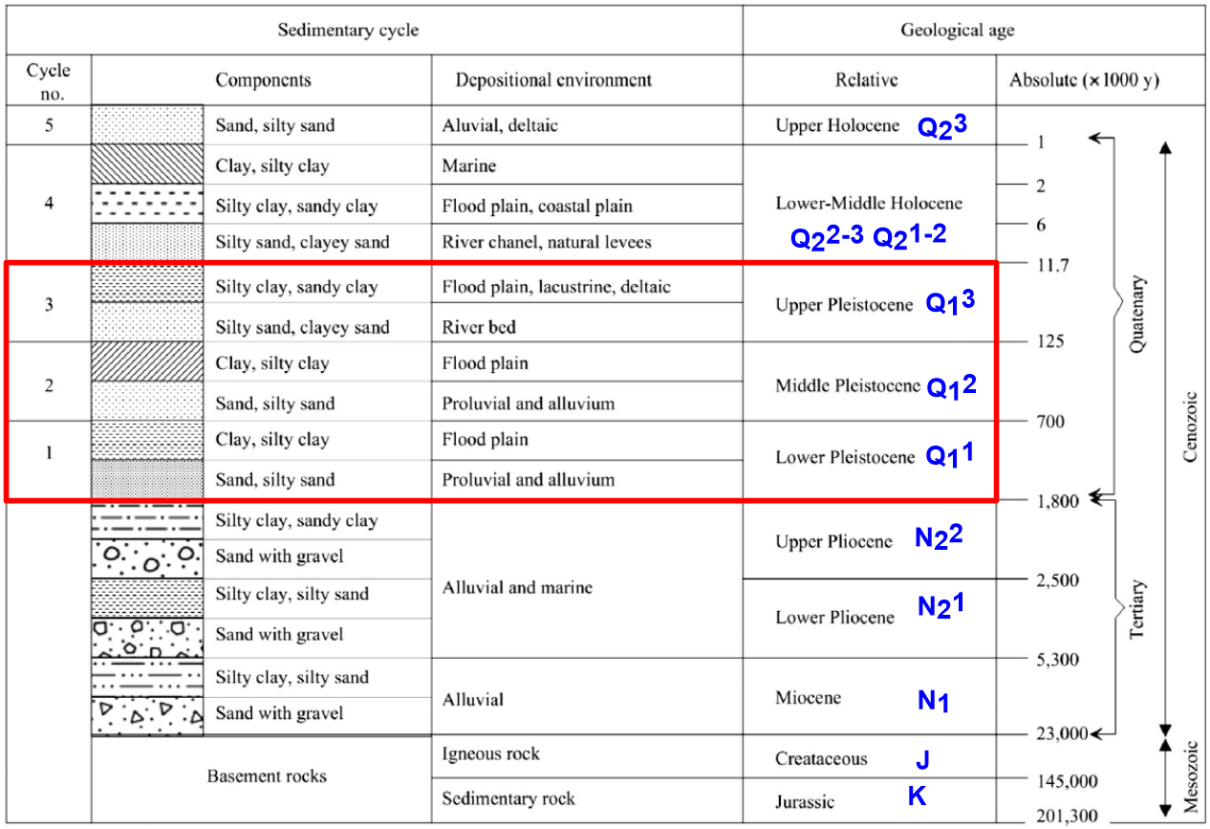

Figure 2.10 Formation and depositional environment of HCM City subsoil (Nghi, et al., 1991) (Thoang, et al., 2015).

This study primarily centers on sediments spanning the Upper Pleistocene to Upper Holocene periods, encompassing ages from 125 thousand years to the present within the Quaternary epoch. The sedimentary environments under investigation include a diverse range, such as riverbeds, floodplains, lacustrine settings, deltas, river channels, natural levees, coastal plains, marine areas, and alluvial deposits (in the red square).

2.2.2 Sediments classification

The sediments in Ho Chi Minh City are formed from two sediment classes corresponding to two periods: Pleistocene and Holocene.

Pleistocene sediments: These ancient alluvial sediments cover the majority of the northern, northwestern, and northeastern parts of the city. They are characterized by hilly terrain with a depth range of 3 to 25 meters. Over time, the Pleistocene sediments have developed into grey soil due to natural factors, erosion, decomposition, and human activities. Grey soil covers an area of 45,000 hectares, accounting for 23.4% of the city's total soil area (Phuoc Van, et al., 2013).

Holocene sediments: These newer alluvial sediments in Ho Chi Minh City originate from coastal areas, bays, riverbeds, and alluvial plains, resulting in the formation of different types of soil. The Holocene sediment includes the following soil types:

- Alluvial soil: Formed in highland terrains with a depth of 1.5-2 meters, primarily found in some areas in Cu Chi and Hoc Mon districts. Alluvial soil covers an area of 15,100 hectares, accounting for 7.8% of the total soil area.
- Aluminum soils cover an area of 40,800 hectares, accounting for 21.2% of the total soil area.
- Alkaline soils: This is the most extensive soil type in Ho Chi Minh City, mainly concentrated in Nha Be and Can Gio districts. Alkaline soil can be further divided into seasonal alkaline soil and salt marsh. Alkaline soil covers an area of 45,500 hectares, accounting for 23.6% of the total soil area.

Our study area displays a diverse range of soil types distributed at varying depths. Research conducted by (Tu, et al., 2022) suggests that the region's shallow formations, particularly in Cu Chi area, contain acrisol soil. This soil type, part of the Aluminum group, is formed through weathering and leaching processes. Characterized by its red or reddish-brown color due to high concentrations of iron and aluminum oxides (Ha, et al., 2019), acrisol has several defining features. It exhibits acidic properties, indicated by a low pH value and a low clay and organic matter content attributable to weathering.

Acrisol plays a vital role as a rainwater filter. Rather than posing a barrier, it facilitates the infiltration of dissolved minerals, notably SiO2, carried by rainwater. Concurrently, acrisol acts as an adsorbent for NO3. Despite the high NO3 concentration in surface water resulting from pollution, the groundwater NO3 concentration remains low due to this adsorption process.

2.2.3 Geological cross-section in the studied area

The geology can be described using Figure 2.11 from Vuong, et al., 2016.

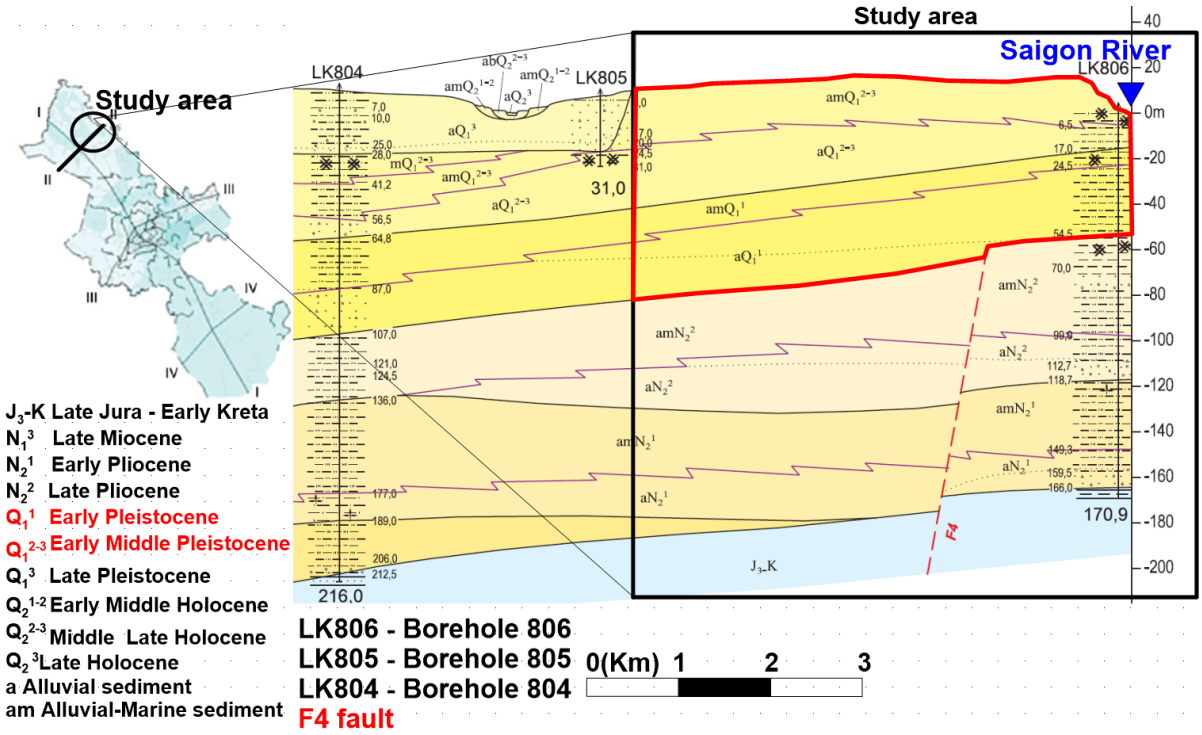

Figure 2.11 Geological cross-section in the study area (Vuong, et al., 2016).

In the study area, deposits of Tertiary and Quaternary sediments overlay the Cenozoic basement. The primary focus of the research centers on the Quaternary sediments.

The Cenozoic sediments include Tertiary and Quaternary formations. The quaternary is formed in five sedimentary cycles corresponding to five phases of marine transgression alternating with marine regression. These cycles, numbered from 1 to 5, are well recognized in the deltas of Vietnam Figure 2.10.

The Late Miocene and Early Pliocene formations consist of weakly cemented sediments of sand, gravel, and clay. Notably, the Early Pliocene strata have a significant proportion of shell fragments, suggesting a high potential for water content.

Late Pliocene formations, belonging to the Ba Mieu Formation, feature mostly sandy sediment at the base and layered clay towards the top. These strata are clayey layers that usually and when possible, serve as marker beds for stratigraphic correlation.

Pleistocene sedimentary formations are classified into three stratigraphic units: the Trang Bom Formation, the Thu Duc Formation, and the Cu Chi Formation. These formations are characterized by a decreasing grain size trend from bottom to top.

Holocene sediment formations, including the Binh Chanh Formation and the Can Gio Formation, mainly comprise sandy clay, occasionally mixed with sand and silty clay.

In some places, a lateritic layer (hardpan and/or diffuse lateritic gravels) has been found 5m deep in Holocene sediments in the Cu Chi area (Pham, et al., 2002). We have observed this layer in our boreholes. Such a layer, if it is widely spread, could play a role in infiltration processes. Actually, hardpans may delay water infiltration, as well as diffuse gravels.

For all those sedimentary sequences (Tertiary and Quaternary) authors note that the electrical resistivity values of these sedimentary sequences (obtained mainly using resistivity

logging in scarce boreholes) depend entirely on their lithological composition and the overall mineralization of the water they contain. With a high proportion of fine-grained sediment and relatively large and widespread thickness, the clayey layers of the Late Pliocene formations can be considered marker beds for stratigraphic correlation based on geological and geophysical data. They are characterized usually by low resistivity values, which distinguish them from the formations above and below in non-saline areas.

2.3 Hydrogeology

In this study, we are considering only shallow aquifers (from the surface down to 150 m) because they are readily accessible and used for individual extraction by households (that could pose also a significant risk), contributing to the potential contamination of shallow aquifers and downward diffusion into adjacent deeper aquifers. Each aquifer layer showcases unique attributes concerning its distribution, composition, depth, thickness, and hydraulic characteristics. While the Holocene aquifer is distributed in a narrow strip and largely excluded from groundwater extraction due to its restricted distribution, the Pleistocene aquifers are more widespread, serving as major sources of groundwater in the region. However, these aquifers also face threats from saline intrusion and pollution, particularly the Upper Pleistocene aquifer.

2.3.1 Aquifer geometry

The hydrogeological system of the rural district of Cu Chi can be described using the general classification of quaternary aquifers described for the entire Ho Chi Minh City region. Hydrogeologists propose to classify seven aquifer layers, from the surface to a depth of 150 m: 1) the Holocene aquifer (qh), 2) the Upper Pleistocene aquifer (qp_3), 3) the Middle-Upper Pleistocene aquifer (qp_{2-3}), 4) the Lower Pleistocene aquifer (qp_1), 5) the Middle Pliocene aquifer (n_2^2), 6) the Lower Pliocene aquifer (n_2^1), and 7) the Upper Miocene aquifer (n_1^3) (Vuong, et al., 2016) (Van, et al., 2018) (NAWAPI, 2022). This description shown in Figure 2.12 (Vuong, et al., 2016) is mainly based on one borehole only (TP 806) which is drilled down top 160 m and reaches the Mesozoic substratum.

- The Pliocene aquifers (n_{22} and n_{21}), found at greater depths, offer a substantial groundwater supply, with the former considered the most favorable for extraction due to its favorable hydrogeological characteristics. However, they are not considered for agriculture yet, being too deep for cheap extraction (Tran, et al., 2016). The Lower Pliocene aquifer, although widespread, is yet to be fully characterized, suggesting potential scope for further groundwater extraction. The deepest, the Upper Miocene aquifer, has been least explored but holds potential for groundwater.

- The six aquifers (excluding the 7th Holocene aquifer) are classified as confined aquifers, separated by aquitards composed of clay, silty clay, and sandy clay, varying in thickness “from 0” to over 10 meters. This means that the lateral continuity of those clay layers is not ascertained: where these aquitards are absent, hydraulic windows may exist, allowing hydraulic connections between the aquifers.

The hydrogeological cross-section built by (Vuong, et al., 2016) demonstrates the horizontal distribution of aquifers in Ho Chi Minh City province and the study area.

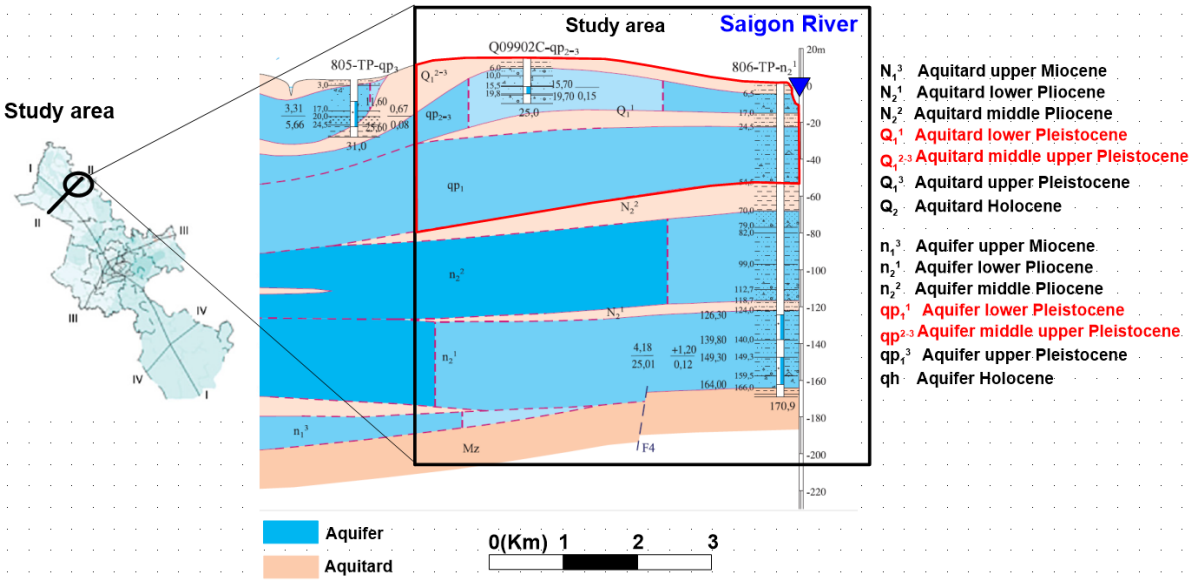

Figure 2.12 Hydrogeological cross-section showing the aquifer and aquitard in the study area (Vuong, et al., 2016).

We can see at the surface the cross section displays a layer marked by a continuous, probably impermeable, clayey barrier layer extending laterally across the entire area. This layer is drawn using similarity between boreholes separated by 3-4 km. This raises a question about constructing these hydrogeological maps and cross-sections: these maps often rely on discrete drilling data for their construction (1 borehole each 3 to 4 km). These isolated data points are then linked together to form a comprehensive profile. While this method may provide a general overview, it can lead to local inaccuracies in areas with complex geology, such as those with intermittent clay layers. Particularly for the study area, our personal field surface observations do not reveal any presence of the clay outcrops on the surface nor any evidence of lateral continuity of those hypothetical clayey layers, which supposedly could act as a protective barrier against potential pollution for the underlying aquifers. This raises doubts about the local accuracy of hydrogeological maps in the study area, or in other words, the geological conditions in the study area may be more complicated than simple continuity drawn between scarce drilling documents, and the reading of the map (or cross sections) could lead to unreliable local information.

Therefore, a more detailed and combined methodology is required to improve the local reliability of the information on these hydrogeological maps and redefine the stratigraphic boundaries accurately. Advancements in geophysical surveying techniques might be of valuable utility in this regard. Additionally, extensive field sampling and laboratory analysis could help validate these maps and potentially reveal geological structures that have previously been overlooked. If our study could bring more local reliable information on surficial clay layer continuity, this, in turn, could have significant implications for water resource management, construction activities, and environmental risks such as groundwater pollution mitigation.

When summarizing the sediments encountered by the boreholes for the aquifer layers, one can note that the total fan of sediment type is represented: “fine sand”, “gray fine sand”, “white-gray silt”, “coarse sand”, “fine to medium sand”, “medium to coarse sands”

Some previous studies bring valuable but scarce information on aquifers Figure 2.13:

- **The Holocene aquifer** (**qh**): The Holocene aquifer consists of unconsolidated sediment deposits from the Holocene age (Q_2). The predominant soil composition of the confined aquifer is fine sand, gray fine sand, and white-gray silt. This aquifer has a distributed area of 196.2 km2, forming a narrow strip in the southwest of Ho Chi Minh City, comprising scattered pockets in Cu Chi District, ThuDuc City, and Binh Chanh District. It has a thickness ranging from 2.5m to 25.5m, with an average thickness of 11 m.
- **The Upper Pleistocene aquifer** (**qp_3**): This aquifer is composed of coarse sands and is widespread throughout the city, except for certain elevated areas in Cu Chi district and District 9. So, it is normally not present in our studied area. It has an average thickness of 23 meters, ranging from 2 to 63 meters. The hydraulic conductivity is measured at 12.8 m/day, and the storativity is 20.3% (Thoang, et al., 2015). This aquifer is primarily recharged by rainfall. The groundwater level in this aquifer fluctuates seasonally, with elevations more than 10.0 meters above mean sea level (MSL) in the northern and northwestern parts and about 1.0 meters above MSL in the southern and southeastern parts. However, this aquifer is prone to saline intrusion and contamination, making it unsuitable for extensive groundwater supply. It is extracted only in small amounts in limited areas.
- **The Middle-Upper Pleistocene aquifer** (**qp_{2-3}**) is widespread, particularly in Thu Duc and Cu Chi districts near the Sai Gon River. It consists of fine to medium sand and is found at depths ranging from 0 to 120 meters, with an average thickness of 27 meters. This aquifer serves as one of the main sources of groundwater supply for HCM City.
- **The Lower Pleistocene aquifer** (**qp_1**): Comprising medium to coarse sands, this aquifer is found at depths ranging from 11.0 to 160.0 meters, with an average thickness of 27 meters. This aquifer also plays a significant role in groundwater supply for HCM City.
- **The Middle Pliocene aquifer** (**n_2^2**): The upper fourth aquifer is composed of medium to coarse sands and is found at depths ranging from 34.0 to 209.0 meters, with an average thickness of 38 meters. It is considered the most favorable aquifer for groundwater extraction and is extensively utilized for industrial and domestic purposes in the city.
- **The Lower Pliocene aquifer (n_2^1)**: The lower fourth aquifer is widespread throughout the city, found at depths ranging from 101.0 to 260.0 meters, with an average thickness of 34 meters. This aquifer has not been extensively characterized yet, with limited pumping tests and well drilling. The clay layer separating it from the overlying aquifer is missing in many locations, suggesting a direct hydraulic connection between the two aquifers.
- **The Upper Miocene aquifer** (**n_1^3**): The fifth aquifer is composed of coarse-grained sand and is found at depths ranging from 116.0 to 304.0 meters, with an average thickness of 35 meters. Only a few wells have been drilled into this aquifer.

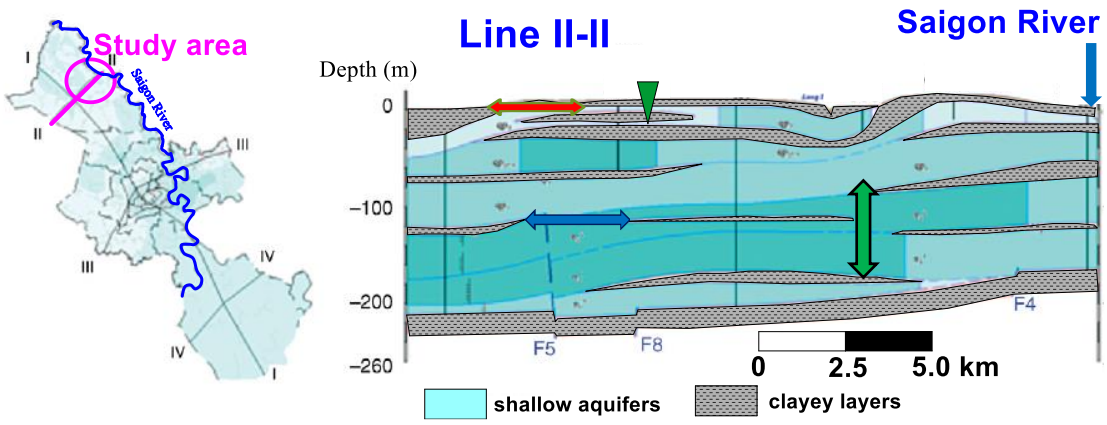

Figure 2.13 Aquifer system in Ho Chi Minh City across the study area (Vuong, et al., 2016). Arrows are described in the text. F4, F5 and F8 are faults.

In Figure 2.14, the hydrogeological section across the study area, as outlined in the Vuong (2016) study, is constructed using data from scattered boreholes. This hydrogeological cross-section depicts the interplay between the shallow and deep aquifers at the marked location of the green arrow. The blue arrow's position shows the horizontal continuous of a deep clay layer plays a role in delineating the separation between the shallow and deep aquifers within the study area. Finally, the accuracy of the previous study findings regarding the presence of a surface clay layer, acting as a protective barrier for the underlying aquifer at the location indicated by the red arrow, needs confirming. Therefore, a more detailed investigation is needed to provide clarity on these matters.

2.3.2 Questions related to the aquifer system geometry

Having described above the main known characteristics of the aquifer system, we summarized here the main questions raised in the frame of the study in the table below. In addition, we indicate whether or not geophysical methods are applied, or other methods. We also indicate the questions that are not directly addressed in the PhD work.

Hydrogeological questions related to geometry	**Proposed methods (geophysics + others)**
How are distributed aquifers in the first 150 m of the subsurface? Actually, for aquifer description and process understanding, there is a lack of knowledge from the previous studies regarding the general organization of the aquifer. If we could answer this question, we could propose a schematic view of the aquifer, hypothesize its genesis, and we may deduce useful information that could be applied in other parts of the region.	• Resistivity sounding methods at large scale: Time Domain Electromagnetism (TDEM) for clayey layers. • Shallow resistivity methods for shallow clay (ERT +FEM). • Borehole coring and grain size.
Is there any hydraulic connection between the rivers and the aquifer? If river systems are subject to pollution, these pollutants can disperse into aquifers in	• Not addressed fully in this PhD

regions where rivers and groundwater interact, contaminating critical freshwater sources. Conversely, contaminants from groundwater can diffuse into river systems. Therefore, there is a need for research to show whether there is an interaction between aquifers and rivers in the study area.	• Shallow Electrical Resistivity Tomography close to the river for shallow clay. • Question addressed by isotope study (Tu, et al., 2022)
Where could be located the zones of recharge? Understanding the areas of groundwater recharge is crucial, as human activities within these regions can significantly influence the recharge process. Indeed, these activities could disrupt the natural replenishment of groundwater and contribute to the introduction and dispersion of pollutants into the aquifer. Therefore, identifying these recharge zones is paramount for the protection and maintenance of groundwater resources. It ensures the smooth continuation of natural recharge processes and helps mitigate any detrimental impacts.	• This question is addressed thanks to the dense TDEM survey that identify shallow resistive structures. • Electrical Resistivity Tomography, FEM at key test sites.
Can we estimate the volume of the aquifer layers? If we could answer this question, we can know the amount of groundwater resources in this area; therefore, we can propose a strategy to protect groundwater in the future.	• This question is not answered in this PhD but could partly be addressed thanks to the dense TDEM survey that identify deep aquifer layers between clayey aquitard
Is there a lateral continuous clay layer at the surface? Is there a risk of vertical infiltration of pollutants through the vadose zone? Indeed, the presence or absence of the clay layers on the surface is a very important point to be studied because it is the conditions for having or not infiltration of pollutants down to the water table.	• This question is addressed thanks to the dense TDEM survey that identify- or not- shallow structures • For detailed continuity: Electrical Resistivity Tomography, FEM in key test sites
Is there a lateral continuity of the laterite layers identified by hydrogeologists? In the same manner, if the laterite layer at a depth close to the surface is permeable or not, its role regarding pollutant transfer has to be investigated. Again, its lateral continuity is an important geometric characteristic to be known.	• This question is addressed thanks to Electrical Resistivity Tomography to laterite parameters in key test sites
Are lateral deep clayey layers continuous, and are they separating aquifers? Answering this question is pivotal in discerning whether aquifers are hydraulically isolated from each other. Such separation could impede the downward diffusion of pollutants from upper strata into lower aquifers. It aids in preventing contamination from the surface to deep	• This question is partly addressed thanks to the dense TDEM survey that identifies - or not- deep conductive structures, but with a decreasing accuracy with depth.

aquifers, thereby playing a significant role in groundwater conservation for future use.	
What is the depth of the substratum? This question is important for groundwater resource estimation as well as the possibility of modeling the groundwater flow.	• Out of the scope of the Ph.D.: In this study, we are not considering this question primarily because we focus on shallow aquifers

2.3.3 Aquifer dynamic

Groundwater head from models

According to Long, et al., (2017), the Saigon Basin has revealed a groundwater flow pattern from the northwest to the southeast within the confined aquifers Figure 2.15. Based on the model results pointed out in the study area, the flow direction is distributed from the aquifer discharge into the Saigon River. In addition, Van, et al., (2018) study also confirmed that in the study area, groundwater from aquifer the discharge into the Saigon River in both the dry and rainy seasons. Therefore, it shows the possibility of interaction between the aquifers and the Saigon River in the study area. However, the location and characteristics of the interaction between the river and the aquifer have not yet been elucidated. There is a need for research on determining the interaction location and the boundary between the Saigon River and aquifers.

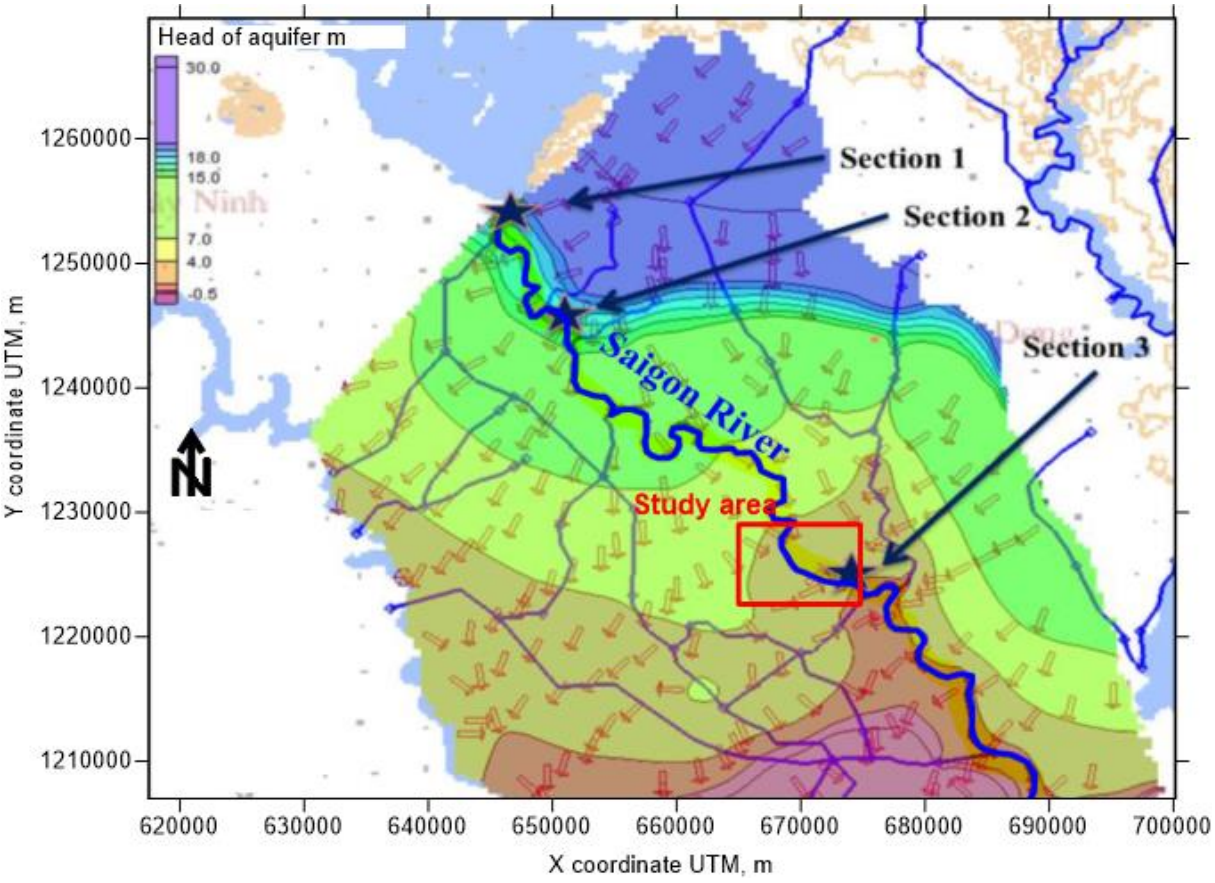

Figure 2.14 Distribution of head and flow direction of groundwater in the Saigon River basin (Long, et al., 2017).

The arrows correspond to the flow direction of groundwater in the Saigon basin, mainly from the Northwest to the Southeast. The coloration on the map in the Saigon River basin area corresponds to the head of the aquifer (in m). Notably, the region with the highest-pressure head is represented by the color purple, ranging from 18 to 30 meters, situated in the north-northeast of the Saigon River basin adjacent to the Dau Tieng reservoir area. Conversely, the South region exhibits the lowest pressure head, indicated by a pale color below the specific sea level elevation of -0.5 meters. Within the study area, the light orange color denotes the reservoir pressure head, fluctuating around 4 meters above sea level.

River-groundwater interactions

Along the entire Saigon River from upstream to the estuary, three aquifers may interact with the river system: The Upper-Pleistocene (qp_3), Upper Middle Pleistocene (qp_{2-3}), and Lower Pleistocene (qp_1) aquifers (Van, et al., 2018) (Long, et al., 2017) (Long, et al., 2020). The Holocene aquifer (qh) is usually disconnected from the river system (Long, et al., 2017). The interaction between the aquifers and the river is usually detected as the river level varies, the piezometer heads in both aquifers oscillate accordingly. In addition, isotopic studies have confirmed the recharge of groundwater at stations 1 to 3 in Figure 5.15, thereby demonstrating the interaction between the aquifers and the river (Long, et al., 2020) (Long, et al., 2017) (Tu, et al., 2022). The conductance values were determined at various distances along the river. At 0 km, the conductance value was computed and validated with field seepage measurement to be 4.5 m^2/day/m. As we move downstream, the conductance values gradually decrease. At 30 km, the conductance value is 4.2 m^2/day/m, at 60 km it is 2.5 m^2/day/m close to the river, at 80 km it is 1.7 m^2/day/m, and at 120 km it reduces to 0.25 m^2/day/m (Long, et al., 2020).

These decreasing conductance values correspond to the changing riverbed materials along the river. In the upstream section, where the conductance is highest, the riverbed consists of sand. As we move downstream, the riverbed materials transition to silt, resulting in lower conductance values. This result is corroborated by the analysis of sediment particle composition in the Saigon River area canal and estuary, indicating a higher proportion of fine particles in the estuarine sediment than in other areas (Babut, et al., 2019). However, there is a lack of specific research that can precisely determine the position and interaction mechanisms between the aquifer and the Saigon River.

Known hydrodynamic parameters and recharge

According to the results of the permeability distribution map for the qp_3 and qp_{2-3} aquifers in Ho Chi Minh City, the study area is in an area with permeability values from 10 to 20m/day (Long, et al., 2017). Previous studies by (Thoang, et al., 2015) (Van, et al., 2018) have given estimates of some properties, measured in far remote boreholes from our zone.

- The Upper Pleistocene aquifer (qp_3): The hydraulic conductivity is measured at 12.8 m/day, and the storativity is 20.3%. This aquifer is primarily recharged by rainfall. The groundwater level in this aquifer fluctuates seasonally, with elevations more than 10.0 meters above mean sea level (MSL) in the northern and northwestern parts and about 1.0 meters above MSL in the southern and southeastern parts.

- The Middle-Upper Pleistocene aquifer (qp_{2-3}): hydraulic conductivity is measured at 15.3 m/day, and the storativity is 6.2%. Groundwater levels vary from more than 6.0

meters above MSL in high-elevation areas to less than 15.0 meters below MSL in low-elevation areas.

- The Lower Pleistocene aquifer (qp_1): hydraulic conductivity is measured at 13.8 m/day, and the storativity is 3.6%.
- The Middle Pliocene aquifer (n_2^2): hydraulic conductivity is measured at 13.9 m/day, and the storativity is 24.8%. Groundwater levels in this aquifer vary from 0.8 meters above MSL to -16 meters below MSL. It is considered the most favorable aquifer for groundwater extraction and is extensively utilized for industrial and domestic purposes in the city.
- The Lower Pliocene aquifer (n_2^1): hydraulic conductivity is measured at 13.6 m/day, and the storativity is 12.5%.
- The Upper Miocene aquifer (n_1^3): Only a few wells have been drilled into this aquifer. The hydraulic conductivity is measured at 10.8 m/day, and the storativity is 3.8%.

According to the study by Tu, et al. (2022), the process of groundwater recharge at Cu Chi was determined through the analysis of $\delta^{18}O$ and $\delta^{2}H$ isotopes and pollutants such as NH_4 and NO_3, which were used to ascertain the recharge process duration for the Pleistocene aquifer. The results indicate that this aquifer replenishes from rainwater over a period of less than 60 years, with the most significant recharge occurring in months where rainfall exceeds 100 mm/month. The study also revealed variations in groundwater recharge volume across the area, explained by the uneven distribution of the shallow clay layer that needs to be investigated. Indeed, the study concluded that the infiltration and recharge process everywhere (with different rates from place to place) contradicts the previous hydrogeological cross-section displaying a continuous thick (5m) clay cap. This finding prompts the necessity for a detailed survey to monitor changes in the shallow clay layer and identify areas with a high recharge coefficient to maintain and protect against potential pollutant contamination transmitted to the aquifer during recharge. The maximum recharge coefficient from groundwater can reach up to 16% in areas without the separating clay layer and less than 5% in areas with this layer.

At a larger scale than the study of (Tu, et al., 2022), the rechargeable areas where groundwater can be replenished, are primarily located in the northern and northwestern parts of the region, encompassing an area of 435 km^2. Notable rechargeable areas include Cu Chi, Thu Duc, and a portion of the Hoc Mon District. A modeling study conducted by (Vuong, et al., 2016) estimated that aquifer recharge can reach 530000 m^3/d.

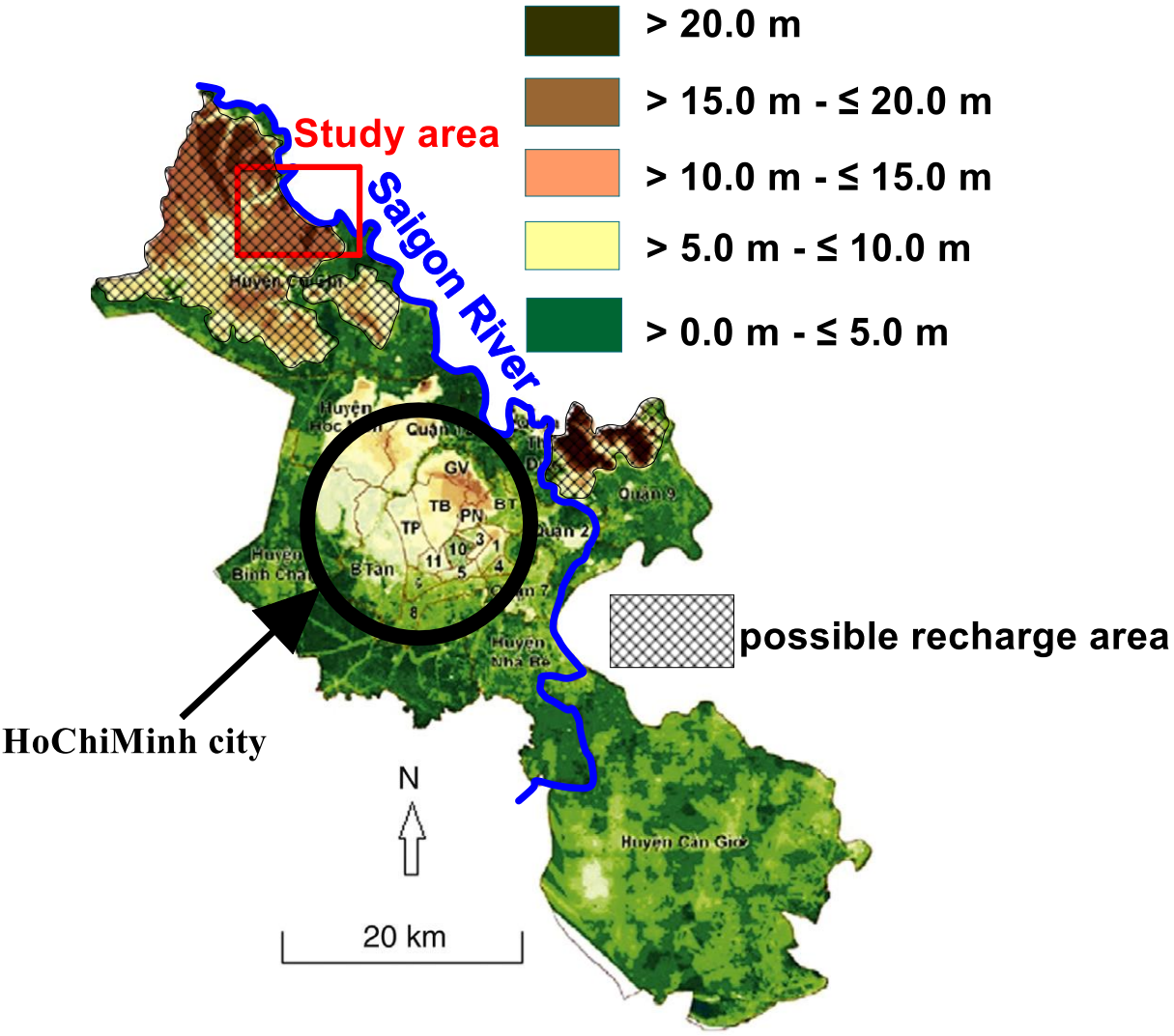

Figure 2.15 Recharge areas in HCMC, Vietnam. The recharge areas are noted here as part of the HCMC province from "Atlas of HCMC" , but other recharge areas exist, particularly at the east of the city (not shown here)

The groundwater recharge areas may coincide with the higher elevation terranes, limited to the northwest area and in the east of the city.

The recharge to the aquifer system occurs through direct infiltration of rainfall in the rechargeable areas and also from the Saigon River in the northern part of the city. The estimated recharge is 530000 m^3/d, accounting for approximately 27.6% of the total rainfall (Vuong, et al., 2016). This value is much higher than the value obtained in the study of (Tu, et al., 2022) 5 to 16%.

Percolation - infiltration in the vadose zone

The study of Long, et al., (2019) investigated some soil hydrodynamic characteristics: Each soil type exhibits different characteristics in terms of deep percolation rates and water infiltration. Sand clay loam has the highest maximum deep percolation rate of 4.5 mm/day, indicating its relatively better ability to allow water to penetrate deeply into the soil. With an annual percolation ratio of 0.34, approximately 34% of the annual rainfall is expected to percolate through this soil type. Sand clay, on the other hand, has a slightly lower maximum deep percolation rate of 3.5 mm/day, with an annual percolation ratio of 0.27. Clay shows

logically the lowest maximum deep percolation rate of 2.4 mm/day, with an annual percolation ratio of 0.04. The average monthly percolation rates also vary for each soil type, ranging from 2-4.5 mm/day for sand clay loam, 1.5-3.5 mm/day for sand clay, and 0.5-2 mm/day for clay, considering a rainfall intensity of 4-14 mm/day. These variations highlight the different water-holding and drainage capabilities of each soil type (Long , et al., 2019). These points out the need for understanding soil characteristics in groundwater management, particularly during consecutive drought years (Long , et al., 2019). In the Ph.D., we contribute to the catalog of values by performing hydraulic conductivity tests on soil samples.

Aquifer exploitation in Cu Chi area

In the Cu Chi area, 90% of the population uses groundwater for daily living needs. Groundwater from residential wells has a greater risk of water quality degradation than concentrated water extraction stations (Tran, et al., 2016). This demonstrates that the water used in the research region is concentrated in shallow aquifers susceptible to contamination. Therefore, easily accessible shallow water sources are the main source of exploitation of households in the area. In addition, agricultural activities are increasingly using groundwater in the dry season (November to April). To date, there are no specific studies that quantify groundwater exploitation in our selected area, or the Cu Chi District.

2.3.4 Groundwater Quality and Aquifer Vulnerability

Surface water Quality in HCMC and Upstream

According to (DNRE, 2022) the surface water quality monitoring results in Ho Chi Minh City in 2021 revealed several noteworthy points. The pH levels dissolved oxygen concentrations, and phosphate levels met the permissible standards for surface water of type B1 (as per QCVN 08-MT: 2015/BTNMT). However, at 44% of the monitoring points, the chemical oxygen demand (COD) concentrations exceeded the Vietnamese standards. Additionally, the suspended solids concentrations did not meet the standards at 50% of the points, while chloride concentrations exceeded the standards at the same percentage of points. Dissolved oxygen levels and coliform counts did not meet the standards at all monitoring points. Furthermore, iron (Fe) concentrations exceeded the Vietnamese standards at 81% of the monitoring points. Therefore, the use of surface water as a supply source for Ho Chi Minh City has certain limitations. This is particularly evident in areas lacking a dedicated water supply system for domestic use. In such areas, the predominant reliance is on groundwater for household needs and agricultural purposes.

Groundwater quality in HCMC region and at the selected study area

The Upper-Middle Pleistocene and Lower Pleistocene aquifers, may not be adequately protected from surface contaminant transfers due to the presence of extended shallow clay layers that do not effectively act as barriers to infiltration. Consequently, contaminants from the surface can potentially infiltrate the shallow aquifers, posing a risk to groundwater quality (Tu, et al., 2022). On the positive side, the North and Northeastern region of Ho Chi Minh City possesses a groundwater resource that has remained unaffected by arsenic contamination. Identifying priority areas for protection is thus crucial to prevent further contamination caused by anthropogenic activities in rural areas. Our study area is a major agricultural area of the region and the use of fertilizers and pesticides in agriculture can have a significant impact on

groundwater resources (Wu, et al., 2021) (Ha, et al., 2022) (Tu, et al., 2022). Fertilizers and pesticides can leach into the soil and groundwater, contaminating the water and making it unsafe for human consumption. This is an urgent issue because it not only affects the health of local residents but can also have long-term environmental impacts on the groundwater resources in the area.

Analysis of water samples from the upper aquifers, including the Upper Pleistocene aquifer (qp_3), Upper-Middle Pleistocene aquifer (qp_{2-3}), Lower Pleistocene aquifer (qp_1), and middle Pliocene aquifer (n_2^2), has revealed the existence of water samples that do not always meet national standards for drinking water. As a result, using these contaminated water sources poses a significant health risk to the population. On the other hand, the groundwater quality in the Upper Miocene aquifer (n_1^3) was found to be quite good, with all components meeting the national standards for drinking water (Vuong, et al., 2016). Furthermore, the data collected from groundwater samples in the three main aquifers indicate an increasing pollution trend, particularly in the shallow aquifer (Pleistocene), although the nitrate concentration remains below the authorized limit. Nitrogen compounds, specifically nitrate, show higher concentrations and distribution in the shallow aquifer compared to the deeper aquifers (Upper and Lower Pliocene). Both geogenic and anthropogenic sources influence the Pleistocene groundwater. Geogenic sources are related to organic matter present in the soil layers of the aquifer, while anthropogenic sources include fertilizers, manure, and septic waste, with the anthropogenic source dominating. Isotopic data confirm the geogenic nitrate source in the deeper aquifers' water. Tracer techniques used to study the infiltration rate and depth of fertilizers and water in areas specialized in legume cultivation also indicate the potential infiltration of water and fertilizers into shallow groundwater (Nguyen, et al., 2013). Effective waste management and treatment measures should be implemented particularly in zones where rainwater contributes to the recharge of the shallow groundwater, such as Cu Chi and Hoc Mon (Nguyen, et al., 2009).

Pollutants

Previous studies show that surface water in Ho Chi Minh City is currently polluted due to agricultural, industrial, and domestic activities (Nguyen, et al., 2020). Pollution indicators in the area where industrial parks are concentrated are related to metal indicators (Phan, et al., 2019) (Nguyen, et al., 2020), surface water in canals and rivers is contaminated with persistent organic pollutants (Minh, et al., 2007) while in suburban areas related to agriculture, pollution indexes related to pesticides and fertilizer (Nguyen, et al., 2020). Besides, groundwater exploited in the city center is also being polluted due to human activities (Nguyen, et al., 2013) (Anh, et al., 2021) (Minh, et al., 2007). Regarding industrial activities, we have only a few industrial zones in the selected area. One can expect pollution due to waste water (Phan, et al., 2019). The main cause of water pollution was the discharge of untreated wastewater directly into surrounding canals by various industrial enterprises (Pham, et al., 2018). Therefore, in an analysis of water samples in the canal in Ho Chi Minh City, it was discovered significant persistent organic pollutants (Minh, et al., 2007). So, there is a need for better management of industrial wastes. In particular, these wastes need to be treated carefully before being discharged into the environment. In the latest research published in 2023 by Caracciolo and colleagues (Caracciolo, et al., 2023), it was shown that the upstream area of the Saigon River

corresponding to our research location, exhibits significant water pollution primarily attributed to insecticides, herbicides, and fungicides originating from agricultural activities.

2.3.5 Questions related to processes, resources estimation, and vulnerability

As previously done for the aquifer geometry, we summarized here the main questions raised in the table below. Not all the questions are treated in the Ph.D. with the geophysical tool, therefore this list of questions can be considered as a wider analysis of the knowledge needed in the near future.

Hydrogeological questions related to processes, resource estimation, and vulnerability	**Proposed methods in the Ph.D. (geophysics + others)**
What are the potential of aquifers? This question is actually linked with the possibility, or not, of determining, from the surface, the types of sediments encountered. This will allow us to estimate the aquifer category (i.e. is it sandy- "good aquifer", loamy rather poor," or clayey "very poor"?)	Attempt to use Nuclear Magnetic Resonance (NMR) at the field and laboratory scale to estimate pore size-related NMR parameter Sieve and laser granulometry Blue Methylene clay estimate
What is the resource available? The resource available depends mainly on two factors: the effective porosity (and storativity) and the recharge rate. Those two parameters are difficult to obtain because we need a borehole, costly pumping tests, isotope analysis, as well as groundwater table monitoring. If any geophysical method can provide fully or partly that information, the contribution of geophysics is a definite advantage.	Attempt to use Nuclear Magnetic Resonance at the field, and laboratory scale to estimate water content NMR parameter Pumping test and tracer test in boreholes
What is the sustainable pumping rate? Could future intensive pumping modify Saigon River (SR) and aquifer interactions? Determining the maximum sustainable pumping rate is essential to ensure groundwater extraction does not induce adverse impacts on the aquifer, such as its depletion due to extraction volumes exceeding natural recharge rates. Should the groundwater level in the aquifer fall below the river level, it could incite a seepage of water from the river into the aquifer, possibly altering the flow direction between them. This could trigger changes in the quality of both river water and groundwater, especially if the river is subject	*Geophysical methods do not contribute directly to this question. Therefore, the evaluation of the pumping scenario is not done in this Ph.D., but some preliminary modeling results towards future simulation are undertaken by the research team using some Ph.D. results*

to pollution. Therefore, it is necessary to determine the optimal pump flow to limit the interaction between the aquifer and the river.	
What is the velocity of infiltration in the vadose zone? Are pollutants infiltrating down to the water table? The velocity of infiltration in the vadose zone depends on several factors, including the type of soil (its permeability and porosity), the pore shape and connectivity, the initial moisture content of the soil, the presence of vegetation, and the intensity and duration of any precipitation or irrigation. Assessing the infiltration rate is crucial for estimating groundwater recharge volume and identifying the potential quantity of pollutants that may infiltrate the aquifer.	*Geophysical methods do not contribute directly to this question. Actually, the geophysical results are used in this question to evaluate the lateral continuity of the vadose zone layers.* *Measurement made in the Ph.D. that can contribute to this question:* A measure of permeability at saturation Ks on core samples Measured with infiltrometer in the field Sieve and laser granulometry data
What is the degree of connection between the Saigon River (SR) and the aquifer? This process affects the recharge or discharge of the aquifer and can participate in pollutant diffusion processes, if any. Therefore, a detailed understanding of the degree of connectivity between the reservoir and the river is required. Several factors that can influence this connection need to be considered, including geological conditions: the type of soils (their permeability and porosity) between the river and the aquifer with the presence (or not) of highly permeable materials like sand and gravel can facilitate a strong connection. Also, when the river's water level exceeds the water table, the river can recharge the aquifer. Conversely, when the water table is higher than the river level, the aquifer can discharge into the river.	*Not addressed fully in this PhD* Shallow Electrical Resistivity Tomography (ERT) close to the river for shallow clay detection Question addressed by isotope study (Tu, et al., 2022)
What is the regional flow? This is driven by variations in the water level or potentiometric surface, which are influenced by topography, recharge rates, and extraction points. Understanding the regional flow is crucial in hydrogeological studies as it provides essential information about the direction and velocity of groundwater flow, which can help predict the movement of pollutants, plan for water supply, and manage water resources.	*This question is not addressed in the Ph.D. The output of the PhD will be however valuable for building a conceptual numerical modeling at a larger scale.*

2.4 Summary

The more elevated area of Cu Chi has an aquifer that consists of the intercalation of sandy, clayey, or loamy layers down to more than 150 m deep. The geology describes many types of quaternary sediments horizontally layered, and the resource is only known from scarce pumping tests partly representative. The hydrogeologist identifies continuous thick clay layers at the surface and at depth from scarce borehole information. Some previous studies raise the question that clay layers may be discontinuous and are not protecting aquifers. In addition, the agricultural zone should release many pollutants that could be flushed away to the river by runoff or most probably infiltrate into the vadose zone. At the end of this chapter, several main hydrogeological questions are therefore raised. This review of the questions allows us to announce the main geophysical and complementary methods used for answering them fully or partly while discarding some of them out of the frame of the work.

CHAPTER 3. GEOPHYSICAL METHODS

This chapter is dedicated to the presentation of the main geophysical methods used in the Ph.D. We present first a brief review of the geophysical studies dedicated to groundwater previously made in the South of Vietnam. Then some main information on the principles, the equipment and the software used are given. We present important synthetic numerical modeling work to evaluate, theoretically, the efficiency of resistivity methods to the presence of clayey layers (that are a key factor in the PhD). At last, the survey design and interpretation strategy of resistivity methods are presented.

3.1 Previous geophysical studies

3.1.1 Regional resistivity survey using Magnetotellurics, VES, and ERT

Pham, et al., (1994) conducted the first regional resistivity survey. They used VES (Vertical Electrical Sounding) and MTS (MagnetoTelluric Sounding) methods in determining shallow and deep aquifers in the Ho Chi Minh City (HCMC) area. The zone of Cu Chi is surveyed with only three VES soundings. For magnetotellurics, only deep structures are revealed (from 50 to 350 m deep). The results from two VES survey lines have shown the presence of a high resistivity layer near the surface in the Cu Chi area with a thickness of 5-10m. This high resistivity layer is explained by the presence of laterite at 5 m deep. However, the survey offers limited insight due to the significant distance separating the soundings, with a gap of 3 km between two VES points. This sparse distribution may affect the comprehensiveness and accuracy of the data interpretation. These results contradict geological cross-sections that suggest the presence of a low resistivity layer above the surface in the study area proposed by the hydrogeological map (see Chapter 2). A very shallow clayey conductive layer would have been detected by VES. Therefore, denser electrical resistivity surveys and integration with other effective geophysical methods are necessary to reassess locally the characteristics of the surface layer at Cu Chi.

Pham, et al., (2002) pursue their study for detailed subsurface investigation with resistivity, at a local scale around HCMC using the Electrical Resistivity Tomography (ERT) technique for hydrogeological purposes. ERT is found efficient in studying and surveying subsurface structures with low resistivity. This method is considered effective in providing more detailed information compared to sparse information obtained from drilling. However, the research density in the area is still limited, so for areas with complex structures and small sizes, a dense survey is required to accurately characterize the structures in the research area. This method appears efficient, but very costly to study large-scale regions, such as our Cu Chi Aquifer, but it can be considered for detailed surveys.

Nguyen Ngoc Thu (doctoral dissertation, 2002, in Vietnamese) uses Vertical Electrical Soundings (VES) focusing on large-scale to study the geology of the Ho Chi Minh City region. By combining the results from vertical electrical sounding (VES) analysis and boreholes, the sedimentary layers of Ho Chi Minh City were divided into seven distinct units. However, the VES profiling results had limited coverage due to the large spacing between measurement points, which spanned 3 kilometers. Consequently, ascertaining at the local scale (few km) lateral variations of subsurface is not entirely possible. Furthermore, the current division of geological layers heavily relies on scarce borehole information, resulting in limited details: for

river-aquifer interaction study, scarce VES are not convenient. To address this limitation, we proposed the use of 2D Electrical Resistivity Tomography (ERT) as an approach to obtain more detailed information on the horizontal variations of sedimentary layers.

3.1.2 Mekong Delta sediment investigation using Time Domain Electromagnetics (TDEM).

Two studies using TDEM have been undertaken in Vietnam

The first one, in 2012, in the red river valley. TDEM method has been employed successfully in northern Vietnam in the Red River sedimentological context (Tran, et al., 2012), at a regional scale with several kilometers separating the soundings, for investigating salted groundwater and aquifer substratum (Tran, et al., 2012). Based on geological observations, geophysical borehole logging, and Transient Electro-Magnetic methods (TEM), researchers have established a distribution map depicting the presence of fresh and saltwater in the Red River floodplain area. With a distance of 2 km between geophysical survey points and a total of 170 TEMs performed, the authors constructed four resistivity cross-sections to display the distribution of deep saltwater aquifers in the study area. The results have demonstrated the effectiveness of the TEM method in identifying sediment layers with low resistivity while confirming its applicability in areas with similar geological environmental conditions.

Bording, et al., (2017) presents the application of the Transient (or Time Domain) Electromagnetic Method (TEM or TDEM) for investigating the subsurface of the Mekong Delta, a region known for its extensive floodplains. They are targeting the groundwater salt intrusion, a major concern in the region. The effectiveness of the TDEM method in identifying low-resistivity layers (below 50 Ω.m) and its capability to study depths of up to 200 meters is confirmed. Combining these interpretation results enables the construction of resistivity-depth maps for specific depths. This approach facilitates the identification of sedimentary structures and helps unravel the region's sedimentary history. However, to enhance the reliability and accuracy of the TDEM method in identifying low-resistivity layers, further validation is required. This can be achieved by integrating additional geophysical methods that efficiently detect resistive layers, such as Electrical Resistivity Tomography (ERT), or for shallow conductive layers, Frequency Electrical Magnetic (FEM). The study of (Bording, et al., 2017), as a preliminary study, suffers from the lack of borehole logging data. Actually, borehole information provides direct measurements of the subsurface properties, allowing for a more accurate assessment of the layer resistivity and thicknesses and reducing equivalence. An internal report (DeltaRes report, Aarhus University, HGP group, Utrecht University, 2016) presents TDEM interpretation based on Lateral Constrained Inversion (LCI). The TDEM sampling interval in the study is 400 to 500 m. The map reveals deep structures 300 to 500 m wide, with low resistivity (1 to 25 Ω.m). For our study in Cu Chi, this large sampling interval (500 m) has been considered too wide and is not suitable for surveying narrow structures that could be present in the subsurface. Also, LCI may have smoothed expected sharp lateral contrasts and will not be applied in our study.

3.1.3 Previous Nuclear Magnetic Resonance (NMR) surveys in Vietnam

Giang, et al., (2012) and Nguyen, (2010) has focused on the delineation of groundwater distribution in the Binh Thuan region of Vietnam, specifically in the dry sand dunes area.

Geophysical techniques, including Direct Current (DC) resistivity, magnetic prospecting, magnetotelluric sounding, very low frequency electromagnetic, transient electromagnetic, magnetic resonance sounding, and seismic refraction, were employed to achieve the objectives of the study. Doing this, they introduced the utilization of the recent geophysical method, the Magnetic Resonance Sounding (MRS), for groundwater exploration in Vietnam. Although affected by environmental noise, the research conducted in the coastal region where the predominant sedimentary environment is sandy deposits has shown results that are highly consistent with the documented outcomes from drilling wells. We proposed in this PhD to apply the MRS method to evaluate its effectiveness in determining the characteristics of the water-bearing layers in the Cu Chi area. We aim to evaluate the effectiveness of the MRS method in assessing subsurface conditions, considering the challenges posed by the interbedded sand-clay deposits that characterize the alluvial floodplain and Pleistocene aquifer.

3.2 Resistivity as a major parameter for hydro geophysics

3.2.1 Definition

For our study, electrical resistivity is a well-adapted parameter because our objective is to discriminate sandy formations (aquifers) from clay formations (aquitard) or any lateral variations of groundwater conductivity (McNeill, 1980). The electrical resistivity (or its inverse, conductivity) is a measure of a material's ability to resist the flow of electrical direct current. To define it, we can consider an electrically uniform cylindrical rock sample with a length of L, the cross-sectional area A through which a current I is flowing Figure 3.1.

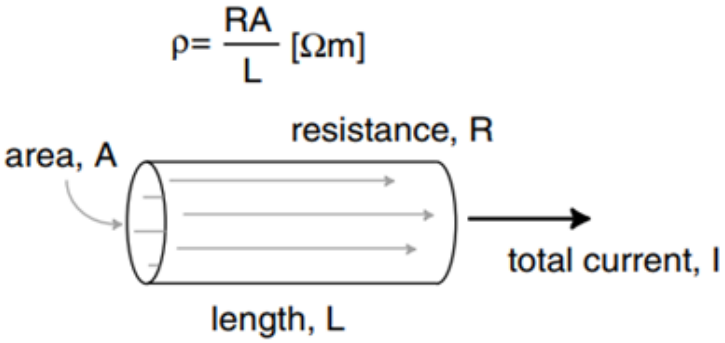

Figure 3.1 Parameters used in defining resistivity.

Definition of resistivity across a cylinder of side length L with an applied current I and potential drop between opposite faces of V. Electrical circuit equivalent, R is a resistor.

$$\rho = \frac{AV}{LI} = \frac{AR}{L} = \frac{1}{\sigma} \qquad 3.1$$

where: ρ =resistivity in Ω.m, *A = surface area in* m^2, *L = length in m, V =voltage in V, I =current in A and σ= conductivity in S/m.*

The unit of resistivity is the Ω.m (or Ω.m) with the conventional units being the Ω for resistance and the meter for length. The electric current in soils and rocks can be conducted through three distinct mechanisms: electrolytic conduction, electronic conduction, and dielectric conduction. In subsurface geophysics, and with Direct Current and Electromagnetic methods, it is the electrolytic conduction that is the predominant phenomenon depicted in Figure 3.2. It involves the movement of ions within an electrolyte (Reynolds, 2011). So electrical current conduction occurs primarily through pore fluids acting as electrolytes.

However, minerals such as clays with good electronic conductivity can have a notable impact on the rock's overall conductivity.

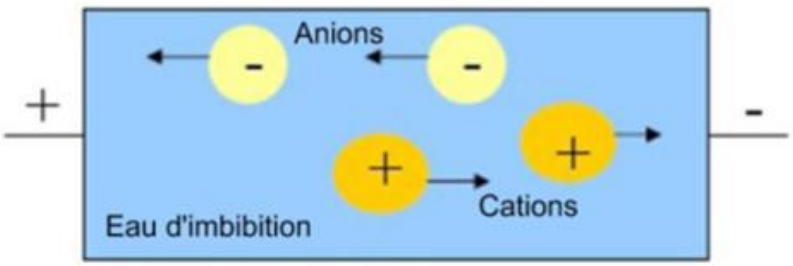

Figure 3.2 Diagram of electrolytic conductivity (Kunetz, 1966)

The movement of conductive ion currents in the fluid environment

The Figure 3.3. presents values of representative resistivity of some rocks more or less saturated with water.

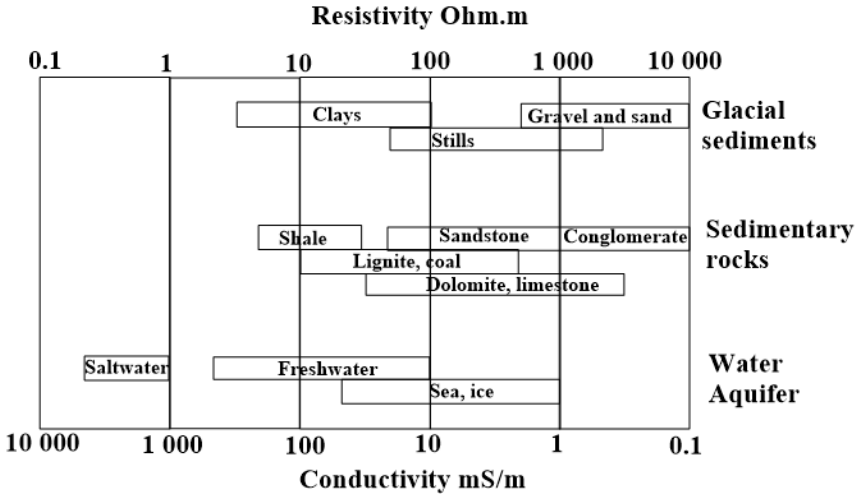

Figure 3.3 Typical ranges of electrical resistivity of earth material modified from (Palacky, 1987).

The resistivity values within the clay strata span a range from a few Ω.m to 40 Ω.m. Conversely, the *resistivity values for the sand deposits in the same area exhibit a broader spectrum, varying from 60 Ω.m to values in the thousands Ω.m range.*

The significant variations in resistivity observed for the same rock type can be attributed to several factors. Incomplete saturation (for sands and gravels), different salinities of the imbibition waters (for the sediments), presence or absence of clays (in sandstones and carbonate rocks). In our study area, characterized by riverine/estuarine sediments and unaffected by salinity intrusion, the differences in resistivity may be primarily attributed to variations in clay and sand. Clay may exhibit a relatively low resistivity value, typically 20 to 30 Ω.m. On the other hand, the resistivity of sand can vary widely, ranging from a few hundred to several thousand Ω.m.

In our geological context of sedimentary quaternary floodplains, clayey deposits and silty to sandy aquifers, resistivity value in clayey layers is also driven by the unique electrical properties of clay soils. Clays are rich in minerals with a layered structure that often carry a net negative charge.

Several factors influence the value of electrical resistivity. They are not described here but can be found in the literature (McNeill, 1980) (Mitchell, et al., 2005) (Ward, 1990). Among them we can cite: the total porosity, the tortuosity, the saturation, the electrical resistivity of groundwater; the temperature, the resistivity or conductivity of the matrix. If Archie's law, first formulated by (Archie, 1942), can be used for understanding the relationship between the electrical properties and the fluid saturation in a porous sand, it applies in "simple" or "clean" formations, i.e., those devoid of clays. In our case, the sediments of the Saigon River contain a significant amount of clay-size minerals that can forbid the use of Archie's law. Therefore, Arche's law will not be used.

3.2.2 Measuring soils and rock electrical resistivity

Electrical-resistivity-based geophysical methods, that includes electromagnetic (EM) and direct current (DC) electrical methods, are widely used in groundwater exploration due to their inherent advantages related to versatility, accuracy, and eco-friendliness (Reynolds, 2011) (D. S. Parasnis, 2012). These methods are measuring electrical resistivity of subsurface materials, which can exhibit significant variation between dry and water-saturated formations (Palacky, 1987) (Telford, 1990).

With the DC resistivity method, the basic idea is to create an electrical current flow into the ground and measure the resulting potential difference, which is then used to calculate the resistivity of the subsurface materials (Telford, 1990) (Kearey, et al., 2002). It is nowadays often used with Electrical Resistivity Tomography (ERT) techniques (Loke, et al., 1996) information about the underlying geology, including the presence of aquifers (Dahlin, 2001) (Reynolds, 2011). Modern advancements in ERT, such as the incorporation of 2D and 3D inversions, have enhanced the technique's precision, accuracy, and depth of exploration, thus making it a powerful tool for groundwater exploration (Dahlin, et al., 2004) (Dahlin, et al., 2002) (Loke, et al., 2013).

With the Electromagnetic (EM) method the basic idea is also to create an electrical current flow in the ground, but using electromagnetic induction principles. EM methods are useful for groundwater exploration due to their capability of rapid surveying over large areas. They are very sensitive to conductive layers (clay, saltwater intrusion, etc.). In its frequency-domain configuration (FEM), EM can provide basic simple multi-layer information (McNeill, 1980) (Nabighian, et al., 2005). In its time-domain configuration (TDEM) it offers a sounding capacity with quantitative layered information and deep penetration (Sengpiel, et al., 2000) (Auken, et al., 2004) (Vest Christiansen, et al., 2012).

Importantly, both DC and EM methods are non-invasive, resulting in minimal environmental impact, which is of particular importance in sensitive areas (Reynolds, 2011) (Fitterman, et al., 1986). They are also cost-effective, especially when employed for large-scale surveys, thus making them preferred tools for groundwater exploration (Ward, 1990) (Zohdy, et al., 1974) (Milsom, 2003).

3.3 TDEM method

3.3.1 Generalities

The Time Domain Electromagnetic (TDEM) method is a widely known geophysical technique. Throughout the 1970s and 1980s, the method was being employed in mapping the depth to conductive bedrock, detecting buried metallic objects, and exploring groundwater resources (McNeill, 1980). The late 1980s and 1990s brought about an enhancement in the interpretation of TDEM data through the advent of 1D inversion models. However, inversion of, 2D, and 3D structures are still under research. For 1D application, a more accurate and comprehensive understanding of subsurface structures can be achieved (Auken, et al., 2004). TDEM in hydrogeological studies has been increasingly highlighted. It's been used to map and monitor aquifers, providing essential data for water management and conservation strategies (Fitterman, et al., 1986). TDEM in environmental and engineering investigations has been used to detect and map subsurface contamination, aiding in the design and implementation of remediation strategies (Guérin, et al., 2001) (Kemgang Dongmo, et al., 2019) (Widodo, et al., 2022) (El-Kaliouby, et al., 2015). Various powerful algorithms for laterally constraining the inversion processes have been developed for some appropriate data set and geology (Auken, et al., 2004). Furthermore, improvements in TDEM equipment, including the miniaturization and increased efficiency of field instruments, have expanded the accessibility and practicality of TDEM surveys (Prakash Maurya, et al., 2019) (Yogi, et al., 2017). The last decade has shown the development of helicopter airborne TEM (Costabel, et al., 2017) (Grombacher, et al., 2022).

3.3.2 Principles, advantages, and limitations of TDEM

Time Domain Electromagnetic (TDEM) uses a large transmitter (Tx) square loop (typically 50x50m² or 100x100m²) and a receiver loop (Rx), both cables laid out on the surface. Rx can be either a small coil with several turns at the center of Tx (central loop system) or the same cable as Tx (coincident loop system, as used in our study). A direct current is injected into Tx, creating a primary static magnetic field that diffuses into the ground. Once the primary magnetic field is established, the current is abruptly turned off, creating a decreasing flux with time. Due to the induction principle, eddy currents are then created in the soil immediately below the Tx cable and flow inside the ground (McNeill, 1994). As time elapses, and because the primary magnetic field no longer exists, the eddy current intensity decreases with time, and further current loops are created deeper and expand laterally in the sub-surface, resembling smoke rings Figure 3.4.

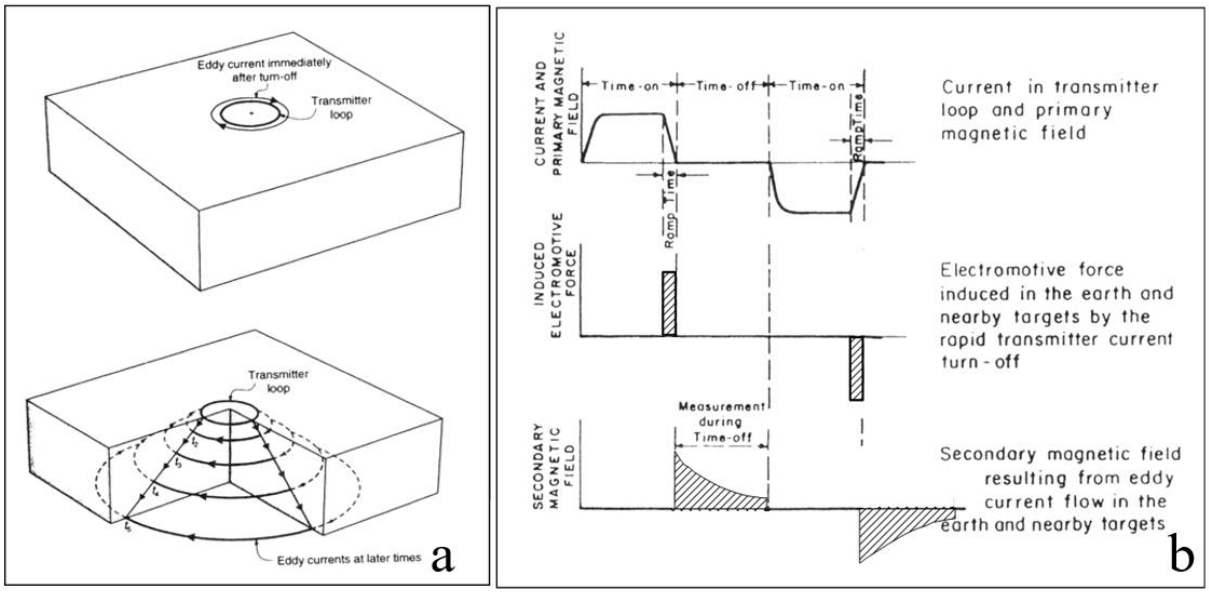

Figure 3.4 Illustration of the basic principles of the TDEM method (McNeill, 1994).

a) Eddy currents within the transmitter loop following its deactivation. As time progresses, the eddy currents visibly expand and penetrate deeper into the material. b) The figure, is a representation of the pulse generating the primary magnetic field, the subsequent electromagnetic force, and the development of the secondary magnetic field.

Each eddy current loop creates a secondary magnetic field (with the same polarity as the primary magnetic field) whose amplitude decreases with time, creating in turn an induced current in the Rx loop. The result of a TDEM sounding is the measure of the decreasing voltage with time. Voltage is determined over time in coincident loop system equation 3.2 (Spies, et al., 1991).

$$V = \frac{\sqrt{\pi} I \sigma^{3/2} \mu_o^{5/2} a^4}{20\, t^{5/2}} \qquad 3.2$$

V voltage (in V) measured by TDEM depends on, I the current injected in the Tx loop in A, the ground conductivity σ in S/m, the permeability μ_o of free space $4\pi*10^{-7}$ N/A^2, the length of the side of the loops Tx and Rx (in m), t the time (in s).

For convenience, this voltage sounding curve is transformed to derive the sounding curve of apparent resistivity variation with time.

$$\rho_a = \frac{I^{2/3} \pi^{1/3} \mu_o^{5/3} a^{8/3} (-v)^{2/3}}{20^{2/3} t^{5/3}} \qquad 3.3$$

Field data are then fitted using a 1D layered resistivity model of the ground through manual and then automatic adjustment. The results are presented as a 1-D (layered) model of the resistivity distribution of the main layers with depth. Further information can be found in the comprehensive review of TDEM for groundwater exploration published by (McNeill, 1994) and (Fitterman, et al., 1986).

The advantages of the TDEM method are numerous.

- This method is effective in determining accurately the resistivity value of the layers below 300 Ω.m. The method is widely considered as an efficient tool for studying saltwater intrusion, clayey zones, and metallic objects.
- Thanks to the fact that the TDEM method is inductive, there is no contact of electrodes with the ground.
- When shallow applications (0-100m) are under a scope, TDEM is user-friendly, and its equipment operation is relatively lightweight, providing significant exploration depth with a limited cable length.
- Some airborne surveys can be proposed in some areas.

The TDEM method also has its own set of limitations.

- TDEM is not sensitive to layers with resistivity values above 300 Ω.m. This means that it is not effective for investigations of sandy aquifers and establishing resistivity-porosity relationships with Archie's law when resistivity is above 300 Ω.m.
- The resistivity values are predominantly influenced by conductive layers where the current flows horizontally. This can lead to underestimating the column resistivity.
- TDEM is subject to external effects that can limit (or even forbid) the interpretation: direct induction into metallic objects (fences, roofs, etc.) around the sounding and interferences from power lines causing potential distortions in readings. In our zones, some places were not surveyed due to a) a high-power line and b) houses and fences.
- TDEM does not allow 2-D interpretations, which can limit its applicability in certain geological situations.
- TDEM can be affected by induced polarization and magnetism effects, which may necessitate additional corrections and considerations during data analysis.
- Lastly, TDEM does not provide high resolution between depths of 0 and 5 meters due to the time necessary to cut off the injection current. This limitation restricts its suitability for investigations that require precise delineation of shallow subsurface features.

In our zone, several technical questions arise when using TDEM

- Firstly, can TDEM accurately detect shallow clay layers, and what is the minimum thickness of these layers that TDEM can detect?
- At what maximum depth can TDEM identify a significantly thick clay layer (i.e. 5m for example)?
- Furthermore, as we must balance the survey duration (cost) with the transmitter loop size, what is the optimum loop size for detecting clayey layers accurately?

To answer those technical questions, we used a synthetic modeling approach and comparison to known boreholes for guiding the appropriate selection of loop size, defining appropriate inversion procedures, and helping to define the density of the surveys.

3.3.3 TEMFAST equipment and TEMRES software

TEM-FAST 48 (AEMR technology, http://www.aemr.net/page2.htm) has been used for our surveys. TEM-FAST 48 is designed to interface with various computing devices. The generator develops rectangular pulses of current, see Figure 3.5.

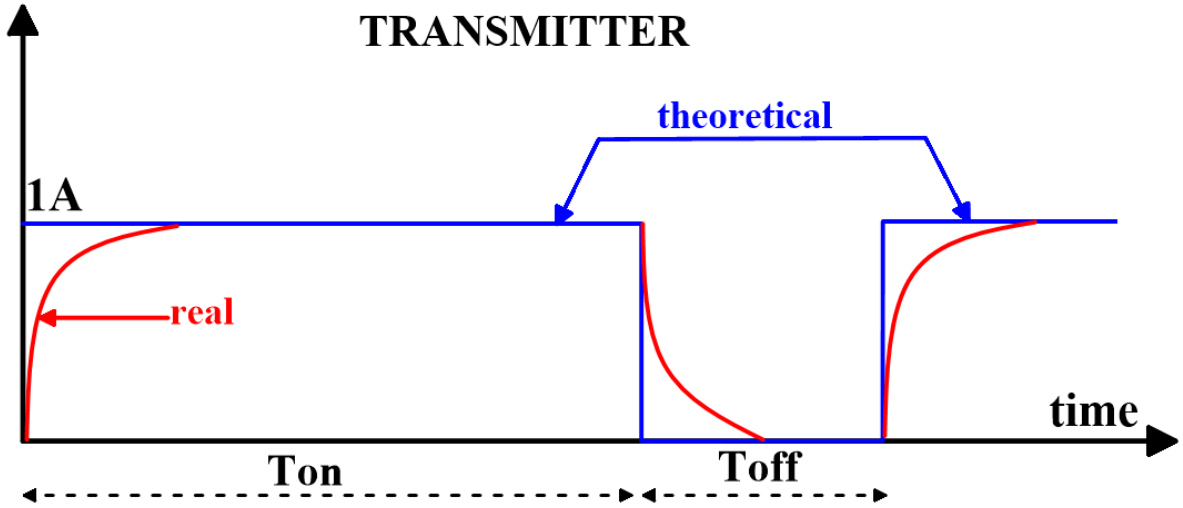

Figure 3.5 The pulses in a transmitter (AEMR technology).

The generator produces square-wave pulses of electric current, and these pulses are subsequently transmitted through the antenna.

Upon signal stacking, the system evaluates normalized voltage/current ratios and root mean square (RMS) inaccuracies of measurements. The algorithms serve to eliminate systematic errors stemming from battery discharge and temperature variations. These algorithms enhance signal-to-noise ratios, especially in scenarios where signal levels are relatively low.

The TEMRES software, developed also by Advanced Earth Monitoring and Research (AEMR), serves as a tool for interpreting and analyzing geophysical data. During data preparation, users can assess the quality of input data enabling the identification and elimination of unreliable data points, including those affected by noise or early-time turn-off effects. External environmental factors, particularly the impact of Induced Polarization (IP) effects or magnetism effects can be taken into account in the interpretation. The software guides the data fitting process and selects the most suitable model that accurately fits the field data.

3.3.4 TDEM sensitivity to clayey layer detection

- **TDEM field data comparison with borehole**

To assess the effectiveness of the TDEM method in identifying conductive clayey layers in the study region, a preliminary investigation was conducted at the BH4 site. At BH4, there is a clay layer 30 m deep and 10 m thick. Three loop sizes were employed for the survey: 25x25, 50x50, and 100x100 m². The comparative analysis between the TDEM data interpretation and the BH4 borehole resistivity and gamma-ray logging data is depicted in Figure 3.6.

Interpretations using the 50x50 m² and 100x100 m² loop sizes point to a conductive layer at a depth of 30m. Meanwhile, the 25x25m loop size places this conductive layer slightly

deeper, at 32m. These results align with the clay layers pinpointed by gamma-ray logging and resistivity logging, both indicating a depth of 30m.

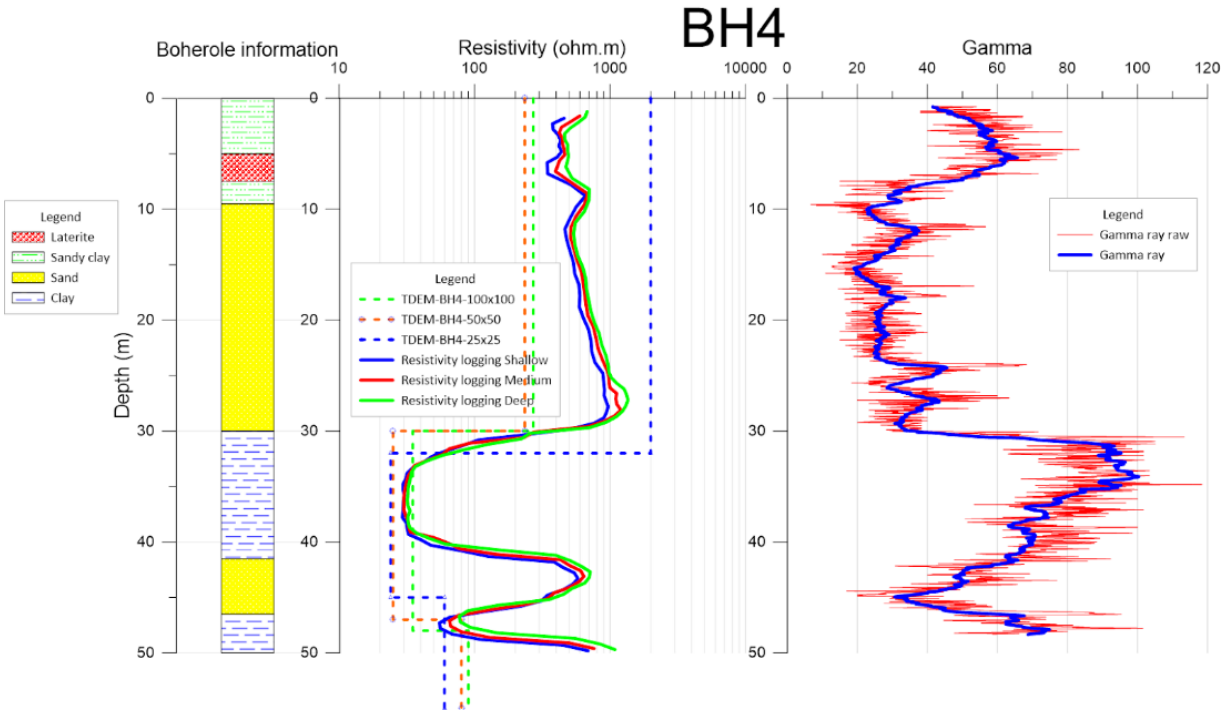

Figure 3.6 Example Interpretation of the TDEM borehole at BH4 and comparison with the gamma-ray logging.

*At left, borehole data derived from drilling are presented, featuring four types of soil by color: green signifies sandy clay, red indicates laterite, blue stripes represent clay, and yellow represents sand. The second column displays electrical resistivity values interpreted from the Time-Domain Electromagnetic (TDEM) data (dashed lines correspond to different loop sizes: blue for 25*25, red for 50*50, and green for 100*100). The resistivity logging is illustrated by solid lines, where blue signifies shallow, red denotes medium, and green represents deep penetration. The third column showcases gamma ray values, with raw data values marked in red and filtered gamma values presented in blue. This arrangement provides a comprehensive overview of the borehole characteristics, TDEM interpretation, and gamma-ray measurements.*

If the top of the layer is relatively well defined, TDEM results overestimate the thickness by 50%. Notably, the loop size of 100x100 m² introduces a slightly higher thickness error compared to the 50x50 m² loop size. From these results, it is difficult to choose the loop size. At this place, a 25x25 m² loop size is able to give the information but could lead to noisy data, even if it would have been convenient for easier surveying. 100x100 m² is difficult to practice close to the villages and roads. Therefore, the most balanced loop size is 50x50 m². It provides optimal accuracy in determining both depth and thickness of the conductive layers. Furthermore, it offers the advantage of reduced data collection time compared to the 100x100m² loop size.

It's worth noting that TDEM failed to detect the sand layer situated between 42m and 46m, primarily due to its low thickness. This underlines the inherent limitations of TDEM in detecting resistive thin layers at depth when they are sandwiched between two conductive layers. The comparison of TDEM depth with BH4 borehole data confirmed, in this particular case, the effectiveness of TDEM in detecting conductive clay layers. However, the BH4 survey area did not identify any conductive layers at the surface. *This raises the question of whether*

the TDEM method is capable of detecting shallow clay layers on the surface, and also at depth. Actually, TDEM is usually considered poor in detecting shallow layers due to the turn-off time delay. In the next paragraphs, we will construct synthetic models to assess the capability of identifying shallow and deep-conductive layers using the TDEM method using a coincident loop 50x50 m² device. This analysis will contribute to further understanding the potential of TDEM in detecting near-surface conductive layers.

- **Is the 50x50 m² loop size efficient?**

As very shallow clay is of utmost importance in our study, is choosing such a 50x50m² TDEM loop able to "see" very shallow with confidence? This question can be answered using forward modeling of TDEM response (see Figure 3.7). Three synthetic datasets have been calculated with a 5 m thick conductive layer with three different resistivity values from 25 to 100 Ω.m. The resulting apparent resistivity-sounding curves are compared to the model without a conductive layer.

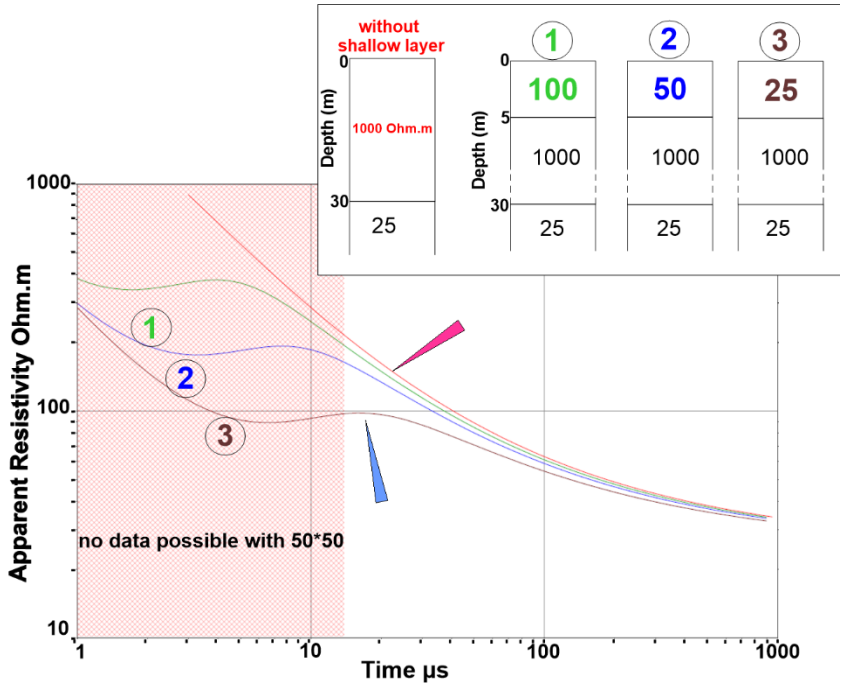

Figure 3.7 Apparent resistivity sounding curves from TDEM synthetic data.

Before 12 µs, the data are not reliable according to our field conditions. The apparent resistivity curves are visually differentiated by colors for clarity in interpretation. The red curves represent synthetic models lacking shallow layers, while the green curves denote a shallow layer with a resistivity of 100 Ω·m. The blue curve is obtained with a shallow layer with a resistivity of 50 Ω·m, and the brown curve with a shallow layer with a resistivity of 25 Ω·m.

At the time of 20 µs, the difference between the curve at 25 Ω.m and the others is significant, thus validating the sensitivity of the loop 50x505m² for thick shallow clay detection. Further synthetic models are thus constructed using this size of loop.

- **TDEM synthetic modeling for shallow and deep clay detection**

It is necessary to conduct a TDEM sensitivity simulation for shallow and deep clay layers to evaluate the effectiveness of the TDEM method in identifying shallow -but also deep- clayey layers. Such simulations assist in pinpointing the maximum detectable limit of the clay layer

and are crucial for establishing the right input parameters and starting models, optimizing the interpretation of actual field TDEM data.

a "Classical" inversion of synthetic dataset with a "free" inversion approach.

The free inversion approach means that the interpreter proposes a 2, or 3, or 4-layer model as a starting solution, and lets the software inverse the data without any constraint (i.e. neither the thickness nor the resistivity are fixed). We have built five synthetic models based on the knowledge of BH4, one without clay and four with 5 m thick clay layer deepening Figure 3.8. The data are calculated for a 50x50 m² coincident loop data.

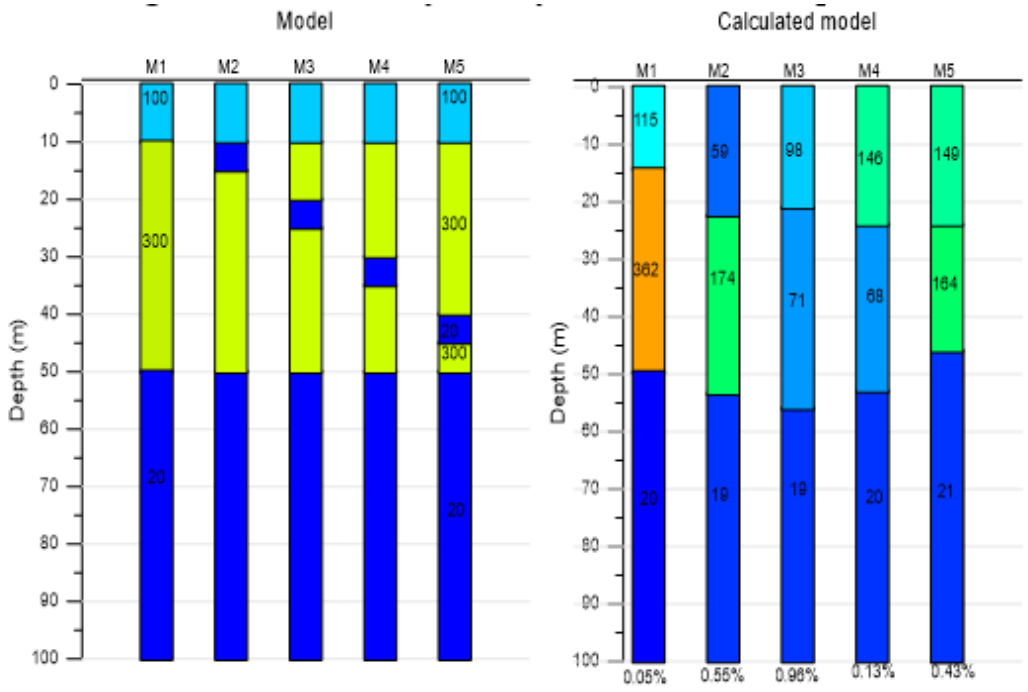

Figure 3.8 Compare resistivity values in the synthetic model and calculated model.

Within the five synthetic models, assumptions about resistivity are made to differentiate various subsurface layers. The aquifer is assigned a resistivity of 300 Ω·m, represented by the color green. Intermediate soil is designated a resistivity of 100 Ω·m, depicted in light blue, while the clay layer possesses a resistivity of 20 Ω·m, represented by the color blue. Synthetic Model 1 features a stratigraphy of 10 m of intermediate soil at the surface, followed by a 40 m deep aquifer, and finally, a 60 m thick clay layer. Subsequent synthetic models (2-5) exhibit alternating 5 m thick clay layers at depths of 10, 20, 30, and 40 meters, respectively.

The free inversion results show that the 5m clay could not be detected in all calculated models with RMS from 0.13% to 0.96%. It is noted that the threshold of noise is about 300 microseconds. This prompts the question: Why does the synthetic model struggle to recognize the presence of an interbedded clay layer? Could it be attributed to the thinness of the clay layer or an interpretation process that lacks optimization? The challenge might stem from an insufficiently precise initial ("starting") model for the inverse process of interpreting TDEM data, and/or also from the lack of constraint during inversion. Hence, a comprehensive investigation into parameter selection is crucial to establish if a user defines an initial - starting-model and constraints could guide the interpretation process towards a better result.

b Constrained inversion of a synthetic dataset with a user-defined "starting model"

We have constructed a simpler model consisting of three layers, where a clay layer is sandwiched between two sand layers with a thickness of 5 meters at a depth of 30 meters Figure 3.9, “a”. This clay layer has a resistivity of 25 Ω.m, a value proposed based on well log measurements in BH4 borehole, and verified with direct resistivity outcrops measurements in the banks of the river and in the paddy field area, which is covered by a surface clay layer along the riverbank. Meanwhile, the resistivity of the sand layers above and below the clay is set at 1000 Ω.m, based on well-log results. From this synthetic model, we have set up a 50x50 m² TDEM data set and limited the time range for inversion from 15 microseconds to 350 microseconds after filtering out early data due to the turn-off effect and late-time EM noise.

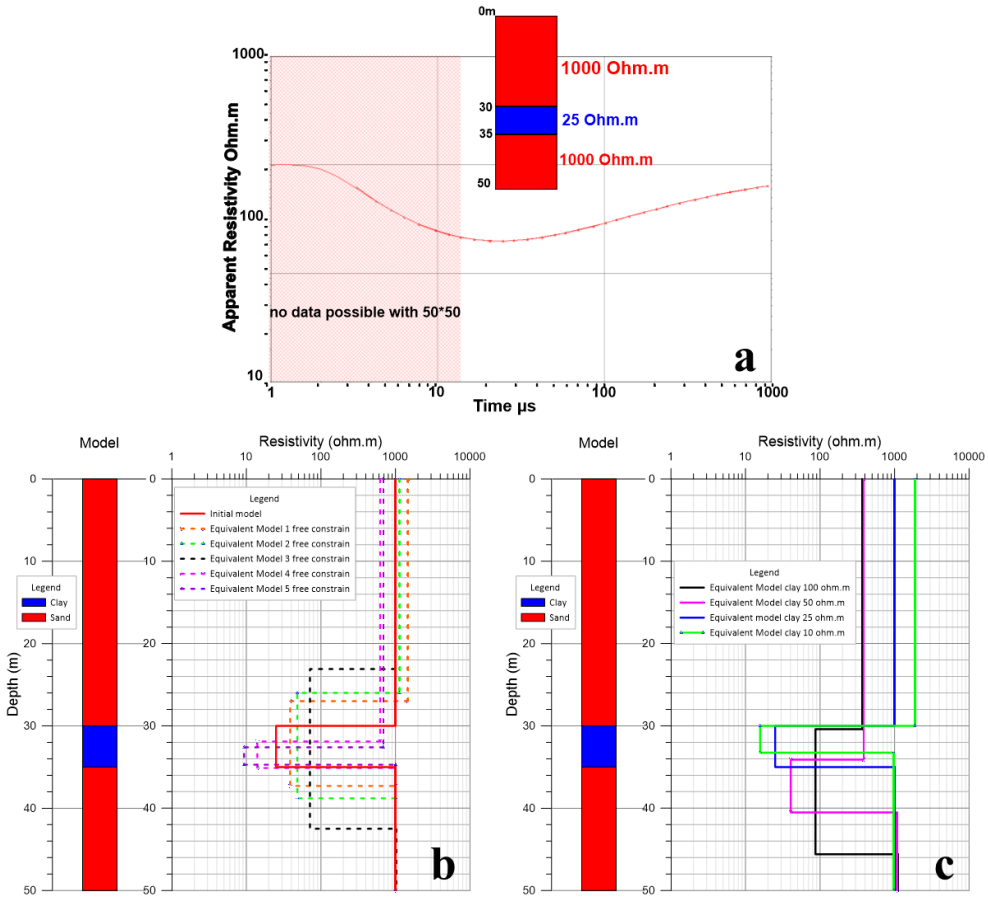

Figure 3.9 Synthetic model and interpretation result with equivalent models.

a) synthetic model and apparent resistivity curve, b) the result of the resistivity interpretation with free constrain the resistivity of clay, c) the result of the resistivity interpretation with initial resistivity proposal corresponding to the resistivity value for Clay layers 10 Ω·m (green), 25 Ω·m (blue), 50 Ω·m (pink), and 100 Ω·m (black)

We are conducting first the inversion of synthetic data, with no prior information regarding the number of layers and the initial resistivity values (Figure 3.9 case “b” above, as “free” inversion case). The results indicate the clay layer with a resistivity of 25 Ω.m at a depth of 30m, cannot be accurately determined through free interpretation. In this context, all equivalent models fail to accurately determine the true depth of the layer while simultaneously underestimating the layer thickness if the resistivity value of the clay layer is lower than the actual resistivity, and overestimating it, if the resistivity value is higher. Note that the root mean square (RMS) coefficients in all the interpretation results are less than 1%, which is acceptable.

Therefore, the question arises: How can we enhance the interpretation process to identify the presence of the clay layer successfully?

We tested the starting inversion model as a 3-layer model (Figure 3.9 case “c”). In this model, the upper boundary of the second layer is situated at a depth of 30 meters, and this layer has a thickness of 5 meters, but not fixed. Several tests are done, using starting resistivity values assigned to the second layer from 10 to 100 Ω.m. Upon examining the interpretation results under these conditions, it becomes apparent that the top boundary of the conductive layer is well-defined. However, the accurate determination of the resistivity value is only achieved when the second layer's resistivity is set initially at 25 Ω.m, as logically expected because it is the resistivity used for generating the synthetic data. This finding underscores the limitation of relying solely on a 3-layer model without fixing the resistivity as an initial approach for comprehensive solutions. Consequently, the question is raised: What happens if we use a starting model with a different value of the depth of the top of the second layer?

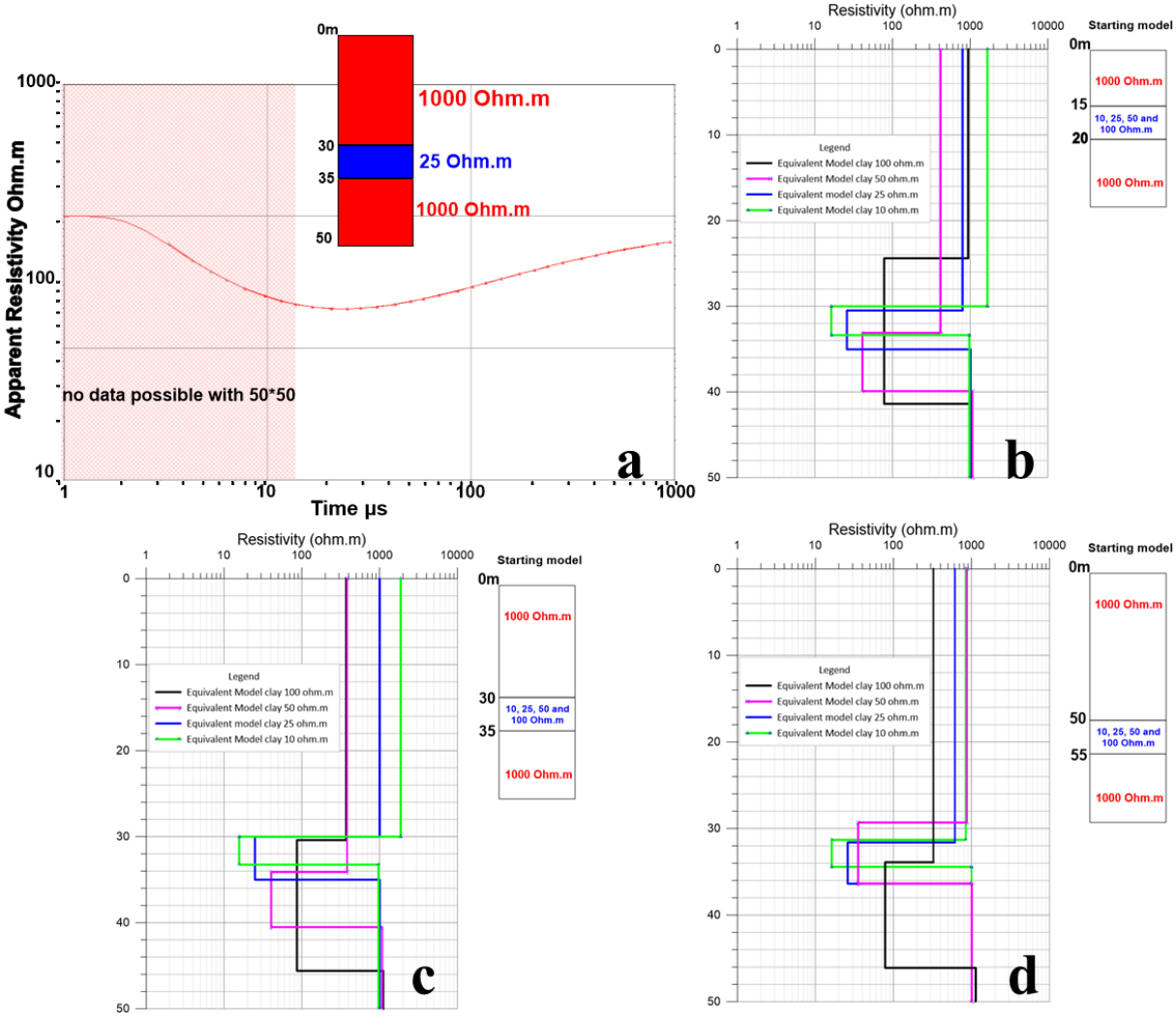

Figure 3.10 Resistivity interpretation results of TDEM synthetic data with depth top second layer at 15m (b), 30m (c), and 50m (d).

The result of the resistivity interpretation with initial resistivity proposal corresponding to the resistivity value for Clay layers 10 Ω·m (green), 25 Ω·m (blue), 50 Ω·m (pink), and 100 Ω·m (black)

To address this question, we analyze synthetic data involving three scenarios: top boundary depths of the second layer is the starting model is set at 15, 30, and 50 meters, respectively. These scenarios are depicted in Figure 3.10, accompanied by interpretation results characterized by root mean square (RMS) coefficients, all well within the acceptable range of less than 1.2%. From these results, we can observe that with the originally proposed model, the resistivity of the second layer at 25 Ω.m yields the most accurate outcomes concerning both the depth and thickness of the conductive layer. Simultaneously, with the depth of the top second layer recommended at 30m, we achieve the most optimal results in terms of both depth and thickness of the second layer after the inversion process. As a consequence, it is only when proposing a resistivity value close to the true value that the inversion leads, logically, to an acceptable result.

The synthetic models highlight the critical influence of the original model and input parameters due to the equivalence problem in inverting the geophysical data. Therefore, the information given by the resistivity logging is extremely important in proposing realistic starting resistivity to interpret TDEM data. Consequently, for interpretation of our field data, we decided to propose a strong hypothesis for inversion: start the inversion with a 3 layers' model, proposing a sandwiched clay layer 5 m thick of 25 Ω.m at 30 m deep between resistive sand layers (1000 Ω.m). This hypothesis is sustained by the fact that the resistivity value of the clay layer is determined from borehole resistivity data and also measured at the surface in the riverbank vicinity. Our strong hypothesis involves the assumption that all the clay layers at all depths may display the same value of resistivity (25 Ω.m) In addition, there are no groundwater conductivity variations around the area, discarding any resistivity changes that could be due to variation of groundwater electrical resistivity. Therefore, our "universal" three-layer starting model is defined as follows

- 0 to 30 m: sand layer, 1000 Ω.m
- 30 to 35 m: clay, 25 Ω.m
- after 35 m: sand, 1000 Ω.m

c Is our "universal" starting model able to reconstruct deepening clayey layers?

In pursuit of this goal, we constructed 13 synthetic models to generate 13 synthetic data sets using a 50x50 m² coincident loop Figure 3.11. These models still incorporate sand characterized by a resistivity of 1000 Ω.m and clay with a resistivity of 25 Ω.m. The clayey layer is 5 m thick and deepens to 90 m. The first model has no clay. The inversions are conducted using our "universal" starting model with clay of 5m at 30m deep. The resistivity, 25 Ω.m, is proposed as either a free value or a fixed value to evaluate the influence of a stronger constraint, i.e. a resistivity fixed. The interpretation outcomes are depicted in Figure 3.11.

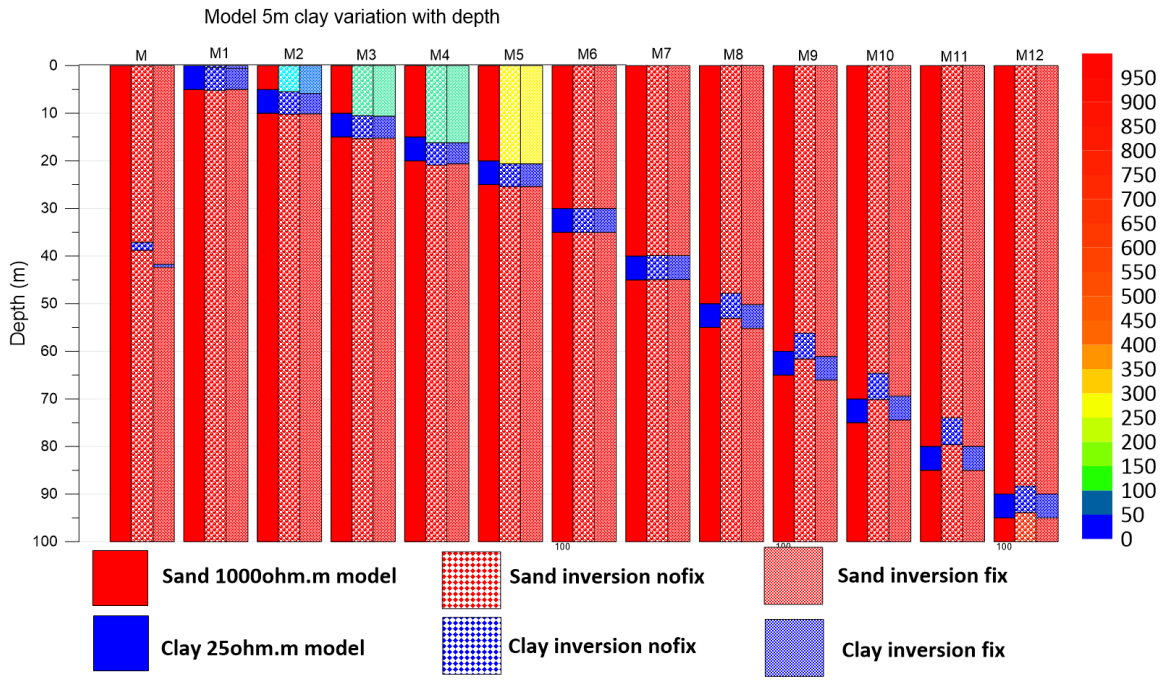

Figure 3.11 Synthetic model and inversion model were obtained using the "universal" starting model.

For each synthetic model, the inversion model includes two cases: no fix and fix, the resistivity value of the interlayer clay layer is 25 Ω.m.

In all inversions, the root mean square (RMS) values remain consistently below 4.16%, demonstrating an acceptable level of accuracy in the inversion model. The results clearly indicate that using our "universal" model as a starting model prior to inversion leads to accurate depth estimation. For the model with no clay, the resulting inverted model shows only a very thin layer (less than 0.5 m) that leads to eliminating it from possible solutions. Furthermore, fixing the resistivity value of the clay layer during interpretation yields (but not significantly) slightly more accurate depth results compared to allowing the resistivity value to vary. Fixing the resistivity is not the crucial point.

d What happens if the resistivity value of the clay in our "universal" starting model varies from 10 to 100 Ω.m?

The tested synthetic data are still constructed as previously, with a clayey layer deepening down to 90 m. An analysis of the RMS of each inversion can help us in answering the question. As seen in Figure 3.12, for the 10 Ω.m starting models, the RMS values vary between 0.08% and 1.55%. With a starting resistivity of 25 Ω.m, the RMS values range from 0.01% to 1.35%. Likewise, for the 50 Ω.m starting models, the RMS values fall between 0.05% and 2.16%. Finally, when utilizing a starting resistivity of 100 Ω.m, the RMS values span from 0.13% to 4.16%. Therefore, this shows clearly that a high resistivity (100 Ω.m) as a starting solution could lead to unwanted high RMS, especially for shallow layers.

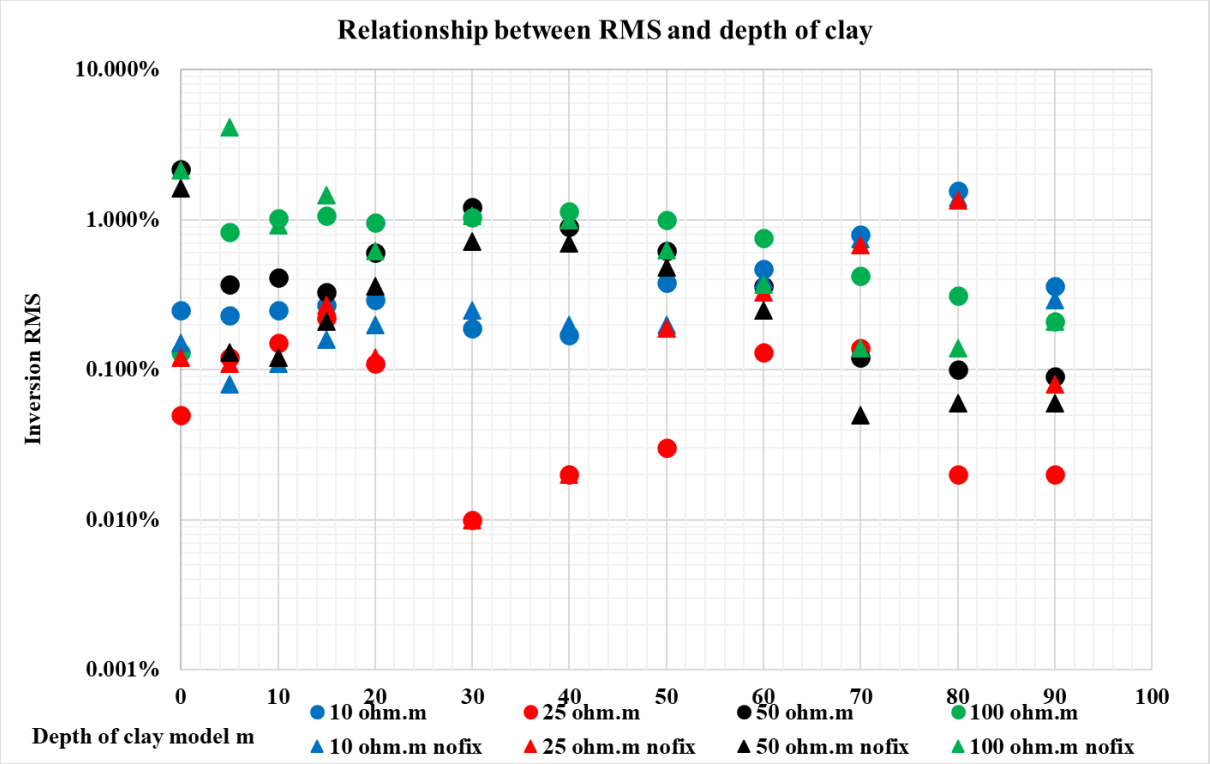

Figure 3.12 Relationship between RMS inversion parameter and true depth of clay.

The depicted diagram illustrates the correlation between the inversion MRS parameter and the depth of a clay layer in a geological model. Circles represent scenarios where the clay layer has a fixed resistivity value, while rectangles indicate instances where the resistivity of the clay layer is free variation. The color scheme signifies distinct starting resistivity values for the clay layer: blue for 10 Ω.m, red for 25 Ω.m, black for 50 Ω.m, and green for 100 Ω.m. In cases where the depth of the clay layer in the model is less than 60 meters, the accuracy of the inversion method with both fixed and unfixed values of resistivity for the clay layer does not exhibit significant differences, especially concerning the starting resistivity of the clay layer.

Additional results (not shown here) also lead to the conclusion that starting with a resistivity value lower than the true resistivity of the clay (i.e. for example choosing 10 Ω.m instead of 25 Ω.m) tends to underestimate both thickness and resistivity. Conversely, initiating the model with a resistivity value higher (100 Ω.m vs 25 Ω.m) often leads to an overestimation of both thickness and resistivity. These results highlight again the significance of the initial resistivity assumption value and its impact on accurately estimating the clay layer's characteristics.

Based on the interpreted results from the synthetic model, the effectiveness of the TDEM method in determining the presence of clay layers at shallow depths, as well as at depths up to 90m, has been confirmed. This modeling also underscores the importance of establishing an initial model before performing data inversion. Identifying and selecting the proposed initial values for the clay layer is also crucial in ensuring accuracy in determining the thickness and depth of the clay layer when it is located at different depths. Specifically, the resistivity value of the clay layer in the research area is proposed to be 25 Ω.m when interpreting TDEM data. Fixing the resistivity value at 25 Ω.m may yield better results regarding the thickness and depth of the clay layer but not significantly.

3.3.5 TDEM field data interpretation procedure

a) Initial inversion

The first step is the selection and exclusion of data points prior to inversion based on the signal-to-noise ratio, filtering out unreliable data points, including those within the early 15 microseconds time window and data points beyond 350 microseconds.

b) A starting initial model is then proposed, equal to our "universal" model tested with a numerical model, with the minimum number of layers aiming to minimize the equivalent model effect in data inversion, as follows:

- 0 to 30 m: sand layer, 1000 Ω.m
- 30 to 35 m: clay, 25 Ω.m
- after 35 m: sand, 1000 Ω.m

c) adding a layer (if necessary)

If the inverted calculated sounding curve doesn't fit the field data (i.e. RMS still higher than an arbitrary value of 2%), the interpreter could propose a number of layers of 4 or 5. It is especially the case when there is a deep conductive substratum, or if very shallow structures are present. If an unrealistic number of layers (i.e. for example 5, 6, or even more) is proposed as a starting model, the RMS can be artificially lowered and lead to unrealistic interpretation. Therefore, we tried to limit the number of layers as low as possible. Lastly, minimizing the number of layers in the inversion process is critical to ensure model accuracy and limit the number of equivalent models during inversion.

d) Checking quality inversion using RMS

The root mean square (RMS) parameter assesses the mathematical accuracy of the inversion, with smaller RMS values indicating closer alignment with the actual data. The proposed RMS value is suggested to be arbitrarily less than 2%. However, this value might be higher in areas heavily affected by noise (and IP effects), but usually less than 5%.

e) Adjustment with nearest neighbor's soundings using a "profile logic"

Once the first (initial) inversion using the starting model is done (and improved by adding 1 or 2 layers more if needed) the inversion model is stored into a general data file. Then, we edited the TDEM model using a resistivity cross-section along key profiles. This allows us to detect some sharp lateral variation of resistivity, and also to evaluate the lateral coherency of the interpretation. If needed, interpretation is harmonized by propagating laterally the model of a sounding to start the inversion of the adjacent sounding, mimicking a "laterally constrained inversion". The only constraint is the neighbor starting model.

f) Estimating the Depth of Investigation (DOI)

The last important step in the TDEM field data interpretation is the estimation of the Depth of Investigation. DOI can be defined as the maximum depth a layer can be detected by the sounding. In the literature, several ways have been proposed to estimate this DOI. In this study, we choose to use a practical approach based on the evaluation of the detection of a deep substratum (that is arbitrarily invented below the sounding point).

First, the resistivity of the substratum is chosen according to the resistivity of the last layer calculated in the last inversion. We choose to add a resistive substratum (1000 Ω.m) if the last layer is conductive. A conductive substratum (25 Ω.m) if the last layer is resistive. Then this substratum is placed at -200 m from the surface. Then we calculate the resulting sounding curve and check the fit with the field data. Then we approach the top of the substratum toward the surface until the fit with the field data is increased by more than 2 %. This is considered as the DOI for the sounding. This DOI value is then used in the resistivity map and profile construction as a blank limit for deeper interpretation.

3.4 FEM method

Frequency-Domain Electromagnetic (FDEM or FEM) methods have been used for numerous applications such as mineral exploration, hydrogeology, and environmental engineering (Telford, 1990). FDEM is non-invasiveness and able to get information about soil salinity and moisture content (Corwin, et al., 2005). Electromagnetic methods were developed for mineral prospecting, primarily for conductive ore bodies (Wait, 1982). Over time, technological advancements led to the development of more portable and airborne systems, expanding the scope of FDEM applications (Palacky, 1987). Hydrogeologists started utilizing these techniques to identify and map water-bearing structures or aquifers in the subsurface (McNeill, 1980). Modern multi-frequency systems and improved data inversion algorithms allow for a more quantitative interpretation of the subsurface in both lateral and vertical dimensions (Vest Christiansen, et al., 2012).

3.4.1 Principle of FEM method

FEM method relies on the measurement of the Earth's electromagnetic response to alternating magnetic fields generated by a controlled source (Telford, 1990) Figure 3.13. This principle is based on Faraday's Law of electromagnetic induction (Nabighian, et al., 1991). An alternating current is passed through a transmitter coil (Tx), creating a time-varying primary magnetic field. The primary magnetic field induces eddy currents in the conductive subsurface (A. Kaufman , 1983). These eddy currents generate a secondary magnetic field that is out of phase with the primary field. A receiver coil (Rx) measures the secondary magnetic field along with the primary magnetic field. The ratio of these two fields provides information about the subsurface conductivity (McNeill, 1980). The coils can be placed in different orientations: horizontal coplanar (HCP, also called VMD vertical dipole mode) or vertical coplanar (VCP, also called HMD horizontal dipole mode). The choice of configuration affects the penetration depth and sensitivity to horizontal or vertical structures (Ward, et al., 1988). The majority of instruments keep the “induction number” low such that the combination of the frequency used and the separation between Rx and Tx is optimized to recover linear response with conductivity (McNeill, 1980). The data obtained is used as a single apparent conductivity value at the center of the device, and if several frequency/inter-coil separations are used, data are often inverted to derive a simple 1-D model of the subsurface conductivity. However, due to the low amount of data (usually 3 to 6 values) the quantitative interpretation capabilities of FEM methods are rather limited. Usually, FEM data are used a) for mapping the apparent resistivity considering a single depth of investigation, b) to get a preliminary indication of how the resistivity is varying with depth (2 or 3 separations needed). In our study, FEM method was considered to evaluate

the presence of a clay layer at the surface, or shallow depth while benefiting from a fast survey production.

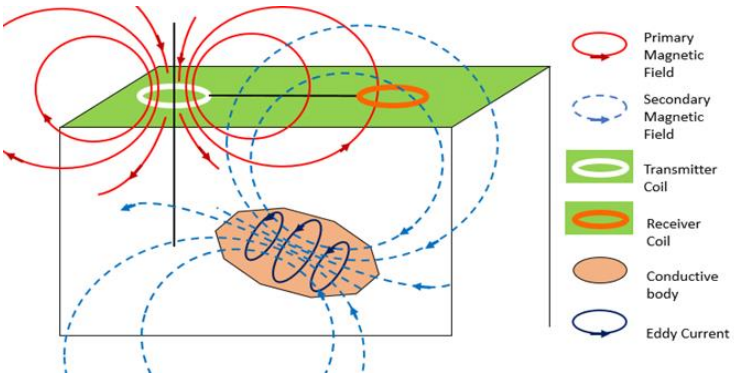

Figure 3.13 The FEM principles are applied to analyze the magnetic field response within a homogeneous half-space, considering the presence of a conductive body, transmitter, and receiver. (Reynolds, 2011).

Illustrating the positions of the transmitter and receiver coils, along with the primary and secondary magnetic fields, following contact with a subsurface target.

3.4.2 Evaluation of FEM sensitivity to clay using numerical modeling

The frequency-domain electromagnetic method (FEM), especially, EM34 instrument measures the conductivity of the underlying earth at different depths of an investigation by changing both parameters: inter-coil spacing and dipole orientation. If several measures are done changing those parameters (i.e. performing a sounding), the measured apparent conductivities can be interpreted into a multilayer 1D model (usually 2 or 3 layers). Our numerical modeling aims to answer the question: "Is EM34 able to detect a clay layer of various thicknesses at various depths and can confirm the presence of a clayey layer (high conductivity layer) immediately close to the surface?". We used the IX1D software (Interpex Ltd). A forward Modeling computes the apparent conductivity instrument readings given a known geological model with the thickness and electrical conductivity of subsurface units. Then the synthetic data set is inverted to produce a multi-layer conductivity 1D model: the electrical conductivity and thickness of each layer are calculated trying to fit to the measured apparent conductivity.

Initially, a series of Synthetic Models (called "SyM") were built based on the resistivity ranges obtained from the borehole log database and direct electrical resistivity measurement at some outcrops. The standard tabular model is set up as base geometries by increasing the depth and thickness to a clayey layer between sand layers. The typical resistivity or conductivity for each component layer is also defined respectively as 20Ω.m (or 50 mS/m) for clays and 200Ω.m (or 5 mS/m) for sand. The clay thickness varies from 0.5 meters to 20 meters: 0.5 m; 1 m; 3 m; 5m; 10 m; 15 m; and 20m. The increasing depth of the top of the clayey layer is at the surface (0 m); 3 m; 10 m; 20 m; 30 m; and 50m Figure 3.14. A total of 42 Synthetic Data (SD) sets created from 42 synthetic models are named from SD01 to SD42. For instance, the SyM14 structure represents a 20-meter thickness of clayey layer bounded by a top 3-meter thin sand and sand substratum and its conductivity value ranges from 5 mS/m (200Ω.m) to 50 mS/m (20Ω.m), and 5 mS/m (Ω.m) respectively. All the geophysical synthetic modeling was carried out with the use of the IX1D software to generate 6 synthetic apparent conductivity values: three with the VMD geometry and three with the HMD geometry, with 10-meter, 20-meter, 40-meter dipole separation for each synthetic model. A total of 252 synthetic data points (VMD-10, VMD-20, VMD-40, HMD-10, HMD-20, HMD-40) are shown in Table 1 42 Synthetic Data + Noise of different thickness and depth of clay models (APPENDIX 1) from 42 synthetic

model. 2% of random noise was added to synthetic data to account for more realistic field conditions from SDn01 to SDn42.

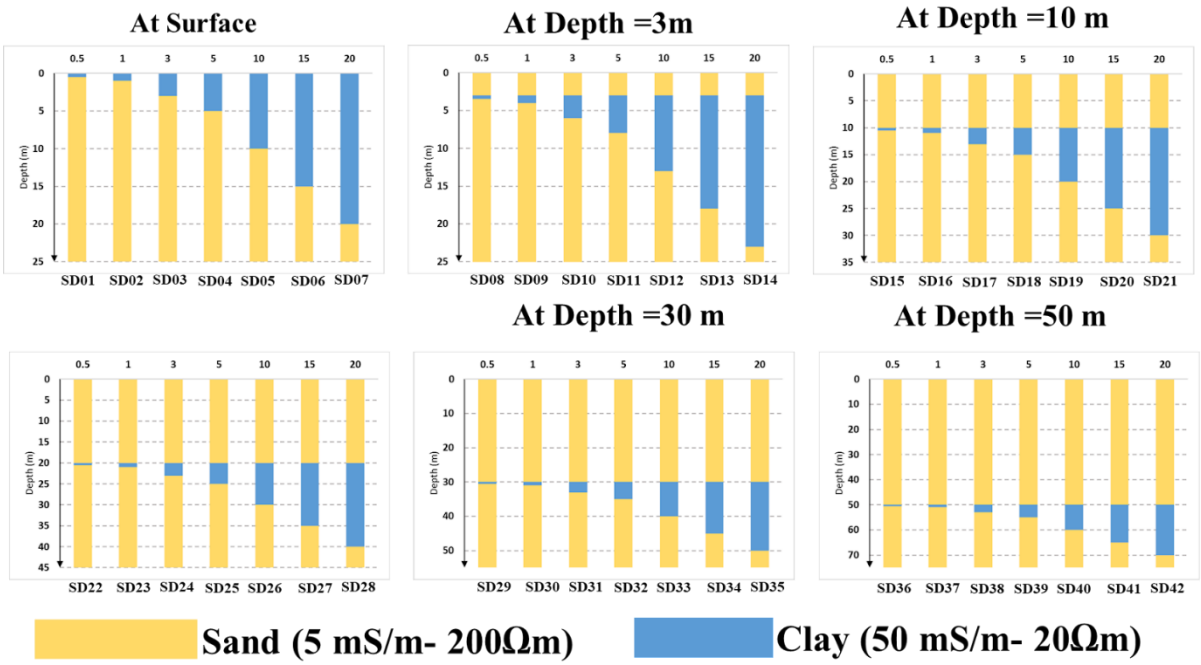

Figure 3.14 42 Synthetic model with different thicknesses and top depth of clay layer.

The synthetic data is subsequently inverted, and a comparison is made between the clay layer's thickness and depth values obtained from the inverted data and those of the original model.

From interpreting each SD synthetic data set, a "Starting Model" (StM) is created manually. To select the suitable StM for inversion, we decided to create two starting models as follows:

- The StM1 is commonly used when there is no information about the geology of subsurface or any additional geophysical survey. When 6 apparent conductivity data points (VMD and HMD) or 3 data points (VMD/HMD) show an increasing pattern with penetration depth, the model structure of the StM has 3 three layers which are increasing in electrical conductivity value with depth and vice versa. The conductivity value of each layer in the model is chosen equal to the apparent conductivity from the dataset. For example, the first model StM1 with 3 layers can be built with a 5-meter thin layer (50 mS/m) at the surface, a thick layer (5 mS/m) at the bottom, and a 15-meter layer (with an average value between 5 mS/m and 50 mS/m, such as 27 mS/m) in the middle.
- StM2 is based on the presence of a clayey layer at shallow depth according to the objective of this study. The model StM2 is similar to test site conditions and describes the presence of clay zones or clayey layers in the subsurface.

To make a comparison between these two starting models StM1 and StM2, we selected two typical SyMs (SD01 and SyM14) because both SyMs give clearly different results when we apply each StM. The two inverted (interpreted) models ("IM") IM01 and IM14 are the result of using successively StM1 and StM2 with two or three multiple cycles of iterations enough to obtain a convergence of the RMS to a stable minimum value. As a result, the StM2 gives a

better fitting and the best StM2 is a 15-meter-thick clay with a conductivity of 50 mS/m (20Ωm) bounded by a top 5-meter-thick unsaturated sand (5 mS/m or 200Ωm) and saturated sand (15 mS/m or 66.6Ωm).

The interpreted models were in a second step obtained by the inversion using only the StM2 for the 42 synthetic datasets with a constant number of iterations. The results were considered acceptable when the root mean square factor (RMS) of fitting error between raw data and calculated data is less than 1.5% due to 2% noise factor. The workflow of synthetic modeling summarized below describes the procedure of evaluating the detectability of a 10-meter-thick clay layer at different depths (at surface, 3m, 10m, 20m, 30m, 50m).

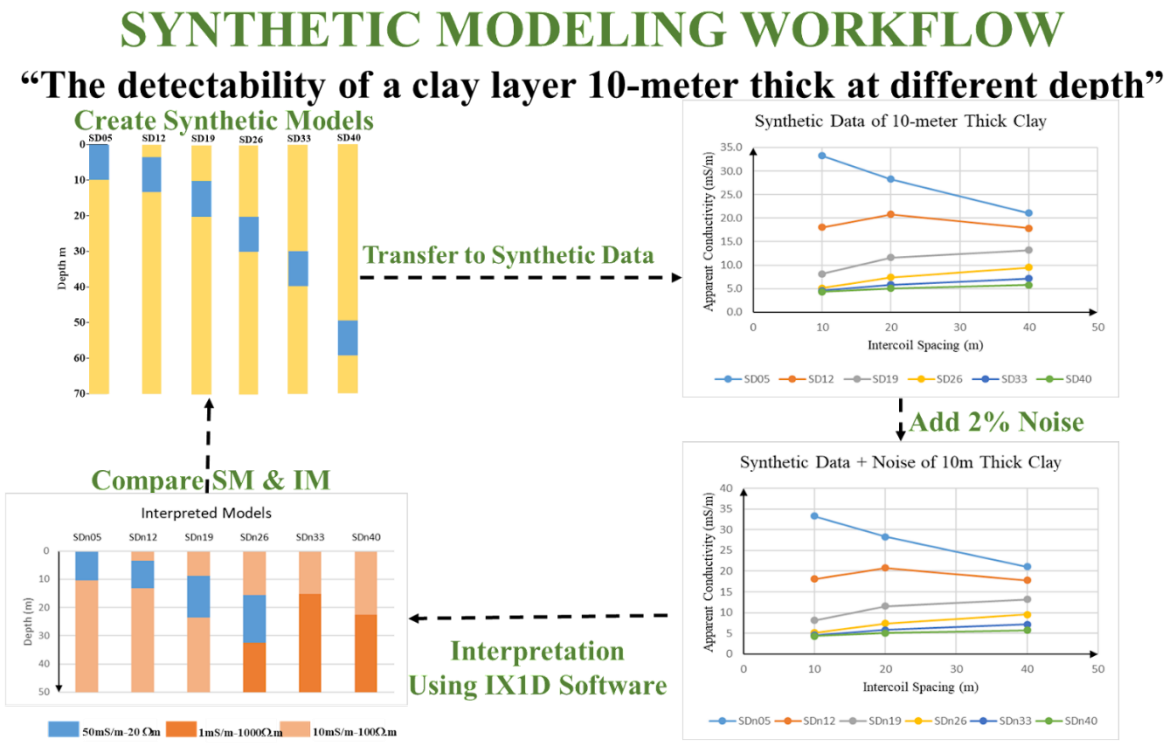

Figure 3.15 Synthetic modeling workflow of EM34 in detecting clayey layer.

The detectability of a clay layer 10 meters thick at different depths.

3.4.3 Results of the FEM numerical modeling

The inversion models result in a three-layer structure that consists of electrical conductivity (EC1) and thickness (T1) of first layer, electrical conductivity (EC2) and thickness (T2) of second layer, and electrical conductivity (EC3) of third layer. If the EC of a layer is very close to the EC of an adjacent layer, we give a two-layer solution using a new layer whose thickness is the sum of two thicknesses and the electrical conductivity is the average EC value of both layers. Results showing various responses of EM34/FEM in detectable clayey layers are presented in Figure 3.16 and showed in Table 2 Interpreted models from 42 synthetic data consist of electrical conductivities and thicknesses in a three-layer solution at APPENDIX 1.

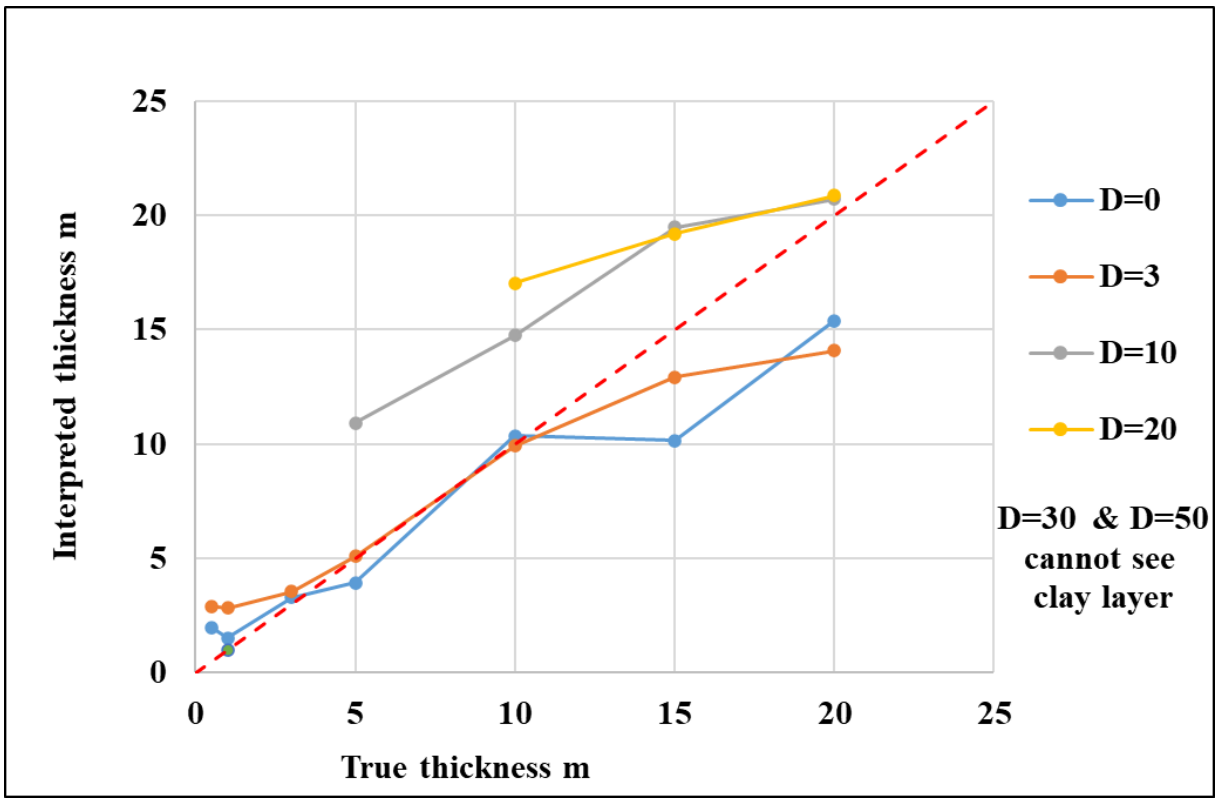

Figure 3.16 Comparison of true thickness and interpreted thickness of clay layer with EM34.

The figure illustrates the correlation between interpreted and true thickness of the clay layer. The comparison results are color-coded: blue corresponds to the surface clay layer, orange to the layer at 3m depth, gray to the layer at 10m depth, and yellow to the layer at 20m depth. Unfortunately, the clay layers at depths of 30m and 50m remain indeterminate. The dashed red line represents the unity line, where interpreted and true thickness values are equal.

The Figure 3.16 shows the comparison between the interpreted thickness and true thickness of the clayey layer at different true depths (D) of a clayey layer. The inversion can estimate the thickness of the clay layer within 25 % to 50% of uncertainty if this layer is situated before 20 m of depth. At the depth of 3 meters and the surface, the interpreted thickness is roughly the same as the true thickness but slightly underestimated after 10m. But for depths 30m and 50m, the inversion does not detect the clay but a more resistive substratum. As a result, the method can detect the shallow clayey layer's thickness which coincides with the interpreted thickness, but as expected, not for deeper clay layers (after 30 m) that are not well defined. The modeling confirms that shallow clayey layer thickness is well detected by EM34.

The Figure 3.17 evaluates the efficiency of the EM34 method in detecting the top depth of a clayey layer. The interpreted depth and true depth in the synthetic model are shown in Table 2 Interpreted models from 42 synthetic data consist of electrical conductivities and thicknesses in a three-layer solution at APPENDIX 1.

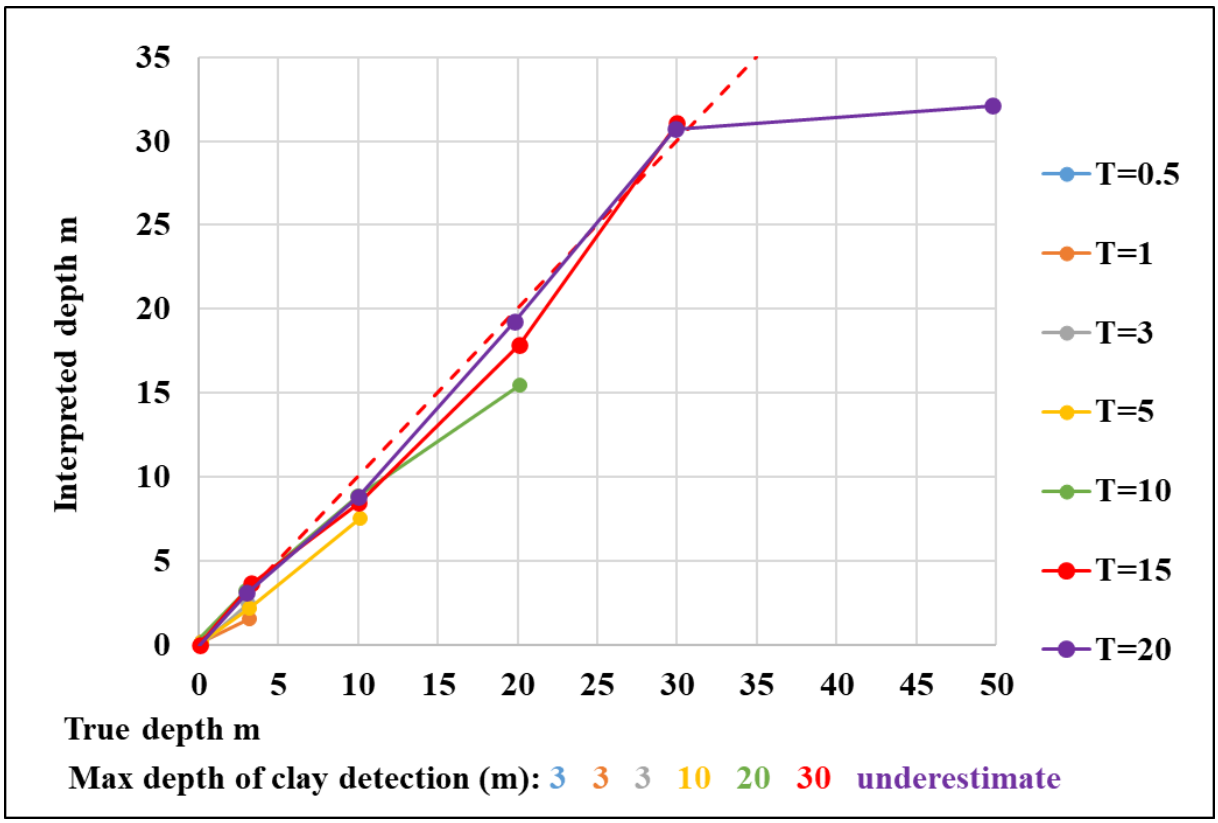

Figure 3.17 Comparison of true depth and interpreted depth of clay layer with EM34.

This graph was constructed to assess the effectiveness of the EM34 method in detecting the top depth of a clayey layer. The line chart presents a comparison between the interpreted top depth and the true top depth of the clayey layer at various true thickness levels. Different colors of lines indicate different true thicknesses of the clayey layer: 0.5m (blue), 1m (orange), 3m (brown), 5m (yellow), 10m (green), 15m (red), and 20m (violet). The red dashed line, marked with the coefficient 1, signifies a condition where the true top depth is equivalent to the interpreted top depth of the clayey layer.

It can be seen that if the clayey layer is thin, it is not detected at depth: for example, a 10 m thick clay is not "seen" if its top is situated after 20 m. The interpreted depth is slightly equal to a true depth from 0 to 30 meters but is underestimated when the clayey layer's top depth is over 30 meters. The maximum depth to which the clay can be detected depends on its thickness. After a certain depth, the calculated conductivity of the conductive second layer is no longer close to the original conductivity of 50 mS/m and drops to lower values, as low as 20 mS/m or even less. Therefore, with such value, the interpreter is no longer able to ascertain the second layer is clay. So, we can call this "max depth of clay detection" as "max depth of true conductivity clay detection". Eventually, the EM34 method is able to detect efficiently the depth to the conductive substratum (clayey layer) up to 30 meters.

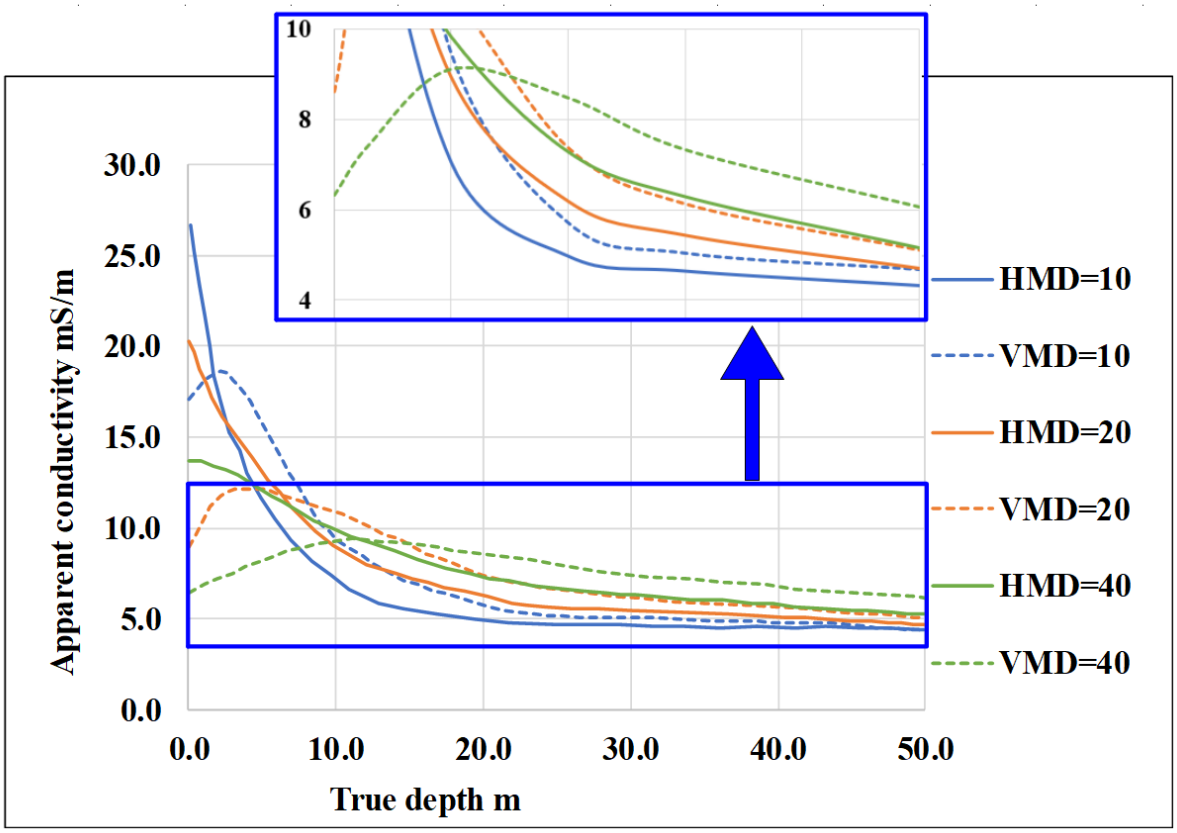

Figure 3.18 Comparison of synthetic apparent conductivity data of a 5-meter-thick clayey layer at different depths using VMD and HMD geometrical Tx-Rx configuration and using three Tx-Rx inter-coil spacings.

The vertical axis indicates the synthetic apparent conductivity data in mS/m in the range from 2.0 to 32 mS/m, the horizontal axis shows the contribution of the true top depth of the clayey layer to the dataset in meters. The different colors of solid lines represent the horizontal mode dipole's data of 10-meter, 20-meter, and 40-meter inter-coil spacing, and the dash lines are conversely vertical mode dipole's data.

The Figure 3.18 represents the comparison of synthetic apparent conductivity data of a 5-meter-thick clayey layer at different depths using VMD and HMD geometrical Tx-Rx configuration and using three Tx-Rx inter-coil spacings. The sensitivity of the method is the best between 0-meter and 10-meter depth because of the significant difference in VMD and HMD data. If the clay is situated between 10 meters and 30 meters, there is still a difference between VMD and HMD. After 30 m the difference between values of VMD and HMD is too small to be ascertained in normal field conditions. If the top of the clay is from 20 to 30 meters, the EM34 method has to measure the apparent conductivity data from 7 to 4.5 mS/m but if the noise is high in the field, it could be difficult to get reliable data. Hence, to obtain the possibility of interpretation of deep clay, a non-noisy area is necessary.

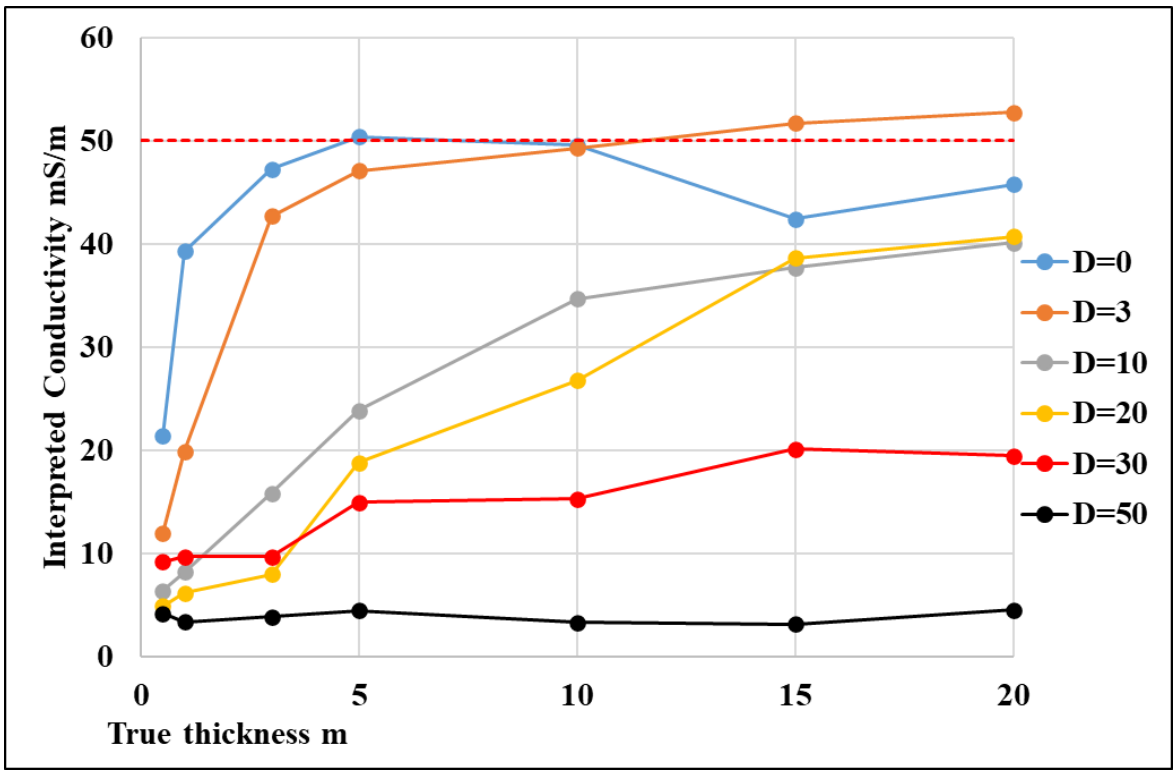

Figure 3.19 Comparison between the interpreted conductivity and true conductivity of clayey layer at different thicknesses and true depth of the top of the clayey layer.

The horizontal axis is the true thickness of the clayey layer in meters, the vertical axis is the interpreted electrical conductivity of the clayey layer in meters. Different line colors describe the true top depth of the clayey layer in meters: at surface (0m), 3m, 10m, 20m, 30m, 50m. The red dash line with the interpreted conductivity of clay is 50 mS/m which means that the interpreted conductivity coincides with the true conductivity of clay or the EM34 method is able to effectively quantify the electrical conductivity of the clay.

Figure 3.19 points out that the clay is truly interpreted as the true value of conductivity when the clay is more than 5 meters thick and close to the surface from 0 to 3 meters in depth. If the clay is deeper, the conductivity may be strongly underestimated.

In general, although the EM34 method is not efficient for estimating the conductivity value of clay, it's well able to detect the presence: of the thickness and the top depth of the clayey layer from surface to 30-meter depth. In contrast, the lack of resolution at depth of the EM34 method increases when the clayey layer is situated deeper than 30 meters. In the field, we used the method on several test sites to illustrate the numerical modeling by true field data, compared to ERT and TDEM.

3.5 Direct current (DC) resistivity methods

Direct current (DC) resistivity method is a prominent technique in geophysics. The foundations of DC can be traced back to the early 20th century, with Conrad Schlumberger first publishing the principles of electrical resistivity prospecting in 1912 (Loke, et al., 2013). DC resistivity methods began mainly in mineral prospecting and oil exploration (Dobrin, et al., 1988). In the 1980s and 1990s saw a broader range of applications for a new technical improvement, the Electrical Resistivity Tomography (ERT). The technique was increasingly being used in hydrogeological investigations, environmental impact assessments, and archaeological studies (Reynolds, 2011). Lastly, the time-lapse ERT approach has

revolutionized monitoring of subsurface processes over time, providing a dynamic view of environmental phenomena such as contaminant migration or groundwater fluctuation (Singha, et al., 2006). The past decade has also seen an increased emphasis on the development of field protocols and standards for ERT surveys (Martin, et al., 2020).

3.5.1 Principle of the direct current electrical method

The DC technique involves measuring the resistivity by injecting a direct current (I) in amperes through two electrodes (A and B, or C1 and C2) using a current generator. Additionally, two other electrodes (M and N, or P1 and P2) are used to measure the potential difference via a voltmeter (as shown in Figure 3.20).

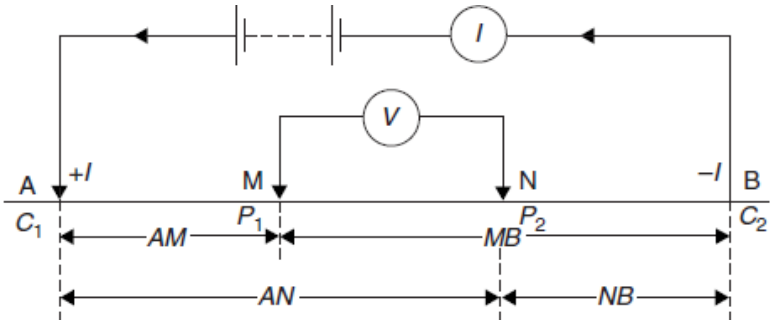

Figure 3.20 Wenner electrode configuration (Reynolds, 2011)

The apparent resistivity is then calculated based on the first resistivity equation 3.4

$$\rho = \frac{K\Delta V}{I} \qquad 3.4$$

The value of the geometric factor K is contingent upon the arrangement of the measuring device's four electrodes aligned in the subsoil

$$K = \frac{2\pi}{\frac{1}{AM} - \frac{1}{BM} - \frac{1}{AN} + \frac{1}{BN}} \qquad 3.5$$

AM = distance between electrodes A and M (in m), same for distances BM, AN and BN.

3.5.2 Concept of apparent resistivity

When the subsoil is homogeneous, the flow of current follows a path without any deformation of the current lines (as depicted in Figure 3.21 a). In this scenario, the measured resistivity value represents the actual resistivity of the investigated subsoil. However, in a heterogeneous subsoil, the streamlines of current are distorted when they encounter zones with different resistivities (as shown in Figure 3.21 b). In such cases, the resistivity value obtained is termed the "apparent resistivity" (ρa). This apparent resistivity is an integrated measure influenced by the varying resistivity zones along the current path. To accurately determine the true resistivity of different zones (or layers) within the subsoil, we need to "invert" the electrical sounding data, enabling the reconstruction of the actual resistivity distribution of the different geological layers or structures present in the subsoil.

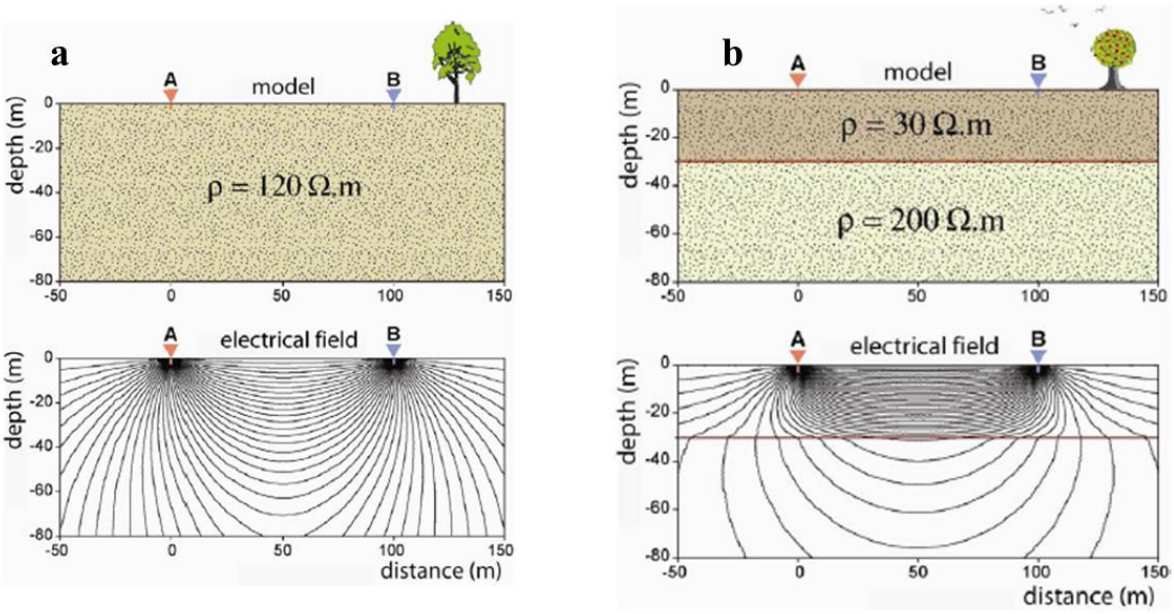

Figure 3.21 Current flow in the subsurface.

a) In a homogeneous subsoil; b) in a heterogeneous subsoil (D. Chapellier, 2000)

3.5.3 Depth of investigation and electrode devices

The depth of investigation is controlled to the first order by the length of the device. The larger it is, the greater the depth of investigation. The second control parameter is the configuration or arrangement of the electrodes (Figure 3.22). Each device has a theoretical depth of investigation depending on the distance between the electrodes.

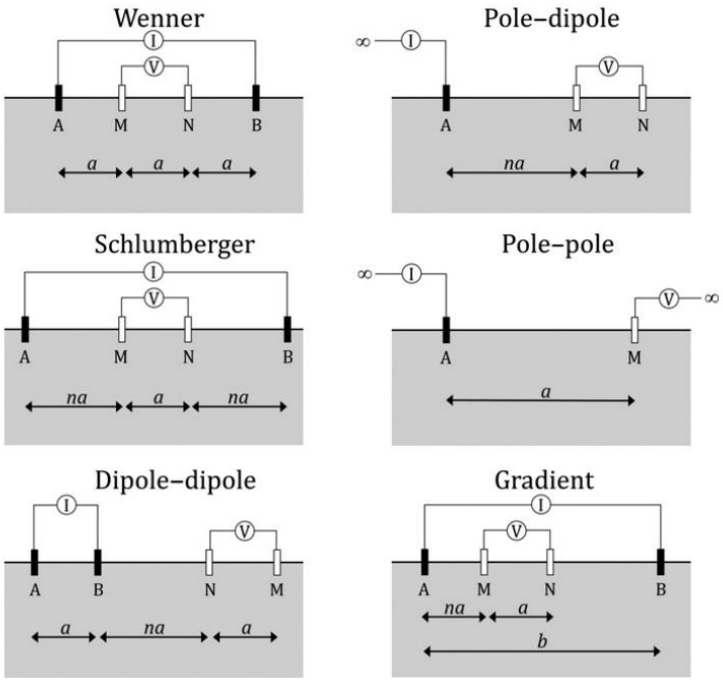

Figure 3.22 The main electrode configurations (Reynolds, 2011).

3.5.4 2D and 3D measurements: Electrical Resistivity Tomography

Electrical Resistivity Tomography (ERT), originating in the early 1990s, is a sophisticated 2D (and 3D) measurement method which employs multi-electrode systems. Pioneered algorithms were crafted for data interpretation (Loke, et al., 1996).

ERT, sometimes referred to as Electrical Resistivity Imaging (ERI) allows for both profiling and electrical sounding acquisition (Dahlin, 2001). For 2D acquisition, the procedure involves connecting in line a significant number of electrodes (such as 24, 48, 72, 96, or more) at regular intervals and perpendicular to the supposed structures. The electrodes function in various capacities, either as an injection (A or B) or measuring electrodes (M or N), providing many device options and quadrupole spacing Figure 3.23.

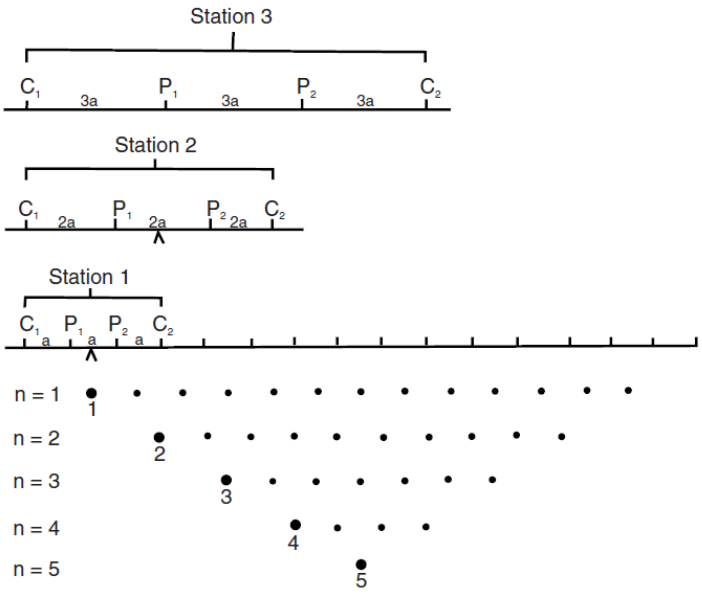

Figure 3.23 A sequence of measurement to build up an ERT pseudo section (Reynolds, 2011)

The measured apparent resistivity section must be inverted to deduce a calculated resistivity distribution. This is achieved through an iterative inversion method, with the assumption that the subsurface structure is 2D. This iterative process starts with a homogeneous model, then calculates a first set of calculated apparent resistivity, evaluates the differences with field apparent resistivity data set, then changes the model according to the difference between calculated and actual apparent resistivity, then runs another second calculated data, and continues the comparison process until the acceptable (low) difference between calculated and actual data is reached. The result is a 2D model of calculated resistivity as a function of depth, presented as a geoelectric section of the subsoil. Notably, the result of inversion might not be unique, and errors in source data can occur. The inversion process can be constrained by utilizing a priori information regarding the structures under investigation to optimize the result. In our study, we used free software like DC2DInvRes and BERT (http://resistivity.net/bert/, (Gürses, et al., 2004)). Several inversion parameters can guide the inversion, with DC2D offering a default setting extensively validated for subsoil characterization.

3.5.5 Modeling the sensitivity of ERT to clay

The primary objective is to determine whether ERT can effectively detect the presence of clay layers in the subsurface. To achieve this, we employ two software tools: DC2DinvRes for building a synthetic initial model and generating synthetic data and Boundless ERT (BERT) for the inversion and interpretation of the data. Three different scenarios were considered. The first scenario involved varying the depth of the clayey layer while keeping other parameters constant. The second scenario examined the ERT method's response to changes in the thickness of the clayey layer. The third scenario focused on varying the resistivity of the upper sand layer while keeping other parameters constant.

The standard array configuration employed throughout the experiments was the Schlumberger array with 48 electrodes spaced at 2-meter intervals. The interpretations were compared with the known initial synthetic models.

- **Variation in the depth of clay**

In this modeling, the clay layer (2m thick) is deepened. Based on the inversion results in Figure 3.24, we can ascertain that the ERT method is effective in confirming the presence of a clay layer on the surface in terms of both its resistivity value and thickness.

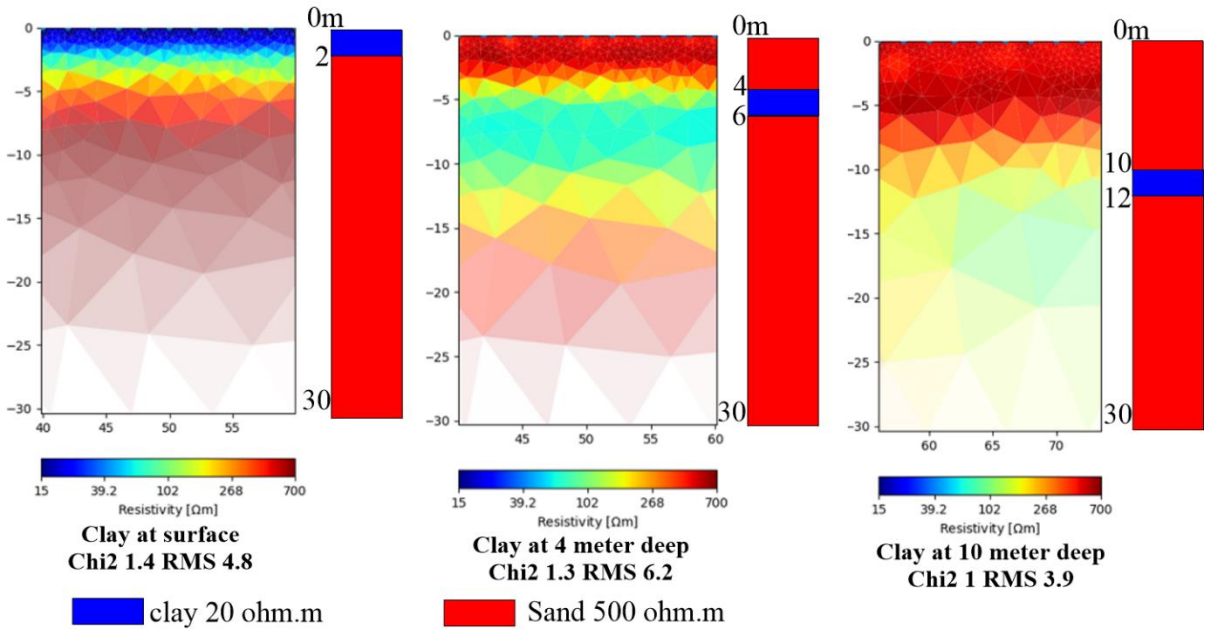

Figure 3.24 Inversion results showing variations in the depth of clay within the synthetic model.

The resistivity value of the clay layer is 20 Ω.m in blue and the resistivity of sand is 500 Ω.m in red respectively.

However, the recognition of clayey layers becomes more challenging as they extend to greater depths. This is primarily due to the increased effect of the resistive layer on the clay making it harder to distinguish from other formations at deeper levels. The determination of the clayey layer's thickness becomes less precise as it goes deeper, leading to potential inaccuracies in the interpretation of the subsurface structure as shown in Figure 3.25.

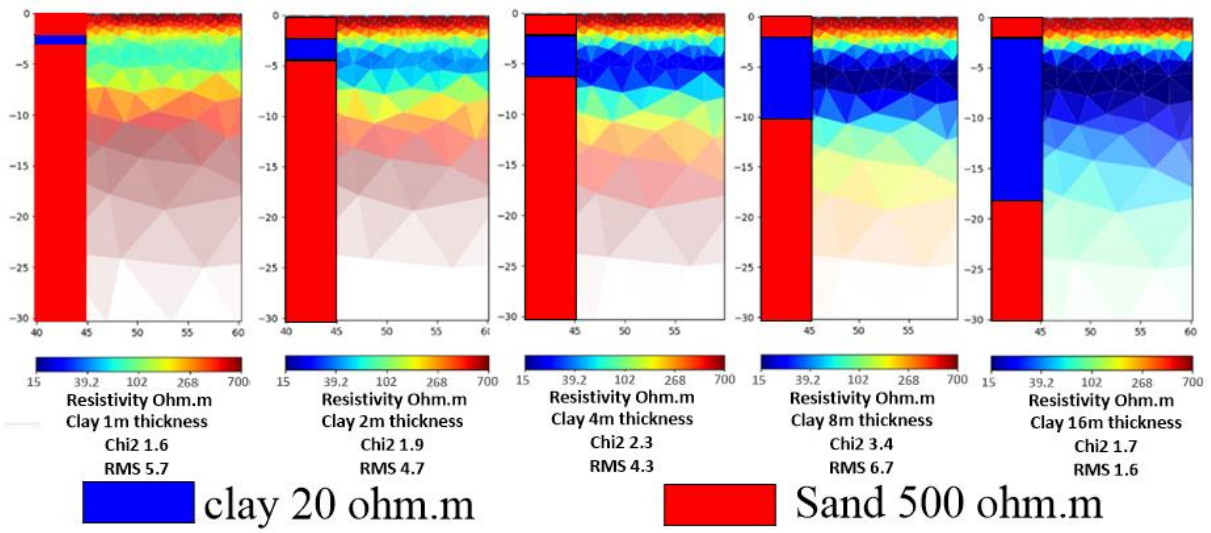

Figure 3.25 Inversion results showing variation in the thickness of clay within the synthetic model

Another significant aspect highlighted is the impact of the clayey layer's thickness on its identification. ERT can still recognize clayey layers even when their thickness increases. However, determining the precise thickness becomes more difficult, which may result in uncertainties when characterizing the subsurface layers. This limitation suggests that additional complementary methods might be required to improve the resolution of ERT data, especially when dealing with thicker clayey layers.

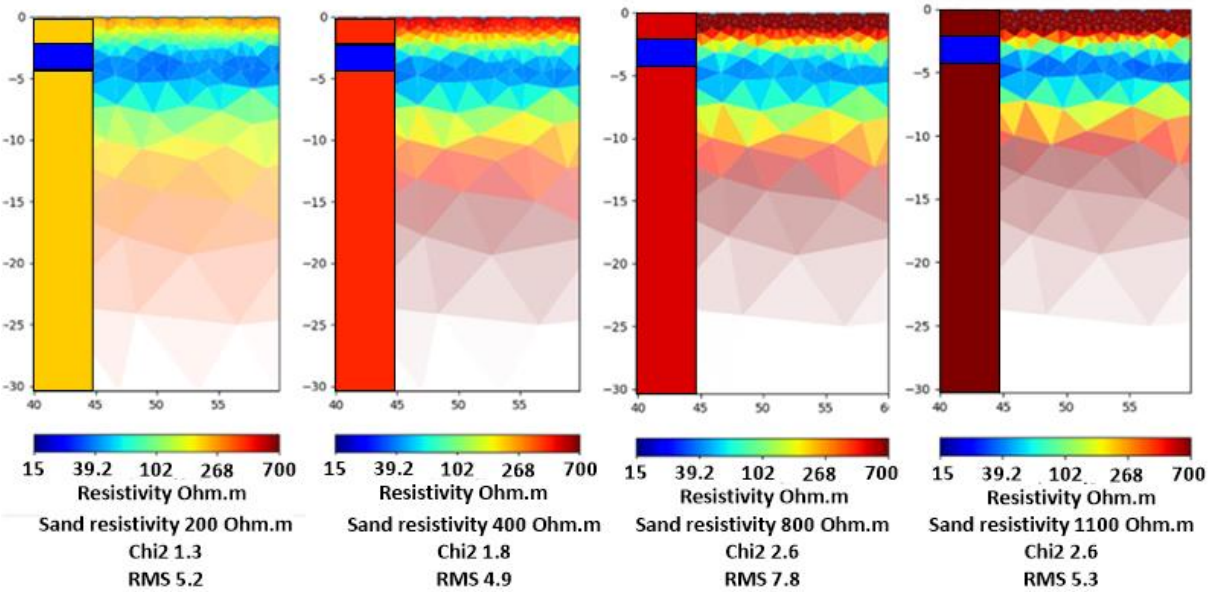

Figure 3.26 Inversion results showing Variation in the resistivity of the sand layer within the synthetic model

On a positive note, the comments also emphasize the stability of the resistivity value for the clayey layer in the presence of changes in the resistivity of the overlying sand layer Figure 3.26. This constancy in the clayey layer's resistivity is encouraging as it provides a consistent marker for identifying the presence of clay despite variations in other geological formations. However, it is crucial to be cautious about potential scenarios where resistivity contrasts between clayey layers and surrounding materials are too low, making accurate identification solely based on resistivity values challenging. Integrating ERT data with other geophysical

methods, such as TDEM, FEM, or borehole data, could enhance the reliability of clayey layer identification.

3.6 NMR method

A key objective of this research is to enhance methodologies not only for geometry but also for analyzing aquifer parameters within the study region, specifically focusing on water content in the aquifer and hydraulic-related characteristics. The Nuclear Magnetic Resonance Sounding (NMR) method was thus proposed, as it directly detects water content within porous materials. This sensitivity to water content was highlighted by (Bernard, et al., 2003). This approach could aid in evaluating aquifer conditions and establishing a link between NMR parameters and aquifer water content, potentially estimating aquifer storage capacity.

The NMR method can be performed at two different scales, the field scale and also at the laboratory (core sample) scale. In this study, we started to test MRS in the field and then, due to difficult results, we explored NMR at the laboratory scale.

3.6.1 Magnetic Resonance Sounding (MRS) method at large -field- scale

The studies of (Vouillamoz, et al., 2014) (Legchenko, et al., 2006) (Descloitres, et al., 2008) have shown that MRS can be an efficient tool to obtain parameters well suited for hydrogeological studies in hard rock or sedimentary aquifers. MRS is a method derived from the NMR (Nuclear Magnetic Resonance) physical phenomenon principle. NMR measures directly the relaxation of the proton H+ of the water molecule when it is submitted to a time-varying magnetic field and plunged into a static magnetic field. This is why we can call NMR a "direct" method because its response comes from the water molecule in the soil only. In hydrogeophysics, the static field is the Earth magnetic field, while the alternative magnetic field is produced by the equipment. Further details on the method can be found in (Legchenko, et al., 2002) (Legchenko, et al., 2004) (Yaramanci, et al., 2002) (Lubczynski, et al., 2003). We call MRS "MR *Sounding*" because using a variable increasing intensity of the electrical current flowing into the surface transmitter loop, the relaxation is produced deeper and deeper in the soil allowing us to derive a sounding information. Currently, available equipment sounds non-destructively the ground in the saturated zone down to 100 meters. At each current intensity step (so at each depth), called "pulse moment", two main parameters are measured with MRS:

The amplitude of the relaxation signal, linked with the MRS water content parameter **θmrs** (W_{NMR}) (in %). In unconfined aquifers, the MRS water content **θmrs** is usually considered as an estimate of the effective porosity if the dead-end and unconnected pores are neglected. In a confined aquifer – that is often the case in a crystalline context or sometimes in our sedimentary context implying clayey layers - **θmrs** is usually linked to the storage coefficient that quantifies the aquifer storativity.

The relaxation time constant **T_1**, linked with the pore size. This relaxation time constant **T_1** (in ms) is determined using a measurement sequence involving two successive electrical current pulses, called FID 1 and FID 2 (FID for "Frequency Induced Decay"). Both pulses generate two decaying signals and result in two different decay curves. Basically, lower the FID2 signal amplitude compared to the FID1 signal amplitude, larger the pore size. Further information on the hydrogeological significance of MRS parameters can be found for example

in (Lubczynski, et al., 2004). Because only two pumping tests are available in the area, we discarded in this study the use of any transformation function to calculate hydraulic conductivity from MRS results because this would have needed numerous pumping tests. In addition, surface large-scale MRS was suffering from high noise conditions.

For MRS, data acquisition involves the deployment at the surface of a cable loop (single turn forming a square or an “8” shape), which is used as transmitter and receiver of the alternating magnetic fields at the Larmor frequency (Legchenko, 2013). It's worth noting the importance of external factors, such as the Earth's magnetic field and anthropogenic noise, which can influence the MRS signal and thus need careful consideration during acquisition (Müller-Petke, 2020). Our tests on 4 test sites at Cu Chi at the beginning of the PhD work were suffering from high noise conditions. Therefore, it has been decided that alongside tests at large-scale MRS in the field, the NMR method could be used at the laboratory scale to determine NMR parameters on core samples extracted from boreholes. The potential of studying cores extracted from the study site may indeed introduce a promising method referred to as "Lab-scale NMR". Thus, one of the objectives of this Ph.D. work is to explore the feasibility of employing lab-scale NMR for studying the Cu-Chi aquifer and potentially other sedimentary aquifers in the country. The objective is to evaluate whether NMR parameters $\boldsymbol{\theta_{mrs}}$ and $\boldsymbol{T_1}$ can be linked with Specific yield - storativity - (Sy) and hydraulic conductivity (K) by acquiring data in the field during borehole campaigns extracting cores, and thus facilitating in-situ parameter assessment without costly pumping tests.

3.6.2 NMR principle

The principle of Nuclear Magnetic Resonance (NMR) phenomenon (or Magnetic Resonance Sounding) is illustrated in Figure 3.27.

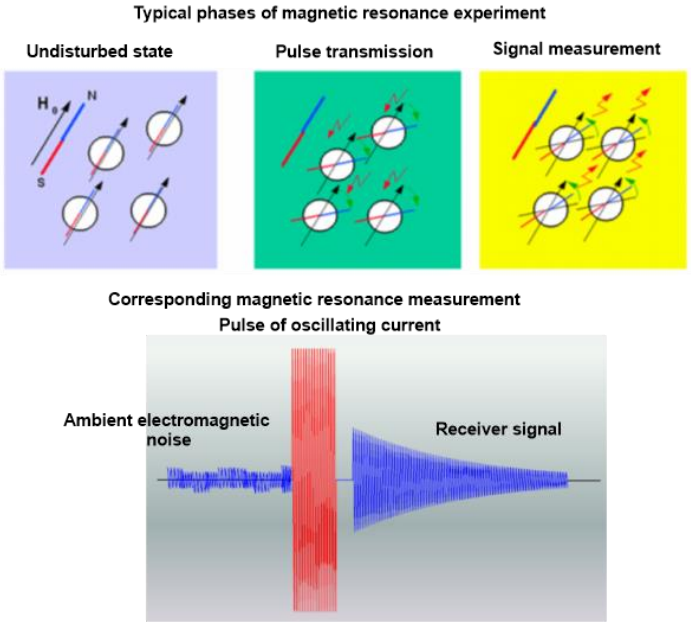

Figure 3.27 Typical phases of a magnetic resonance experiment.

The first is an undisturbed phase for measuring electromagnetic noise; the second is pulse transmission to generate the oscillating current; and the last phase is the signal measurement to receive the signal response. iris-instruments.com

In their natural, undisturbed equilibrium state, all magnetic moments (M) align with the geomagnetic field (Bo) and do not generate any signal. Proton nuclei (H+) are capable of absorbing electromagnetic energy at the Larmor frequency (Legchenko, 2013). The Larmor frequency is determined by the equation:

$f_o(Hz) = 0.04258 \times B_o\,(nT)$ 3.6

The Bo value of the Earth geomagnetic field is established through standard magnetic surveys using a magnetometer and averaging readings. When a sample is exposed to an oscillating electromagnetic field, magnetic moments deviate from equilibrium. This exciting field is generated by an electric current passing through a loop for surface MRS or a coil for laboratory NMR, operating at the Larmor frequency (f). The intensity of the current (I) and its duration across the loop or coil define the exciting field and is called 'pulse moment". Ideally, the external field should be perpendicular to the geomagnetic field. The H^+ nuclei generate a magnetic field when excited by this external oscillating field. The initial signal amplitude is given by the expression:

$$Eo = \int 2\pi f B(r) M_o \varphi(r) \sin\big(0.5\gamma B(r)\big) Q dv \quad 3.7$$

Mo is the proton's magnetic moment H

φ or WNMR is its water content dimensionless

BL is the stimulated field component that is perpendicular to the static field.

When the external field is switched off, the particles return to their initial positions, creating a relaxation secondary magnetic field that decays over time at the Larmor frequency. This field is measured using a receiver coil or loop. Data acquisition involves injecting an oscillating current pulse at the Larmor frequency into the transmitting coil. After the pulse ends, the magnetic resonance response is measured in the receiving coil (which can be the same as the transmitting coil or loop) at the same frequency. The response is given by the equation 3.8 (Legchenko, 2013)

$$E = E_o \exp(-t/T_2^*) \cos(2\pi ft + \varphi) \quad 3.8$$

T_2* is the free induction decay (FID2) time constant ms

φ is its water content dimensionless

f Larmor frequency Hz

The parameters for NMR measurements are

- E_o is the amplitude of the MRS measured signal. Its magnitude is directly proportional to the quantity of proton nuclei (H) present in the sample or the subsurface material.
- T_2 and T_2* are transverse relaxation times associated with the component of the proton magnetic moment (M0) that is perpendicular to the Earth's magnetic field. In a measurement utilizing a single pulse technique, T_2* is the parameter used to characterize the decay of the signal amplitude, as shown in Figure 3.28.
- T_1 refers to the longitudinal relaxation time. It is related to the component of the proton magnetic moment (M0) perpendicular to the Earth's magnetic field. Magnetization along the longitudinal axis cannot be directly measured; it must be measured along the transverse axis. T1 is typically determined using two pulse sequences.

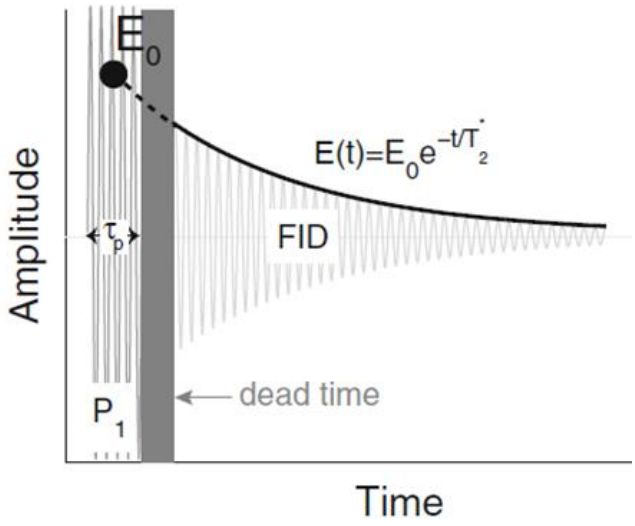

Figure 3.28 FID pulse sequence (Behroozmand, et al., 2015)

The single 90° energizing pulse, denoted as P1 is emitted at the local Larmor frequency. After P1 is deactivated, allowing for a measurement dead time (indicated by the shaded gray box) to pass, a single Free Induction Decay (FID) is recorded, ideally oscillating at the same frequency as P1. Subsequently, employing envelope detection on the FID yields the effective transverse relaxation time, T_2, and the initial amplitude, E_0.

3.6.3 Laboratory scale NMR equipment and data acquisition

Previous tests of surface large-scale MRS were suffering from high noise conditions in the Cu Chi area. Therefore, it has been decided that alongside tests at large-scale MRS in the field, NMR method could be used at the laboratory scale to determine NMR parameters on core samples extracted from boreholes. The potential of studying cores extracted from the study site introduces a promising method referred to as "Lab-scale NMR." Thus, one of the objectives of this Ph.D. work is to explore the feasibility of employing lab-scale NMR for studying the Cu-Chi aquifer and potentially other sedimentary aquifers in the country. We used a laboratory Earth's field NMR prototype instrument developed at IGE Laboratory (Legchenko, 2022). Most of the figures and measurement procedures below are extracted or summarized from the equipment manual written by A. Legchenko (Legchenko, 2022). Figure 3.29 illustrates a schematic of the equipment, including the equipment components and installation procedure.

Figure 3.29 Lab scale laboratory NMR instrument

The Lab NMR device is designed with two parallel coils: a transmitter coil and a receiver coil. Both coils have their axes perpendicular to the north direction, but they are oriented in opposite directions. One of the coils acts as a measurement coil, while the other, with identical characteristics, acts as a noise measurement coil. This noise measurement coil is used to reduce the overall noise level in the data. The coils are positioned at a 3-5 m distance from other

equipment systems to minimize interference. A proton magnetometer is used at the installation site to monitor any fluctuations in the Earth's magnetic field.

It's essential to select an appropriate Larmor frequency for the Lab NMR device's operation using a bottle full of water (that maximizes the amplitude of the signal). Some measurements can be done a few Hertz away from the Larmor frequency to avoid harmonics of 50 Hz or other perturbing EM noises. The quality of the data collected is assessed using the signal-to-noise ratio. Additionally, the form of the amplitude spectrum contributes to determining data quality. In cases where the signal-to-noise ratio is low during the measurement, the stacking index can be increased. It's crucial to ensure that the installation site is as free as possible from electromagnetic interference sources like power lines, passive conductors (such as buried pipes or buildings), and surrounding fences.

3.6.4 Determining T1

The objective of calculating T1 value is first to classify the aquifer's quality and second to obtain T1 mean value for setting the duration of the pulse for the water content procedure (described after this paragraph). Figure 3.30 illustrates how to measure the signal from the core sample using at least two distinct duration polarization times to compute the T1 value. Better T1 characterization is obtained if more than two pulse durations (“pulse delay”) can be measured. In this study, we used 5 successive E measures with 5 different duration pulses.

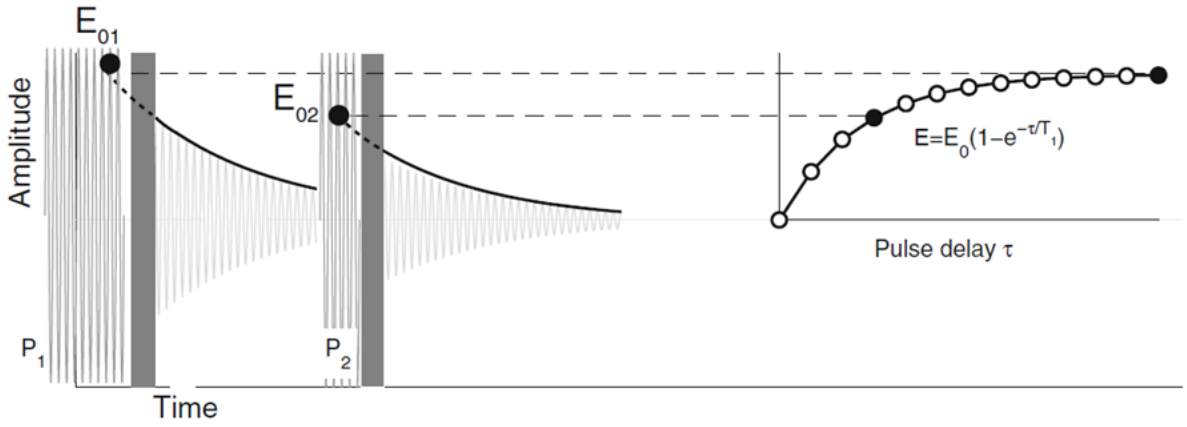

Figure 3.30 Saturation Recovery pulse sequence. The measurement initiates with a single 90° energizing pulse, denoted as P1, resulting in a corresponding Free Induction Decay (FID1).

Following a delay time, a second 90° pulse, P2, is administered, generating the corresponding FID curve (FID2), which is then recorded. This sequential process is replicated with varying delay times, and the initial amplitude of FID2, represented as E02, is utilized to construct the T1 recovery curve. (Behroozmand, et al., 2015))

The expression for the amplitude signal measured in duration polarization time is

$E_{meas} = E0 \times (1\text{-}\exp(-D_p/T1))$ 3.9

E_{meas}: amplitude signal measure in D_p duration polarization time

In the PhD work, two periods of lab scale NMR on borehole cores have been considered: The first year, a first set of cores have been measured in Grenoble. In the second year, the second set was acquired in Vietnam in a remote place to avoid EM noise. In Vietnam, similarly

to Grenoble procedure, the following procedure is achieved to get data with acceptable quality for calculating T1.

- The device's operating frequency has been chosen at 2020 Hz, around 17 Hz away from the actual Larmor frequency, to avoid a disturbing internal frequency. Even lowered by this technical procedure the signal at the actual Larmor frequency is still measured and used for our measurement.
- A real-time filtering is applied, and contains a filter with a bandwidth range of 25 Hz and 100 stacks in a single measurement, which is sufficient to stack noise below 30 nV.
- Successive automated measurements are made to record the raw signal at polarization duration times ranging from 80 to 1030 milliseconds.
- We regularly check the signal-to-noise ratio, the signal amplitude, and the frequency shape of the amplitude spectrum. When the signal-to-noise ratio is low and the spectral signal frequency reaches the bulk water frequency of around 2003 Hz, this means that the measurement is good quality.
- After the raw measurements with several pulse durations, the data are post-processed: undesired noises are filtered out, and the signal-to-noise ratio is enhanced by stacking. We use the software NumisPro for processing the raw data.
- The curve of pulse duration versus NMR signal amplitude is plotted and T1 value is extracted from a curve fitting adjustment.

3.6.5 Determining NMR water content

Once the T1 parameter is known from the previous experiment, the objective is to calculate the water content of the saturated core sample (Legchenko, 2013). The NMR method is utilized to ascertain the water content within the core sample, encompassing both free water (which includes water in a mobile state) and a portion of "inactive" water referred to as trapped water.

The water contained in the core sample is determined based on a simple procedure (see Figure 3.31)

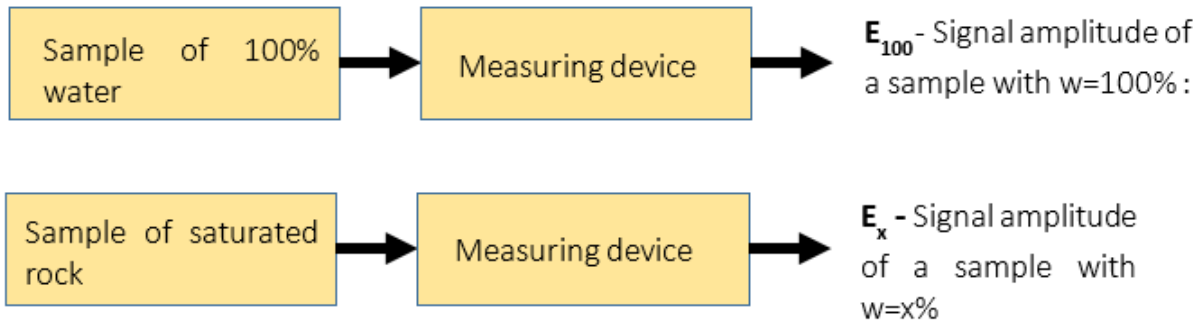

Figure 3.31 Procedure to measure the water content (Legchenko, 2022)

The water content is the ratio of the sample signal to the bulk water signal.

The water content is calculated $W_{NMR} = 100\% \times E_x / E_{100}$ 3.10

The value of E depends on the duration of polarization time and the amount of water in the sample. For a 100% water content (i.e. the bottle of water) we need a duration of polarization

time long enough to get the actual value of E_{100}. Then for measuring the water content of the sample E_x, we use E_{100} amplitude to adjust the device before measuring E_x values. The water bottle for calculating water content must have the exact dimensions of the core sample to be measured.

3.6.6 Measuring NMR water content of the core sample

To accurately record the energy amplitude associated with the core's water content, an automated measurement function is configured with a polarization time of 1000ms. Given that the T1 value of the sample is less than 1000ms, a 1000ms polarization time enables the capture of the actual amplitude signal of water in the sample. Successful measurement is indicated by a high signal-to-noise ratio and a signal amplitude spectrum frequency close to the frequency of the water used for initial correction within the 2003 Hz range.

After completing the measurement, it is necessary to correct the measured amplitude at t = 20ms value by calculating the original true amplitude E_o at t= 0ms. E_o represents indeed the signal amplitude extrapolated to the delay time (20ms) as shown in Figure 3.32. This 20-millisecond delay time corresponds to the period before signal measurement. The T_2* value, which is the transverse relaxation time constant, is employed to determine the signal amplitude related to the water content of the core sample.

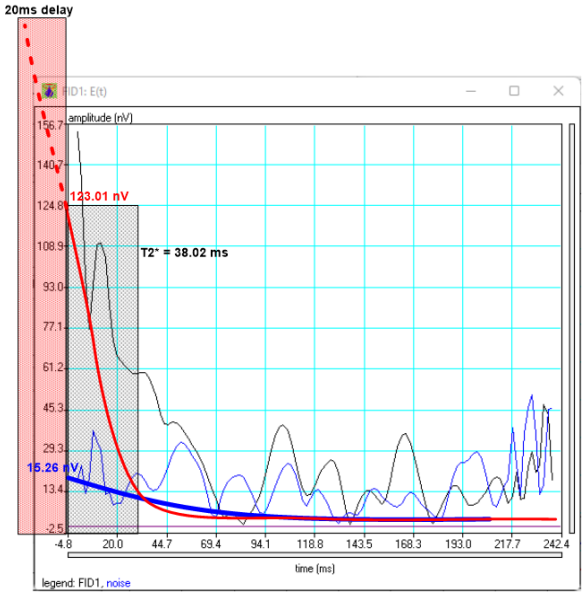

Figure 3.32 T2* and extrapolation of the signal to 20ms delay time before

"Bottle of water" E_o measurements:

Using a bottle with 100% water, the signal amplitude determines the water content in the core sample. Figure 3.33 shows the method used to figure out how much water is in the core sample. The water bottle is measured with polarization times ranging from 1000ms to 5000ms. The measurement data are processed and calculated based on the correspondence between the model line and measurement data shown in Figure 3.33. We determine from the matching model that the amplitude of the water bottle is, in this example, 4097nV.

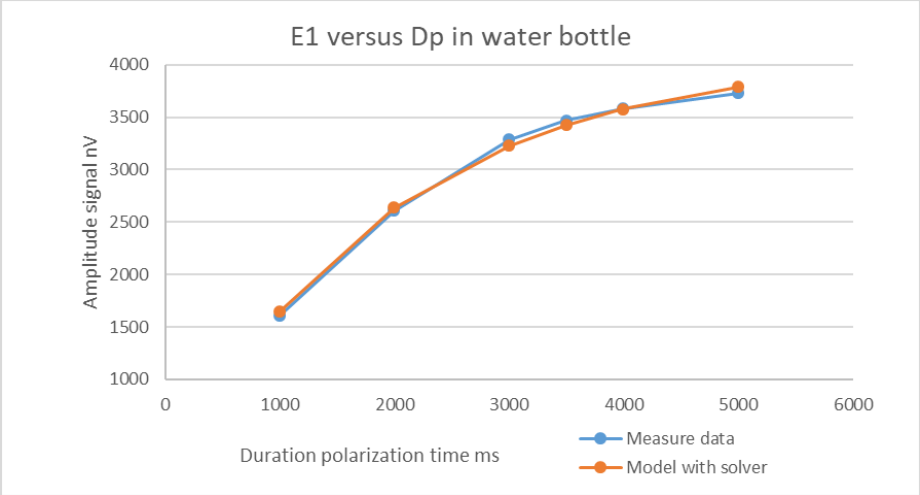

Figure 3.33 Amplitude versus duration polarization time for a bottle of water

Verifying the NMR sensitivity to water content using a "perfect saturated sand."

This "perfect sand" bottle measurement experiment is made to ensure that our device correctly estimates the water content in a homogeneous sample of "ideal" saturated coarse sand. The saturated coarse sand bottle contains 33% water based on weighing measurements. The sand bottle is measured using various polarization durations ranging from 80ms to 3000ms. After data processing and analysis, we can determine that the water signal in the sand bottle is 1287nV Figure 3.34.

Using equation 6, we can calculate the water content in the sand bottle as follows:

W_{NMR} = 100*1287/4097 = 31.4%

Compared to the value of the water content in the sand bottle as measured by the weighing method, the error result is acceptable at 5%.

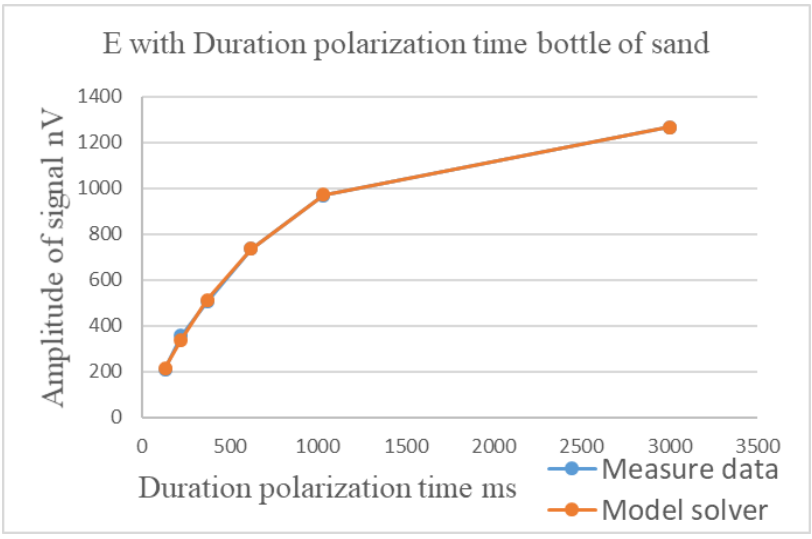

Figure 3.34 Amplitude of signal versus duration polarization time in sand bottle

The NMR water content deduced from the perfect sand bottle is nearly equal, in this experiment, to its total porosity, and we could have hypothesized that it is equivalent (or close

to) to its effective porosity (i.e., the connected porosity which allows the water flow through the coarse sand) since the sand in the bottle is homogeneous and free of clay.

3.7 Location of geophysical measurements and boreholes observation

3.7.1 TDEM survey strategy

The key issue was to define the spacing distance between sounding points. These spacing plays a key role in the accuracy and resolution of the TDEM measurement as well as the optimization of the time during data collection. The spacing between TDEM measurement points aims to strike a balance between optimizing data collection time and ensuring the ability to detect subsurface structures effectively. To achieve this balance, we estimated the size of subsurface structures based on the actual topographic features and current geological structures. Observations from studies of the surface topography of the Saigon River provide valuable insights. The meandering patterns of the Saigon River typically exhibit a wavelength of 500 meters to 1 kilometer, with the river itself measuring around 100 meters in width within our study area. In addition, the current floodplain area can extend to more than 500 m in width. Consequently, we can anticipate the presence of similar subsurface structures below the surface. Taking this into account, we propose a spacing of 200 meters between measurement points. Shorter distances between TDEM soundings (50 and 100 m) have been also tested in two test sites (BH4 and rubber tree area) and the results show that, as expected, some conductive deep clay anomalies are larger than 100 m, this being detectable by a TDEM survey with 200m between the soundings. The “routine” spacing between TDEM measurement points has been set at 200 meters. As defined in the 3.3.4 section, the chosen loop size is 50 by 50 meters. The major consequence of choosing the 200 m spacing as a compromise is that structures below 50m wide cannot be reliably mapped by the TDEM survey. Further studies are needed to estimate the lateral detectability of small-size clay layers using a 2D modeling approach, not used in this study.

The research area encompassed various topographical features, each with distinct land characteristics, where geophysical surveys were conducted from the right bank of the Saigon River in the Cu Chi district (“CCxx” points) to Ben Cat in Binh Duong Province (“BCxx” points) separated by the Saigon River in between Figure 3.35. These included highland regions, predominantly rubber plantations hosting long-standing industrial trees like rubber, accompanied by shrubs. The subsequent survey zone comprised areas with short-cycle crops, focusing on two observable crop types: sugarcane and maize. A more challenging access zone for investigation was the paddy field area, characterized by flood-prone conditions and primarily cultivating rice and fruit-bearing trees. Additionally, the dense vegetation areas adjacent to rivers were selected for study to explore the interaction between the groundwater layer and the river. In line with the diverse topographies described above, the geophysical surveys, including TDEM investigations, were carried out at over 315 measurement locations. Some soundings were conducted with loop sizes of 25x25 and 100x100m². Notably, the majority of soundings employed a loop size of 50x50m², which was found to be adequate for exploring the water-bearing layer and the potential presence of surface clay in the study area. These TDEM measurement points were widely distributed throughout the research area, encompassing even the most challenging zones, such as the paddy fields.

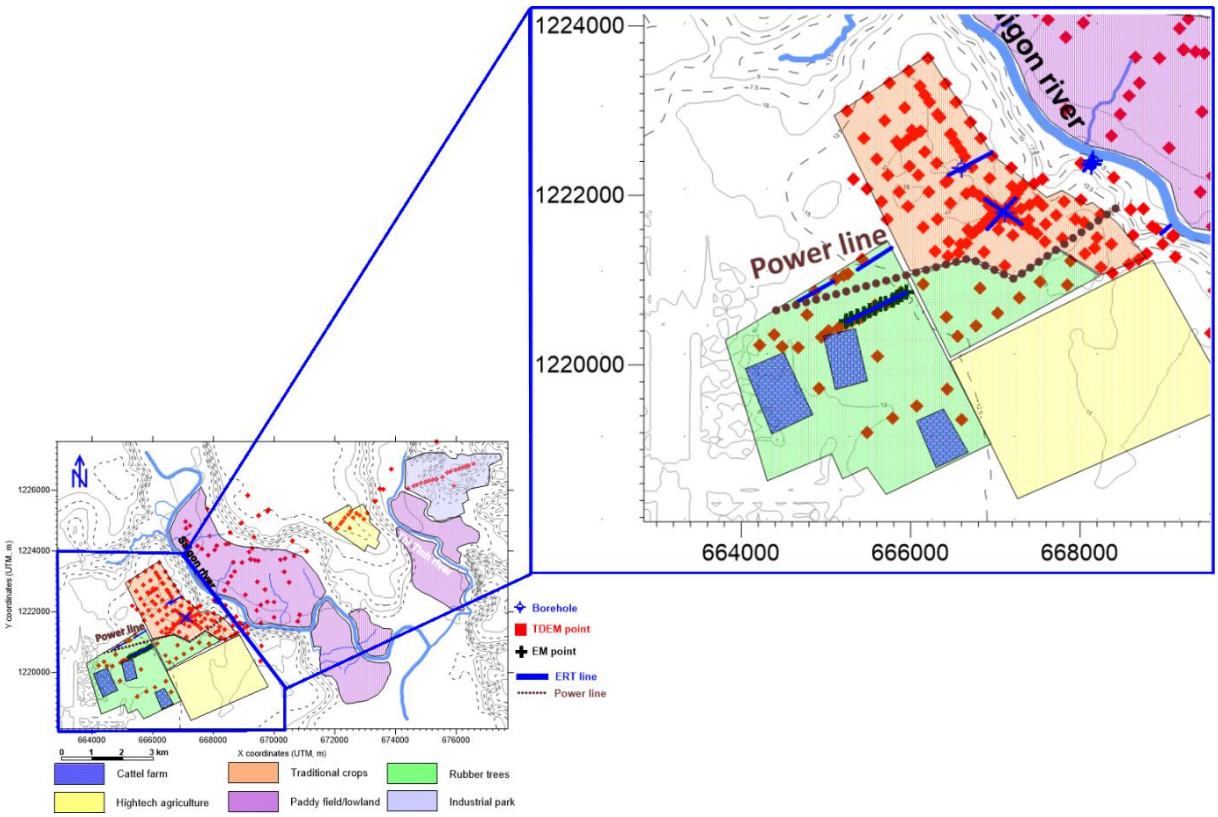

Figure 3.35 Study area with TDEM, ERT, and EM survey location.

3.7.2 Test sites for detailed investigations

Several hydrological and geological questions are raised and tackled at a smaller scale for studying in detail Figure 3.36.

First, we needed to confirm the presence of shallow clay within 10 m from the surface. Second, as some laterite layers have been seen by previous studies (Pham, et al., 1994) and hydrogeologists (Vuong, et al., 2016) and also encountered in our borehole between 5 and 10m deep, we needed to confirm the lateral continuity of those layers, as they may play a role for shallow hydrological processes. Last, third, the river-aquifer geometry is not known and could be tackled by surveys close to the river (a cross-river survey was considered since the beginning but remained unachieved for now). The test sites are as follows and located all on the Cu Chi side:

- A rubber tree plantation site
- A laterite outcrop site
- Two Boreholes BH4 and BH5 test sites
- Two river sides test sites

FEM surveys were conducted to assess the presence of shallow clay layers on the surface in the research area. Due to constraints, FEM surveys were only possible at two measurement lines in the Cu Chi area, covering both the rubber tree and short-term crop planting areas, for comparison with ERT and TDEM results. The distance between survey points on each line was 50 meters, with varying electrode separations of 10, 20, and 40 meters. Measurements were

taken with the measuring instrument aligned horizontally and perpendicular to the Earth's magnetic field.

Subsequently, ERT data were collected along the same survey lines as the FEM surveys, in combination with TDEM survey points. Through comparing the results from all three methods, we identified locations for borehole surveys (BH4 and BH5) to verify the geophysical results and conduct pumping tests. Comparative analyses of TDEM, ERT, and FEM were conducted in the rubber tree area, and another survey point was selected in the BH4 area, involving ERT, FEM, and TDEM. Additionally, at BH5, we compared ERT and TDEM to re-evaluate the subsurface geology of the area and assess the lithological characteristics. Two ERT survey lines were conducted along the riverbank area to confirm the presence of high-conductivity sediment layers at the surface. The objective was to determine the interaction between the Saigon River and the water-bearing layer within the research area to confirm the presence of high-conductivity sediment shallow layers on the riverbank area of the Saigon River.

The measurement activities shown in Figure 3.37 include TDEM, ERT, EM34 survey, and borehole logging.

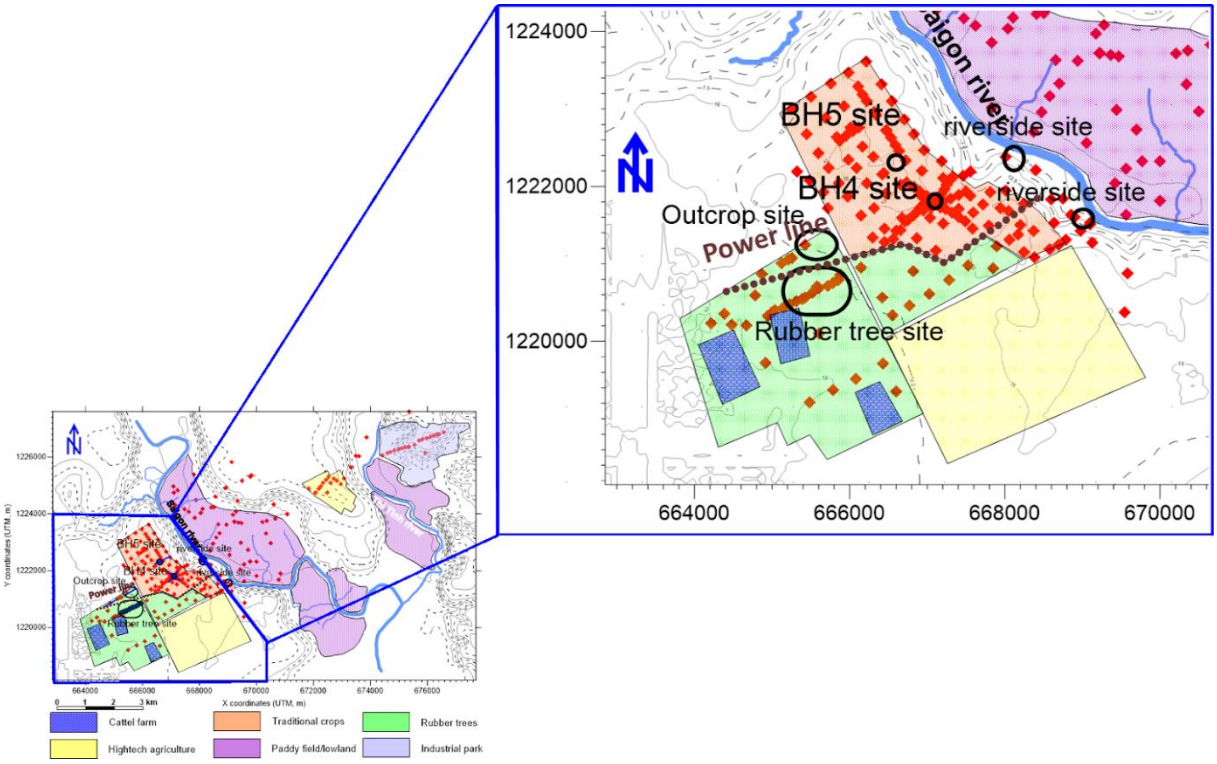

Figure 3.36 Local site for detailed investigation

Figure 3.37 Geophysical measurements include TDEM, EM34, MRS, ERT, and well logging.

CHAPTER 4. AQUIFER AND AQUITARD GEOMETRY CHARACTERIZATION

This chapter presents the results to answer the first series of hydrogeological questions raised in the introduction (and chapter 2) regarding mainly the aquifer geometry estimation:

> How are organized aquifers and aquitards layers in the first 150 m of the subsurface? Are the clayey layers (aquitards) extending laterally and separate aquifer layers, or are they continuous? This question is mostly addressed on a large scale using the main geophysical method, TDEM.

> Is there a continuous clay layer at the surface (as displayed by hydrogeologists) that protects the first aquifer from surface pollution? This question is addressed not only with TDEM but also on a smaller scale using ERT and FEM

> What are the types of sediments encountered? This question is addressed when discussing the geophysical results using grain size analysis and other laboratory and field observations

> What is the river-sediment geometry in the vicinity of the river? This question is partly addressed on a smaller scale using ERT and FEM.

Discussions will revolve around their formation processes, leading to hypotheses about their characteristics and assessing the vulnerability of the aquifer to pollution within the research region.

4.1 TDEM for large-scale aquifer and aquitard mapping

Due to its sensitivity to low-resistivity layers, the TDEM survey was primarily dedicated to mapping the clay layer extension by determining, using 1D models, the thickness and distribution of clay layers. The interpretation of 1D layers is then gathered to build the resistivity cross-sections and contour maps of resistivity according to depth in the study area. Besides, the result should help in detecting the geometry of possible ancient channels of the Saigon River in the past (if any) and therefore could give clue guidelines to understand how the sedimentation is organized in the sub-surface.

4.1.1 TDEM maps at different depths

We conducted interpretations for all TDEM measurement points within the research area, including loop sizes of 25x25, 50x50, and 100x100 m². During the interpretation process, we determined the depth of investigation (DOI) as described in chapter 3. We built a dataset that represents the distribution of electrical resistivity values by (X, Y) coordinates and depth at the survey points. This dataset was then integrated into Surfer 9 software (Golden software) using kriging (using a standard linear variogram) to create contour maps that illustrate the spatial distribution of electrical resistivity values in the research area. The resistivity maps were drawn at depth intervals of 5 meters for different depth levels ranging from +10 asl to -35 meters. Subsequently, the depth spacing between resistivity maps is 10 meters from -40 to -150 meters. In total, there are 22 resistivity maps distributed across depths from +10 meters to -150 meters asl. As an example, we present and analyze in this chapter five resistivity maps at +10 meters, 0 meters, -30 meters, -70 meters, and -130 meters in Figures 4.1, 4.2, 4.3, 4.4, and 4.5. The other maps at other depths are in appendix 2.

We took advantage of having a preliminary description of the sediments made by the driller as well as a resistivity logging in 2 boreholes (BH4 and BH5). We have considered that the conductive values from 5 to 120 Ω.m reveal clayey, silty, and loamy sediments. Below the values of 25–30 Ω.m, according to logging results (see chapter 3), the layers are clearly clayey. In addition, an outcrop resistivity measurement has been done in dark muddy sediments on the river's banks, both at the Cu Chi side (right bank) and Ben Cat (left bank), and the resistivity measured is 25 Ω.m. Thus, we can hypothesize that these muddy sediments are clayey and typical for bank and floodplain deposits, and probably river bed. In the maps, this resistivity range below 25 Ω.m is represented by colors ranging from violet to dark blue and light blue. Above 120 Ω.m more resistive layers (displayed in green, yellow, and red colors) may correspond to more silty to sandy aquifers. In the logging, the aquifer appears to be resistive, at least above 120 Ω.m and even reaching a value of more than 2000 Ω.m.

In the surface resistivity map at +10m elevation (Figure 4.1), we observe the following regions: In the Cu Chi area (on the right bank of the Saigon River, W and SW of the investigated area), the entire surface is covered by a layer of high-resistivity sedimentary deposits, characterized by electrical resistivity values ranging from 200 to 2000 Ω.m. These values are represented by a spectrum of colors ranging from green to orange and red. This indicates that at the surface level in this surveyed area, there is a complete absence of conductive clay or silt layers. The part along the Saigon River bank has no data due to its low elevation. In contrast, in the Ben Cat area (on the left bank of the Saigon River, NE direction) at an elevation of 10 meters, the surveyed area contains only a few points that are present at +10 m and feature high electrical resistivity values spanning from 200 to 2000 Ω.m. in Ben Cat also, no clays are seen at this altitude.

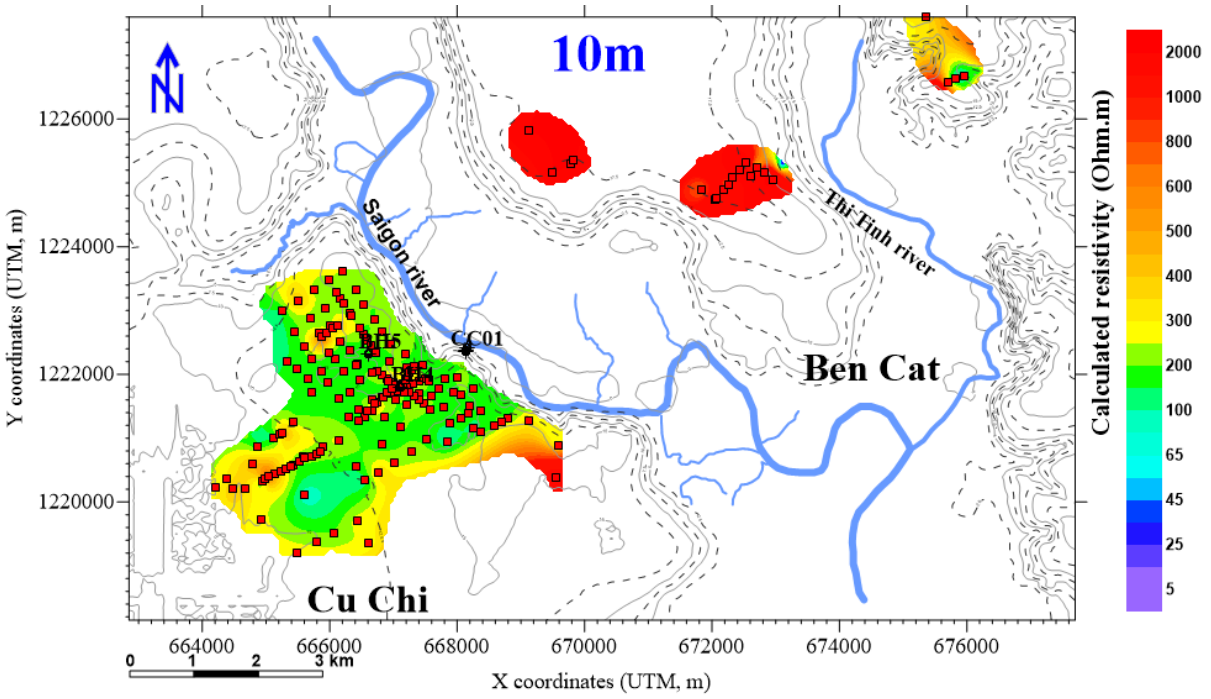

Figure 4.1 TDEM resistivity contour map at elevation +10m above sea level.

Red squares indicate the location of TDEM data points. The study region is split into two segments: the Cu Chi area is positioned on the left bank of the Saigon River in the southwest (SW), while the Ben Cat area is situated on the right side in the northeast (NE). In Ben Cat, only a few points are at +10 m high that explains why there is almost no data displayed.

The resistivity map at an elevation of 0 meters is presented in Figure 4.2. We observe distinct patterns in the Ben Cat and Cu Chi areas: in the Ben Cat area, the resistivity map displays resistivity values within the range of 5 to 25 Ω.m. These colors signify the presence of floodplain deposits. As we move towards NE in areas with higher elevations, the electrical resistivity values gradually increase. The highest resistivity value recorded in this region reaches 2000 Ω.m, represented by colors ranging from green to red. The boundary between the low resistivity zone (violet to dark blue) and the high resistivity zone (green to red) coincides with the 2-meter elevation contour. This boundary indicates the boundary of the current Saigon River floodplain.

In contrast, the Cu Chi area predominantly exhibits a color gradient from green to red on the resistivity map, corresponding to electrical resistivity values fluctuating between 200 and 2000 Ω.m. This suggests that, for the most part, the Cu Chi area lacks clay or silt layers down to a depth of 10 meters. However, in a small area adjacent to the Saigon River and within paddy fields at low elevation, we observe the presence of a conductive layer similar to the Ben Cat side, indicated by colors in the violet to dark blue range.

In summary, the resistivity map at an elevation of 0 meters reveals significant geological and hydrological insights. The Ben Cat area showcases a clear transition from low resistivity (indicative of floodplain deposits) to higher resistivity values as elevation increases. This demarcates the Saigon River floodplain boundary. The Cu Chi area is characterized by a relatively uniform distribution of moderate to high resistivity values, indicating a lack of clay or silt layers down to 10 meters, with only localized areas showing conductive features near the river and paddy fields.

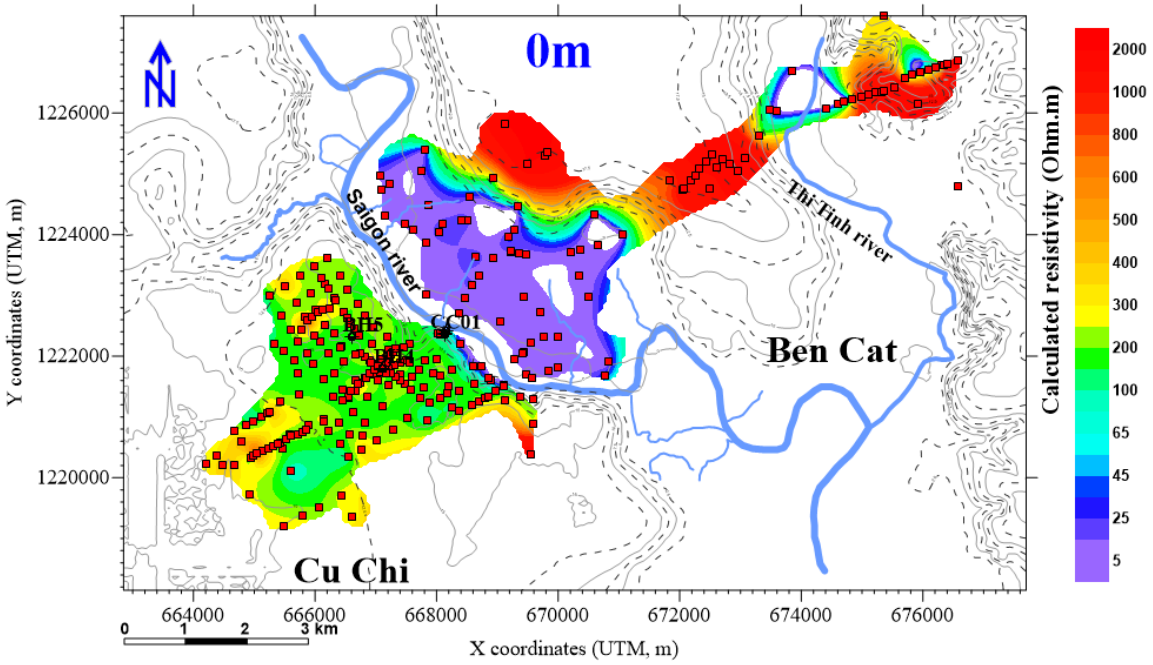

Figure 4.2 TDEM resistivity contour map at elevation 0m.

The black line delineates the boundaries between the low resistivity zone (< 120 Ω.m) and the high resistivity zone.

The resistivity map at a depth of -30 meters reveals a clear contrast between the Ben Cat and Cu Chi areas in Figure 4.3.

In the Ben Cat area, the entire region is depicted in shades of red, with a small section along the river highlighted in green. This indicates that at a depth of 35 meters, the Ben Cat area is predominantly characterized by high-resistivity sedimentary sediments and corresponds to a loamy to sandy aquifer. The electrical resistivity values fluctuate from 200 to 2000 Ω.m, with most of the area exceeding 1000 Ω.m. Conversely, the Cu Chi area features a significant portion covered in violet to dark blue, indicative of deep riverbed sediments and floodplain sediments, corresponding to resistivity values ranging from 5 to 25 Ω.m. The presence of a conductive layer at -30 m is confirmed at the test site of borehole BH4. The remaining area is primarily displayed in shades of green to orange, with resistivity values varying from 100 to 600 Ω.m, representing the aquifer layers identified also in BH4 between the surface and -25m.

In Cu Chi, the conductive layer doesn't cover the entire area, while the Ben Cat area exhibits continuous coverage by sand layers, with a notable absence of clay. We hypothesize that at a depth of 30 meters, an ancient Saigon River riverbed was dug entirely within the Cu Chi area. This may signify a change in the morphology and transformation of the flow and activities of the Saigon River from the past to the present. This hypothesis will be further discussed.

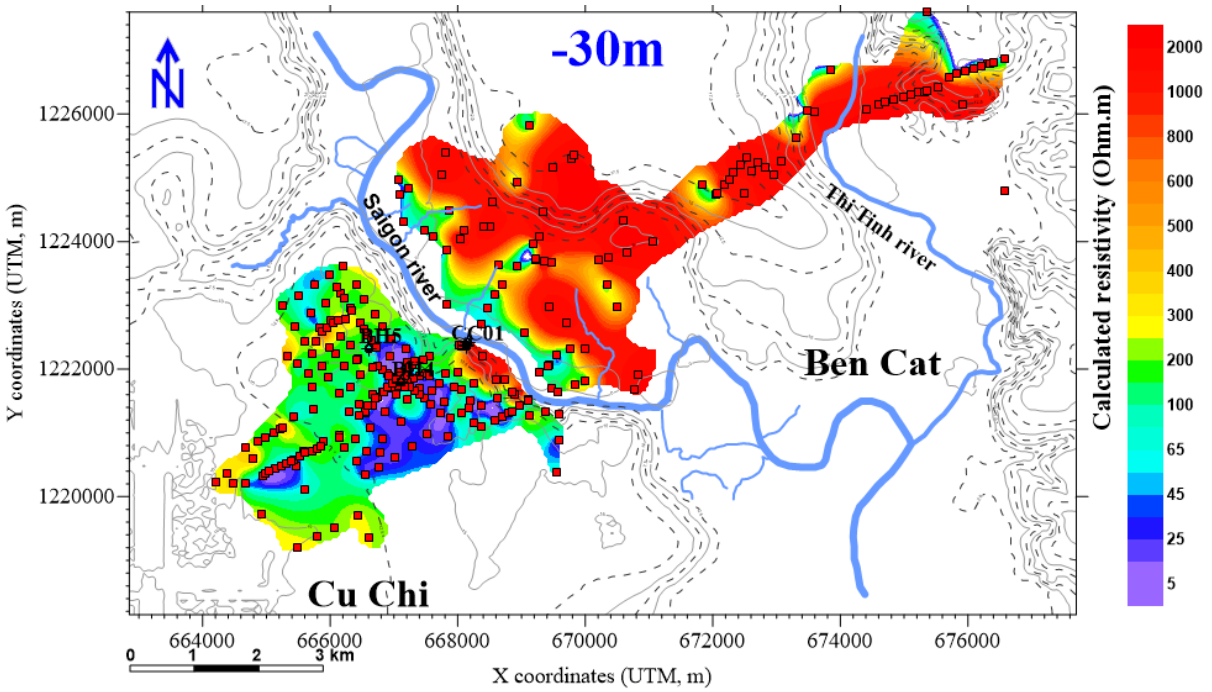

Figure 4.3 TDEM resistivity contour map at depth -30m below sea level.

The electrical resistivity map at a depth of -70 meters Figure 4.4 reveals layers of sediment with resistivity ranging from 5 to 120 Ω.m. High electrical resistivity characterizes the aquifer layers in the research area, represented by colors ranging from green to red, with resistivity values ranging within the range of 200 to 2000 Ω.m in both the Cu Chi and Ben Cat regions.

Furthermore, at this depth, we note that an ancient channel (oxbow) is seen from right to left bank crossing the current river bed direction, in continuity from Cu Chi to Ben Cat, confirming our logic of interpretation. Therefore, it can be concluded that over time, the Saigon River has undergone multiple changes in its influence domain, affecting both the Ben Cat and Cu Chi areas. This led to a complex ancient river bed and flood plain geometry, changing the Saigon River system with time and as a consequence of the aquifer structure.

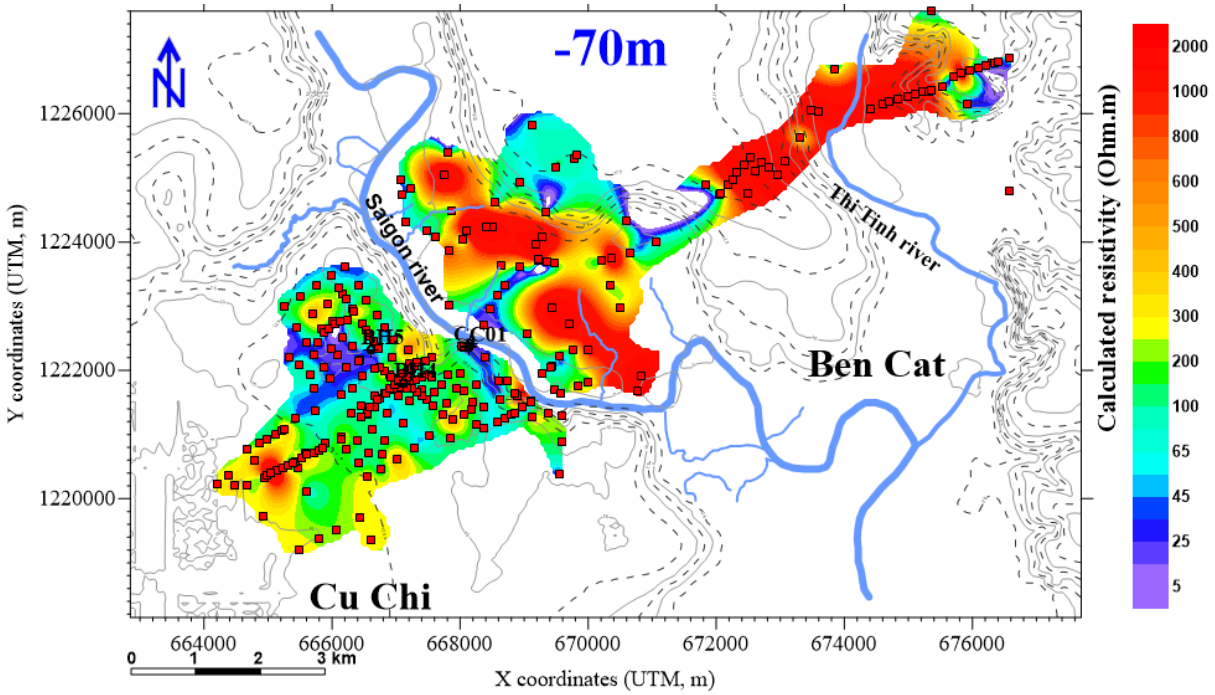

Figure 4.4 TDEM resistivity contour map at depth -70m bsl.

The ancient meander system channel, oxbow and meandering are underlined with red lines

The resistivity map at a depth of -130 meters Figure 4.5 continues to show the presence of an ancient meander system channel and meandering. This is depicted by colors ranging from violet to dark blue, which are characteristic of resistivity values ranging from 5 to 25 Ω.m, typically associated with clay sedimentary. However, it's worth noting that the distribution area of the resistivity map gradually narrows with increasing depth due to the limitations of the depth of investigation of the TDEM.

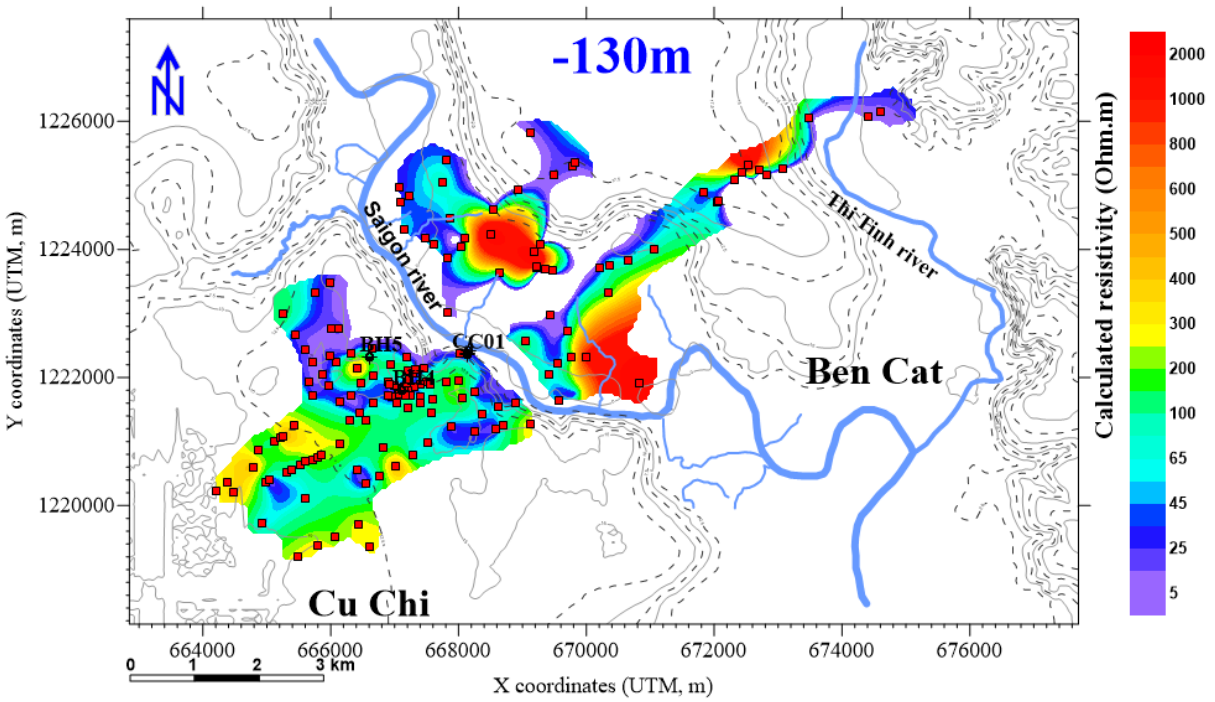

Figure 4.5 TDEM resistivity contour map at depth -130m bsl.

The ancient meander system channel, oxbow and meandering are underlined with red lines

The synthesis of electrical resistivity maps at various depths, ranging from the surface to a depth of 150 meters, in the research area is presented in Figure 4.6. This figure illustrates sedimentary characteristics in both the Cu Chi and Ben Cat areas.

In the Cu Chi region, there is an absence of conductive sediment (depicted by violet to dark blue colors, corresponding to resistivity values of 5 to 25 Ω.m) from the surface down to a depth of 20 meters. Conductive sediments start appearing at a depth of 25 meters and continue to be distributed in interbedded high-resistivity sediment (green to red colors, corresponding to resistivity values of 200 to 2000 Ω.m), which characterizes the aquifer layers, down to a depth of 150 meters. This indicates a complex sediment deposit and aquifers in the Cu Chi area.

Conversely, in the Ben Cat area, from the surface to a depth of -20 meters, both conductive sediment and high-resistivity sediment coexist. Conductive sediment is present in the low-lying areas (paddy fields), while high-resistivity sediment is found in the higher-elevation regions. From a depth of 20 meters to 150 meters, there continues to be an interbedding between conductive sediment and high-resistivity sediment, demonstrating the complexity of the aquifer system in the study area.

The TDEM interpretation maps will provide valuable information for constructing a 3D model of the entire groundwater system. Such a model (not done in the frame of this PhD) will provide valuable insights into the distribution and properties of sediments and aquifers at various depths, aiding in groundwater resource management.

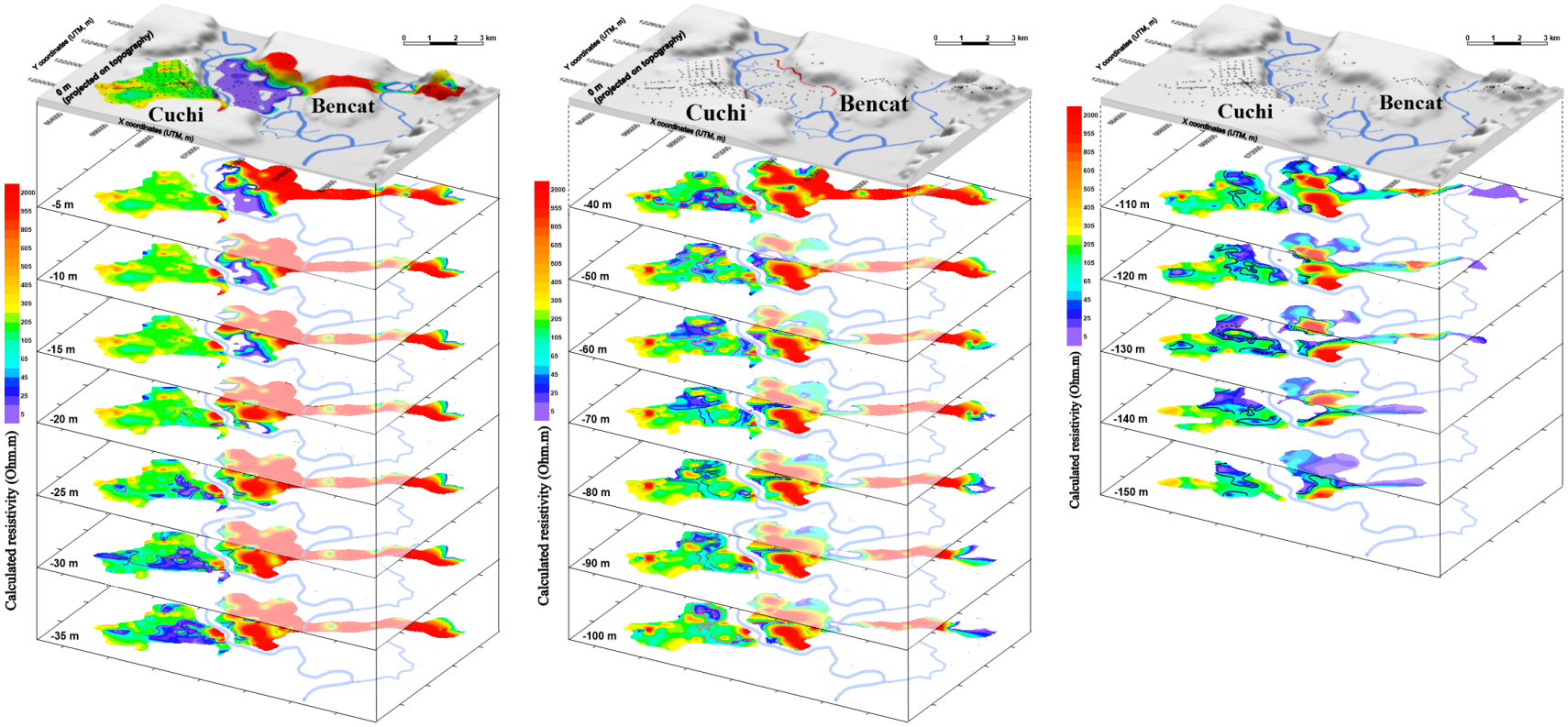

Figure 4.6 TDEM resistivity maps from 0 to -150m depth.

To show the historical evolution of the Saigon River valley from the past to the present, we present the boundary time-lapse evolution between low-resistivity and high-resistivity sediments at various depths: 0m, -10m, 20m, and 30m, as shown in Figure 4.7. This boundary is defined based on contour lines of resistivity at 120 Ω.m (a transition value between sand and clay determined from well log data-gamma ray). We simplified the color scale to represent resistivity values, making it easier to visually distinguish between high-resistivity and low-resistivity sediments as well as the boundaries between them. Clayey sediments, corresponding to resistivity values ranging from 5 to 25 Ω.m, are depicted in dark blue. Transition resistivity values ranging from 25 to 120 Ω.m are represented in light blue. Meanwhile, higher resistivity sediments, with the highest resistivity value of 300 Ω.m, are depicted in orange. Since the TDEM method is not sensitive to sediments with resistivity values higher than 300 Ω.m, we grouped all layers with resistivity values greater than 300 Ω.m into a single category, characteristic of the aquifer layer in the area. In Figure 4.7 the Saigon River valley shifts from the Ben Cat area to Cu Chi as you move from the surface to deeper depths.

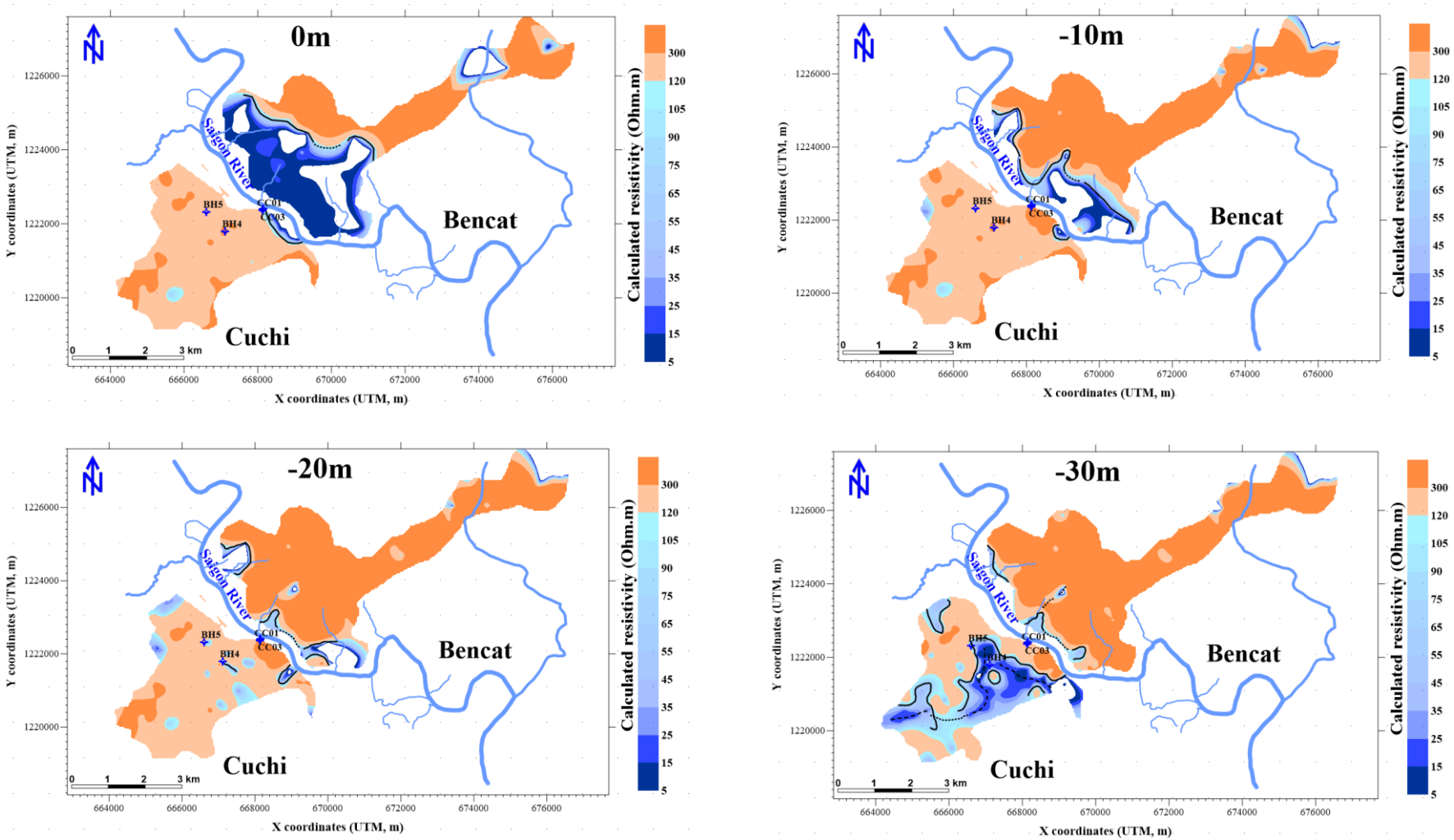

Figure 4.7 Resistivity contour maps at depth 0m, -10m, -20m and -30m with a simplified resistivity scale.

Dark to light blue indicates low-resistivity sediments (clay and silt from ancient floodplains) and orange indicates high-resistivity sediments. The black line marks the boundary between them corresponding to the location of the ancient Saigon River bank.

To provide a clearer understanding, we simultaneously display the boundary between low resistivity and high resistivity at different depths on the same map, as shown in Figure 4.8. This visualization shows the shifting boundary over time. In this representation, the arrows indicate the direction of the boundary's movement from the past to the present. Specifically, at a depth of 30m, in the past, this boundary was entirely located within the Cu Chi area. However, over time, sedimentation gradually occurred, and the course of the river changed. At present, the entire flood plain area lies on the side of Ben Cat at the surface.

From this, we can conclude that throughout the historical sedimentation activity in the research area, the Saigon River has undergone continuous migration. The characteristic feature of the river's activity is the extensive inundation area, which deposits low-resistivity sediments. To further substantiate this hypothesis, a comparison between the conductive sediments at a depth of 30m in the Cu Chi area and the surface sediments in the Ben Cat area will be presented in the discussion section.

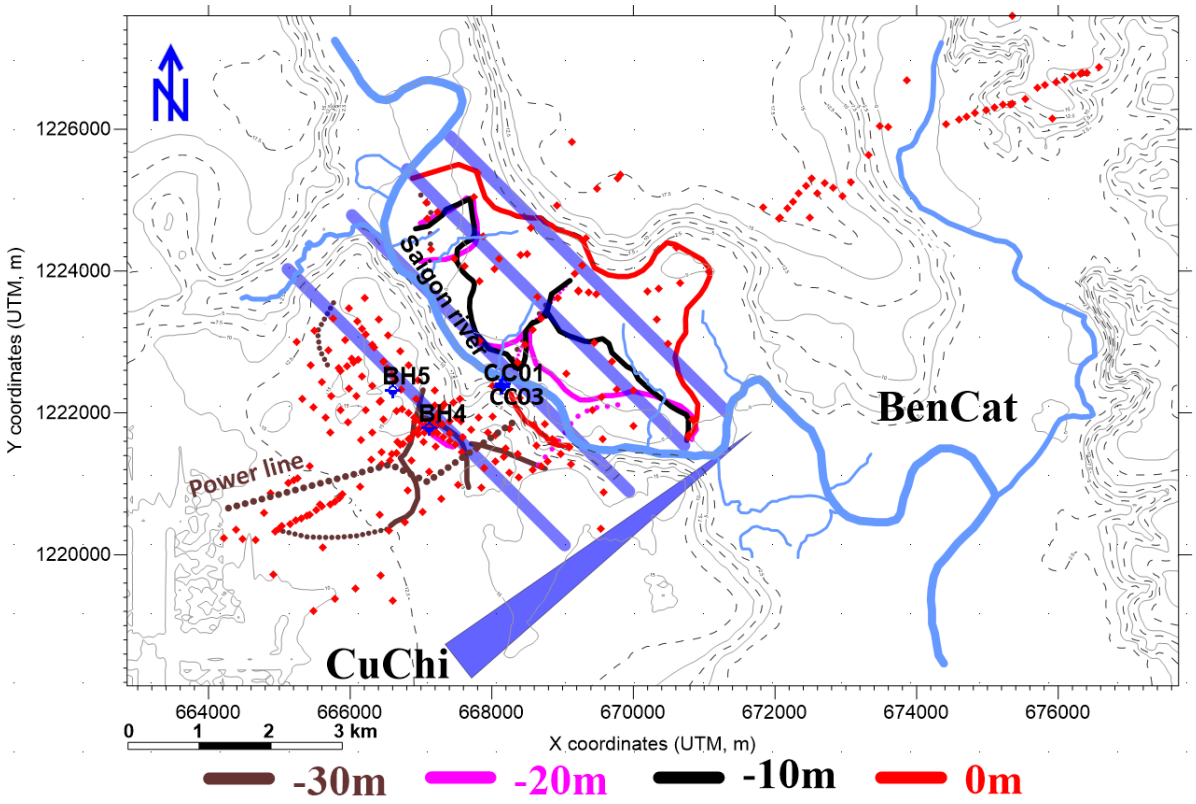

Figure 4.8 Evolution of the ancient banks limits at depths from -30 to 0m deep.

The arrow shows the direction of the evolution from the past to the present day of the left bank limit, moving towards the NE.

In summary, based on the results of the TDEM electrical resistivity map analysis in the research area, we have been able to identify the historical “footprints” of the Saigon River at different depths, reconstructing the sedimentary process from the past to the present in the region. We also have confirmed the absence of clayey layers (low resistivity) on the surface in the Cu Chi area. At depth, the complex structures between conductive layers and high-resistivity layers raise questions about the continuity of the conductive sediment (silt or clay) layers and their potential impact on aquifer continuity. These questions can be addressed

through further analysis of the variation of resistivity with depth in the study area using TDEM profiles.

4.1.2 TDEM profiles

To better understand the changes in electrical resistivity within the research area at different depths and assess the continuity of clay sediments, we have implemented a series of resistivity cross-sections across the study area to clarify this matter figure 4.9. The longest cross-section extends from the Cu Chi area to the Ben Cat area, aiming to elucidate the subsurface structure between these two regions as well as explain the contrasts on the electrical resistivity map, both at the surface and at various depths. In the Cu Chi area, we established a total of 11 cross-sections, comprising 5 parallel to the NW-SE direction alongside the Saigon River, designated as CCNW-SE1 to CCNW-SE5. Furthermore, six cross-sections perpendicular to the river in the SW-NE direction were created, denoted as CC SW-NE1 to CC SW-NE6.

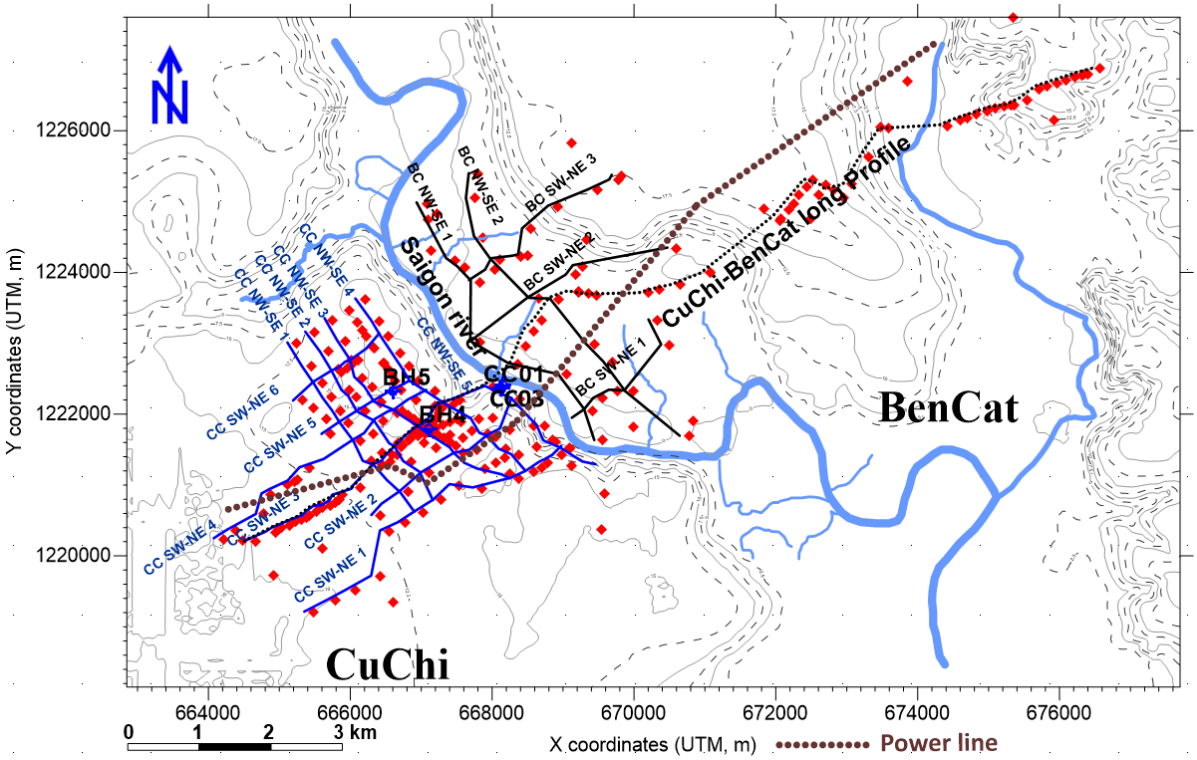

Figure 4.9 Map of the position of resistivity profiles.

In the Ben Cat area, we also constructed 5 cross-sections, which is fewer than in the Cu Chi area due to the lower density of data collection points. Among these, 2 profiles parallel to the Saigon River and are labeled as BC NW-SE1 and BC NW-SE2. Additionally, 3 cross-sections are oriented perpendicular to the Saigon River, labeled as BC SW-NE1 to BC SW-NE3.

In this segment, the PhD will present a comprehensive longitudinal profile of the Cu Chi-Ben Cat region to highlight and compare distinct sedimentary characteristics in these two areas. Specifically, the dissertation will feature three cross-sections traversing BH4 and BH5 to confirm the result of TDEM with borehole information including CC SW-NE3, CC SW-NE5,

and CC NW-SE3, additional cross-section CC SW-NE1 to show the aquifer system inland of study area.

Transitioning to the Ben Cat part, the PhD study will showcase the BC NW-SE2 cross-section parallel to the Saigon River, the BC SW-NE2 and BC SW-NE3 cross-section perpendicular to the river. These depictions aim to unravel the intricate aquifer structure prevalent in the Ben Cat region. The remaining cross-sections will be diligently presented in Appendix 3 for a comprehensive reference.

To calculate the resistivity cross sections, we used an interpolator algorithm (nearest neighbor) that avoided smooth transition between two soundings, and displayed the results as close as possible of the true inverted resistivity 1D model. This procedure produces sharp contrast between some soundings especially when dilating the vertical scale.

4.1.3 Analysis of the long cross section from Cu Chi to Ben Cat

Based on the results of the long profile displayed in Figure 4.10, we use the Saigon River to divide the area into two regions.

- The Cu Chi region, in the SW

This region is entirely absent of low-resistivity clay or silt sediment on the surface. In the first 30 meters, characterized by green to red colors, it exhibits electrical resistivity ranging from 200 to 1000 Ω.m, representing the water-bearing layer in the research area. The water table in this area is at -7 m from the surface at BH4. This confirms the absence of impermeable sediment layers on the surface and creates favorable conditions for the groundwater recharge process. It also raises concerns about the potential for contamination if agricultural or industrial activities occur on the surface, as pollutants could easily permeate and contaminate the underlying aquifer.

Besides, in a small band at the bank of the Saigon River within the Cu Chi region, there is the presence of low-resistivity clay sediment, depicted by violet to dark blue colors, with resistivity values ranging from 5 to 25 Ω.m, extending to a depth of approximately 10 meters. Immediately below this clay layer, there is a layer with a resistivity fluctuating around 200 Ω.m, indicated by the green color. So, the question arises if the Saigon River is “penetrating” into an impermeable layer or into a more sandy layer. Our work cannot answer this question because we should have performed TDEM measurements directly on water. This work has been planned for the future. If the interaction process occurs, it will impact both the replenishment of the groundwater layer and the potential risk of contaminant transmission from the river to the underlying aquifer or vice versa.

At a depth of 30 meters, we observe the presence of a low-resistivity layer with resistivity values ranging from 5 to 25 Ω.m, as. Based on borehole information and the correlation between resistivity and gamma ray value in well logging, as well as descriptions of core samples, and grain size analysis (see after in this chapter), it has been confirmed that this layer is clayey sediment. However, the distribution of this clay layer is not continuous, creating “windows” of possible hydraulic connectivity between the shallow and deeper aquifer layers, potentially posing a risk of contaminant transmission.

Additionally, on this cross-section, we observe a “valley” in the middle (between X=1000 and 2000 m) where the clay layer appears at greater depth, extending down to approximately 50 meters. Deeper, a conductive substratum is “seen” by some soundings. This geological information indicates a complex subsurface in the Cu Chi region, with potential pathways for hydraulic communication between different aquifer layers and the risk of contaminant migration.

- The Ben Cat area (left bank)

This area can be divided into two distinct zones based on elevation. The lower-lying zone along the riverbank is covered on the surface by a layer of low-resistivity sediment with resistivity values ranging from 5 to 25 Ω.m. This sediment layer characterized the floodplain areas. Immediately beneath this layer is an aquifer with high resistivity, fluctuating between 200 to 2000 Ω.m.

As we move gradually towards higher elevations, the absence of the low-resistivity sediment layer on the surface becomes apparent, similarly to the Cu Chi area. However, in the higher elevation region of Ben Cat, there is no presence of an interbedded low-resistivity sediment layer to separate the shallow and deep aquifer layers. Therefore, only a single aquifer exists above, with the majority of resistivity values above 1000 Ω.m, represented in red, accompanied by areas with intermediate resistivity values around 200 Ω.m in green. Similar to the Cu Chi area, the Ben Cat region exhibits a deep substratum with a layer of low-resistivity sediment.

This geological information highlights the distinct hydrogeological characteristics of the Ben Cat area, with a clear separation between the surface sediment layer in the lower-lying zone and the deep aquifer in the higher elevation zone, which lacks the interbedded low-resistivity sediment layer.

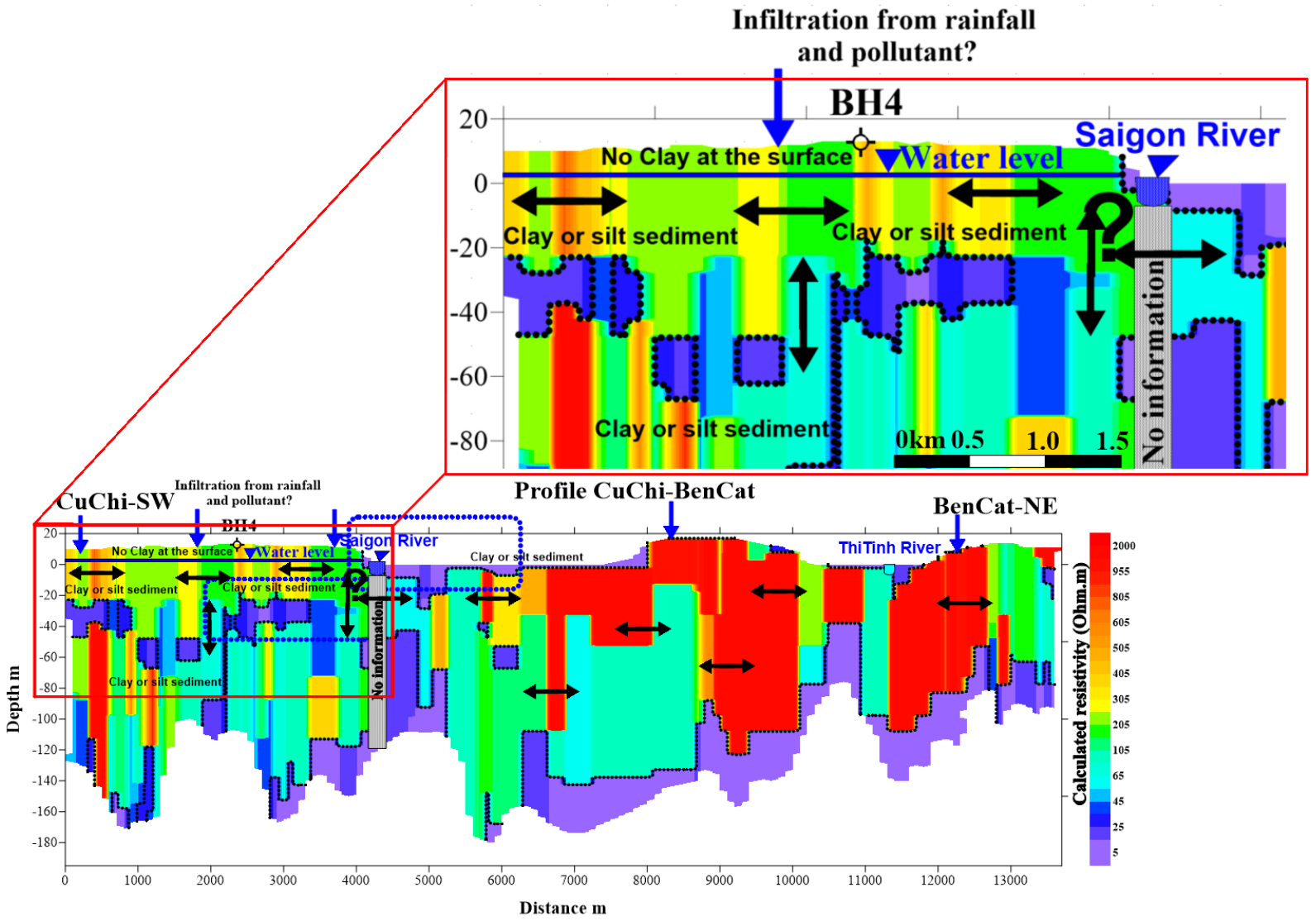

Figure 4.10 TDEM resistivity profile extending from Cu Chi in the southwest (SW) to Ben Cat in the northeast (NE)

4.1.4 Analysis of the shorter cross sections

- **In Cu Chi area**

In the Cu Chi area, there are 11 short survey lines that have confirmed the absence of a low-resistivity layer on the surface (appendix 3). Specifically, surface layers in the CC NW-SE and CC SW-NE profiles are characteristic of sediment with high resistivity ranging from 200 to 2000 Ω.m. Except for a small area near the Saigon River, which has low resistivity ranging from 5 to 25 Ω.m, depicted in shades of violet to dark blue. These results align with the resistivity maps confirming the absence of a conductive sediment layer on the surface. This indicates the potential for pollutant transmission from the surface to the underlying aquifer layers, particularly in areas with extensive agricultural activities, including traditional crops, high-tech agriculture, and rubber trees using fertilizers and pesticides. Additionally, there are farms at risk of discharging untreated waste materials outside. This also confirms that this is an area with the potential for groundwater recharge.

Figure 4.11 (profile-oriented NW-SE) illustrates the presence of a low-resistivity sediment layer starting to appear at a depth of 30m. This corresponds with the analysis results from borehole information and well logging, confirming the existence of this low-resistivity sediment layer at this depth of around 30m. This result is also confirmed through the perpendicular section CC SW-NE3 Figure 4.12, which shows that at location BH4, the clay layer is located at a depth of 30m, and the low resistivity sediment layer is absent on the surface. To further verify the accuracy of the TDEM results at section CC SW-NE5, the clay layer depth appears to be about 35m, coincide the results in well BH5 through resistivity logging and gamma-ray data.

Moreover, based on these resistivity profiles, this low-resistivity sediment layer appears to be nearly continuous laterally. It divides the aquifer into two separate layers: a shallow aquifer and a deep aquifer. This helps prevent the infiltration of pollutants from the surface to the deeper aquifer layers in the Cu Chi area. But the lateral continuity is not perfect as the layer is discontinuous. Figure 4.13 points out the discontinuity of this layer located on the left (SW) side of the SW-NE1 profile, from X = 0 to 1400m, corresponding to areas with farming activities and rubber trees. Conversely, towards the NE at a distance of 1500m to over 4000m towards the Saigon River, there is a continuous clayey layer acting as a barrier between the shallow and deep aquifer layers. Therefore, in the SW region of the Cu Chi area, there is also a significant concern about the potential spread of contaminants from the shallow aquifer to the deeper aquifer layers below, posing a major challenge in managing and safeguarding groundwater quality for the future.

Similarly, to the Ben Cat area, to assess in more detail the potential transmission of pollutants from the surface to the underlying aquifer layers, a periodic monitoring process involving water sampling in the research area is necessary to determine the mechanisms and process of pollutant transmission, but this study is not conducted in the frame of the PhD.

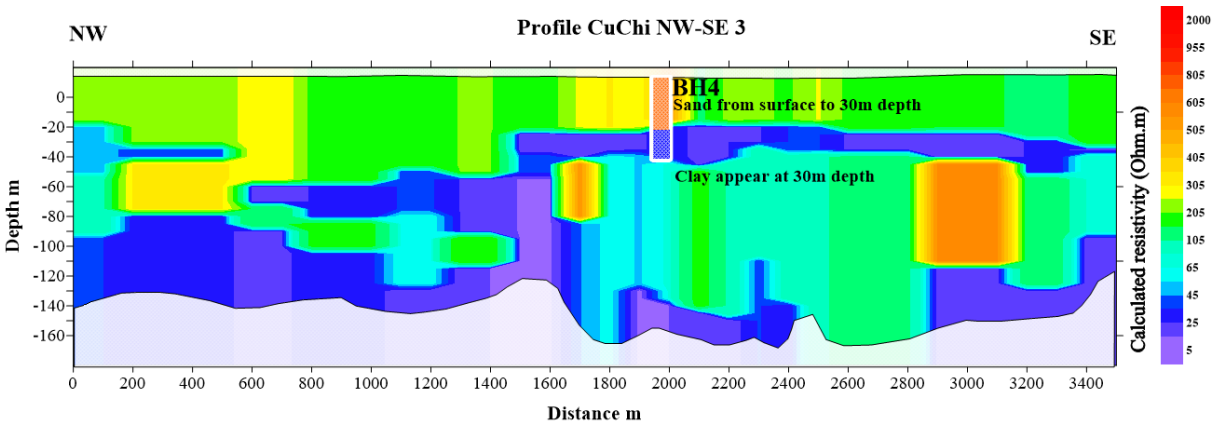

Figure 4.11 TDEM resistivity cross-section CC NW-SE3.

The TDEM resistivity results are validated using well information from BH4, including well-logging resistivity and gamma-ray measurements to identify the depth of the clay layer.

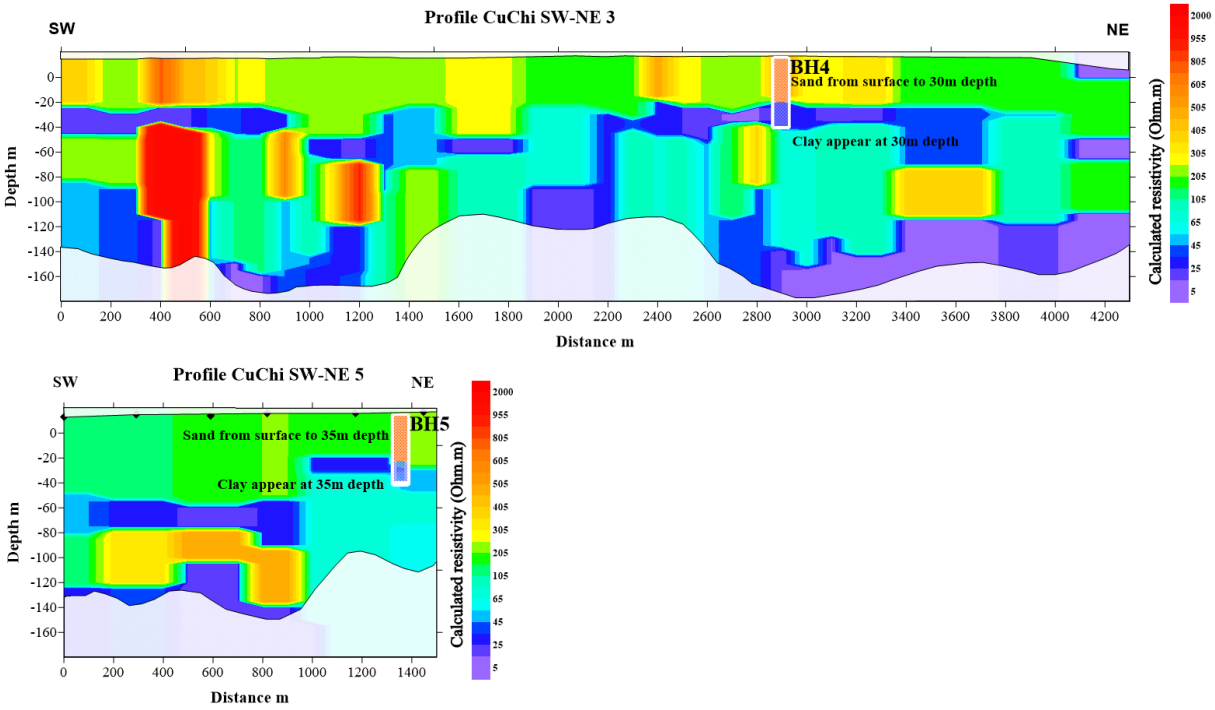

Figure 4.12 TDEM resistivity cross-section CC SW-NE3 and SW-NE5.

The TDEM resistivity results are confirmed by incorporating well information from BH4 in cross-section CC SW-NE3 and BH5 in cross-section CC SW-NE5. This validation includes well-logging resistivity and gamma-ray measurements to ascertain the depth of the clay layer.

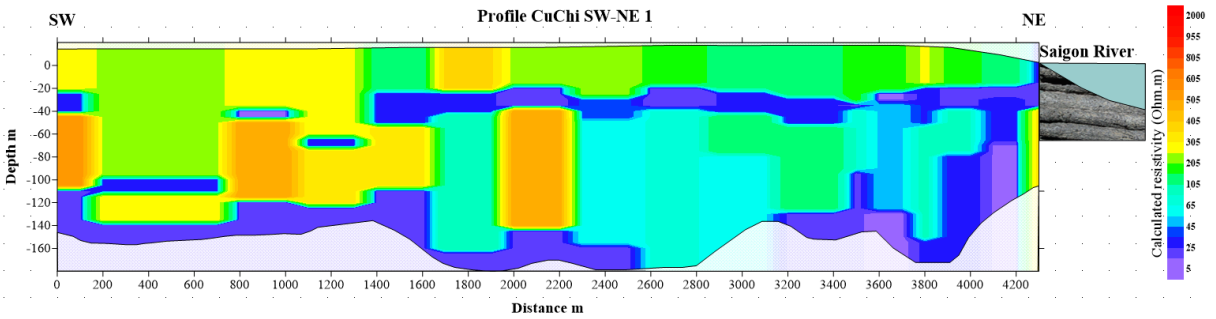

Figure 4.13 TDEM resistivity cross-section SW-NE1.

In this cross-section, the discontinuous clay is evident at depth at the southwest (SW), while a continuous clay layer is observed in the northeast (NE). Particularly notable in the NE profile near the Saigon River, low-resistivity sediments are at the surface, distinguished by a violet color.

- **In Ben Cat area**

Almost all results of short electrical cross sections in the Ben Cat area, including BC NW-SE2, BC SW-NE2, and BC SW-NE3 indicate shallow surface conductive layers in the low elevation part, characterized by resistivity ranging from 5 to 25 Ω.m violet color Figure 4.14. The presence of this surface sediment layer likely limits the infiltration of pollutants such as fertilizers and pesticides used in agricultural activities from reaching the groundwater layers below. Moreover, immediately below this layer, there is a high-resistivity layer ranging from 200 to 2000 Ω.m, displayed in shades of green to red, characteristic of the aquifer in the area. This high-resistivity sediment layer has a significant and continuous thickness, lacking the intercalation of the low-resistivity sediment layer seen in the transition from shallow to deep aquifers.

Furthermore, in the SW-NE3 line and the Ben Cat portion of the CC-BC big cross section, when moving from the paddy field area (Figure 4.9, low altitude) to the higher altitude area, the thickness of the low-resistivity sediment layer (clay sediment) covering the top surface gradually reduces and is nearly absent in areas with high resistivity (high-tech agriculture and industrial park). The absence of the sediment layer in these areas suggests the potential for pollutant transmission from agricultural and industrial activities to the aquifer below. Therefore, further in-depth studies are needed by collecting water samples for analysis of water quality to assess infiltration of pollutants.

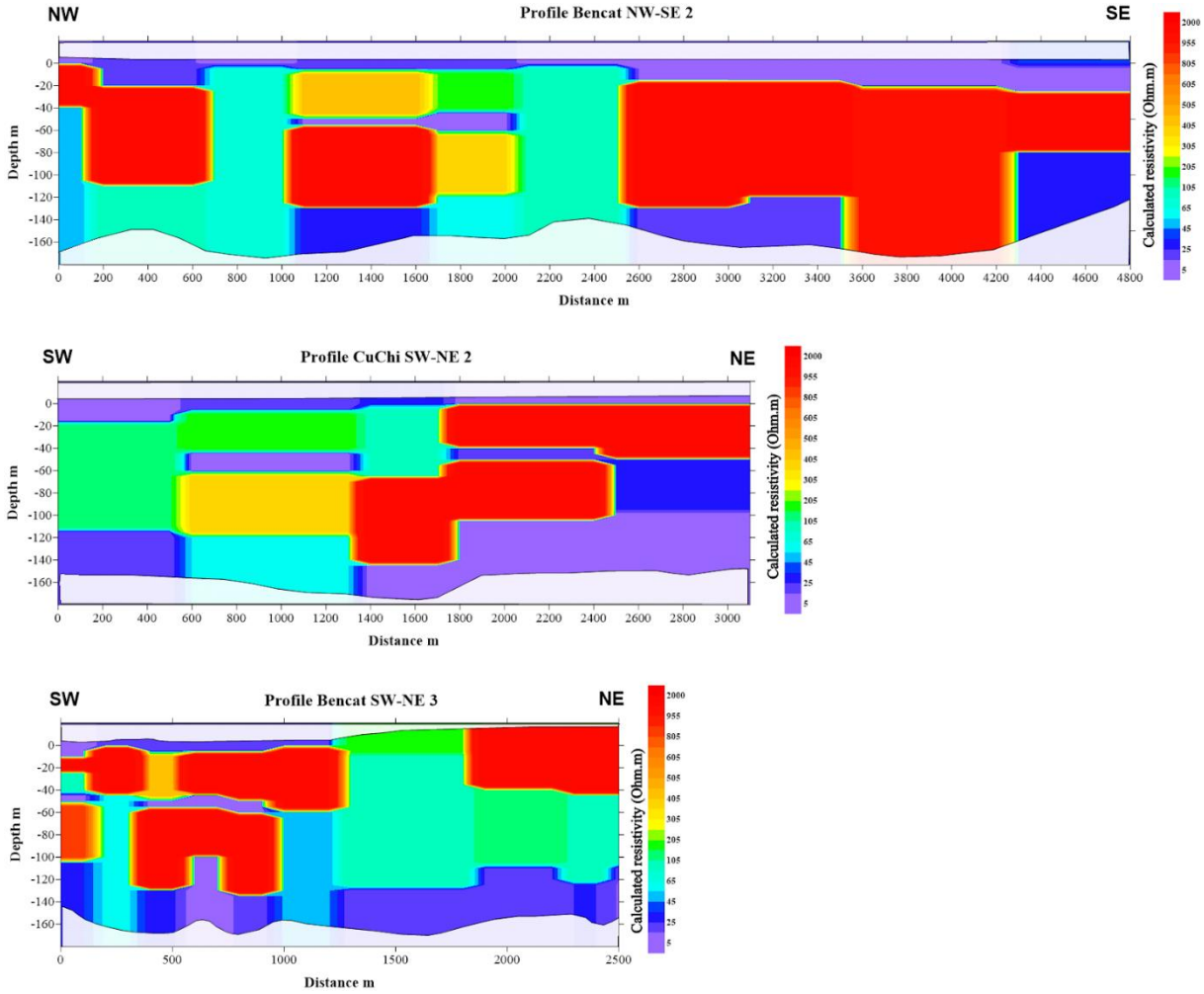

Figure 4.14 TDEM resistivity cross-section BC NW-SE2, BC SW-NE2 and BC SW-NE3.

The resistivity cross-sections in the Ben Cat area exhibit a distinct contrast between sediments with violet low resistivity values and sediments with red high resistivity values.

4.1.5 Conclusion at large scale

Based on the results of resistivity analysis from resistivity maps and resistivity profiles, it has been confirmed the absence of a low-resistivity sediment layer at the surface in the high-elevated area of the entire research area, including the Cu Chi area and the high-altitude area in the Ben Cat area. This facilitates the infiltration and recharge of groundwater for the area, but it poses a risk of spreading pollution due to agricultural and industrial activities in this area. Moreover, intercalated non-continuous layers with low resistivity pose a potential risk of contaminants spreading from shallow aquifers to deeper ones. If this is not a conductive sediment layer on the surface, what kind of sediment is it that has been previously identified as clayey sediment in prior geological and hydrogeological studies?

Only a small part of Cu Chi near the river and the entire paddy field area along the riverbank in the Ben Cat side (left bank) is covered by a layer of low-resistivity sediment on the surface attributed to clayey and silty sediments. On those surfaces, pollutants from agriculture may be washed out down to the river with surface runoff in the rain season.

Furthermore, to affirm the absence of a low resistivity sediment layer on the surface, as indicated by the TDEM method, additional validation from other techniques like ERT and FEM are necessary at a smaller scale for a better lateral sampling of the subsurface.

In addition, we hypothesized that TDEM is detecting old positions and shapes of the Saigon River. We need further detailed studies to determine the composition of these conductive sediment layers as well as the sediment formation process.

4.2 ERT, FEM results at small scale for shallow clay or laterite detection

4.2.1 FEM results on test sites

The objective of the FEM survey along the test profile in the rubber tree plantation was to evaluate if the method and EM34 equipment, employed at several coil spacing and coil orientation (-i.e. in "sounding" mode) is able a) confirm the absence of conductive layer at the surface with a small spacing between measurement points (25 m or less), b) detect the clay layer at depth, and c) detect the discontinuity of the clay layer at depth seen in TDEM survey.

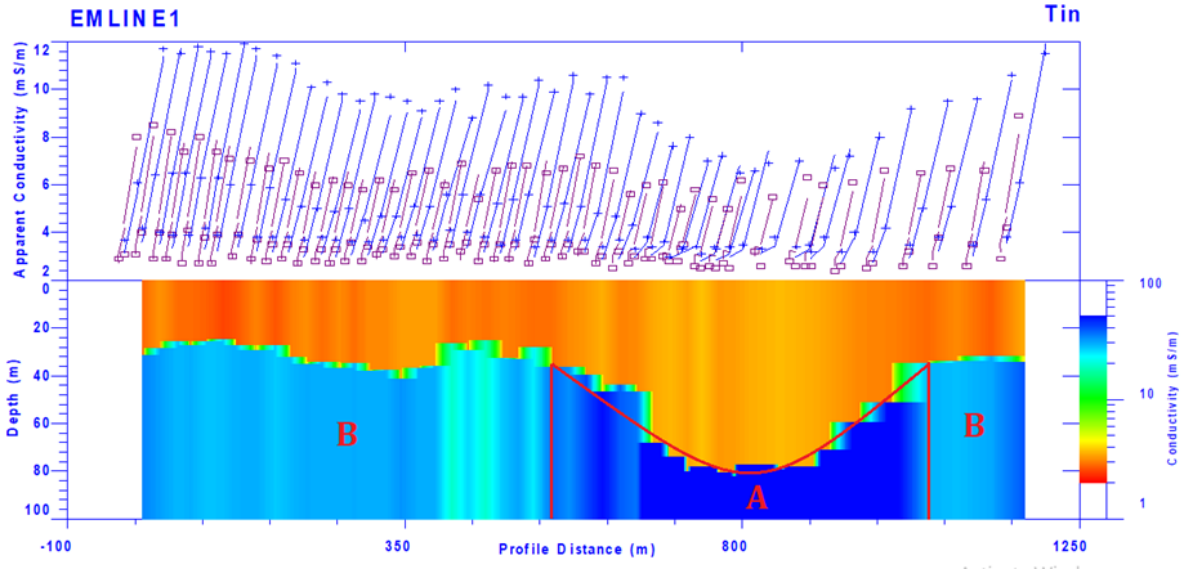

Figure 4.15 EM34 field data and interpreted result (2D model reconstructed from 1D interpretations) of EMLINE1 survey, respectively showing (A) the presence of "valley"; (B) shallower clay at roughly 30 meters.

The apparent conductivity values and the 2D conductivity model for the EMLINE1 section, shown in Figure 4.15, indicate that the section has a deep clayey layer. The 2D conductivity model was interpreted from 47 soundings with a simple two-layer solution because the two-layer solution was enough to fit the data. Some tests have been done taking the three-layer starting model used for the synthetic modeling. Even doing so, the final model displays a two-layer solution because the clayey layer present in this site is deep. Although the EMLINE1 section does not appear to have a strong effect by some source of noise at the field measurement, some fittings do not comply with an acceptable RMS of less than 5% because of the discrepancy of HMD and VMD fitting in the interpretation. Additionally, the pattern of HMD and VMD apparent conductivity data at each sounding is relatively similar; HMD and VMD show a sharp increase in conductivity with depth. Although the segment from stations 665m to 1,030m has a lower value of conductivity than the others, the HMD and VMD reading conductivities of this segment still increase with depth.

After inversion of the field data, the EMLINE1 section indicates that there is a high conductivity layer (blue zone) at depth of 30m which is an intermediate depth of the clayey layer. Along the profiles, there is no evidence of shallow clayey layers (0-15-20 m). The clayey layer underlines a resistive layer about 2.5 to 3.7 mS/m at nearly 30-meter depth. A 500-meter-long inner valley was seen at the distance between 530m and 1030 m in the section. At the valley the clay has a higher value of conductivity from 50 to 220 mS/m that the conductivity increases significantly with depth, while the ordinary value of conductivity of clay beside the valley is approximately 27 to 31 mS/m. These results may indicate that (1) there is a lateral geologic change of clay nature in the subsurface or (2) there is a problem with the accuracy of EM34 for the deep layer which is the fact revealed also by synthetic modeling in chapter 3. In both segments, the thickness of the clayey layer is not defined because this conductive layer acts as a "barrier" from deeper electromagnetic induction: any additional resistive layer deeper, if it exists, would produce too weak a signal to influence the data. We are here in a typical situation where the depth of investigation of inductive geophysical methods is limited due to the presence of conductive layers, acting like a "mask" for deeper layers. Eventually, the interpretation results of segment B are potential results according to synthetic modeling works.

- Efficiency of FEM in detecting shallow clay and laterite

The comparison of the EM34 method was made with 13 soundings of the TDEM method located near EMLINE1. Figure 4.16 shows the interface's continuity of the clayey layer from the interpreted EM34 results (pink solid line) overlapping the result of interpreted TDEM result (background) at the same scale Figure 4.16. The EM34 interface layer matches the clay's top depth of TDEM at nearly 30-meter depth, corresponding to segment B in Figure above. At the "valley" segment, the EM34 indicates the presence of clay at a deeper depth than the TDEM from 50 to 60 meters. It is similar to the statement of the synthetic modeling that EM34 is not well estimated at the clay's top depth of over 30 meters. Meanwhile, the electrical conductivity of clay from EM34 is about 30 mS/m which means the resistivity is about 33.3 Ω.m, the TDEM has a higher value of resistivity 55 Ω.m. Because the TDEM method can estimate effectively the value of resistivity of the conductive layer at shallow depth, it indicates that the EM34 result slightly underestimates the electrical conductivity of the clayey layer.

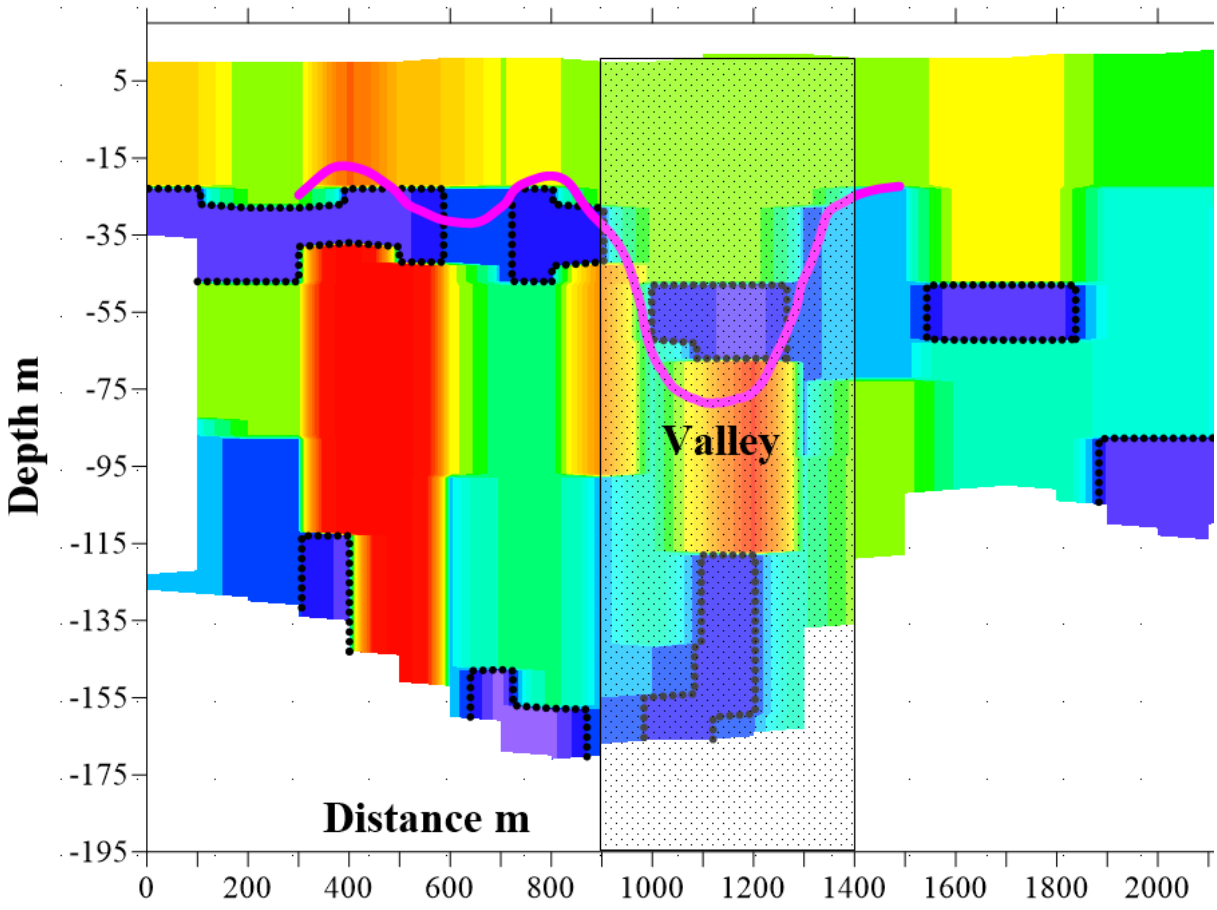

Figure 4.16 Comparison between EM34 and TDEM methods.

The interface between resistive and conductive layers of EM34 is shown with pink line on TDEM results

To summarize, the TDEM confirms EM34 with an underground "valley" in the range from X=900 to 1400 meters, but the EM34 over-estimate the depth to the clay layer. The TDEM also confirms the efficiency of the EM34 method at intermediate depth to detect clay from 0 to 50 m deep, but not the thickness of the clay. Both TDEM and EM34 results confirm the absence of the clay layer at the surface in the study area. FEM sounding appears not as suitable as TDEM for deep investigation of the clayey layer after 50-60 m. In addition, the use of FEM in sounding mode takes time in the field, time similar to TDEM layout and measurements.

The entire FEM survey, its synthetic modeling (chapter 3) and field results has been published in the first year of the work as paper "Synthetic modeling of EM34 in detecting the shallow clayey layer in aquifer system" Thanh Quoc Truong, Vietnam Journal of Construction Vol 10, 2021 (Truong , et al., 2021).

4.2.2 ERT results on test sites

Therefore, to elucidate the small-scales lateral variation of electrical resistivity horizontally within these high-resistivity sediment layers, the Electrical Resistivity Tomography (ERT) method is proposed due to its better sensitivity to such layers. The density of survey points in the ERT method yields a higher horizontal resolution compared to the TDEM and EM34 methods. A total of 10 electrical resistivity tomography (ERT) survey lines were conducted in the area, with survey line lengths ranging from 96m to over 800m, corresponding to electrode spacing of 1m (for very shallow investigation) and 5m (for deep

investigation). 96 electrodes were used. Wenner and dipole-dipole arrays were chosen for their sensitivity for horizontal and vertical changes in resistivity. Both arrays are inverted jointly. Default parameters were chosen for inversion. The results interpreted from these ERT surveys are presented from Figures 4.17 to 4.23. The information on ERT lines summarize in table 4.1

Table 4.1 Summary ERT line survey in the study area

ERT N°	**Name**	**Objectives**	**ERT lines /remarks**
1	BH4	compare all methods investigate resistivity of laterite / clay	spacing 1m and 5m
2	BH5	compare all methods investigate resistivity of laterite / clay	spacing 5m
3	"Outcrop"	evaluate the resistivity of a thick laterite layer outcropping	spacing 1m and 5m
4	"Rubber tree"	investigates the rubber tree valley for comparing the FEM and TDEM results	spacing 5m/ length of survey 1200m
5	Near river 1	investigates the boundary between aquifer and Saigon River	spacing 1.5m
6	Near river 2	investigates the boundary between aquifer and Saigon River comparing with borehole information	spacing 2m

- **Site BH4**

The ERT survey at the BH4 test sites is presented in Figure 4.17. The depth range from 0 to 30 m is characterized by high resistivity sediments ranging from 200 to 2000 Ω.m. ERT surveys confirm the absence of the surface conductive clay layer confirming at smaller scale the TDEM results. The laterite pebbles and soils encountered in BH4 between 5 and 8 m depth are not clearly "seen" by ERT. They are included into the high resistive first layer. Even with a 1 m spacing, it is impossible to discriminate between resistivity differences. Deeper at 30-40 m, the conductive clayey layer seen in the borehole is not clearly seen with ERT, displaying a conductive layer but at 100 Ω.m, four times higher than the clay. This is a confirmation of the lack of resolution of ERT at depth.

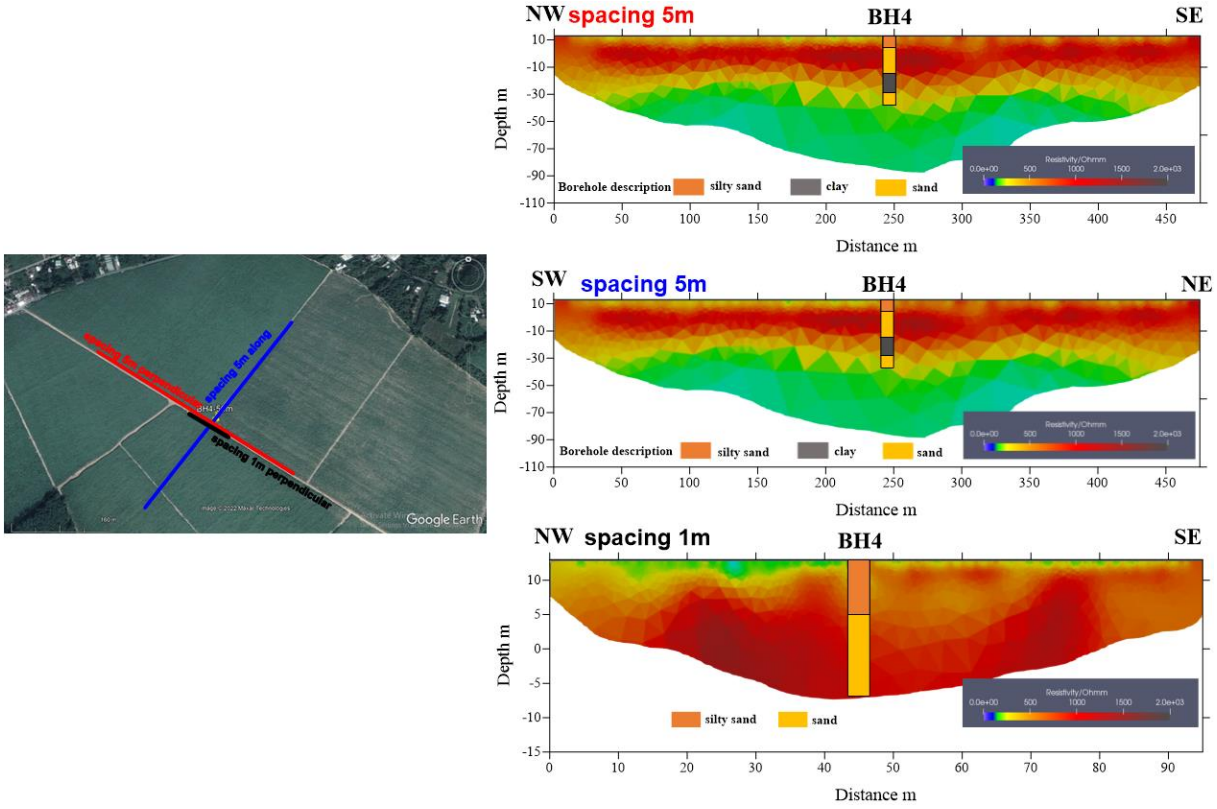

Figure 4.17 ERT results at BH4 with electrode spacing 5m to 1m.

This figure displays high-resistivity sediment at the surface, characterized by a red color.

- **Site BH5**

The ERT survey at the BH5 test sites is presented in Figure 4.18 The depth range from 0 to 30m is characterized by high resistivity sediments ranging from 200 to 2000 Ω.m. However, contrary to the BH 4 site, the resistive layer is "cut" by more conductive material at X=180 m and 400m. At X = 300 m, a more conductive zone is encountered (resistivity close to 40-60 Ω.m) that is probably not clay but a more silty zone. ERT surveys also confirm the absence of the surface conductive clay layer. Deeper at 40 m, the conductive clay layer seen in the borehole is not clearly seen with ERT as at BH5 site. The ERT image confirms that the sedimentation in the first 30 m is not as homogeneous as the BH5 site was indicating.

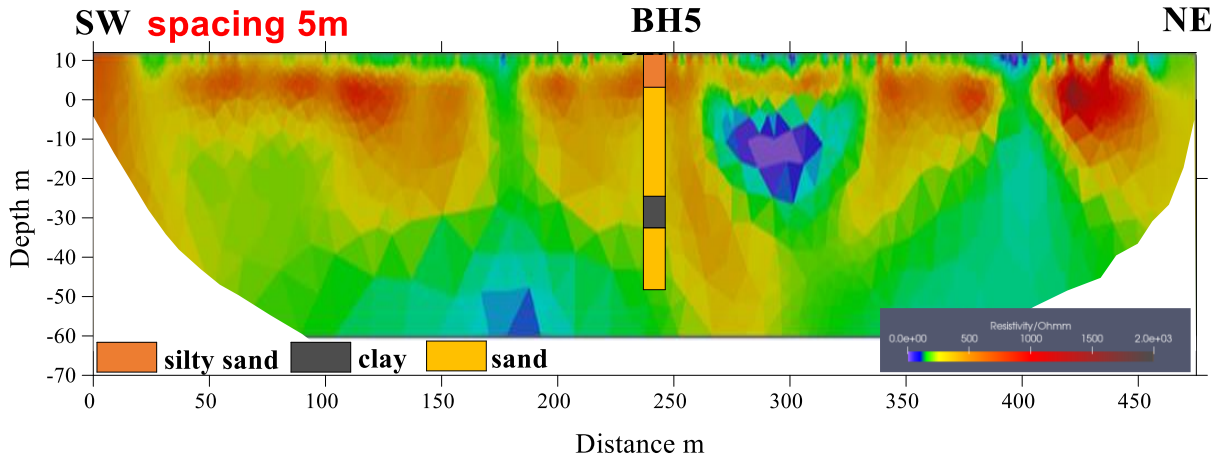

Figure 4.18 ERT results at BH5 with electrode spacing 5m

- **“Laterite outcrop” test site**

The ERT survey, similarly from the BH4 site, shows the depth range from 0 to 30 m is characterized by high resistivity sediments ranging from 200 to 2000 Ω.m appearing very homogeneous Figure 4.19. The thick laterite layer seen at the pond nearby Figure 4.20 appears as very resistive and seems continuous laterally. The weathered laterite strongly dissolves the surrounding sedimentary materials near the rock matrix, suggesting that the washed-away components non clay minerals. This is corroborated by the high resistivity observed in the ERT profile and well-log resistivity data when measured within the laterite layer.

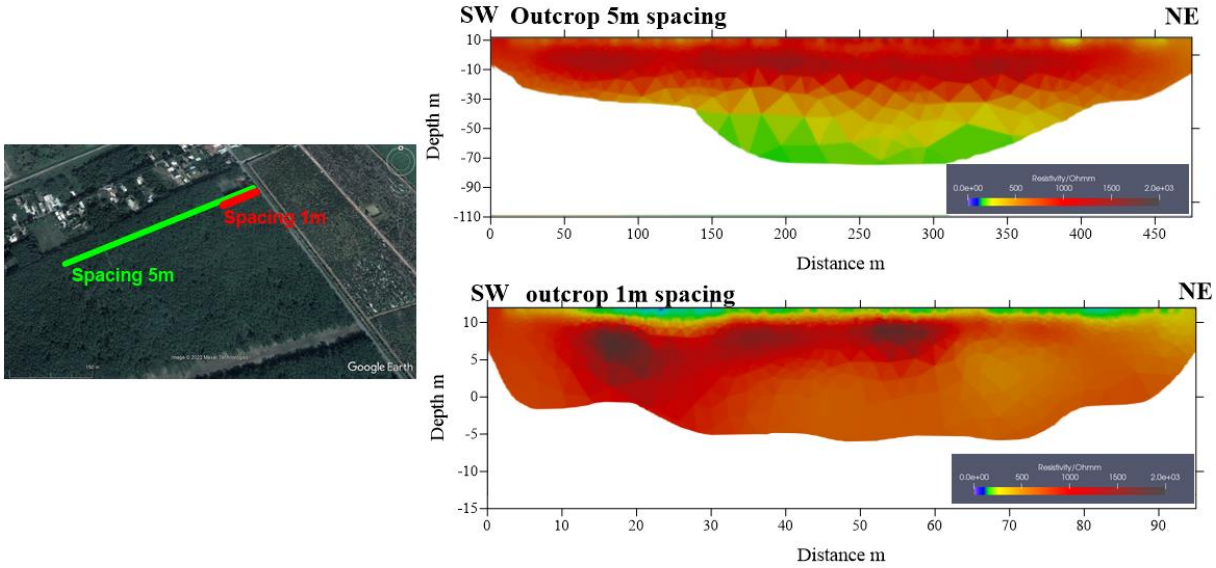

Figure 4.19 ERT results at outcrop site with electrode spacing 5m and 1m.

Figure 4.20 Laterite outcropping at the” outcrop” site.

The laterite is heavily cemented, but a large connected porosity is present.

- **“Rubber tree” test site**

The ERT measurement reveals mainly four layers, Figure 4.21. The first resistive layer is situated from ground surface to 3 to 5-meter deep whose resistivity is about 740-800 Ωm (1.25

– 1.35 mS/m). The second layer is a slight les resistive layer with resistivity roughly 630 Ωm (1.59 mS/m) and 350 Ω.m (2.85 mS/m) at some distance from 70m – 150 m. The third resistive layer is located from 10 to roughly 35m deep with resistivity about 740-1000 Ωm. The conductive substratum has resistivity from 200 to 350 Ω.m (2.85-5 mS/m). Between X=400 and 550 m, the conductive substratum is "pierced" by the third layer: We have here a clear confirmation of the discontinuity of the clayey layer, as seen as a "valley" by TDEM and EM34.

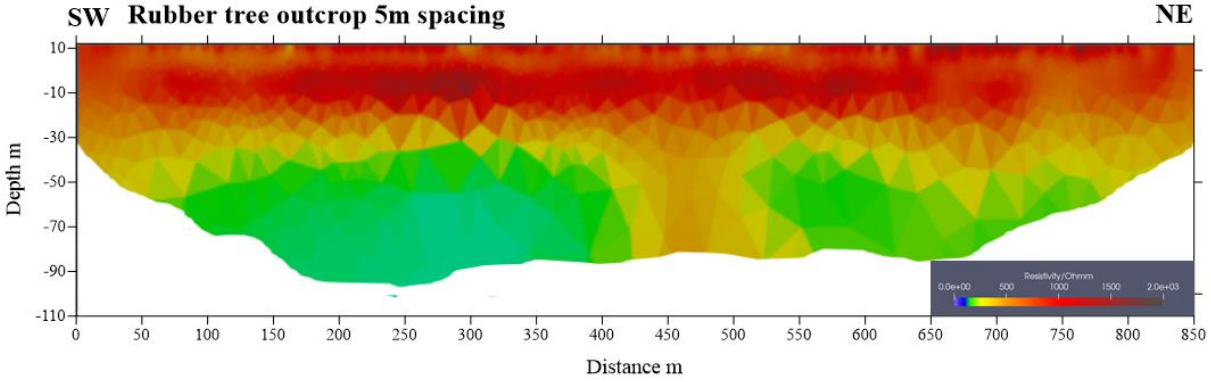

Figure 4.21 ERT results at" rubber tree" site with electrode spacing 5m

The comparison of the EM34 and TDEM method was made with the use of ERT method situated right at EMLINE1 location figure 4.22. The interface between conductive (clayey layer) and resistive layer from the interpreted EM34 results (purple solid line) overlaps the result of interpreted ERT results (background) at the same scale. An ERT interface between the resistive layer (dark red zone) and conductive (light blue zone) is also described as a green solid line. The EMLINE1 profile of EM34 method is longer than the ERT 850-meter profile in which the first and last electrodes begin at EM16 and finish at EM48. This line coincides with TDEM profile CC SW-NE3 from 700m to 1550m.

Hence, ERT method confirms with EM34 and TDEM that (1) the top depth of conductive substratum (top depth of clayey layer) is averagely 35-40 m due to the variation of the interface of ERT method, and (2) the presence of "valley" from clayey zones located from 300 to 700m long. However, the "valley" from EM34 is also deeper than the ERT and TDEM method so it reconfirms the detectability of clayey layer over 30 meters of EM34 cannot be taken with confidence. The resistivity value of ERT of the conductive clay substratum cannot be used for comparison with EM34 or TDEM because the sensitivity of ERT at depth > 30-40 m is very poor for conductive substratum. For an accurate determination of deep substratum resistivity with ERT, we would have needed to use much longer electrode spacing (up to 2 to 5 times more) to be able to get the data required for resolving the resistivity correctly. However, operating ERT with such a large survey line demands high costs and may not be suitable. Meanwhile, TDEM has demonstrated the ability to identify clay layers at greater depths and with higher accuracy. Therefore, the primary advantage of the Time-Domain Electromagnetic (TDEM) method compared to the Electrical Resistivity Tomography (ERT) and EM34 methods is its ability to better identify conductive layers in terms of depth and resistivity values.

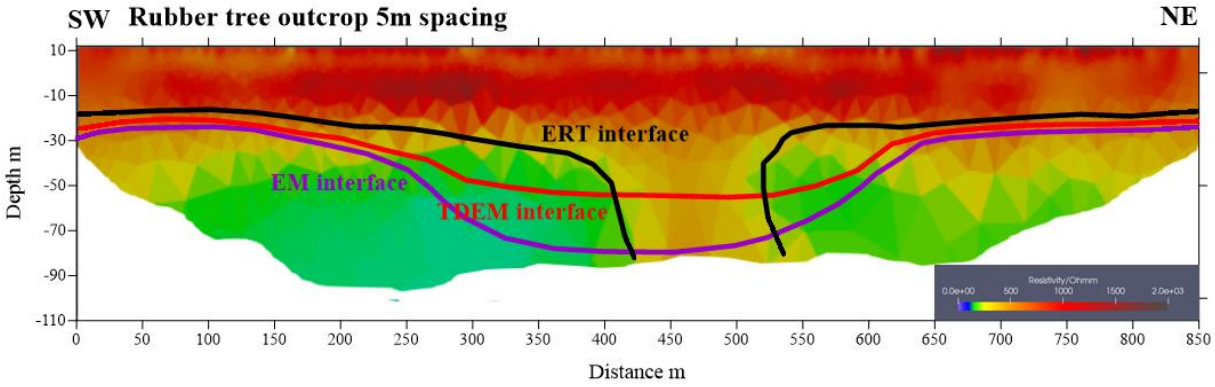

Figure 4.22 Comparison of resistivity results between EM34, TDEM and ERT at rubber tree outcrop. EM34 (purple), TDEM (red), ERT (black)

To summarize ERT results on the Cu Chi elevated plateau, the electrical resistivity tomography confirms the absence of a superficial clayey layer. These results also demonstrate the possible continuity of the laterite layer in the study area, found at depths fluctuating between 4-10m. This laterite layer is identified as a high-resistivity layer. The resistive layer from 0 to 30-40 meters appears in some sites as heterogeneous. The deep clay layer (at 50m) is not well defined by ERT (its resistivity is much higher than the resistivity calculated by TDEM) could be discontinuous. This discontinuity "paths through the clay" confirms TDEM results.

- **River bank test sites**

The ERT results at sites 1 and 2 near river right bank reveal the presence of a low-resistivity sediment layer near the surface in the vicinity of the Saigon River with resistivity values ranging from 5 to 25 Ω.m Figure 4.23 and Figure 4.24. This indicates that the interaction between the river and the aquifer may be not active laterally down to a depth of 15m. Below the river however, we cannot conclude with ERT if the river is touching the sandy-silty aquifer below or if the bottom of the river is made of impervious clayey layers.

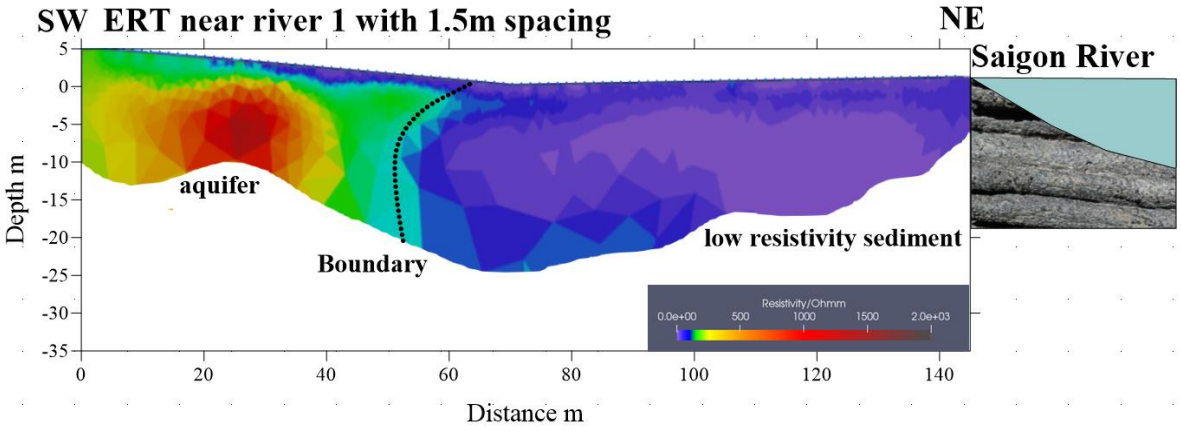

Figure 4.23 ERT line near the river 1.

This figure illustrates the boundary between high-resistivity sediment (red color) and low-resistivity sediment (violet color).

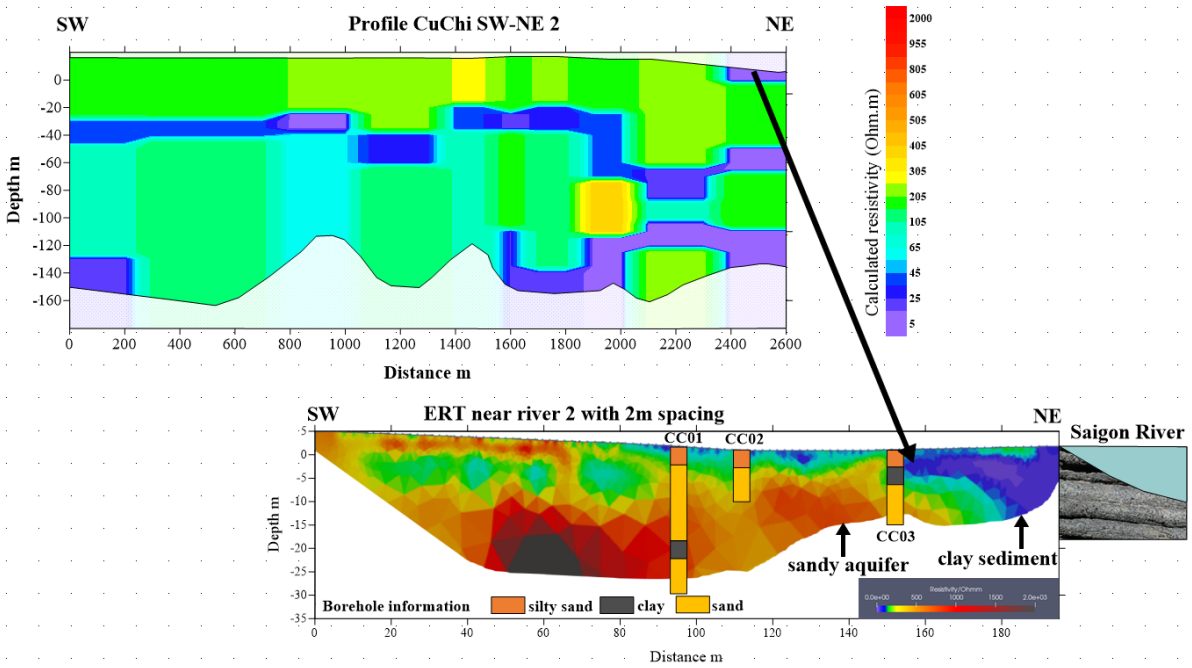

Figure 4.24 ERT line near the river 2.

Comparison between TDEM and ERT result on the river bank

4.3 Discussion

The geophysical survey results, including TDEM, ERT, and EM 34, have confirmed the absence of a clay layer on the surface in the Cu Chi side of the study area (high elevated area). However, geologists and hydrogeologists have pointed to the presence of a clay layer on the surface. This discrepancy led us to analyze soil samples collected at two locations, BH4 and BH5 sites, to confirm the presence - or absence - of a clay layer on the surface in the study area and to assess the permeability of the laterite layer. We conducted a particle size analysis using the sieve method to determine the particle size distribution in the core samples extracted from our test and confirm the presence of clay using the methylene blue staining method. Furthermore, the grain size analysis will help in making correlation with geophysical parameters and Nuclear Magnetic Resonance (NMR) presented in chapter 5.

4.3.1 Grain size analysis

The objective of the grain size analysis is to classify the petrographic composition and evaluate the nature of the sediments of the aquifer and aquitard. Besides, the particle composition analysis may determine the clay content in the formation and help in qualifying the nature of the underground meanders.

- **Sieve granulometry**

Sieve grain size analysis is a widely used method for determining the particle size distribution of granular materials, such as soil, sand, gravel, and crushed stone. It involves passing a sample of the material through a series of sieves with progressively smaller openings or mesh sizes. This analysis is typically conducted using two main methods: sieve analysis and hydrometer analysis, each tailored to different particle size ranges. According to ASTM D1921-18 standards for sieve grain size analysis. This method is employed for particles larger than 0.075 mm in diameter. It involves passing a dry soil sample through a series of sieves with

progressively smaller openings, typically using sieves with designations such as U.S. Nos. 4, 10, 20, 30, 40, 60, 140, and 200. The soil is oven-dried and any lumps are broken into smaller particles before shaking it through the sieves. The mass of soil retained on each sieve is determined, and for cohesive soils, mixing with water and washing may be necessary. The key steps include determining the mass of soil retained on each sieve, the total mass of the soil, the cumulative mass of soil retained above each sieve, the mass of soil passing through each sieve, and calculating the percentage of soil passing through each sieve. The results are then plotted on a semilogarithmic graph, creating a particle-size distribution curve.

Hydrometer analysis: This method is suitable for particles smaller than 0.075 mm in diameter. It involves creating a soil suspension in water and using a hydrometer to measure the settling rate of soil particles in the liquid. By tracking the sedimentation over time, the particle-size distribution can be determined. The hydrometer analysis is typically conducted in a graduated cylinder, and the process involves measuring the initial and final hydrometer readings to calculate the particle sizes.

A total of 32 samples were analyzed at the GEOPET laboratory for grain size composition at the BH4 site, including 9 samples from the shallow layer, 4 samples from the aquitard layer, and 19 samples from the aquifer. Similarly, at the BH5 site, 37 samples were analyzed, with 9 samples from the shallow layer, 4 samples from the aquitard layer, and 24 samples from the aquifer. These analysis results were then plotted on a ternary diagram to classify the soil based on the proportions of sand, silt, and clay in the analyzed samples, using the U.S. Department of Agriculture textural classification (USDA) Figure 4.25.

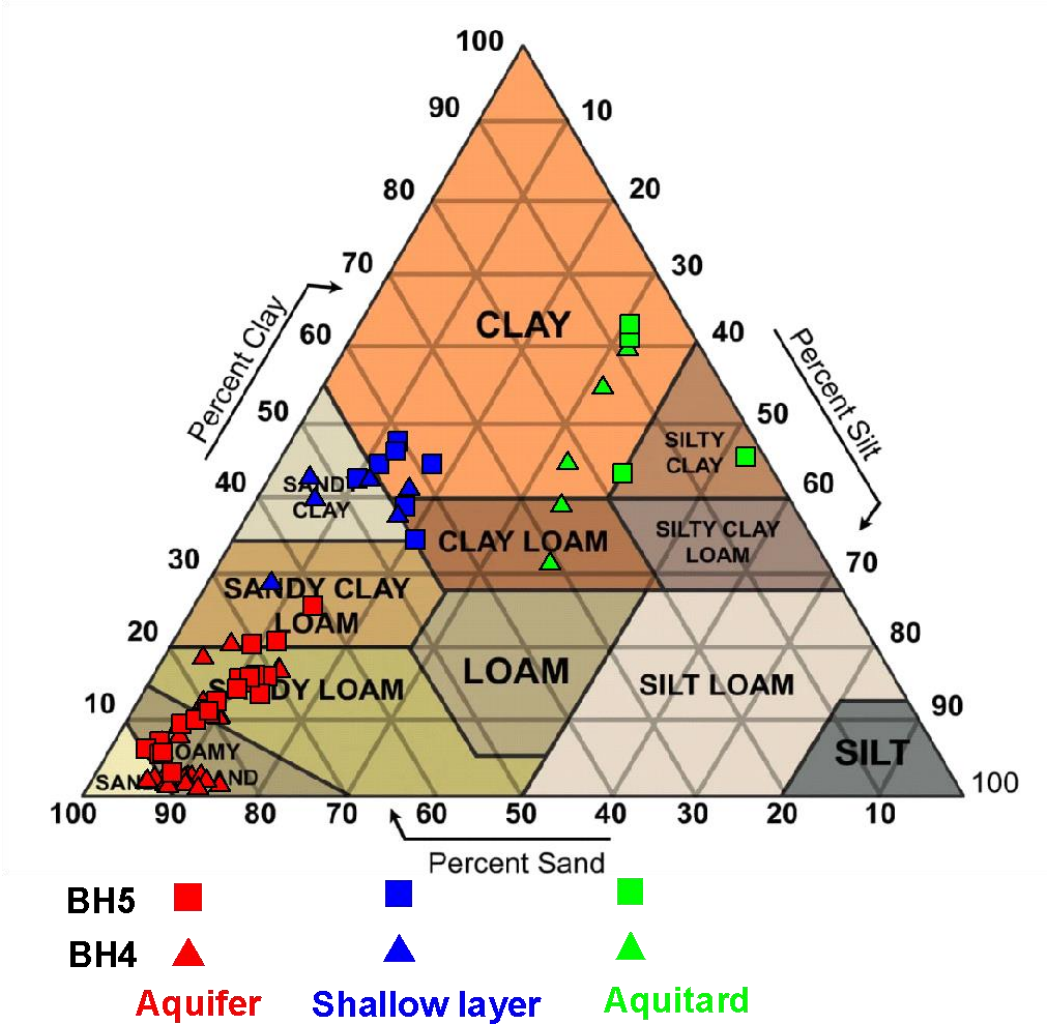

Figure 4.25 Texture triangle chart for the Sieve Grain Size Analysis to classify the soil (texture)

Figure 4.25 illustrates the soil classification results based on the particle composition. The BH4 site is represented by a triangular symbol, and the BH5 site is represented by a square symbol. The red color represents samples from the aquifer, the green color is characteristic of samples from the aquitard, and the blue color signifies samples from the shallow layer.

The analysis shows that the aquifer in the study area is classified as sandy loam to sand, with a high sand content ranging from 70 to 90%, silt content ranging from 10 to 20%, and silt content ranging from 5 to 15%. In addition, the aquitard samples have a high clay content, ranging from 40 to 60%, with sand content ranging from 10 to 20% and silt content from 30 to 40%, and can be classified as “granulometric” clay. The shallow “clay” layer seen by the hydrogeologist with the same sieve analysis appears with our sieve analysis into the category of “sandy clay”, “clay loam to clay”, with a relatively high clay content ranging from 35 to 50%, while the sand content ranges from 40 to 50%, and the silt content ranges from 5 to 20%.

To summarize, in the sieve analysis, the particle composition of the aquifer was clearly classified, ranging from sandy loam to sand, with sand being the predominant component. Particularly, the shallow layer exhibited a high clay content, ranging from sandy clay to clay.

However, there is a contradiction between the results of sieve particle composition analysis and the geophysics data results for the shallow layer. Specifically, the results of particle

composition analysis indicated that the analyzed samples fell into the “granulometric clay region”. However, the electrical resistivity values obtained from well log data were high, ranging from 300 to 800 Ω.m, and the gamma-ray values ranged from 40 to 60 cps, which is not characteristic of the clay layer at all. So, what is the actual type of sediment of these soil layers in the shallow layer?

To ascertain the presence or absence of mineralogical clay in the sediments it is necessary to conduct the Methylene Blue method test to confirm the presence or absence of mineralogic clay. Mineralogic clay produces low resistivity values, while granulometric clay may be formed by very fine particles but not always by true mineralogical clay particles. Methylene Blue will help clarify the discrepancies and confirm the true composition of the soil layers in the shallow layer.

4.3.2 Methylene Blue Method

The methylene blue test is a technique for identifying clay minerals in aggregate fines (Yukselen, et al., 2008) (Chiappone, et al., 2004). This testing approach operates on the basis of chemical reactions initiated by an excess of negative electric charges present in the clay particles and/or the ionic exchange phenomena occurring between easily exchangeable cations in the clay and the methylene blue cations released as methylene blue decomposes in water. In the adsorption process, the material undergoes specific steps to evaluate its interaction with methylene blue. First, the material is prepared by pestling in a mortar after drying in an oven at 72°C for 24 hours to ensure uniformity. A 20g specimen, featuring a grain size less than 2mm, is used for the experiment. This specimen is soaked in a container with 200 ml of distilled water while maintaining constant stirring to ensure thorough mixing. Unit doses of 5 mL of methylene blue solution, each with a concentration of 10 g/L, are successively added to the mixture.

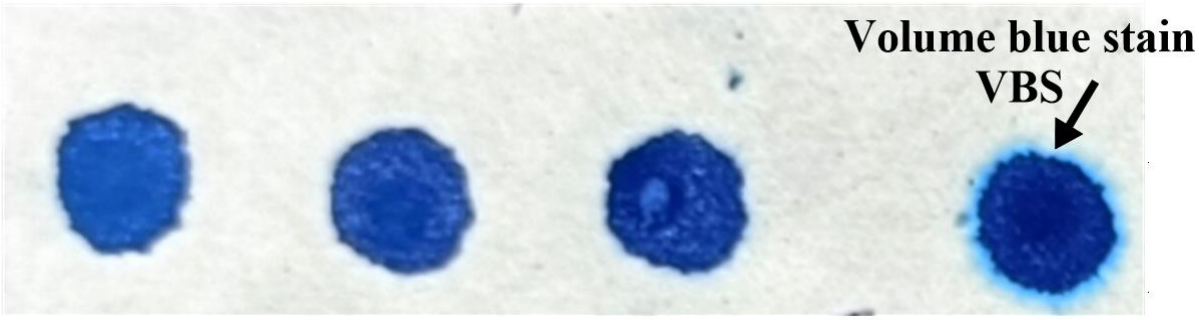

Figure 4.26 The trace of blue stain in Methylene blue experiment

Following the addition of each unit dose, a small portion of the suspension is carefully collected using a glass rod, allowing a small drop to fall onto filter paper. This produces a dark blue stain, surrounded by a clearly defined colorless wet area, as illustrated in Figure 4.26. Additional units of methylene blue (MB) are continued to be added until drops are deposited on the filter paper, forming a bright blue halo within the wet area. This alteration signifies the presence of an excess quantity of methylene blue that is no longer being absorbed by the clay mineral and thus remains within the mixture. At this juncture, no further methylene blue is introduced, and the suspension is closely monitored at 1-minute intervals to assess the stability of the light blue halo. If the halo remains stable and persists after 5 minutes, it indicates that a

sufficient quantity of methylene blue has been added. On the contrary, if the halo does not sustain its stability, the titration process is continued until the halo achieves the desired stability.

The uncertainty in the test results is estimated at around 5%. It represents imprecision in terms of dosage: the quantity of blue added per dosage being 5 ml and the glass rod being graduated to the fifth of a milliliter, we could find ourselves, by imprecision, where applicable, with quantities of 4.8 ml or 5.2 ml which would cause an uncertainty of + or – 0.2 ml and which would represent 4% of 5 ml. Hence an estimate of uncertainty at 5%.

The clay content is determined by the amount of methylene blue "VBS" (Value of blue stain) expressed in grams of methylene blue adsorbed per 100 g of soils. If the methylene blue solution is used at a concentration of 10 g/l (as for this study), we use equation xx to calculate VBS (Tran, 1980).

$$VBS = V*C*100/M \qquad 4.1$$

with: V = volume of the adsorbed blue solution (ml), C the concentration (g/cm^3) of the methylene blue solution used, M = mass of the sample (g).

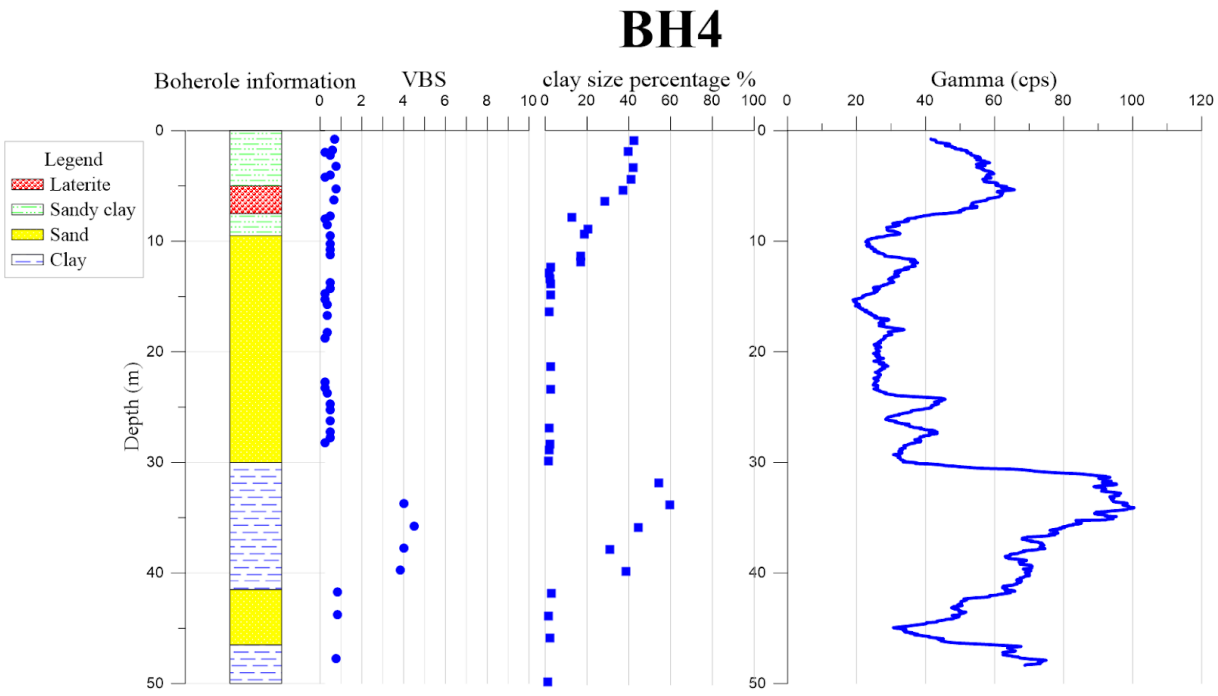

Figure 4.27 The correlation at BH4 site with VBS and well logging and clay size sediment

At the BH4 site Figure 4.27, grain size analysis was conducted in the Geopet laboratory to determine the particle composition of a total of 32 samples. Among these, 9 samples were close to the surface with granulometric clay content ranging from 12.7% to 64.5%. However, the VBS values ranged from 0.3 to 0.8, indicating the soil absence of clay. Respectively, the electrical resistivity values varied between 300 to 800 Ω.m, and the gamma-ray values ranged from 23 to 62 cps. This confirms that the near-surface sediment layers have particle sizes corresponding to clay-sized particles. However, in terms of mineralogy, they are not clay. For the aquifer, the granulometric clay content ranged from 1.3% to 2.9%, with VBS values

between 0.3 and 0.9. The electrical resistivity varied from 300 to 1400 Ω.m, gamma values from 19 to 42 cps.

In the deep clay layer identified in well logging, the granulometric clay content ranged from 31.1% to 59.6%. The corresponding VBS values ranged from 3.9 to 4.5, gamma values ranged from 60 to a peak of 100 cps, and electrical resistivity values ranged from 30 to 40 Ω.m. The analysis results have confirmed the suitability for clay layers with low electrical resistivity, indicating a high mineralogic clay particle content. Consequently, their ability to absorb methylene blue is higher compared to non-clay soil layers.

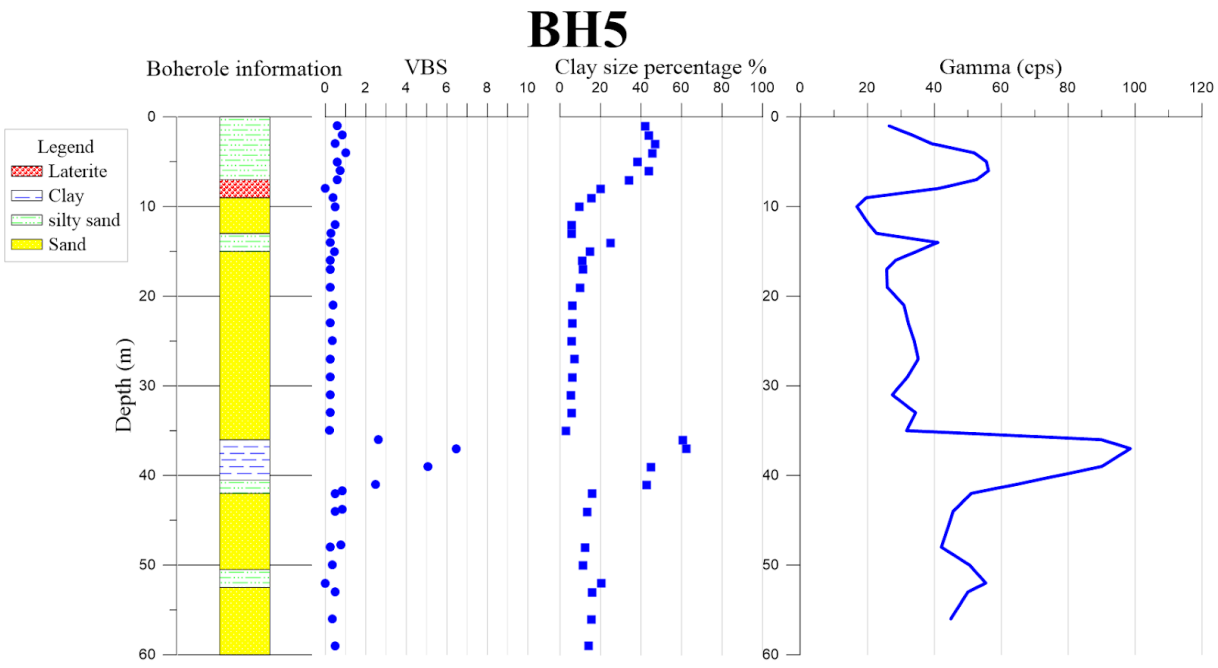

Figure 4.28 The correlation at BH5 site with VBS and well logging and clay size sediment

At the BH5 site Figure 4.28, similarly to BH5, grain size analysis was conducted in the Geopet laboratory to determine the particle composition of a total of 37 samples. Among these, 7 samples were close to the surface with granulometric clay content ranging from 34% to 47%. However, the VBS values ranged from 0.6 to 1, indicating the soil absence of clay. The electrical resistivity values varied between 300 to 800 Ω.m, and the gamma ray values ranged from 23 to 58 cps.

For the aquifer, the granulometric clay content ranged from 3% to 23%, with VBS values between 0.2 and 0.5. The electrical resistivity varied from 300 to 1400 Ω.m, and gamma values ranged from 19 to 50 cps.

In the deep clayey layer identified in the geological document for the drilling well, TDEM, and core samples, the granulometric clay content ranged from 42.7% to 62.5%. The corresponding VBS values ranged from 2.5 to 6.5, gamma values ranged from 60 to a peak of 100 cps, and electrical resistivity values ranged from 30 to 40 Ω.m.

Therefore, we can conclude that there is no mineralogic clay on the surface in the highly elevated area in the study region with VBS values less than 1. This is further confirmed by the high resistivity ranging from 300 to 800 Ω.m based on surface geophysical and borehole logging. Additionally, the low gamma ray values ranging from 19-62 in the well logging data

also support this conclusion. For further studies using TDEM resistivity, the relation between resistivity and VBS, shown in Figure 4.29, gives us a clear limit: below 60 Ω.m (a range of values easily identified by TDEM), we are sure to have clayey layers.

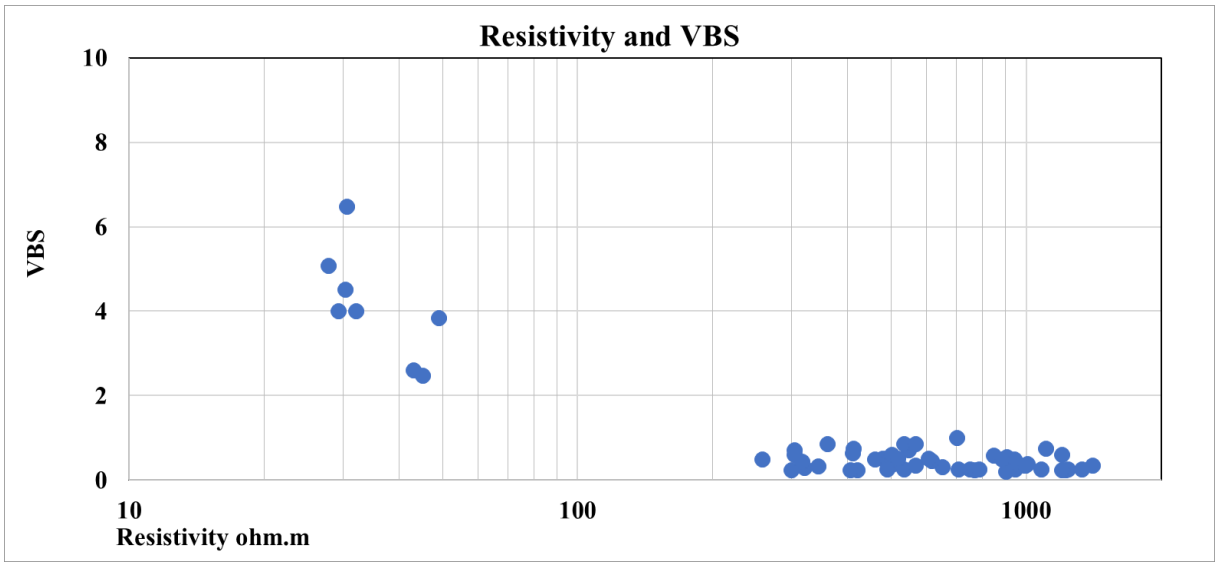

Figure 4.29 Relationship between well log resistivity and the VBS value obtained from the Methylene Blue experiment.

In addition, when having a look to the correlation between resistivity (obtained by logging) and the amount of sand in the aquifer samples (obtained by analyzing the core at the corresponding depth), and discarding the shallow unsaturated layer, we see in Figure 4.30 that the resistivity values above 200 Ω.m indicate an amount of sand above 60%.

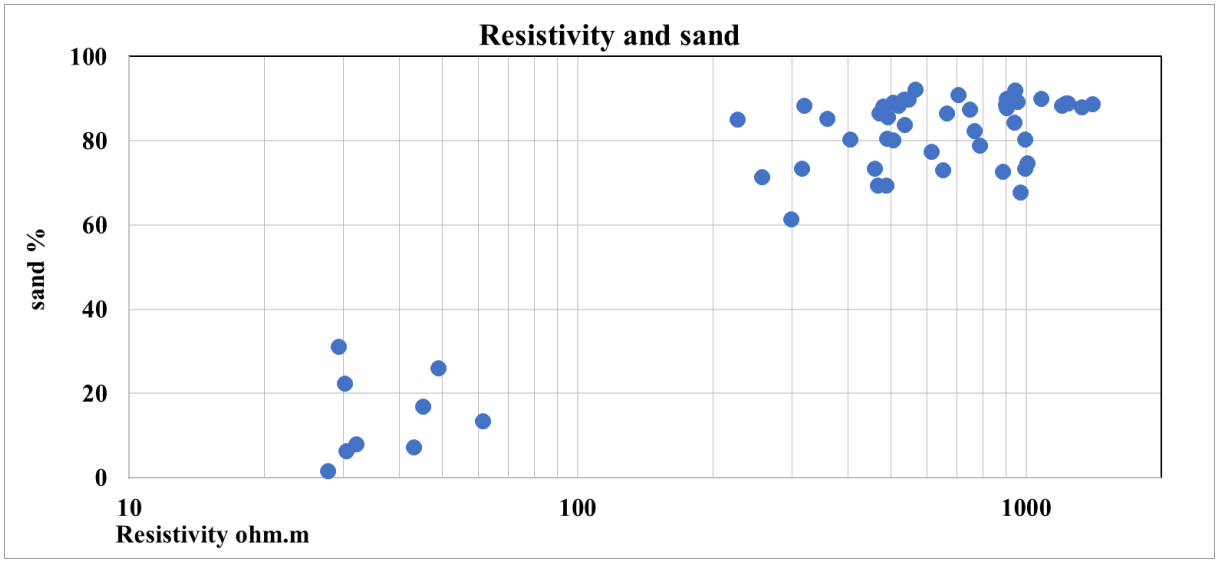

Figure 4.30 Correlation between well-log resistivity and the percentage of sand size in core samples

However, it is not possible to propose a clear relationship between resistivity and sand content. Further studies could be proposed to deconvolute the resistivity value using additional parameters (silt content, resistivity of the water, pore shape, etc., as proposed for example in Archie's law).

- **Specific case of the laterite**

The results of analyzing the laterite core samples using the sieve method revealed that particles larger than 2mm (gravel) ranged from 25-30%, and the granulometric clay particle content, smaller than this size, varied from 15-20%. This indicates that the laterite layer possesses poor sorting due to its wide particle size distribution and low permeability. However, when determining the granulometric clay content within the laterite sediment using the methylene blue staining method, it was observed to be relatively low, with VBS values ranging from 0.5 to 0.7. These values are consistent with the shallow-depth sediment layers in the study area. This suggests that the laterite layer could be permeable, although it is lower compared to the layers above, due to its lesser sorting grain size. Therefore, the laterite layer may still allow water to pass through, contributing to the recharge of the groundwater system with rainwater. However, this also poses a potential risk for the transmission of surface pollution.

- **Specific case of the river banks and paddy fields**

In order to investigate the resemblance between electrically conductive sediment at various depths and sediment with low electrical resistivity in the vicinity along the riverbank (Cu Chi area) and the paddy field area (Ben Cat area), we carried out sample collection in these specified locations. We conducted particle analysis utilizing the Sieve technique, followed by ascertaining the existence of clay through the employment of the Methylene Blue method.

The analysis results, depicted in Figure 4.31, reveal significant findings. For samples taken from the Cu Chi riverbank area, the clay content, determined using the MB method, showed a VBS value of 4.3, corresponding to a clay content of 55.5% by the sieve method. On the other hand, samples collected from the Ben Cat paddy field flooding area exhibited a clay content of 51.2% with a VBS value of 4. The analysis results of the particle composition for these two samples were plotted on a ternary diagram and fell into the clay classification zone. Those values are close to those of the sediments appear as electrically conductive at depth in the Cu Chi area. In the Cu Chi area, the clay content varied from 40% to 60%, with corresponding VBS values ranging from 2.5 to 6.5, as determined by the MB method.

Those similarities reinforce our hypothesis that the electrically conductive sediments at depth, well detected by TDEM, are indeed formed under floodplain conditions (or old channels filled by marine or estuarine clay). The evidence of mineralogic clay presence in the floodplain areas, as indicated by particle analysis and the Methylene Blue (MB) method, suggests a strong correlation between the conductive sediment and floodplain conditions.

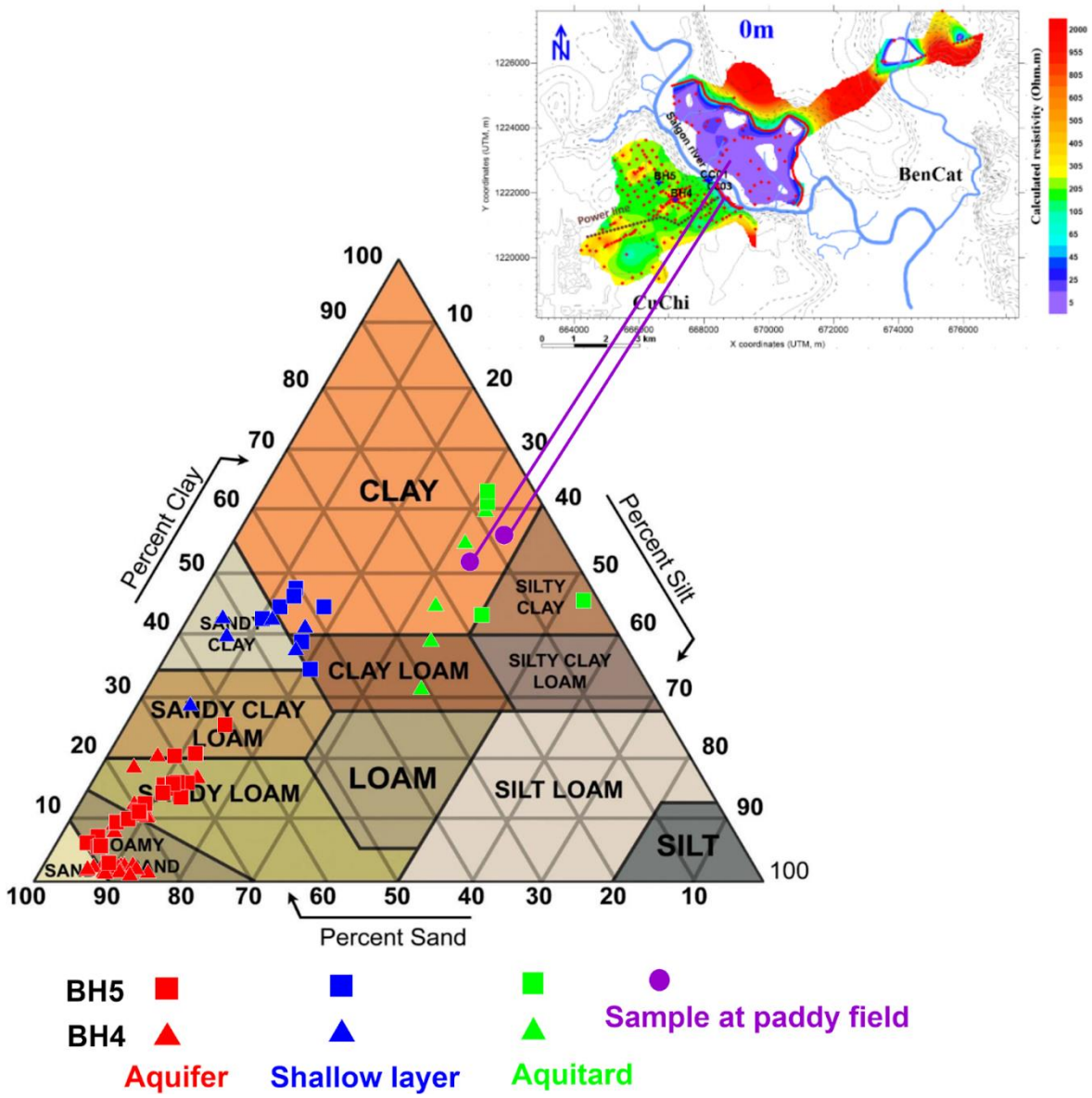

Figure 4.31 Texture triangle chart for the Sieve Grain Size Analysis to classify the soil including samples from the paddy field in the Cu Chi and Ben Cat area.

In this figure, the triangle symbol represents core samples from well BH4, while the square represents core samples from well BH5.

The red color is characteristic of core samples extracted from the aquifer layer, based on drilling data, well logging resistivity (ranging from 300 to 1400 Ω.m), low gamma ray below 60 cps, and VBS values between 0.4 and 0.75. The soil composition in the reservoir spans from sandy loam and loamy sand to sand. The blue color designates shallow layers with high resistivity values (300-800 Ω.m) and high gamma, classified as sandy clay and clay loam, with VBS values ranging from 0.4 to 1. Core samples from the aquitard layer are represented in green, indicating low resistivity values (30-70 Ω.m) and high gamma values exceeding 60 cps. These samples are classified as clay and silty clay, with VBS values ranging from 4 to 6.5. Additionally, two sediment samples from the paddy field areas in Ben Cat and Cu Chi, located in regions of low resistivity according to TDEM and ERT data, have VBS values measured at 4 and 4.3, respectively. These values fall within the same classification range as aquitard, and the soil composition is primarily clay.

4.3.3 Conclusion from the sediments type analysis

Based on the particle analysis and methylene blue results, the presence of mineralogical clay is observed in the floodplain current sediment of Ben Cat and river banks. Additionally, the aquitard layer in the study area exhibits a mineralogical clay V_{BS} value similar to that of the floodplain current sediment of Ben Cat and river banks, concerning particle distribution and V_{BS} values, as well as resistivity values determined through geophysical methods.

Therefore, considering the similarities in mineralogical clay content and resistivity values between the floodplain current sediment and the aquitard layer, the hypothesis suggesting that resistivity maps constructed from TDEM may reveal the presence of an old river channeling and floodplain system is reinforced. Sediment at depths less than 10m has indeed been confirmed to be non-mineralogical clay, this is why they are high resistivity values ranging from 300 to 800 Ω.m from various electrical methods. However, particle analysis using the sieve method indicated a notably high content of fine particles -even in the clay-sized domain, consequently leading to a layer with low permeability. This shallow layer, seen as “clay” by hydrogeologists in previous literature, may be not as impermeable as expected.

4.3.4 Geological investigation

From our results, two explanations can be proposed to explain conductive sediments delineated by geophysics. They can correspond to ancient river bed and continental floodplain as seen nowadays in Ben Cat area. This interpretation is probably the correct one for flood plains. But having very fine sediments deposited at the bottom of the river remains contradictory to the fact that, usually, it is rather sandy sediments that are dispositioned at the bottom of the stream. In addition, several boats are dragging sand in the rivers. A second explanation that could explain clayey (or very fine sediment -silts) deposits is to invoke an old sedimentation process that originated from an estuary environment with mangroves as seen at the south of HCM City. The question arises: how the channels detected by geophysics could originate from an estuary depositional system?

An answer to this question is given by the paper of (Thanh, et al., 2021) describing the sediment deposit dynamic history in the Mekong Delta close to Saigon River basin in the quaternary period. The sedimentary processes include transgressive and regressive phase of sedimentation in regression phase, this includes a process characterized by river incision, resulting in the surface being weathered and forming boundaries for this type of sediment. After, the transgressive process leads to the infilling by fine sedimentary deposits of valleys eroded. This can elucidate how the old channels, formed by river incision during regression and erosion phases, might have been filled with very fine estuarine deposits during the transgression phase Figure 4.32.

To track the existence of the regression-transgression process in our area, we surveyed a unique major geological (man-made) outcrop. The outcrop reveals oblique dandy to loamy sediments Figure 4.32 that can be characterized by a deposit process similar to the sedimentary model of the Mekong Delta. Specifically, on the outcrop surface, we observed oblique sediments corresponding to those formed by the sea level fall process (regression).

This geological (sedimentological) history can elucidate why the sediments from the ancient Saigon River detected by geophysics exhibit fine sediments with low resistivity, high

clay content, a possibly indicating an estuarine depositional context during the transgressive phase. This includes also the process of old flat areas (flooding plains) associated with mangroves.

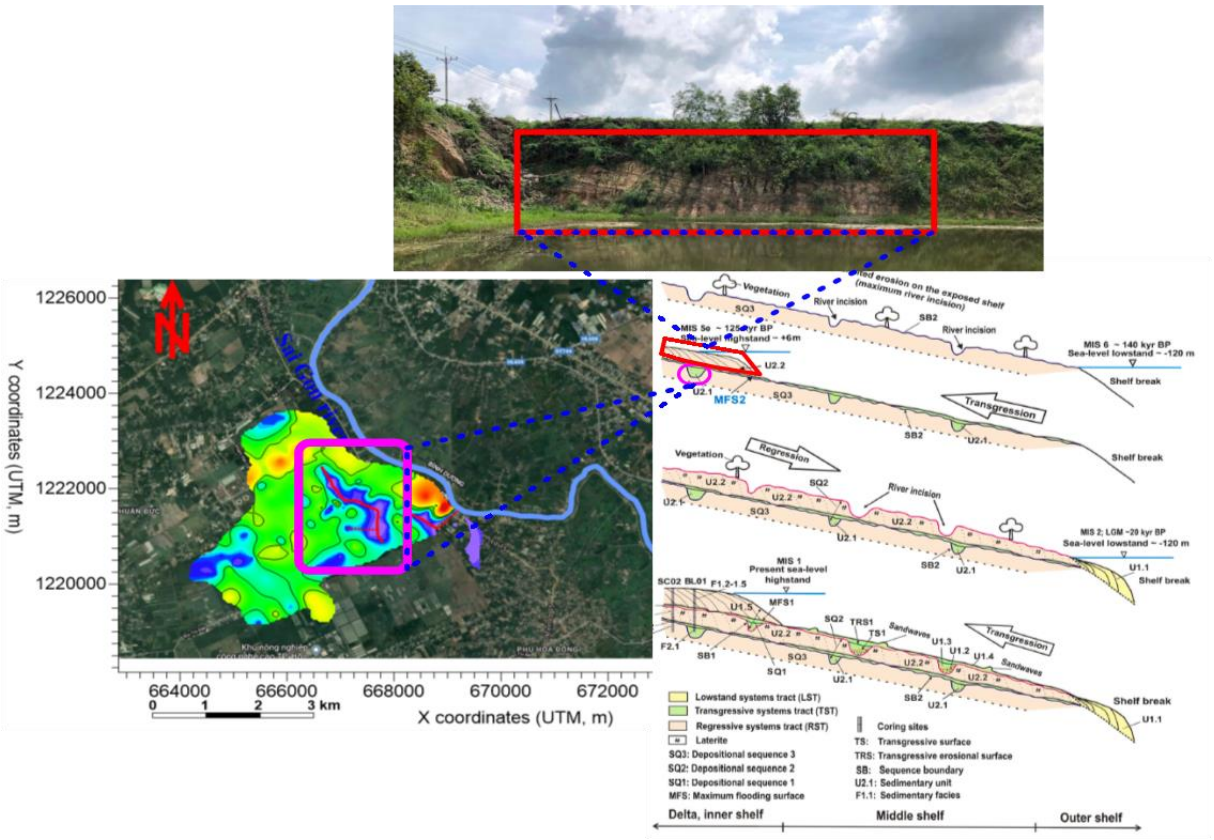

Figure 4.32 Example of TDEM map (-30m), picture of sandy outcrop related to the conceptual model of (Thanh, et al., 2021)

4.4 Conclusion on aquifer-aquitard geometry

Shallow layers in elevated zones (Cu Chi area) primarily consist of sandy-clay to clay loam sediments rather but without true mineralogic clay (thus appearing as resistive for geophysics). Their sandy-clay to clay loam texture suggests that they may present a low to intermediate value of hydraulic conductivity, therefore a potential for infiltration. This is confirmed in chapter 5 by intermediate hydraulic conductivity (Ks) values. This analysis is an important output of the study: this means that water and pollutants can permeate these layers, to some extent. Therefore, the shallow (0-50 m) aquifer can be considered as vulnerable to pollution. Still in the elevated area, laterite layers are probably continuous, but remain difficult to "see" with resistivity because these layers are as resistive as the aquifer. They appear to be either porous on some outcrop, with cemented big pebbles and large voids, either made of pebbles and surrounding matrix made with sandy-clay to clay loam sediments. Thus, the hypothesis is that the laterite layer may play the role in delaying the infiltration rate in some places.

Shallow layers in the current low elevated zones (river banks in Cu Chi and paddy fields in Ben Cat) are rich in clay-size sediment containing "true" mineralogical clays, thus with low electrical resistivity. Clay-rich sediments are likely to be much more impermeable than silty sediments or should exhibit low permeability, restricting the infiltration of fertilizers and

pesticides into the aquifer. Below the floodplain, shallow aquifers may be less vulnerable to infiltration of surface pollution. Clayey sediments may also favor lateral runoff to the river.

Deeper aquitard layers (30-50m) are mainly encountered in the Cu Chi area. In some places, they are almost continuous laterally, but not totally and therefore cannot protect the second deeper aquifer from pollution. The arrangement of aquitard follows the ancient meandering of the Saigon River and its floodplains, filled by silty-clay to clay loam sediments and clayey sediment. The ancient beds are probably filled by fine estuarine sediments from the last transgressive period.

Shallow and deep aquifers appear as intermediate to resistive layers, interconnected. They are mainly sandy to loamy. Our study doesn't investigate the layers immediately below the Saigon River and further studies are required to evaluate river-aquifer interactions.

The Time-Domain Electromagnetic (TDEM) survey appears as a very efficient tool in our study. TDEM results also described the geological characteristics within the area, especially when the information is sparse from borehole data. TDEM has revealed crucial insights into the subsurface structure of the study area, particularly with regard to the ancient geomorphological features of the Saigon River channel and floodplains system. Conductive channels and floodplains have been identified at depth, shedding light on the region's geological history. In elevated areas, TDEM does not indicate the presence of conductive surface clay, aligning with observations from Electrical Resistivity Tomography (ERT) and Frequency Electromagnetic Method (FEM) studies at a smaller scale. This suggests that elevated regions may be more susceptible to infiltration, despite the sediment's composition being sandy-clay to clay loam particles, which can potentially reduce the infiltration rate. The laterite layer, prevalent across some test sites, may influence surface infiltration dynamics and may be widespread across the entire area. Consequently, vadose zone modeling should consider the presence and role of this laterite layer in governing infiltration patterns. Additionally, TDEM identifies substantial and widespread thick clayey layers in the lowest areas, suggesting a natural barrier that could impede in some places deep percolation of pollutants, underscoring the potential protective role of these clayey layers in groundwater quality preservation.

A known limitation of the TDEM method is its less sensitivity to high-resistivity sediment layers, specifically above 300 Ω.m. Therefore, direct use of the resistivity values determined by the TDEM method to estimate the saturation or porosity of the formations in the research area is not feasible. Additionally, the electrical properties and conditions at the survey location significantly impact the data collection and interpretation of TDEM materials, including influences from power lines, electromagnetic noise from local activities, and the induced polarization effect caused by the peculiarities in the geological formations.

Based on the mentioned outcomes, in the future, applying TDEM for surveys on Saigon rivers will clarify the subsurface geological structure beneath the riverbed, aiding in clarifying the interaction between the river and the adjacent aquifer layers within the area. Moreover, for areas with complex topography and large areas, implementing airborne TDEM is a practical and effective proposal for expanding research in the future.

Based on the interpretation and analysis of TDEM results, we attempted to explain the history of sediment formation in the research area within the first 150 m from the surface in this

typical rural area. The major result is that the aquifer is vulnerable from surface pollution. Connections are possible between aquifers at depth. By understanding the history of the formation of soil and sediment layers, we also can propose appropriate geological hypotheses for other areas, especially those on a larger scale. The TDEM results can assist in determining geological structures and understanding the history of the formation of sedimentary layers, thereby providing appropriate solutions for resource management and environmental issues. In particular, based on the geophysical results obtained, a 3-D hydrodynamic hydrogeological modeling and vadose zone infiltration modeling exercises are undergoing, but not presented in this PhD work, which serves as preliminary work for aquifer management.

CHAPTER 5. AQUIFER PROPERTIES ESTIMATION USING MAGNETIC RESONANCE AND HYDROLOGICAL METHODS

In Chapter 4, we presented how the geophysical methods based on resistivity give results a) delineating aquitard, and ancient river features and b) identifying more resistive zones corresponding to more silty to sandy aquifers. However, due to the fact that TDEM is poor in giving reliable resistivity values above 300 Ω.m (and thus forbid the use of Archie's law), the TDEM resistivity parameter cannot be easily used directly for giving an estimation of the aquifer properties in the Cu Chi-Ben Cat area.

Pursuing the objective of the Ph.D. work in exploring the possibility of geophysical methods for aquifer parameters characterization, chapter 5 introduces the Nuclear Magnetic Resonance method for this purpose. The chapter will present briefly the results obtained in the field in 2018 with the field scale Magnetic Resonance Sounding (MRS) mode. As those field results were unsuccessful, the second part of the chapter will present the NMR results obtained at the laboratory scale, which is a novel method currently tested at the IGE laboratory and with its partners in some sites in the world using a prototype device built by A. Legchenko (Legchenko, 2022). The Vietnam data set acquired in the frame of this PhD is therefore a part of a novel research effort to characterize aquifer properties in some studies. NMR results obtained at the laboratory scale (cores sample scale) are discussed using a) a field scale pumping test and b) a hydraulic conductivity test and grain size analysis obtained with the core samples.

A preliminary conclusion will be derived regarding the applicability of the NMR method in our field context.

5.1 Field scale Magnetic Resonance Sounding (MRS)

5.1.1 MRS set up

During a PhD preliminary work (2018-2019), we aimed to assess the effectiveness of Magnetic Resonance Sounding (MRS) in determining aquifer properties within the designated study area in Cu Chi. To achieve this goal, a total of four MRS data collection points were established Figure 5.1. Among these, three locations (MRS 1, MRS 3, and MRS 5) are situated in proximity to the Saigon River. The purpose of collecting data at these locations is to conduct a comparative analysis with the findings of aquifer isotope research conducted by the GEOPET and CARE laboratories team (Tu, et al., 2022).

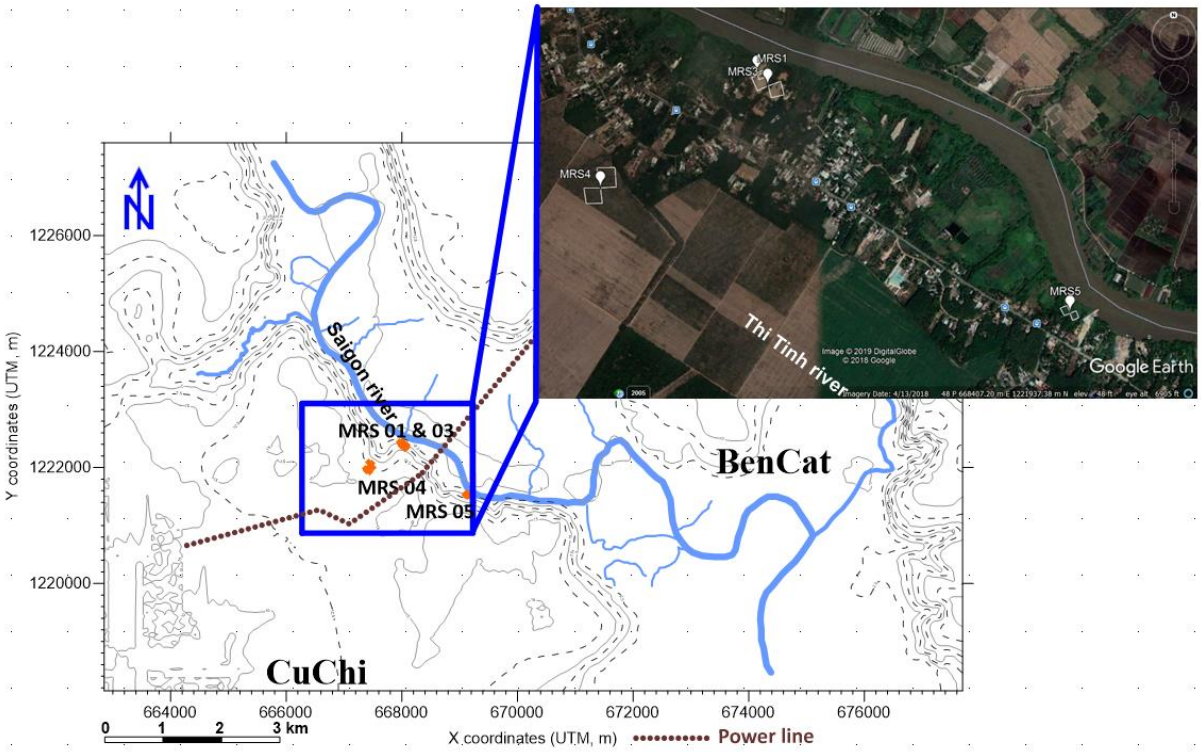

Figure 5.1 Location of MRS soundings in the study area.

Additionally, a MRS measurement point denoted as MRS 04, was designated for testing within the inland region. This specific data collection point was chosen to evaluate the characteristics of the aquifers present in the area. In our survey Magnetic Resonance Sounding (MRS) involved the setup of a wire loop on the ground arranged in an "8" shape with dimensions ranging from 25 to 50 meters. The eight-loop has been employed to enhance the signal-to-noise ratio (S/N) Figure 5.2.

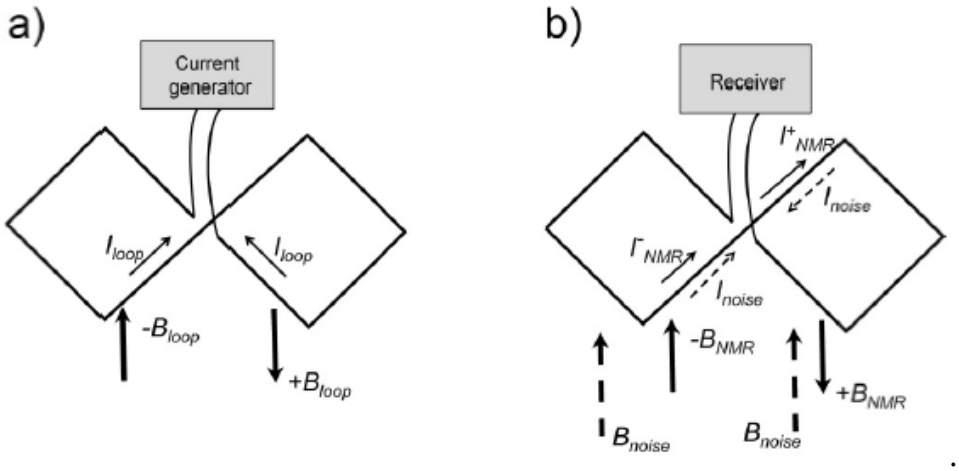

Figure 5.2 Principle of noise cancellation using the figure-eight loop (Legchenko, 2013).

The transmitting current pulse I is applied to the figure-eight loop and produces the magnetic field B. b) Receiving MRS signal and noise: As a result of the configuration of the figure-eight loop, MRS signals induced in each square exhibit inverse polarity. Notably, the noise magnetic field induced currents "Inoise" in each square with a reverse polarity that tends to cancel the noise.

The design of the "eight-loop" allows the currents induced in each square to be interconnected in such a way that they subtract from each other. This leads to the doubling of

the desired signal, while simultaneously canceling out unwanted noise, as the survey is very close to a high-power line (see Figure 5.1)

The Larmor frequency was determined by measuring the geomagnetic field (B) at the surface with a proton magnetometer. At Cu Chi, the Larmor frequency was 1819.7 Hz. Measurements of the magnetic resonance signal are carried out by varying the pulse moment, the configuration of the MRS surveys is provided in Table 5.1. The over quality of the soundings was found to be “highly noisy” despite the 8-shaped loop.

Table 5.1 Specific parameters for MRS sounding

No location	No Sounding	Loop size	Turn	Stacking	Quality
MRS 1	Sounding 1	25*25	2	400	highly noisy
MRS 3	Sounding 2, 3	50*50	1	200	highly noisy
MRS 4	Sounding 4	50*50	1	400	highly noisy
MRS 5	Sounding 5	25*25	2	400	highly noisy

5.1.2 MRS result

The collected data was processed and interpreted by A. Legchenko and the team using the Numis inversion software (Legchenko, 2022). An example of signal and noise levels is displayed for the MRS01 sounding close to the river in Figures 5.3a and 5.3b. A total of seven signal pulses were obtained with 400 stacking, with measurement intervals pulses spanning from 55ms to 1996ms. Notably, both the signal amplitudes from Free Induction Decay (FID1) and the Mean Signal recorded are very close to the noise level post-processed. We conducted an interpretation to determine the distribution of water content according to depth. The water content must be considered as the maximum value of the water content that could be present in the soil. The poor quality of our data cannot lead to a quantified value of the actual water content. Figure 5.3c presents this calculation. At an interval depth of 6 to 15 meters, an aquifer could be present with an MRS water content of 20% maximum. This section is highlighted in red, and it exhibits a very low T1 value of 100ms, which is characteristic of a very fine-grained aquifer. Again here, those values can be considered also as “a high noise data interpreted as an aquifer”. Below, a lower water content value of 12.5% is calculated and could be either an aquifer or a noise signal. The calculated T1 value is 150ms, again typical for aquifers with a fine-grained composition, following the classical MRS aquifer classification (Legchenko, 2013).

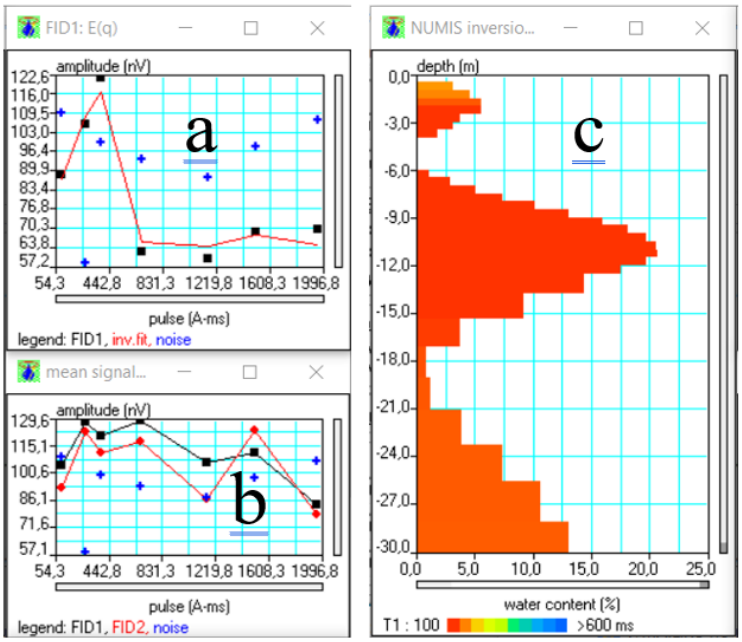

Figure 5.3 Example of the interpretation of MRS 01 sounding.

a) Raw amplitude of the MRS signal and b) Amplitude of the mean of the MRS signal. The MRS signal measured is shown as black squares, the noise as blue crosses. c) Attempt to calculate an aquifer parameter considering that the noisy data could be an aquifer. As written in the text, this interpretation could also be a noise interpreted wrongly as an aquifer.

Similarly, the data from MRS03 and MRS05 underwent processing steps before interpretation. The processing outcomes at these two measurement locations reveal that the measured signal's amplitude is nearly indistinguishable from the accompanying noise, as illustrated in Figure 5.4. Therefore, it is impossible to conduct an interpretation to determine the water content contained in the aquifer as well as determine the T1 value to classify the aquifer based on the size of sediment particles.

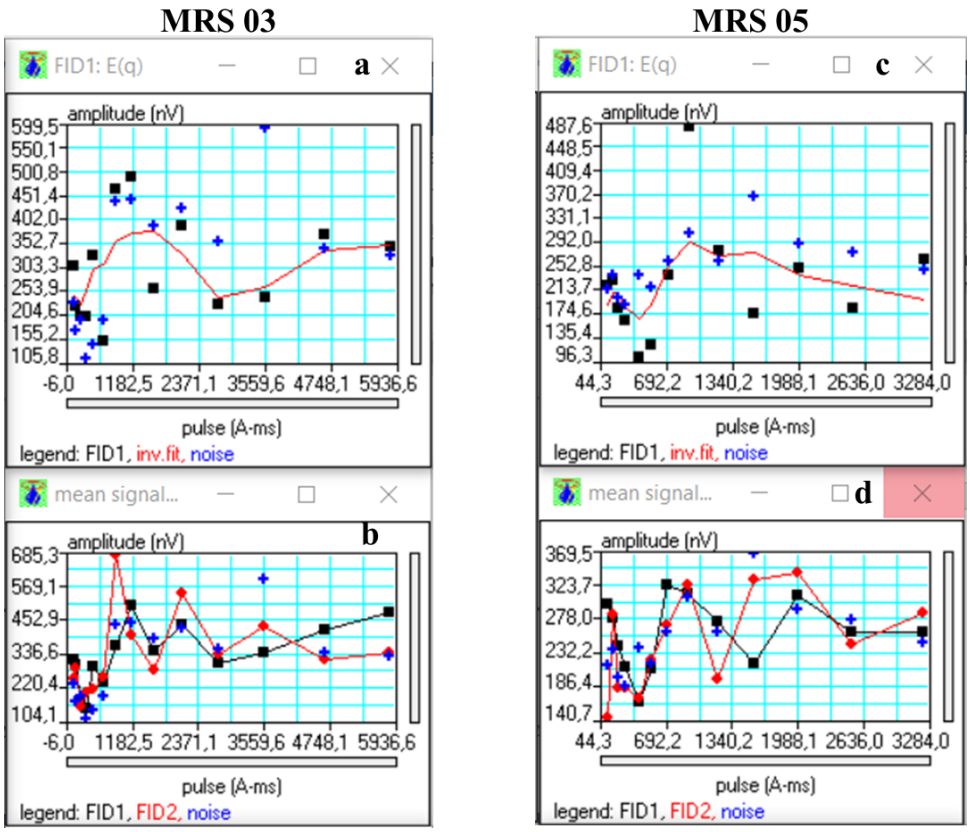

Figure 5.4 Results of the processing of MRS03 and MRS05 data, indicating a too noisy site.

The horizontal axis represents the measured pulse time in milliseconds, while the vertical axis represents the measured amplitude value. In the illustration, noise is represented as a blue plus sign, while the received signal (FID1) is depicted as a black square and the red square is the FID2 signal. The red solid curve represents the inversion fit of the measurement data.

From the survey findings, it becomes evident that in the riverside area, the feasibility of interpretation of MRS data is limited.

We conducted MRS 04 on agricultural land planted with cassava, located approximately 500m away from the Saigon River. Similarly, to the previous survey along the river, the signal amplitude aligned closely with the amplitude of the accompanying noise as seen in Figure 5.5. Consequently, it proves challenging to distinctly discern between the actual signal and the noise. As a result, the post-processed data cannot be effectively interpreted to determine the aquifer's characteristics, including water content and sediment particle size.

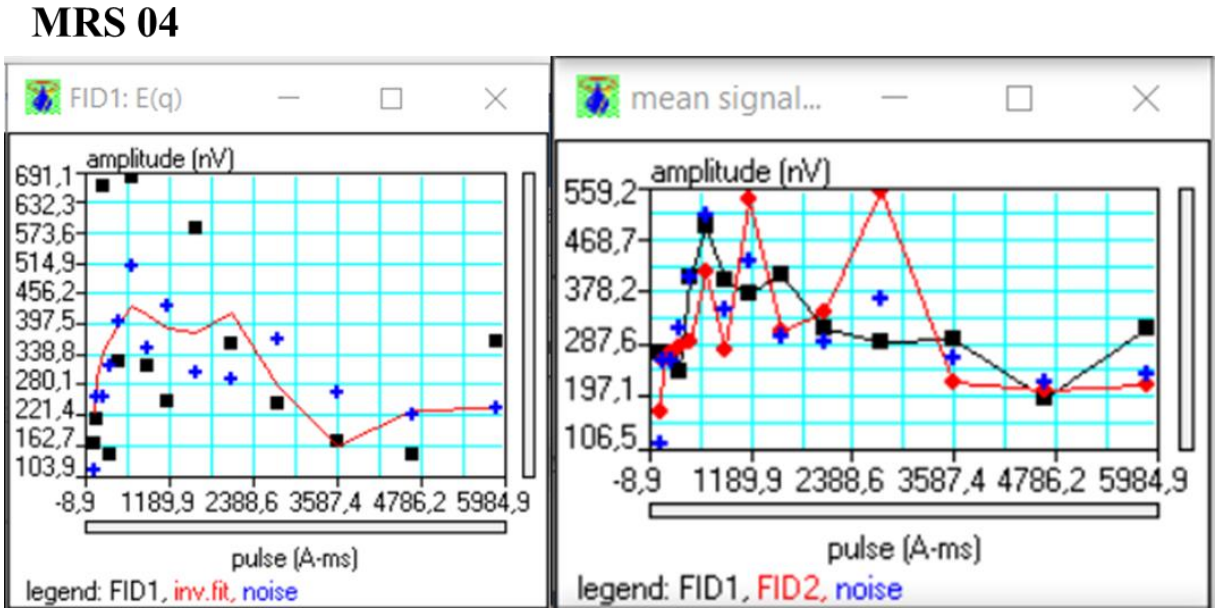

Figure 5.5 Results of the processing of MRS 04 data.

The information values depicted in the figure same as those found in MRS03 and MRS05

5.1.3 Conclusion on MRS at the field scale

The outcomes of processing and interpreting MRS data at the field scale reveal that the post-processed signals are predominantly closely aligned with the noise signals. Consequently, employing the post-processed MRS data for interpretation to determine the aquifer characteristics within the study area is unfeasible with our data obtained with small-sized eight-shaped loops. Only for the sounding MRS 01, the MRS signal amplitude could be considered as equal to the noise (and above the noise for some pulse moment) which could lead to an analysis that, if an aquifer exists below the loop, it has a maximum water content of 20%, and the maximum T1 value is 150ms, characteristic of an aquifer with fine particles (i.e. a “poor” aquifer). For longer time of survey, it could be possible to obtain better results by stacking the signal and reducing the noise to acceptable levels.

In conclusion, the MRS data collection conditions in the study area proved challenging due to the high EM noise. Therefore, to assess the applicability of the MRS method at the field scale, additional MRS tests are imperative in various locations within the research area, along

with considerations such as augmenting loop size and the number of turns during data collection, as well as a longer stacking procedure. The initial results suggest that the aquifer might consist of fine sand or a silty composition, featuring a relatively low water content and T1 value. To validate this outcome, more comprehensive MRS surveys are required at the field scale that couldn't be performed in the frame of this Ph.D. due to the lack of equipment in Vietnam (the tests were done during a summer school in 2019). Therefore, it was decided to explore another application of the MRS but at the laboratory scale (core sample scale).

5.2 Laboratory-scale Nuclear Magnetic Resonance (NMR)

The objective of NMR at the laboratory scale is to obtain an aquifer parameter using the cores extracted from our test boreholes. Actually, if this is validated, NMR core analysis could be considered as an alternative way to obtain aquifer parameter estimates without performing costly pumping tests, keeping in mind that the scale from a core to a pumping site is different. We benefit from the study of the low-cost sampling possibilities in Vietnam. Our goal in this context is to collect a substantial dataset comprising a minimum of 30 samples. To ensure the reliability and accuracy of the collected data, four boreholes were drilled in the frame of the PhD to minimize potential local biases. By analyzing the NMR results in conjunction with other key parameters such as grain size, well logging data, and clay content, the objective is to establish a more comprehensive understanding of the aquifer for providing valuable insights that are essential for effective groundwater resource management and environmental monitoring.

5.2.1 Core sampling

The borehole location aligns with the field-scale MRS site. This includes the well locations of CC01 and CC03, positioned near the river and corresponding to MRS 01 and MRS 03. Two wells inland are situated in the same topographical situation as the field-scale MRS04 site. These wells have been sampled for NMR laboratory-scale analysis as seen in Figure 5.6.

Simultaneously, pumping tests and tracer tests were conducted at two separate locations, BH4 and BH5, aimed at determining hydraulic conductivity and effective porosity.

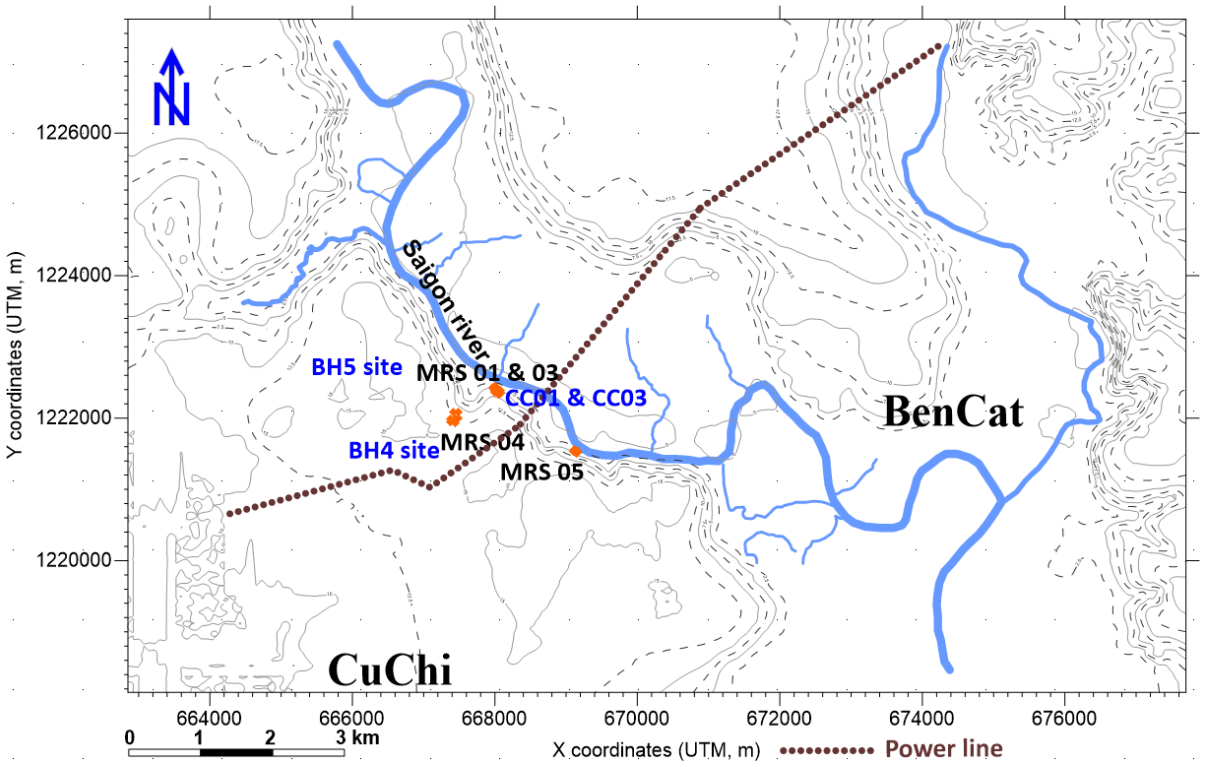

Figure 5.6 Location of borehole sites for NMR sampling.

In the study area, we conducted borehole investigations at four locations. Two boreholes are situated near the rivers: CC01, with a depth of 16 meters, and CC03, with a depth of 50 meters. Additionally, two boreholes were drilled inland: one at the BH4 site, reaching a depth of 50 meters, and another at the BH5 site, reaching a depth of 60 meters.

In Figure 5.7, it can be seen that our primary objective was to extract cores from the so-called aquifer level in several boreholes. For each core, after the NMR core analysis, additional measurements have been done: first a sieve grain size analysis, then for some samples a methylene blue test for confirming (or not) the presence of true clay minerals, then hydraulic conductivity (Ks) measurements using constant head and variable head procedures.

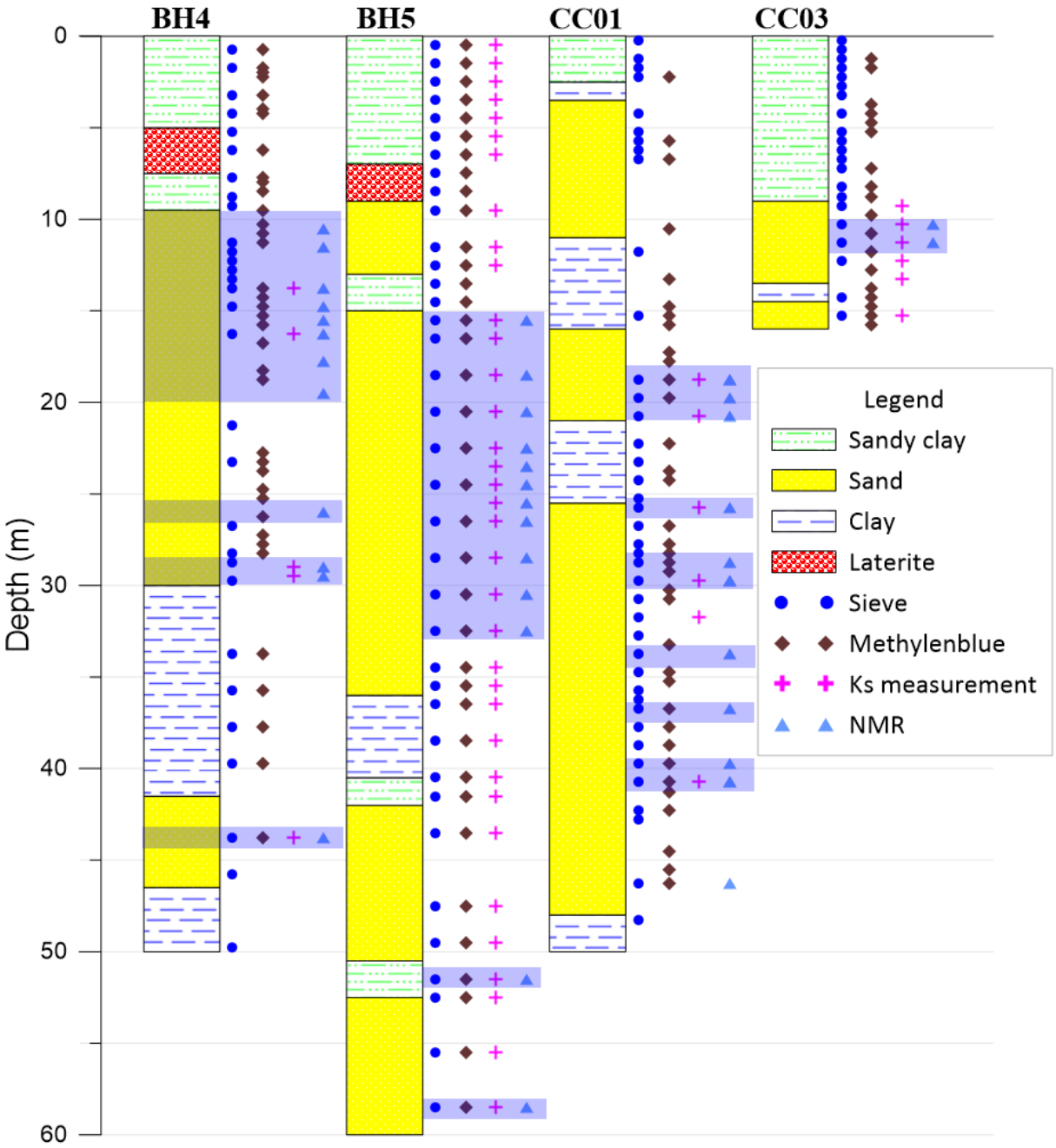

Figure 5.7 Sampling strategy in the boreholes.

The blue shaded frames indicate the cores where NMR tests have been done jointly with other tests to provide data for comparison. This mainly concerns the aquifer layers.

5.2.2 Estimation of the water content of the sample

The objective is to get an estimate of the water content of the samples using classical laboratory methods to be able to compare the NMR water content with two "types" of water content. For this, we considered the total porosity and the specific yield Sy that could be also called "drainage water content" (DWC).

The total porosity is expressed as a percentage of the total water content in the aquifer. The "drainage water content" is expressed as the percentage of water that can be extracted from the aquifer by gravity. Besides, the parameters specific yield (Sy) and water retention (Sr) are

parameters that characterize the characteristics of the reservoir in terms of water content in the reservoir as well as the amount of water that can be exploited from the reservoir.

Specific yield (Sy) is a hydrogeological term used to describe the portion of water that drains from an aquifer in response to gravity and can be extracted or pumped from the ground figure (Johnson, 1967) (Woessner, et al., 2020). It is expressed as a percentage and represents the ratio of the volume of water that drains from the aquifer to the total volume of the aquifer. Specific yield is a key parameter in hydrogeology and is used to calculate the amount of groundwater that can be sustainably pumped from an aquifer.

$$S_y = V_d/V_t \quad (5.1)$$

S_y = specific yield (dimensionless)

V_D = volume of water that drains by gravity (L3)

V_T = volume of sample (L3)

Specific yield is influenced by the porosity and permeability of the aquifer material. Porosity refers to the amount of open space (voids) within the rock or sediment, and permeability describes the ability of these voids to transmit water. Aquifers with high porosity and permeability typically have a higher specific yield because they can store and release more water.

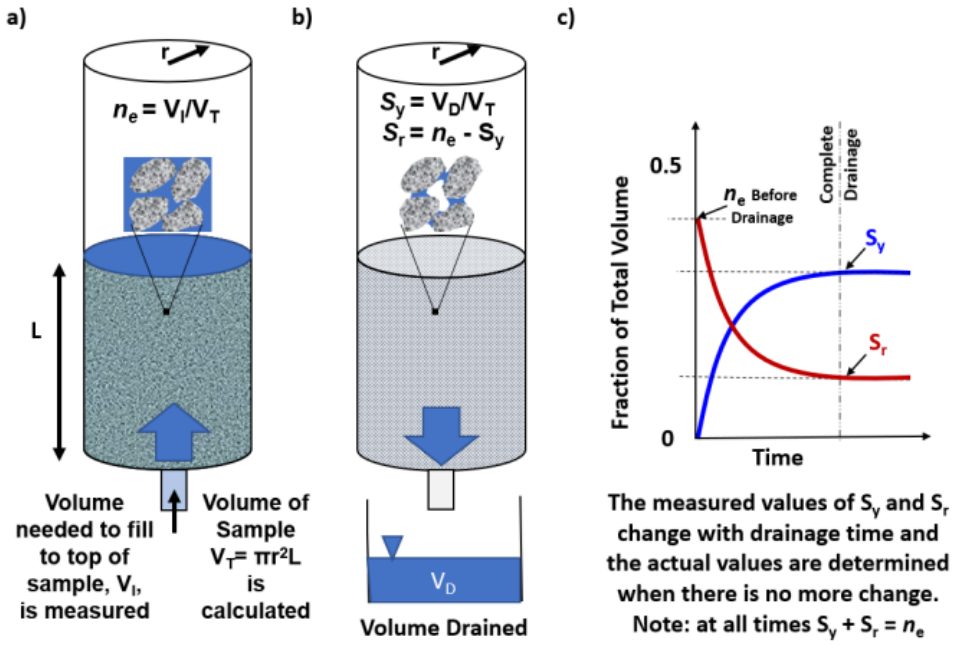

Figure 5.8 The determination of effective porosity (ne), specific yield (Sy), and specific retention (Sr) involves a multi-step process:

To find the effective porosity (ne), start by measuring the total volume (VT) based on the sample's geometry. Then, measure the interconnected pore volume (VI) by saturating an initially dry sample from below and calculate ne. b) For specific yield (Sy) and specific retention (Sr), drain the sample and measure the volume of water drained (VD). You can compute Sy and Sr by analyzing the data. c) It's important to note that the measured value of Sy will increase, and Sr will decrease as the drainage process continues in step (b). Keep in mind that neither value is accurate until the drainage process has completely ceased (Woessner, et al., 2020)

Table 5.2 Summary of specific yield values of common earth materials compiled by Morris and Johnson (1967) with additional data from Rivera (2014), Freeze and Cherry (1979), and Domenico and Schwartz (1998) (Woessner, et al., 2020).

Material	Number of Samples	Range of Specific Yield %
Unconsolidated Sediments		
Clay	27	1 – 18
Silt	299	1 – 40
Loess	5	14 – 22
Eolian sand	14	32 – 47
Sand (fine)	287	1 – 46
Sand (medium)	197	16 – 46
Sand (coarse)	143	18 – 43
Gravel (fine)	33	13 – 40
Gravel (medium)	13	17 -44
Gravel (coarse)	9	13 – 25

The sample saturation and drainage methods involve the process of draining saturated columns by gravity, with a focus on determining both the volume of drained material and the volume of extracted water. The drained water volume can be directly measured by weighting after the drainage process.

Specific Yield estimated with grain size analysis

We also tried to get a value of Sy using a proposed relationship between these parameters and particle size in the literature. This allows for an estimation of the specific yield, specific retention, and effective porosity based on the characteristics of the material's particle size distribution.

Johnson 1967 has considered the particle composition of the sample. In this method, he employs a triangular chart Figure 5.9 using the percentage of sand, silt, and clay in the sample to determine these parameters. From this location, Johnson can deduce the specific yield of the material.

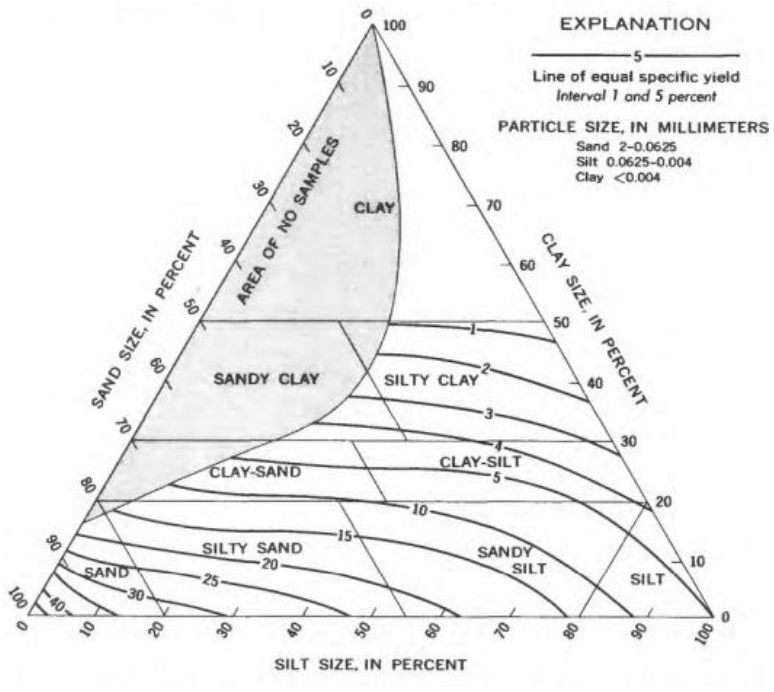

Figure 5.9 Soil classification triangle that illustrates the correlation between particle size distribution and specific yield (Johnson 1967)

The triangular chart in Figure 5.10, based on the Johnson 1967 framework, categorizes the core samples into three distinct zones. The first zone, highlighted in blue and characterized by a clay content of 30-70%, falls within the range of clay silt to silty clay. This zone is identified as an aquitard layer, corroborated by drilling data, gamma ray logging, and resistivity well log measurements. The specific yield values are typically below 4%, the majority falling below 1%.

The second zone, depicted in gray, shows core samples with a higher clay content (20-50%) and significant silt content (40-70%), while sand content remains below 20%. These samples, extracted from a depth of 0-10 meters and primarily composed of laterite layers rich in fine particles, range from clay sand to sandy clay soil types.

The third zone, in orange, represents core samples identified as aquifers. These samples, as determined through drilling and gamma-ray and resistivity measurements, show a grain-size distribution ranging from silty sand to sand, indicative of aquifer layers. The specific yield values in this zone range from 10 to 35%, distinguishing these samples as potential aquifer materials.

At first glance, there is a strong variability observed in the specific yield value (Sy) within the aquifer of our study area. Figure 5.11, illustrates the Sy results obtained for the aquifer layers only, from each borehole. Borehole BH4 exhibits higher Sy values, characterized by a range oscillating between 30% and 35%. In contrast, the Sy values observed in wells BH5, CC01, and CC03 display a wider spectrum, ranging from 10% to 35%. This pronounced disparity underscores the heterogeneity of the aquifer and suggests a relatively lower quality at sites BH5, CC01, and CC03 when compared with borehole BH4.

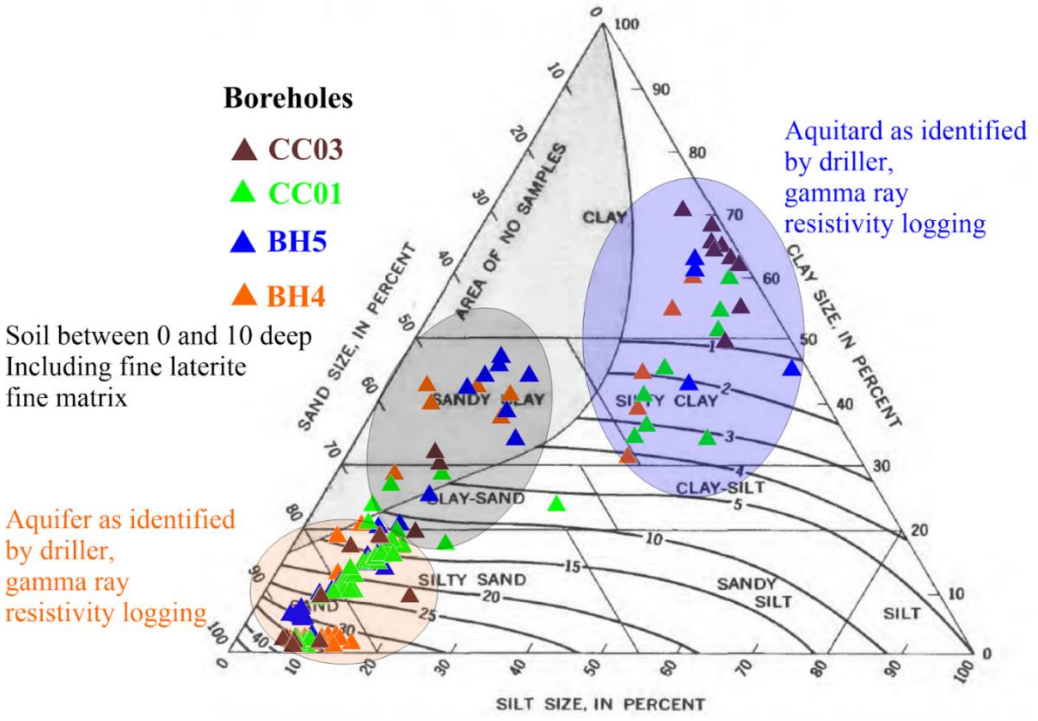

Figure 5.10 Particle composition values of core samples from wells CC01, CC03, BH4, and BH5 superimposed with the Johnson triangle to determine the specific yield parameters for the aquifer in the study area.

In the illustration, core samples from drilled wells are depicted as triangles on the graph, with each color corresponding to a specific well: brown for well CC03, green for well CC01, blue for well BH5, and orange for well BH4. The data points are categorized into three main groups representing different soil components. The data group within the orange ellipse area represents error samples originating from the aquifer layer, the blue ellipse encompasses data from the aquitard layer, and the remaining black ellipse area includes core samples from the soil layer in a shallow depth range of 0 to 10 meters, including the laterite layer. Information about rock layers is determined through drilling data and well log data, which includes gamma ray and resistivity logging.

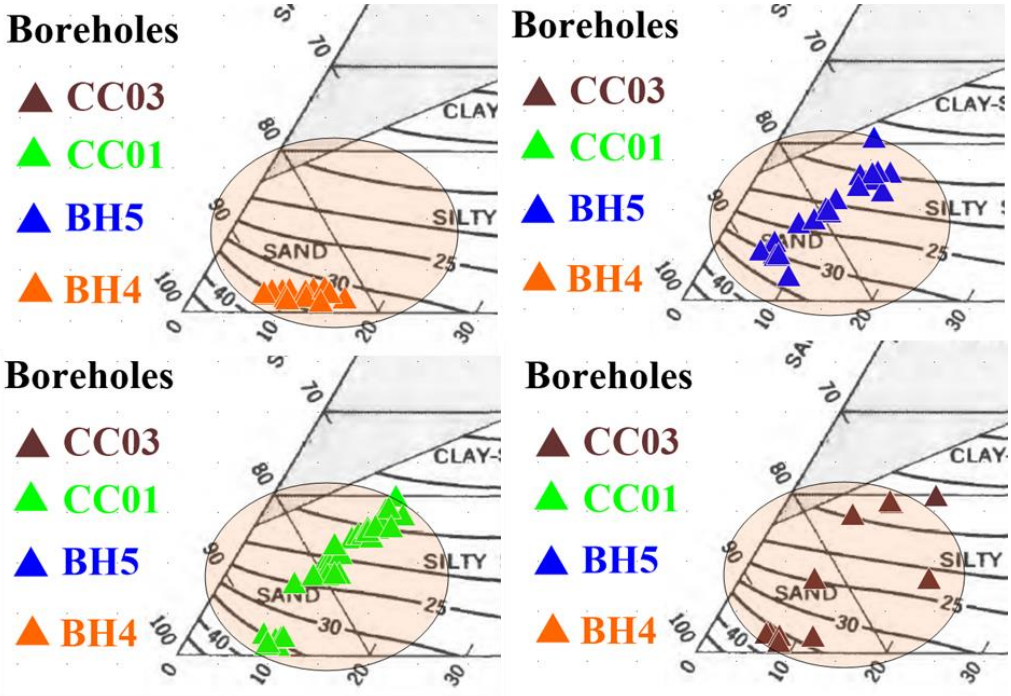

Figure 5.11 The classified specific yield (Sy) at CC01, CC03, BH4, and BH5 for the aquifer layer.

Further substantiating this assertion are the findings derived from pump tests and tracer tests, as expounded upon in section 5.4.2. These tests confirm that the aquifer at well BH4 exhibits higher quality when compared with its counterpart at well BH5.

Drainage water content (DWC) simplified measurement (48h)

For precise Sy determination, testing would have necessitated the use of an 8-foot-long and 5-inch-diameter core sample, with a total survey time potentially extending up to 2.5 years Johnson 1967. Even though several authors advocate for the use of very long columns to prevent an excessive portion of the column from being taken up by the capillary fringe and also observed the drainage over a very long period, we wanted to obtain a first rough estimate for a so-called "drainage water content" (DWC) with a simple drainage period of 48 h using our short cylinders. The core samples were preliminary re-saturated and NMR measurements were done. Employing formula 5.1 and factoring in the volume ratio between the released water content and the initial sample volume, we calculated a drainage water content parameter ("DWC"). To display DWC results we drew on Figure 5.12 a correlation between the DWC after 48 hours of measurement and the Sy value determined through the Johnson method.

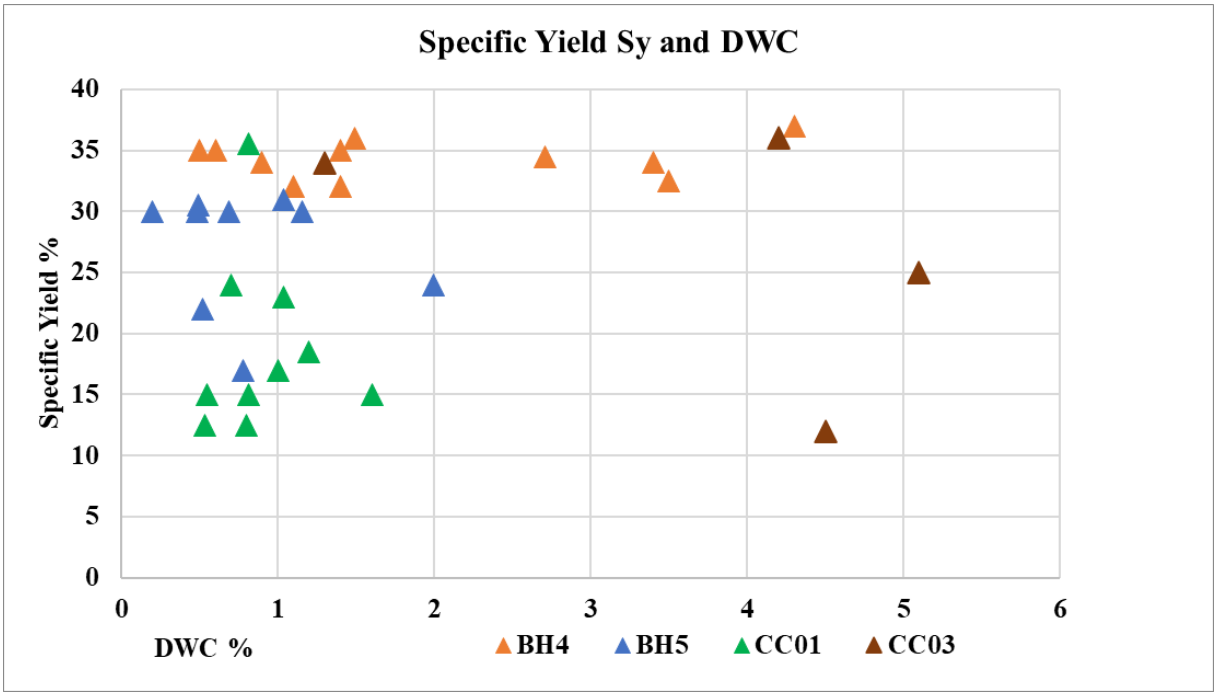

Figure 5.12 Relationship between specific yield (Sy) proposed by Jonhson's triangle and drainage water content (DWC).

The horizontal axis represents the DWC value in percentage, while the vertical axis depicts the specific yield from Johnson in percentage

Figure 5.12 shows that the DWC value ranges from 1-6% while the textured triangle proposed by Jonhson is in the range of 10 to 35 %. There is no relationship between DWC and Sy. The "drainage water content" (DWC) obtained may be a poor estimate of the actual effective porosity. The DWC value underestimates drastically Johnson's Sy. A large amount of water may have been retained by capillarity inside the core.

Indeed, the described experiment highlights the complexity and challenges associated with accurately determining the Sy value under laboratory conditions. Factors such as the size

of the core sample, the duration of the experiment, and the capillary water contribute to the intricacy of the process. The decision to use a smaller core sample and limit the experiment duration to 48 hours was driven by our limited experimental time. These challenges emphasize the importance of careful consideration and methodology refinement in the pursuit of precise Sy determinations in such experiments. Therefore, we needed the field scale measurement (pumping test) to estimate the effective porosity and specific yield in the aquifer.

5.2.3 Hydraulic Conductivity measurements of the samples

Hydraulic conductivity Ks could be a key parameter to be compared to the NMR time constant parameter "T1" usually considered as representative of the dynamic characteristic of an aquifer, being linked with the pore size. This is why we put efforts into getting several series of Ks values. We also choose to fully describe the in Chapter 5 the Ks measurements. A total of 56 depth intervals were examined to assess saturated permeability in both the borehole and site. The study encompassed 17 full-core samples, with saturated permeability determined through constant head measurements at Geopet and Grenoble laboratories Figure 5.13. Additionally, 35 smaller core samples were analyzed at the Geopet lab, employing falling head measurements as illustrated in Figure 5.14. Furthermore, at the BH4 site, permeability tests were conducted at four different depths close to the surface using an Aardwark field permeameter as depicted in Figure 5.15

The constant-head permeameter stands as a widely employed laboratory instrument for determining saturated hydraulic conductivity (Ks) under controlled conditions. The procedure is comprehensively documented and adheres to established standards such as ISO 17892-11:2019. In this laboratory configuration, the water supply at the inlet is regulated to maintain a constant difference in head between the inlet and outlet throughout the test duration. Once a steady flow rate is achieved, the collected water is gathered in a bowl and subsequently weighed. Given the assumed density of water as 1 g/cc, it becomes possible to calculate the rate of water flow through the core sample over time. By employing Darcy's law, we can determine the saturated permeability of the core sample.

$$K = QL/AH \qquad 5.2$$

K saturated permeability in the core sample cm/s A cross-section of the core sample cm^2

Q flow rate cc/s H constant head cm

L length of the core sample cm

In the falling-head permeability test, as depicted in Figure 5.14, water is directed through the soil from a standpipe. The initial head difference (h_1) is measured at the beginning of the test (t = 0), and the water is then allowed to permeate through the soil specimen until the final head difference at time $t = t_2$ is recorded as h_2.

The rate of water flow through the specimen at any given time (t) can be expressed as:

$$K = 2.303\ aL/(At)*\log(h_1/h_2) \qquad 5.3$$

q: flow rate cc/s L: length of core cm

a: cross-sectional area of the standpipe cm^2 $t = t_2$ s

A: cross-sectional area of the soil specimen cm^2 h_1, h_2 pressure head cm

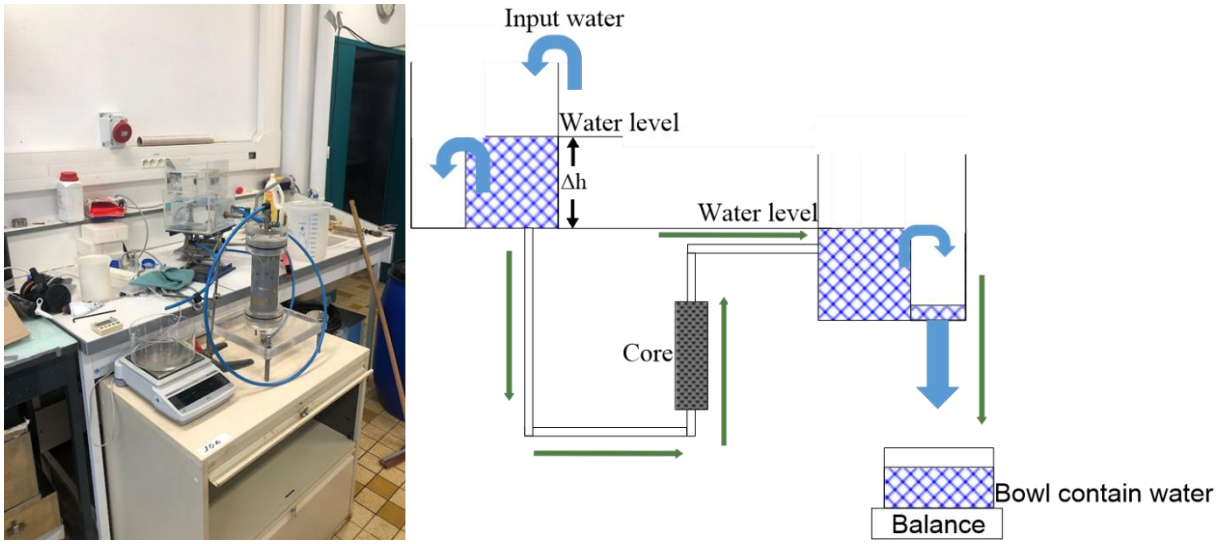

Figure 5.13 Procedure for measuring saturated permeability in the core sample with a constant head.

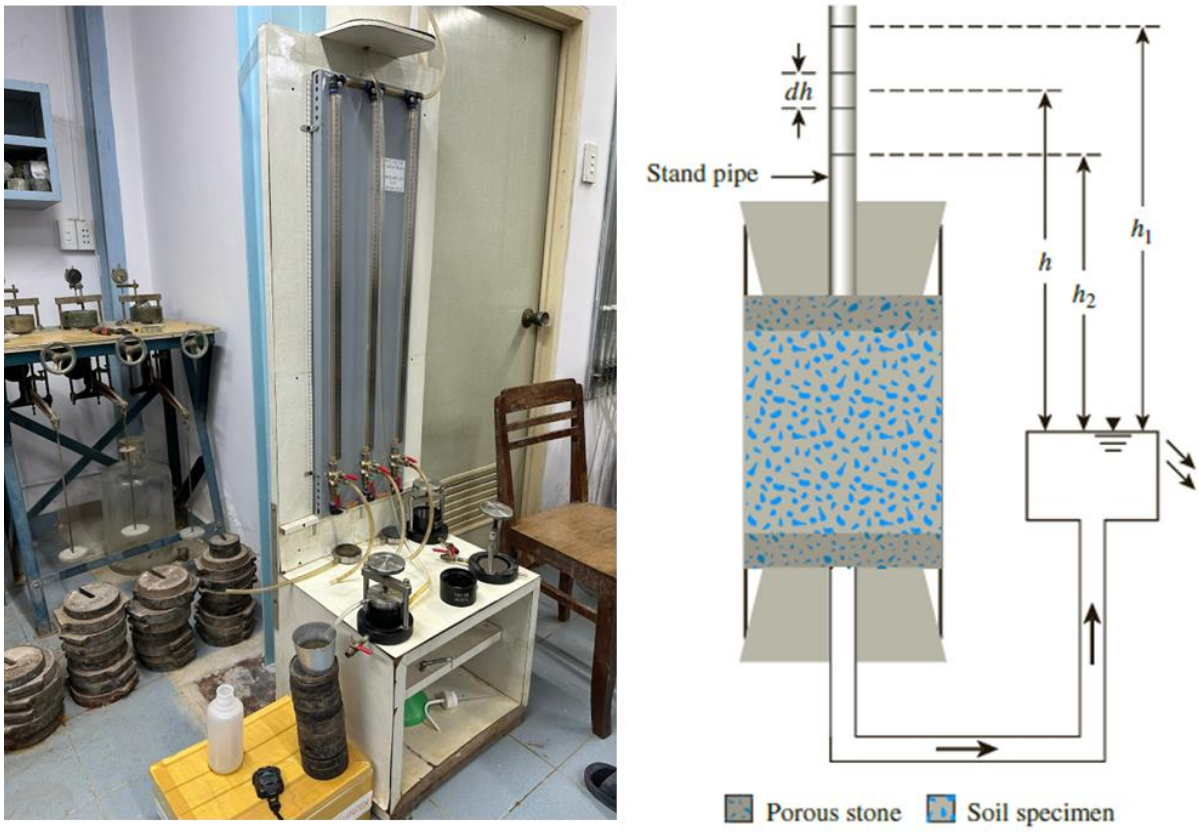

Figure 5.14 Procedure for measuring saturated permeability in the core sample with a variable head (Braja, et al., 2016)

The Permeameter operates as a constant head, maintaining a consistent water depth (h) in the borehole throughout the measurement period Figure 5.15. This ensures that measurement conditions remain stable. The rate of water supplied reflects the soil infiltration rate from both the bottom and side surfaces of the testing borehole. By measuring the amount of supplied water (d) at regular intervals Figure 5.15, equivalent to the water infiltrated by the soil, the

Permeameter estimates soil hydraulic conductivity. The soil-water infiltration rate, representing the percolated water over time and analogous to the reservoir flow rate, is continuously monitored. The measurement concludes when the reservoir flow rate (soil-water infiltration rate) stabilizes, and soil hydraulic conductivity (Ksat) is then calculated using this steady flow rate (Q).

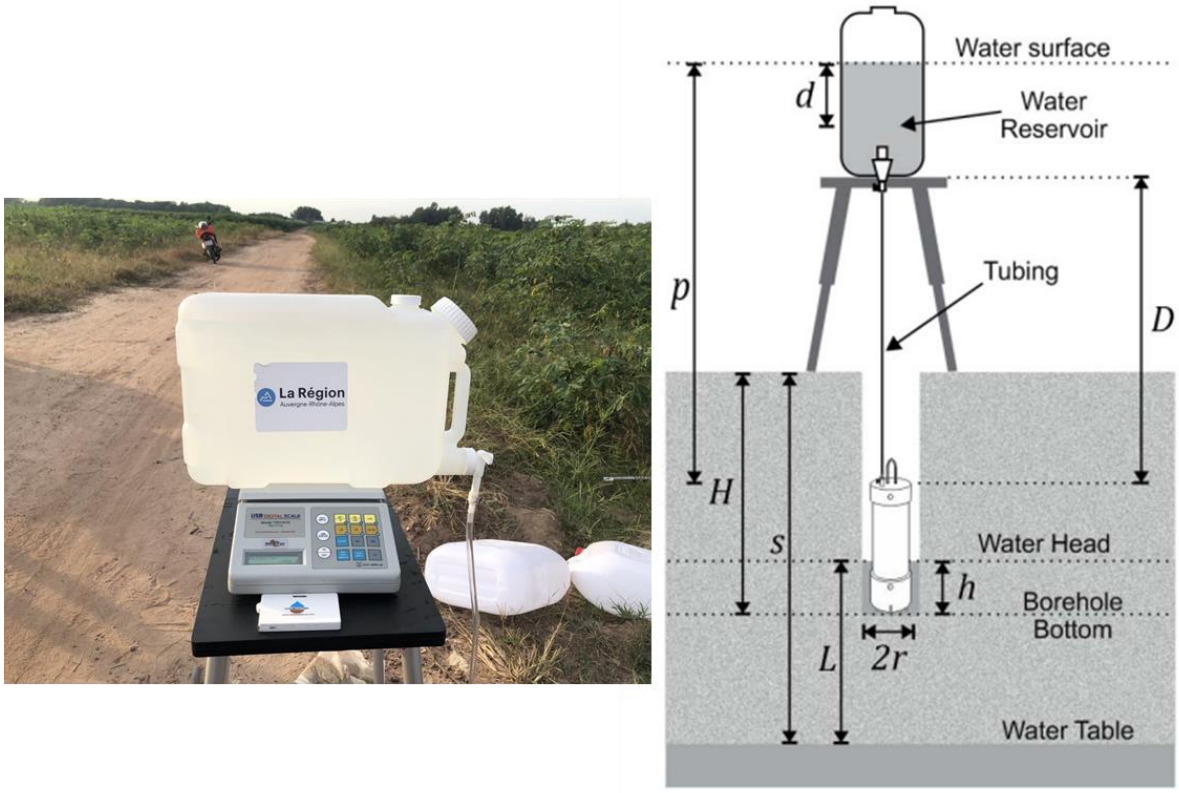

Figure 5.15 Permeameter test at the field BH4 site.

Schematic of a Standard Setup of Permeameter Equipment (PE). Where d is a drop in reservoir water level, D is the vertical distance between the Reservoir and PE, H = borehole depth, r = borehole radius, h = constant water head height in borehole, p = vertical distance between the water surface in a reservoir and constant water head, s = water table depth, and L = the vertical distance between constant water head and water table / impervious layer.

The results of measuring the saturated permeability of core samples in the laboratory and saturated permeability in the field are compared with other parameters of core samples such as VBS value and clay size content.

Ks and clay size content

To investigate the relationship between the Ks value in the core sample and particle composition from sieve analysis, we aim to establish a correlation between the experimental Ks value and the clay size content obtained from the sieve analysis in Figure 5.16. In the clay size domain above 40%, Ks ranges from 2*10e-6 to 5*10e-2 m/day. A clear separation exists between aquitard sediments and shallow-layer sediments. For aquifer layers, Ks ranges above 10e-2 m/day with clay size content less than 20%. Therefore, based on the clay size content obtained from sieve analysis, we can categorize it into three value ranges corresponding to soil classifications: aquifer, aquitard, and shallow layer. This classification aligns with the general

trend were, as clay content decreases, permeability increases. It's important to note that there is no discernible relationship between clay size content and Ks.

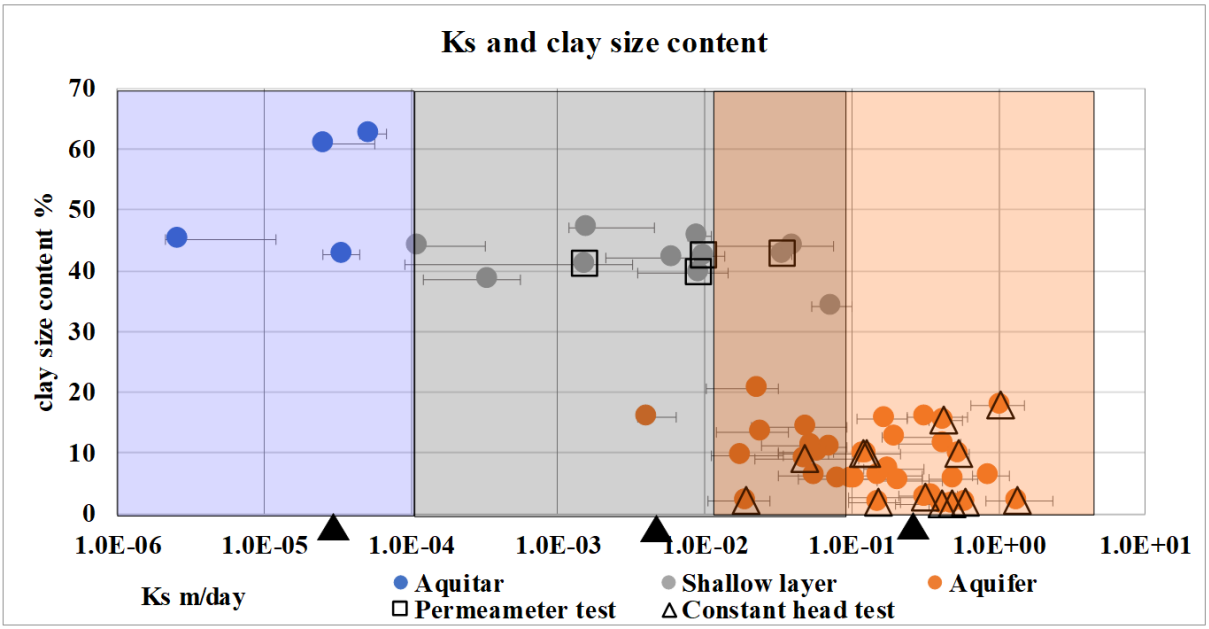

Figure 5.16 Correlation between saturated permeability and clay size content.

The chart illustrates three value regions: the blue region represents core samples in the aquitard layer, the gray region signifies core samples in the shallow layer, and the orange region denotes core samples in the aquifer layer. The core samples with Ks values determined by the permeameter test method are marked with a black square, a black triangle denotes those determined by the constant head method, and the remaining samples' Ks values are determined using the variable head method.

Ks and VBS value

We further investigated the relationship between the Ks value and clay content in the core sample, using the VBS values from the methylene experiment in the figure 5.17. The results reveal two distinct value ranges in the core sample based on VBS values greater than 1 and less than 1, corresponding to two separate permeability ranges. Notably, the lowest Ks values below 10e-4 m/day are attributed to the presence of bull clay minerals (VBS >1 from 2.5 to 6.5). The existence of mineralogical clay (VBS) emerges as a key factor resulting in very low Ks (<10e-4 m/day) in the aquitard layer, as confirmed by the driller and supported by well-logging gamma ray and resistivity measurements. Conversely, when VBS values are <1, the Ks values exhibit a larger variation, ranging from 5 m/day to 10e-4 m/day.

To summarize, in cases where there is no mineralogical clay but a high percentage of very fine sediment (clay size content 40-50%), the Ks values are low but not extremely so, ranging from 10e-4 to 10e-2 m/day, characterizing the shallow layer from 0 to 10m depth. Conversely, when the percentage of fine sediment (clay size content < 20%) is low, the Ks values are higher, ranging from above 10e-2 to 1 m/day. This characterizes the aquifer, with a mean value of Ks at 2*10e-1 m/day.

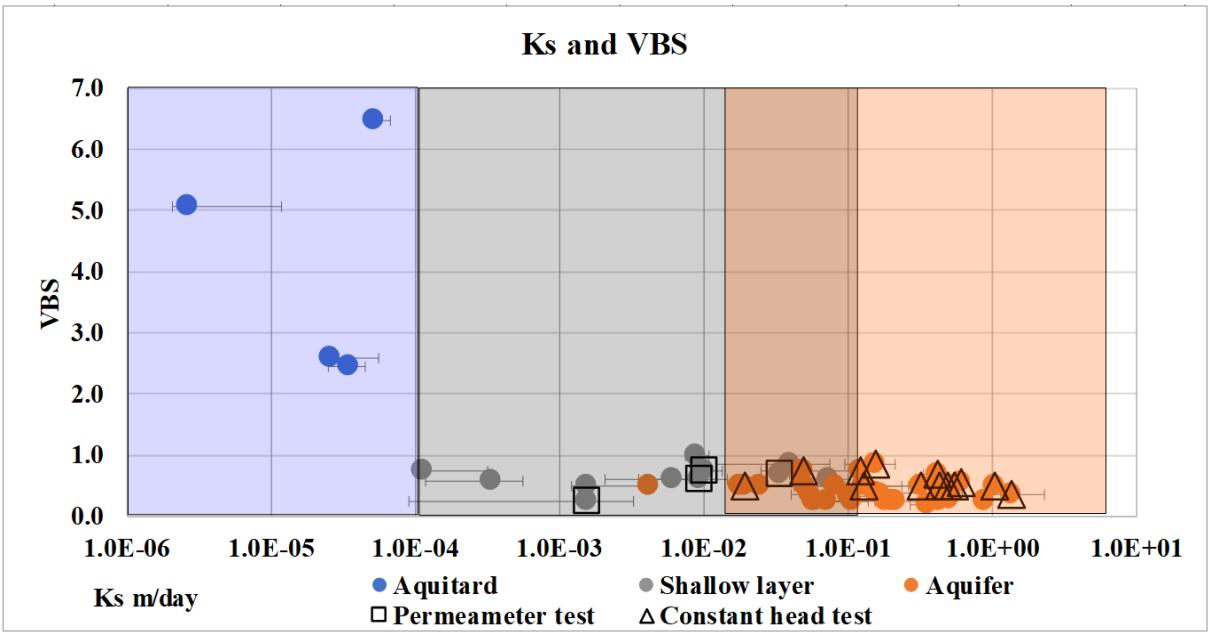

Figure 5.17 Correlation between saturated permeability and clay size content estimated by the VBS value obtained with the methylene blue test

Correlation between Ks and well-logging data

The saturated permeability value Ks is compared with the well-logging data: Figure 5.18 and Figure 5.19 illustrate the correlation between Ks and gamma-ray or resistivity, respectively.

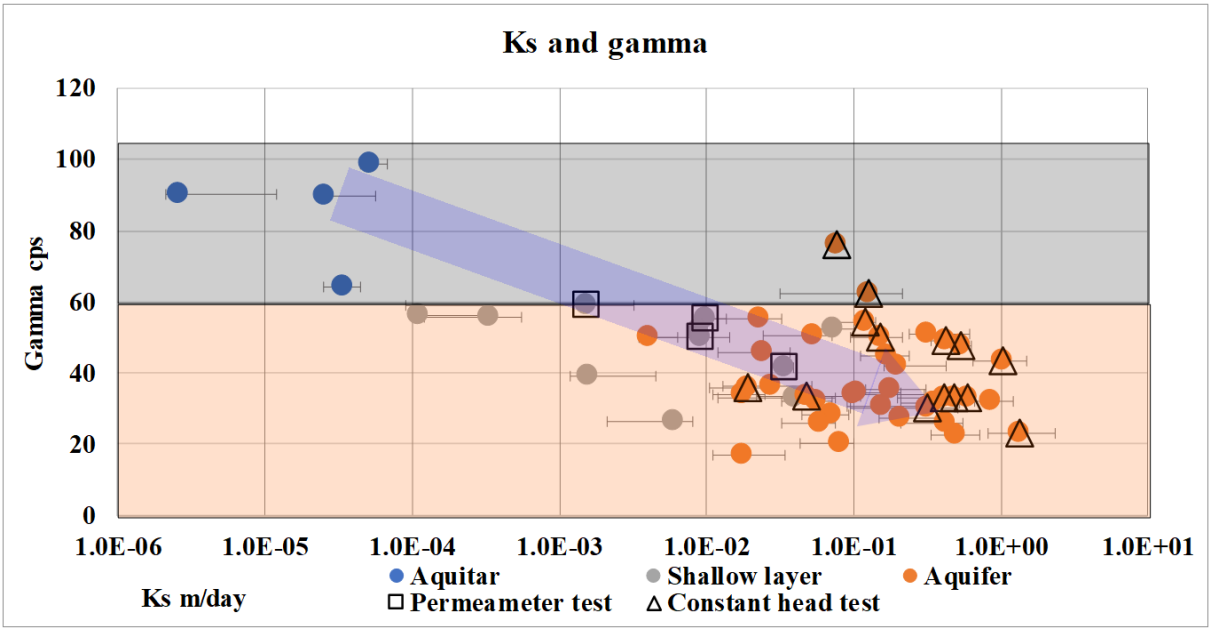

Figure 5.18 Correlation between saturated permeability (m/day) and gamma-ray (in count per second)

In Figure 5.18, the correlation trend between gamma-ray values and saturated permeability (Ks) shows logically that low gamma-ray values correspond to aquifers with high Ks values, while high gamma values correspond to aquitard layers with low Ks values, typically lower than 10e-4m/day. The gamma-ray values are thus dividing two domains: values less than 60 cps characterize the aquifer and shallow layer, while values higher than 60 cps characterize the aquitard layer. However, distinguishing between the shallow layer and the reservoir layer is challenging with gamma-ray values of less than 60 cps.

Figure 5.19 illustrates a general trend where high resistivity values characterize high-permeability aquifers, while low resistivity values characterize low-permeability aquitards. The resistivity values are divided into two domains: values less than 100 Ω·m, which are typical for the aquitard layer, confirmed by gamma-ray values; and high resistivity values ranging from 200 to 1200 Ω·m, characterizing the aquifer and shallow layers. However, it is not possible to rely on resistivity values to clearly distinguish between the shallow layer and the aquifer.

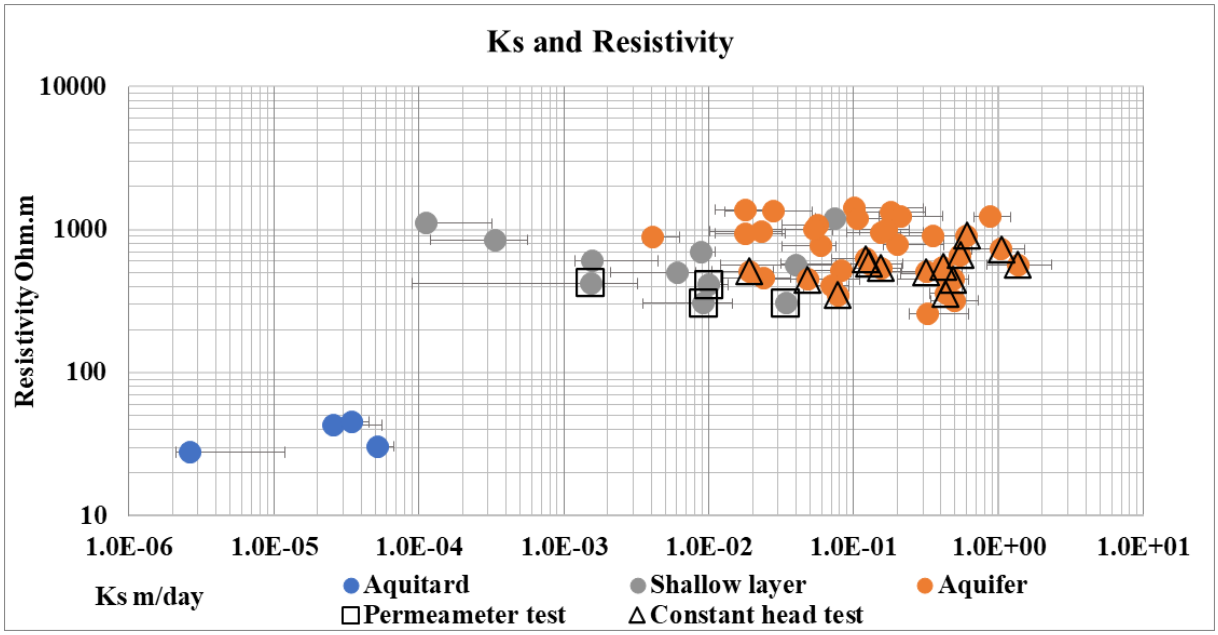

Figure 5.19 Correlation between saturated permeability and resistivity logging

5.3 NMR results

5.3.1 Preparation of the samples and interpretation procedure

The standard core sample used in this study measures 25 cm in length and 75 mm in diameter, and it was placed inside a PVC tube with the same length but a slightly larger diameter for protection. In the field, the core was wrapped with a thin food wrapping paper to fix it in place before being placed in the prepared PVC tube. To ensure proper saturation, two pieces of hard mica with holes were used to seal the ends of the tube.

The saturation process began with placing the tube in a vacuum chamber to remove any air gaps in the porosity of the core. The length of time required for saturation varied depending on the time since the extraction of the core, with “fresh” cores requiring 1-2 hours and older cores (extracted 1 or 2 years ago, at the beginning of the PhD) needing 2-3 hours for full saturation.

Throughout the process, the mass of each state was carefully measured and recorded. This included the mass of the core, the mass of the core and PVC tube, and the mass of the core both before and after saturation.

In addition, we also made a PVC tube full of water with the same length of 25 cm and diameter of 90 mm. This water sample was used to compare the NMR signal amplitude of the core sample and of the water sample, enabling us to determine the NMR water content from the NMR method. Furthermore, the difference in diameter between the core sample and the water sample will lead to a correction in the result during interpretation.

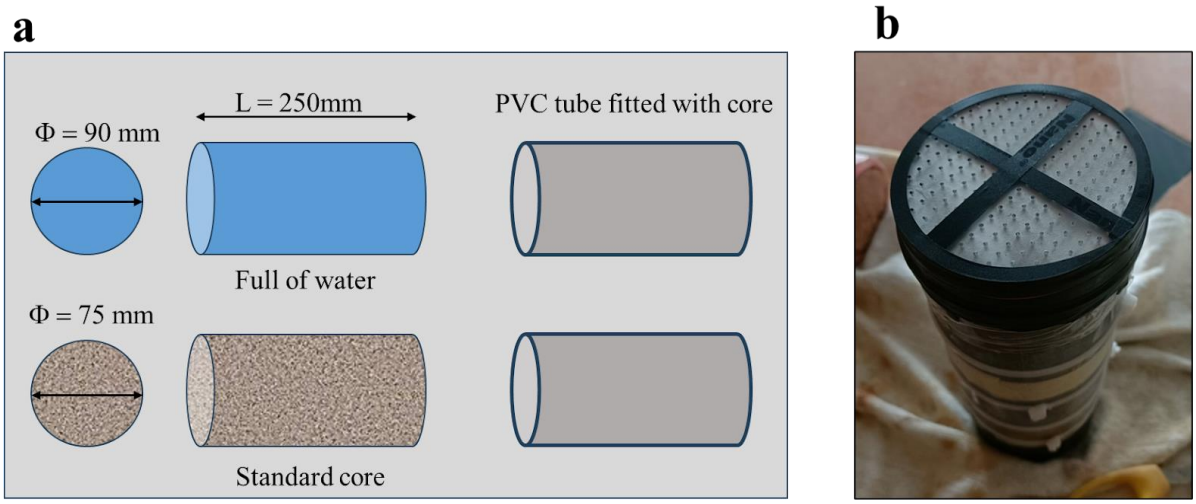

Figure 5.20 a) core sample and water sample tubes, b) Core sample after preparation before saturation step

A comprehensive procedure for measuring one standard core using NMR equipment in the field will be briefly described. We choose to describe the procedure used in Vietnam while the procedure adopted in France for the first measurement is similar with slight differences due to the noise conditions. It is worth noting that the detailed description of measuring and interpretation can be found in the "User's Guide Processing Core Samples in Vietnam " developed for the purpose of the PhD by (Legchenko, 2022). The measuring sequence with the “FID2” is used, and the time sequence of the injection of the current pulse duration, dead time duration, and noise measurement duration is set according to a specific table that takes into account various factors such as the core diameter, length, and water content.

The measurement procedure for each core involves a three-step procedure: 1) first take three NMR measurements using the full water sample tube at different relaxation times (600ms, 800ms, and 1000ms) to establish a reference signal for the core sample, 2) then five measurements of the core sample itself at various relaxation times (1000ms, 700ms, 400ms, 200ms, and 100ms) to capture a range of signals that can provide the necessary data to calculate the water content, and 3) at last three additional measurements of full water sample at the same relaxation times as before to ensure the stability of the reference signal. The frequency used for Vietnam in the 2023 procedure is 1819.7 Hz, which is carefully chosen to maximize the sensitivity of the NMR measurements while minimizing the impact of environmental noise. Both the core sample and water need to be weighed before and after measurement to ensure the accuracy of the measurement.

For the core sample, the frequency stack applied is typically around 200-400 stacks, depending on the level of noise compared to the signal. The experiment was made in Vietnam a few kilometers from the MRS field test, but in lower noise conditions away from the high-power line. The signal from the core is logically a lot weaker than that from the water sample due to the lower water content. Therefore, a higher number of stacks is often needed to obtain a reliable measurement. In contrast, for the water sample, the frequency stack is usually between 15 – 25 stacks, as the signal is much stronger and more stable. Each core sample takes approximately 3 – 4 hours to complete, which includes the time required for setting up the equipment, preparing the core sample and the water sample, and conducting the measurement.

The raw data obtained from NMR measurements needs to be post-processed and interpreted before it can be used to make meaningful conclusions. The post-processing and interpretation of NMR data are critical steps, and some examples of the post-processing parameter are given using screen-shots of specialized software programs such as NumisPro and Samovar (Figure 5.21, 5.22).

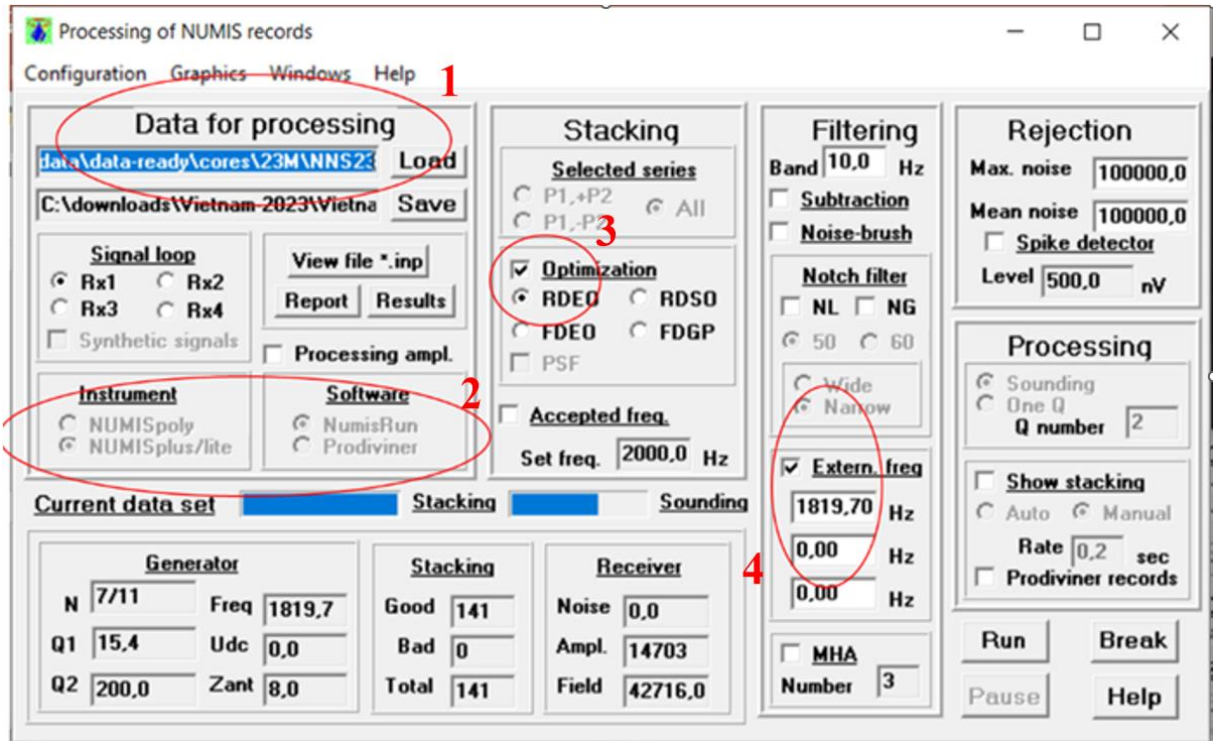

Figure 5.21 NUMIS PROGRAM for optimization, filtering, and stacking data before inversion.

In Step 1, the dataset can be loaded or saved using the 'Load' and 'Save' buttons. Moving on to Step 2, the measuring device selected for this study is the NUMIS plus/lite device. Step 3 involves stacking, which can be performed without any optimization (just the addition of records) or by utilizing optimization algorithms such as RDEO (Raw Data Energy Optimization), assigning higher priority to records with smaller energy. This option is commonly used in NumisRun. Finally, in Step 4, the Lamor number at the survey location, specifically in the research area, is determined to be 1819.7 based on geomagnetic field values.

After the raw NMR measurements are taken in the field with our saturated cores, the data are processed using the “NumisPro” software that filters and stacks the records to produce relevant information. The “Samovar” software is then used to compute signal amplitudes, which are an important parameter for calibrating water content. The next step in the interpretation process is to extract the relevant information from the ".nov" raw file and proceed with basic analysis using Excel tables. The interpretation process involves calculating parameters such as the amplitude of the NMR signal versus P1 duration, the mean NMR signal versus P1 duration, and the NMR signal moment versus P1 duration. These parameters are used to compute T1 and water content using the Solver tool, a part of the Excel calculation sheet.

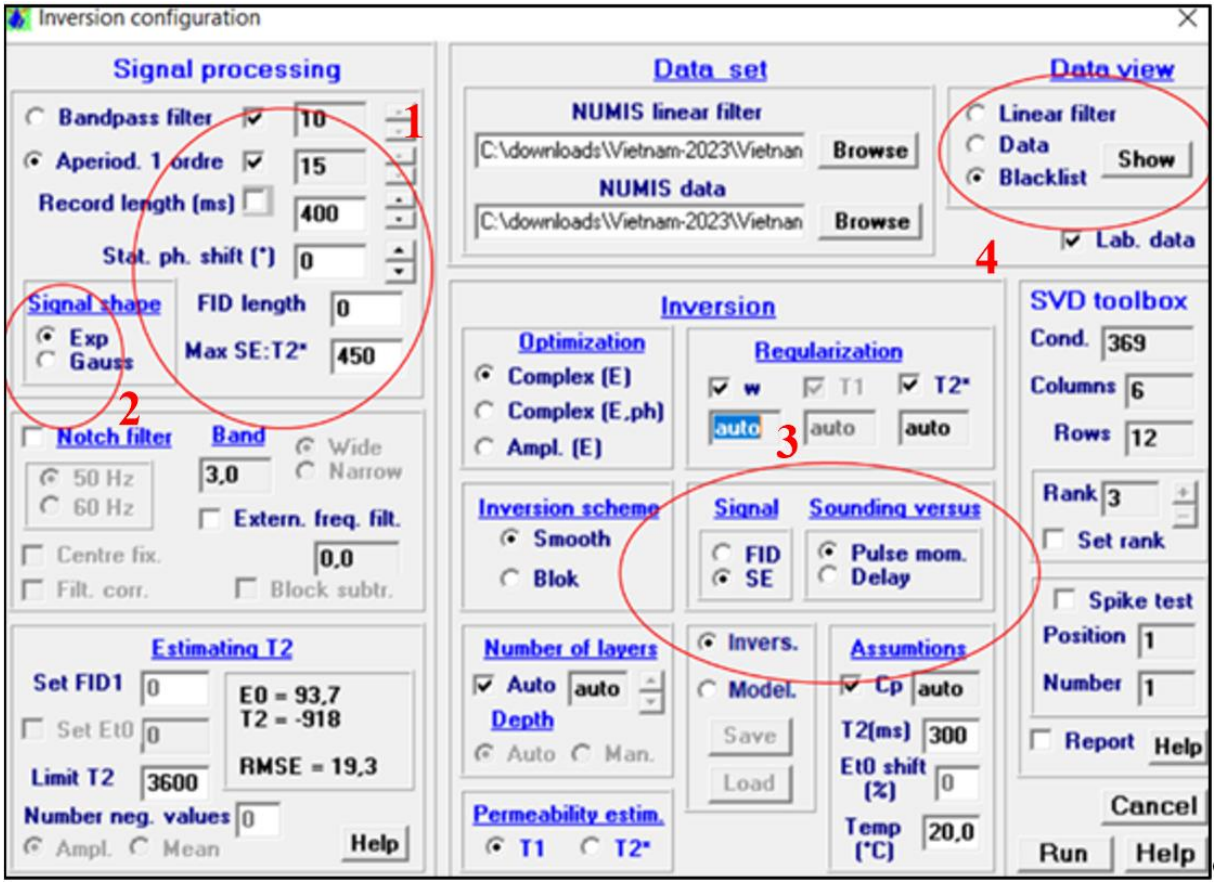

Figure 5.22 SAMOVAR program before inversion of the core data, to obtain the ".nov" result file.

The processing process consists of several steps. In Step 1, the bandpass filter and measurement pulse time are selected. Moving on to Step 2, the data fitting model is chosen, either in exp or gauss format. In Step 3, the input data parameter is determined, which could be SE, FID, or Signal moment. Finally, Step 4 involves removing bad measurement data pulses identified in the blacklist section

To enhance the T1 parameter determination, the procedure involves three methods for computing T1, and this allows us to evaluate the T1 range of deviation. Finally, the output of the interpretation process is a summary table that includes parameters such as T1 (in ms) and water content (in %).

5.3.2 NMR T1 results

A total of 42 core samples were selected in the aquifer layers of the 4 wells (Figure 5.7). The NMR response of a sample can be characterized by three values including amplitude, mean amplitude signal, and signal moment Figure 5.23. The noise is estimated using mean and moment noise signals only.

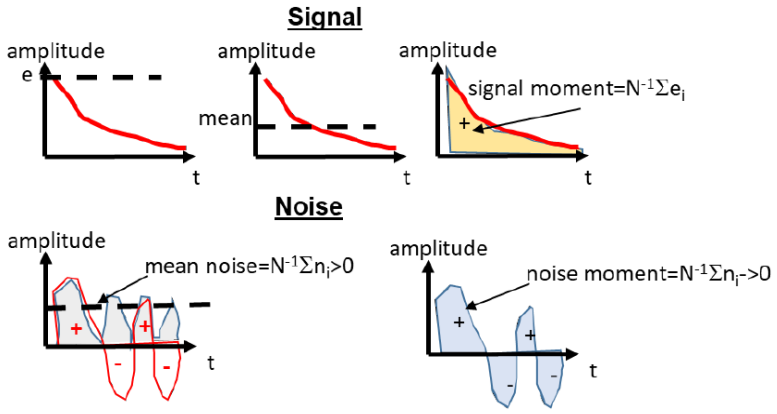

Figure 5.23 Three different ways to calculate the amplitude of NMR signal and noise in NMR measurement

Each sample underwent analysis with five different polarization durations: 79ms, 222ms, 370ms, 620ms, and 1030ms. As the duration of the NMR pulse increases, there's a corresponding increase in the recorded signal. The signal amplitude may be smaller than E_{fid} and for computing E_{fid}, one has to apply the T1 correction.

$$E_{fid} = E_{meas}/(1 - \exp(-t_p/T1)) \qquad 5.4$$

E_{fid} is signal amplitude Free Induction Decay nV

E_{meas} is measure signal amplitude nV

This model allows us to match actual measurements and theoretical values, leading to the estimation of the T1 value. The three determinations of T1 involves an analysis of three key NMR parameters: amplitude, mean amplitude signal, and signal moment value for the selected pulse moment duration. These parameters are illustrated in Figures 5.24, 5.25, and 5.26, corresponding to core samples from wells BH4 at a depth of 16.25m, CC01 at 33.75m, and CC03 at 10.25m, respectively. We choose to present those examples as good, intermediate, and bad quality T1 determination.

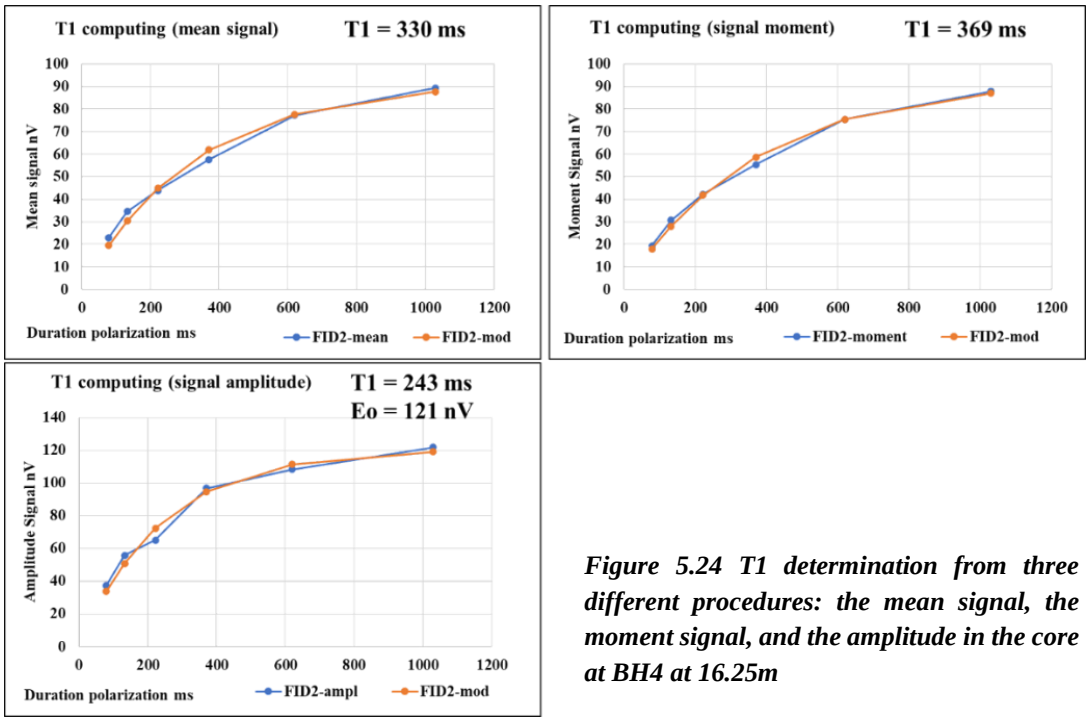

Figure 5.24 T1 determination from three different procedures: the mean signal, the moment signal, and the amplitude in the core at BH4 at 16.25m

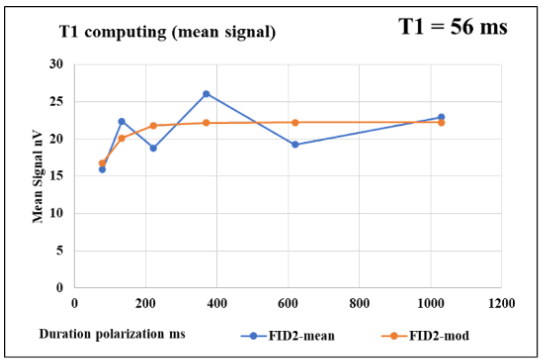

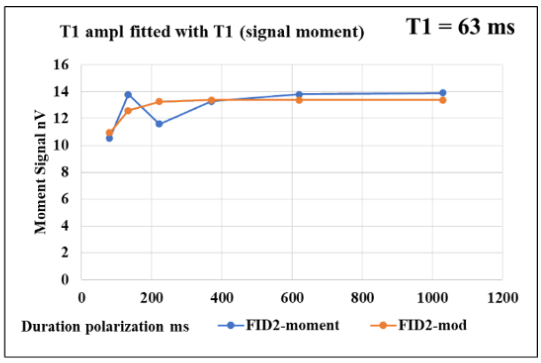

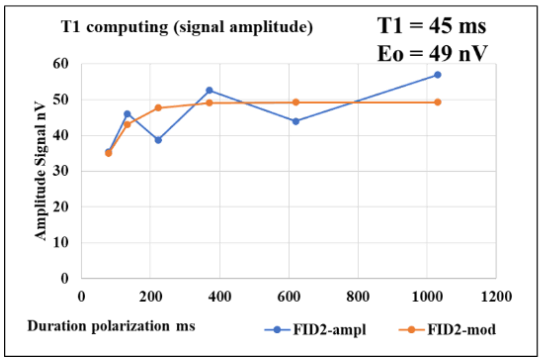

Figure 5.25 T1 determination from three different procedures: the mean signal, the moment signal, and the amplitude in the core at CC01 at 33.75m

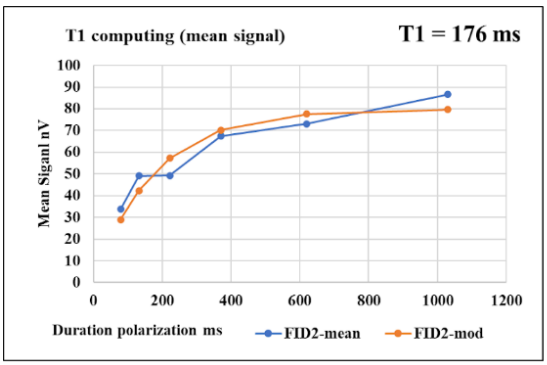

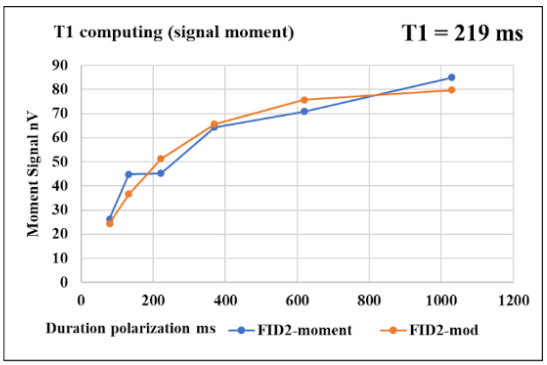

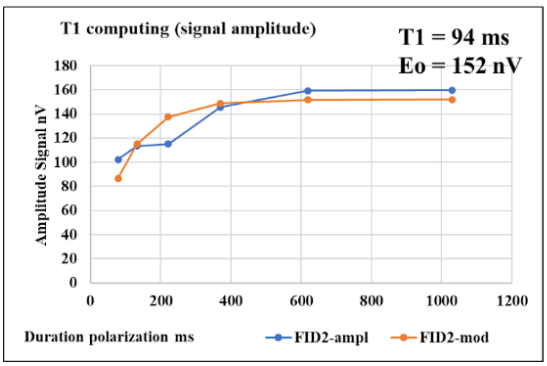

Figure 5.26 T1 determination from three different procedures: the mean signal, the moment signal, and the amplitude in the core at at CC03 at 10.25m

The core sample from well BH4, shown in Figure 5.24, exhibits the highest amplitude at a depth of 16.25 meters. This sample also demonstrates the most accurate fitting between the measured data (blue curve) and the theoretical model (orange curve). The T1 values for this sample range between 243ms and 369ms, with an average of 314ms. In contrast, the sample from well CC01 at a depth of 33.75 meters, presented in Figure 5.25, gives an example of bad-quality data with the smallest T1 values. This sample is characterized by lower amplitude readings and a significant discrepancy between the measure and theoretical model data. The T1 range for this well is 45 to 63ms, averaging at 56ms.

Figure 5.26 illustrates the intermediate quality results for well CC03 at 10.25 meters depth, where T1 values span from 94 to 219ms, with a mean of 163ms. The comprehensive T1 value analysis for all 42 core samples is summarized in Figure 5.27.

NMR T1 and "Johnson's Sy"

To investigate the relationship between the NMR T1 value and various reservoir parameters, we establish the correlation between NMR T1 and the specific yield from Johnson, as illustrated in figure 5.27. In this figure, T1 relaxation times measured at wells BH4, BH5, CC01, and CC03 are depicted using green, blue, orange, and brown triangles, respectively, each accompanied by error bars.

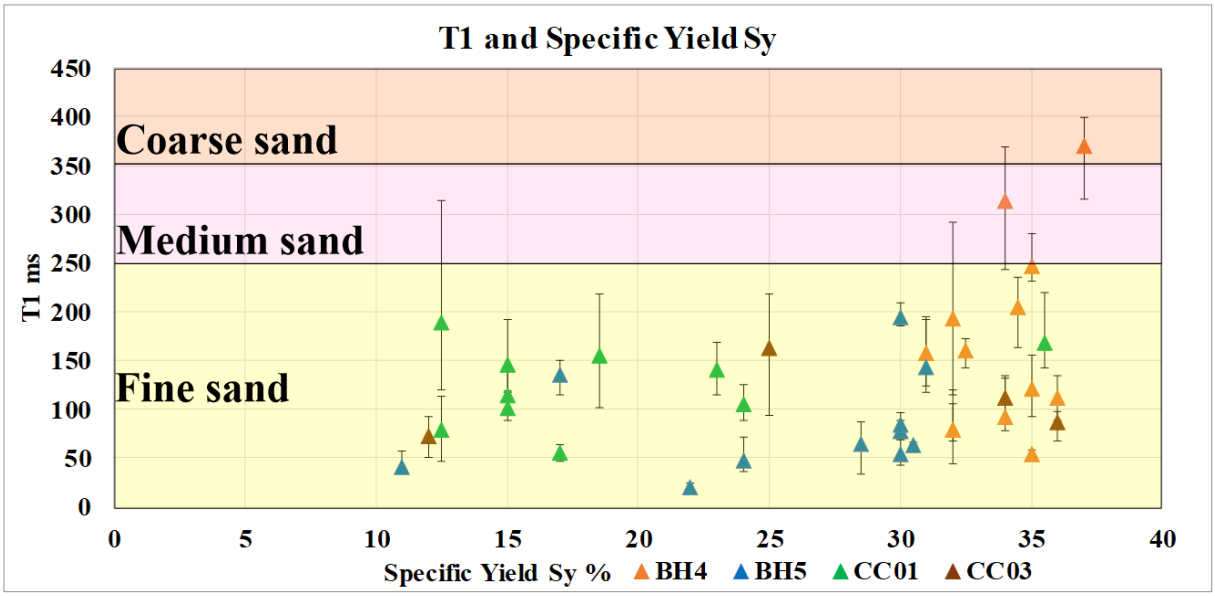

Figure 5.27 Relationship between T1 and specific yield (Sy).

The horizontal axis represents the specific yield from Johnson in percentage, while the vertical axis depicts the NMR T1 value in milliseconds. The figure illustrates three distinct value ranges: the yellow region corresponds to the T1 value of 0-250ms, representing the characteristic fine aquifer; the pink region signifies the medium aquifer with a T1 value ranging from 250-350ms, and the orange region represents the coarser aquifer with a T1 value above 350m.

These findings predominantly indicate that the T1 values for the majority of the tested aquifer core samples fall within the 0-250ms range. This is the major result of our NMR core sample analysis: This T1 characteristic classifies our aquifers as "fine sand". This result is in accordance with the supposed T1 value calculated during our field test site CCO1 (Figure 5.3). Furthermore, the figure reveals a lack of correlation between the T1 values and the estimated "Johnson's specific yield" of the aquifer, as determined from the grain composition of the core samples, when evaluated against Johnson's classification for granular composition. Most T1 measurements suggest a "very fine aquifer" classification, yet Ks at BH5 is substantially lower than at BH4, as corroborated by pumping and tracer tests (see further in the chapter).

NMR T1 and Ks

Another important output of the T1 NMR core analysis is to evaluate if T1 values can be used as an indicator of permeability, specifically KS permeability. This is important for assessing how easily water can flow through the aquifer material. Figure 5.28 depicts the general trend where an increase in hydraulic conductivity (Ks) corresponds with an increase in

T1 value. However, the general trend is observed on a very scattered data set, and the data corresponding to borehole 5 (BH5) exhibits both low Ks and low T1 values, diverging from the expected range of 0.3 to 20 m/day.

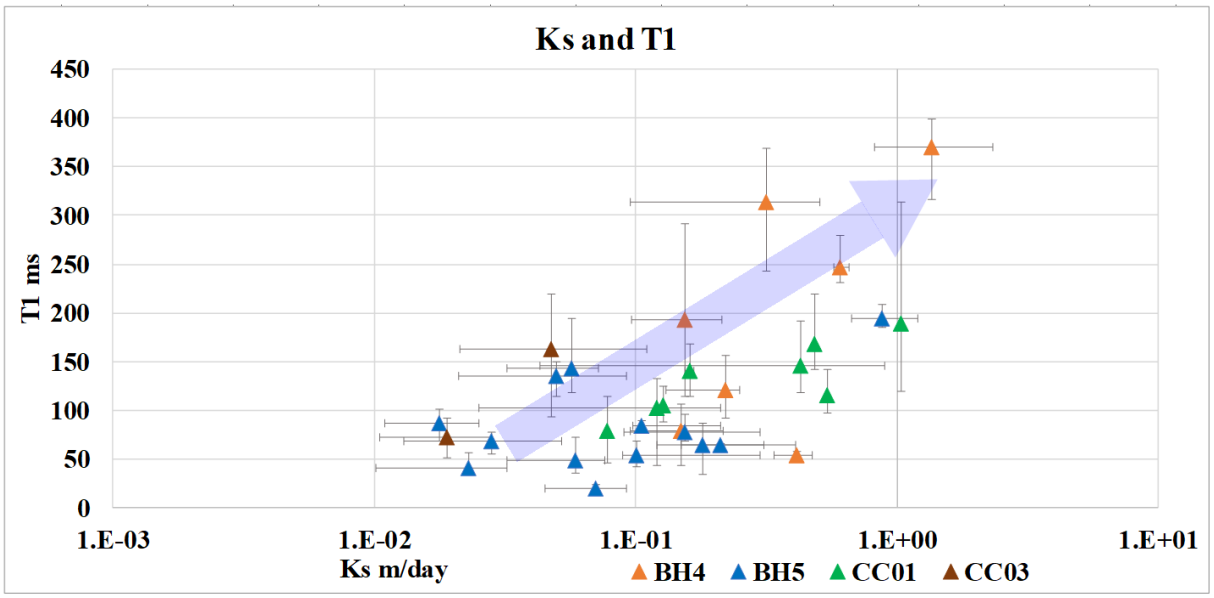

Figure 5.28 Correlation between Ks and T1

To validate the observed trend, further investigation encompassing aquifers with medium to coarse granularities and Ks values exceeding 1m/day is necessary. Enhancing our understanding of the T1-Ks relationship could render the NMR T1 parameter a robust proxy for estimating Ks at the core scale.

5.3.3 NMR water content

To determine water content, it is necessary to calculate the initial amplitude of the NMR signal produced by both the soil sample and the equivalent cylinder full of water. This involves extrapolating over the dead time and accounting for incomplete polarization. Incomplete polarization leads to a reduced amplitude, and adjustments are made to extrapolate it toward complete polarization. The dead time extrapolation takes into account the dead time value used in the pre-defined measurement sequence.

Measurements with soil sample: During the interpretation, we noticed that for the Vietnamese samples, the signal envelope deviates from a classical exponential form, therefore we chose a Gaussian model to fit the envelope. To compute the initial amplitude, T1 values are derived using both the amplitude and signal moment estimations. Since the mean signal is more sensitive to noise, its corresponding T1 is usually omitted. The measured amplitude against pulse duration is then fitted using two predetermined T1 values, yielding the minimum and maximum measured amplitudes. The corresponding initial amplitudes are determined by extrapolating over the dead time. Utilizing amplitude data, we modify the T1 value determined from the parameters of mean signal, moment signal, and amplitude to redefine the original signal amplitude value. The outcomes of these calculations for three representative core samples are depicted in Figure 5.29.

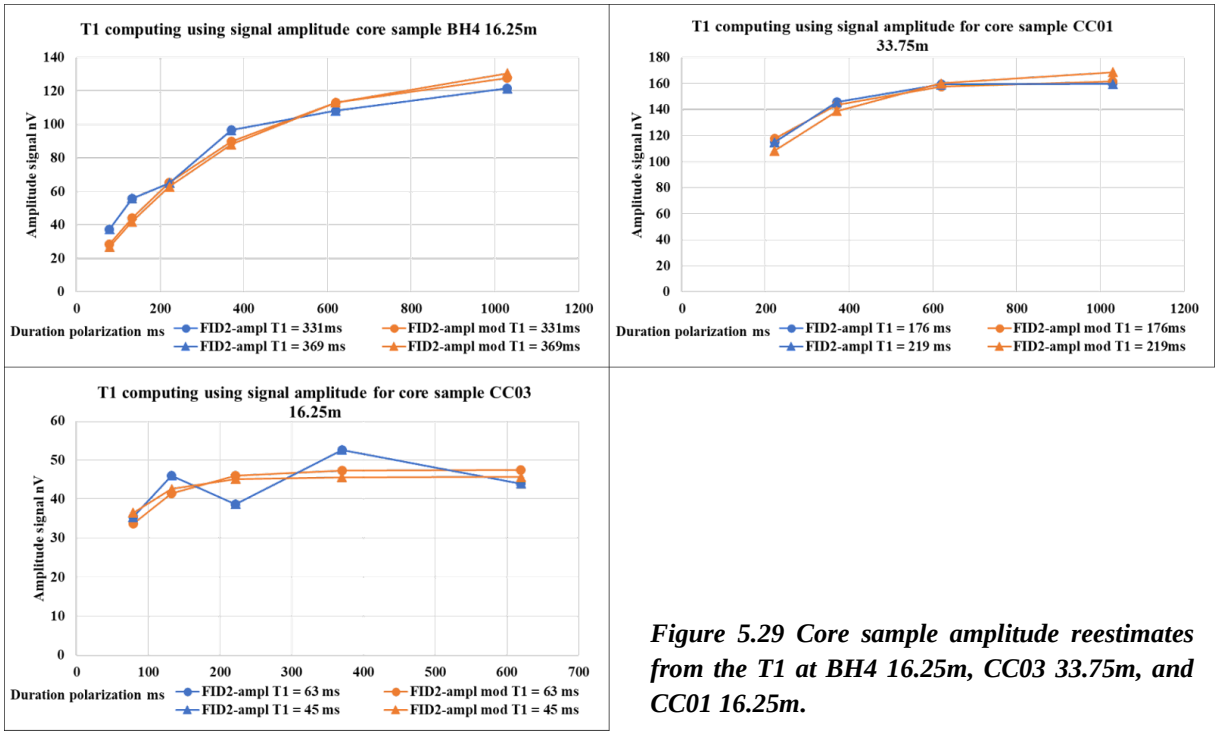

Figure 5.29 Core sample amplitude reestimates from the T1 at BH4 16.25m, CC03 33.75m, and CC01 16.25m.

Measurements with a cylinder full of water, the "water sample"

T1 time constant for "full water" can be accurately determined by using the mean signal, amplitude, and signal moment, given the high signal-to-noise ratio. This involves fitting the measured amplitudes while accounting for the minimum and maximum values of T1 and extrapolating over the dead time

The measured data exhibit a good fit and the computed T1 values for the water sample are displayed in Figure 5.30.

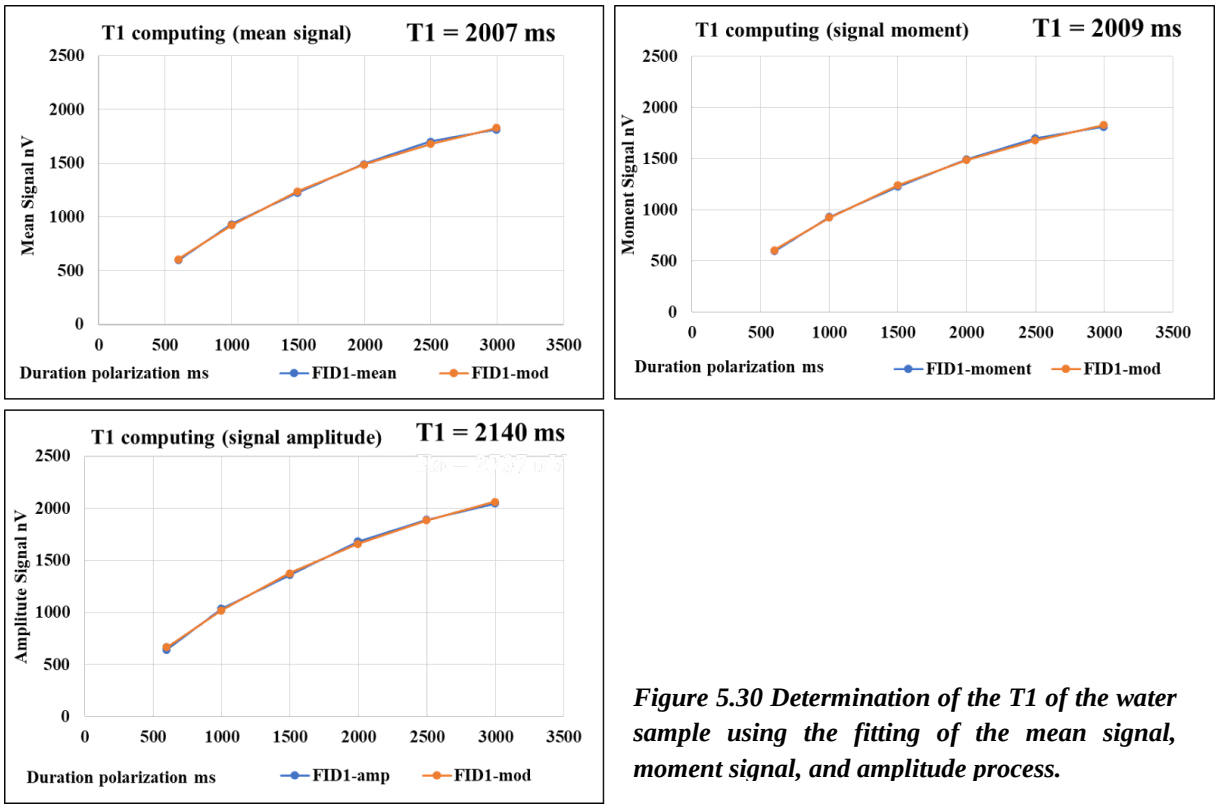

Figure 5.30 Determination of the T1 of the water sample using the fitting of the mean signal, moment signal, and amplitude process.

Based on the data from Figure 5.30, the T1 value for the water sample is estimated to be between 2007ms and 2140ms. In this analysis, the Gaussian model is utilized. To determine the initial amplitude, T1 values are calculated using estimates of both amplitude and signal moment. Then using the min and max values of T1, the interpreted signal amplitude values for the water sample are calculated and shown in Figure 5.31. It ranges from a minimum of 2640nV to a maximum of 2737nV

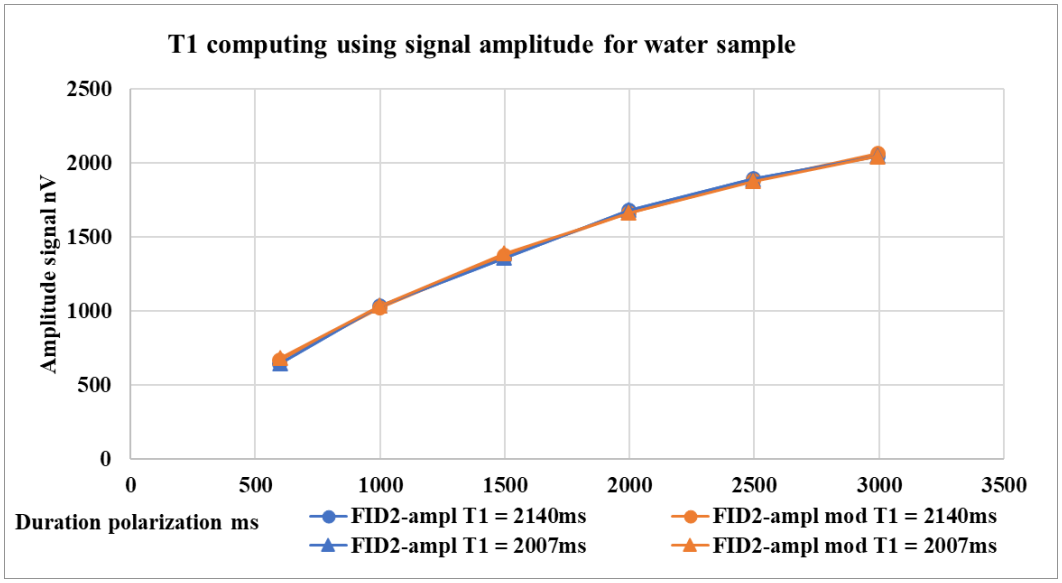

Figure 5.31 Water sample amplitude reestimate with min and max values of T1 = 2007ms and T1 = 2140ms

Calculation of the NMR water content of the core samples

Having calibrated the measurement with the full water sample, the last step is to calculate the water content in the core sample by determining the ratio between the amplitude of the soil sample (adjusted for dead time and sample size) and the amplitude of the water sample. This ratio serves as an indicator of the water content in the core sample. As said earlier, corrections due to the geometry of the cylinder are applied for a precise estimation of water content. Table 5.3 presents the example of the results from the three cores taken as examples above. Logically, the Core 01 "33.75m" has a very low NMR water content between 1.4 and 1.5%. The core CC03 "10.25m" has a higher NMR water content between 4.9 and 5.3 %.

Table 5.3 Water content in the Core Samples

Core sample (Borehole and depth)	Water		Core Sample		NMR Water Content (%)		NMR Water Content (%) after correction	
	Eo min	Eo max	Eo min	Eo max	Min	Max	Min	Max
BH4 16.25m	2640	2737	134	139	4.9	5.2	3.7	3.9
CC01 33.75m	2640	2737	46	47	1.8	1.9	1.4	1.5
CC03 10.25m	2640	2737	162	171	6.1	6.7	4.9	5.3

Correlation between T1 values and the actual NMR water content in the core samples.

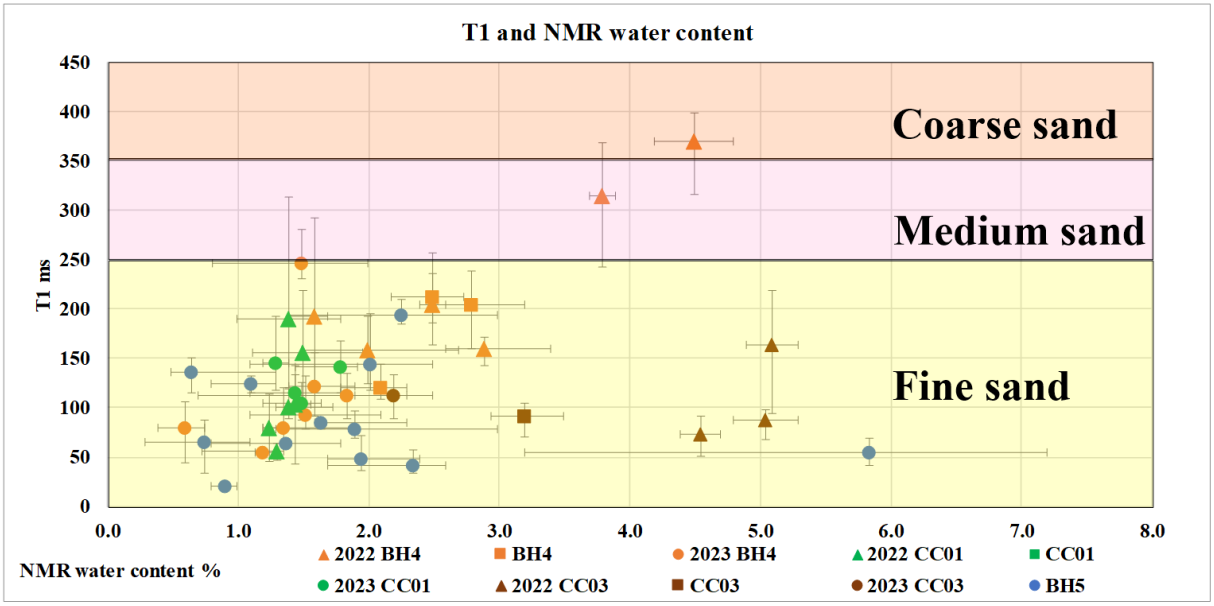

Figure 5.32 Relationship between T1 and NMR water content

Figure 5.32 indicates that there is no reliable correlation between the T1 value and the NMR water content. Even if we discard some data obtained in 2022 for borehole CC03 (brown triangles at the right) and one data obtained from the borehole BH5 (blue circle at the right) it remains difficult to propose a general trend "higher the T1, the higher the water content" because the relation appears very scattered. The NMR measurements indicated that the water content at BH5 varied between 0.6% and 2.5%. In contrast, at BH4, the NMR water content values were found to be between 0.5% and 4.5%. These findings show a slightly higher water content in BH4 compared to BH5, suggesting superior aquifer quality at BH4 with a possible higher storativity. This hypothesis will be further validated through the pumping test and tracer test, discussed in Section 5.4.

NMR water content and DWC, total porosity and "Johnson's Sy"

When plotting NMR water content versus our simplified Drainage Water Content (DWC) in Figure 5.33, we found surprisingly a general trend increase in water content leads to an increase in DWC.

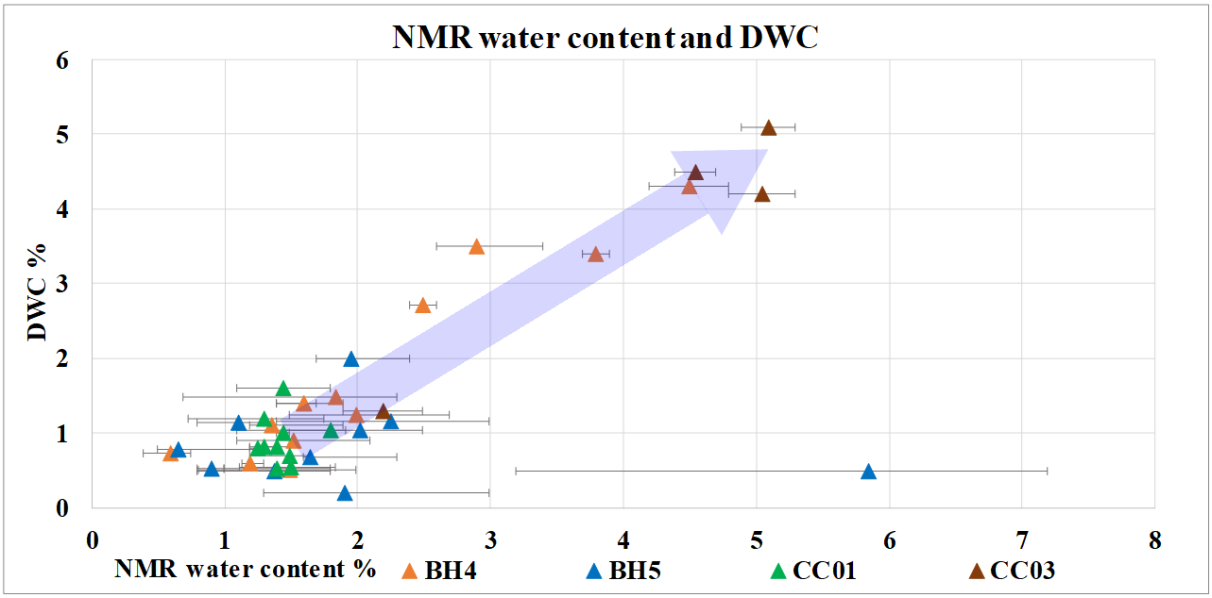

Figure 5.33 Relationship between NMR water content and drainage water content (DWC)

Figure 5.33 demonstrates that Borehole 5 (BH5) has an NMR water content ranging from 0.8 to 2.1% and a drainage water content (DWC) between 0.5 to 2%, whereas Borehole 4 (BH4) shows for some cores higher values for DWC ranging from 1 to 4.5%. Interestingly, DWC values above 2.5% correlate with higher NMR water content values of 2.5 to 5.2% in 7 data points. This trend suggests a potential linear correlation between NMR water content and our simplified DWC parameter. DWC is highly underestimating the true effective porosity and this implies that NMR water content may also undervalue effective porosity. Attempts to refine this relationship with additional data points in 2023 were unsuccessful, as the cores examined were at the lower end of the NMR water content spectrum (<3%). Further measurements are essential to confidently assess NMR's capability to estimate effective porosity in a wider range of sandy to silty aquifers. It is also compulsory to build a more reliable laboratory experiment that could measure a better estimate of the true specific yield.

In Figure 5.34 presents data showing no correlation between total porosity and NMR water content. Despite a constant total porosity of 30%, NMR water content varies significantly from 0.6 to 5.6%.

Figure 5.35 indicates that there is no relationship between Johnson's specific yield (Sy) and NMR water content. This suggests that the NMR water content is not influenced by the clay content within the core sample, which is a primary factor in calculating Johnson's Sy.

Partial conclusion on NMR at the core scale

To summarize our results obtained with the NMR water content as well as the T1 experiment at the lab scale, it is worth noting that the NMR results, when compared to parameters obtained at the same scale on core samples and grain size analysis, are still difficult to be analyzed. This is due to both difficulties in getting reliable data when the NMR signal is small, and also to the difficulty of getting reliable data from sample water content itself. On the positive, and encouraging, side of the work, a correlation between T1 and Ks can be suspected, but requires a larger range of aquifer quality. The NMR water content gives quite low values below 5% in accordance with the T1 NMR classification of “very fine” aquifer.

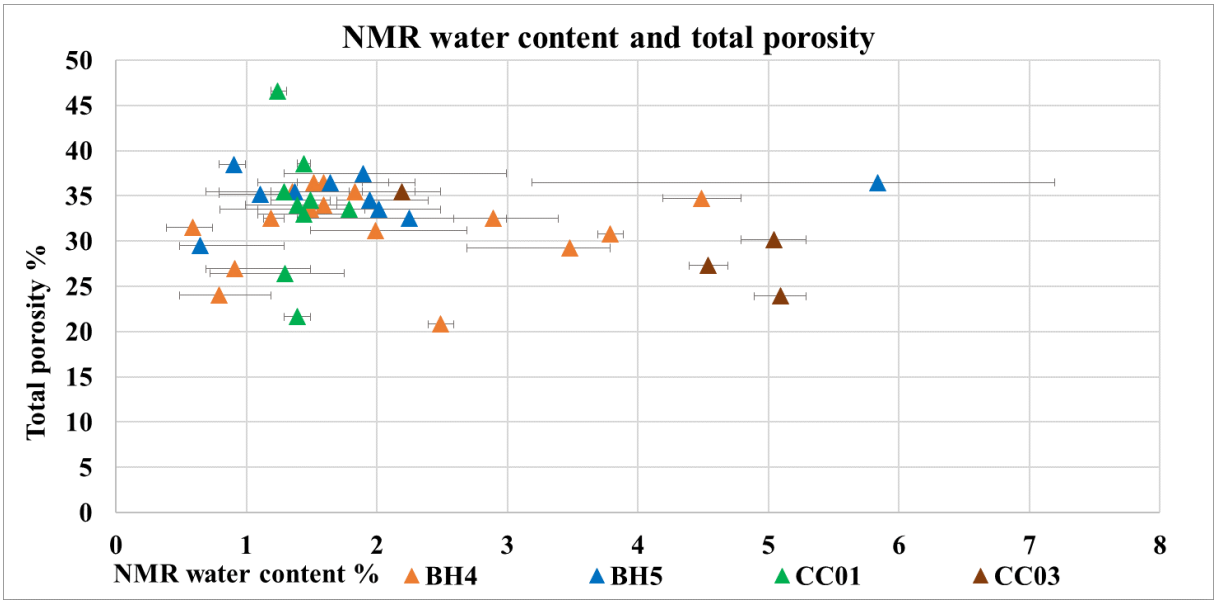

Figure 5.34 Relationship between total porosity and NMR water content

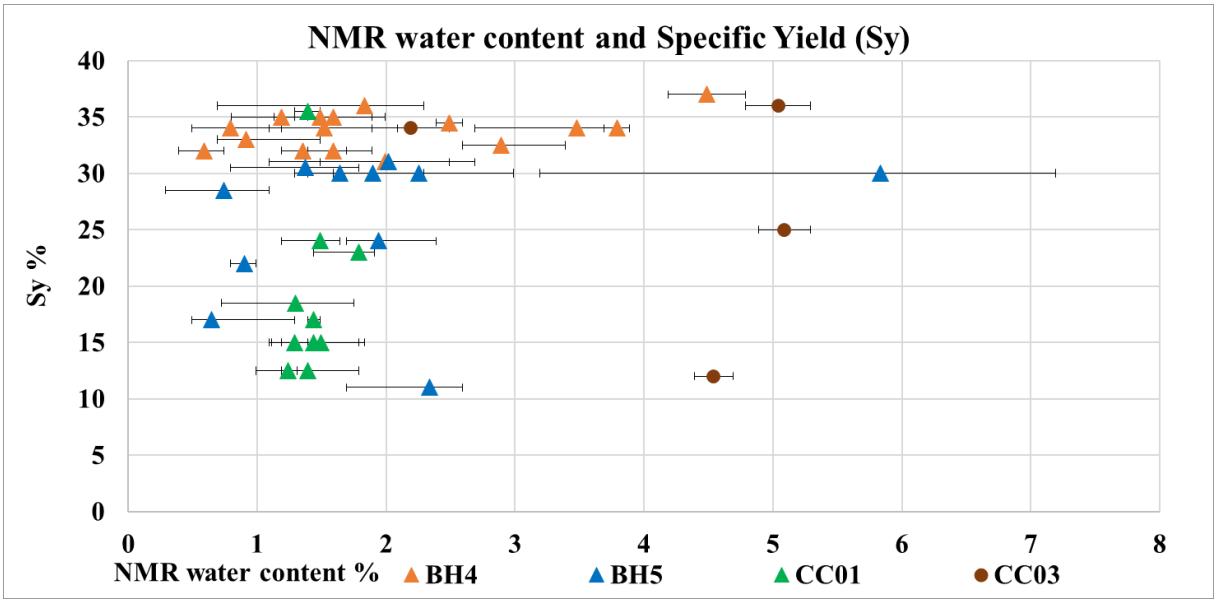

Figure 5.35 Relationship between NMR water content and specific yield (Sy).

5.4 Comparison between NMR with pumping and tracer test

A pumping test involves the controlled pumping of water from a well or borehole. The response of the aquifer to this pumping is monitored, and data collected during the test are used to calculate hydraulic conductivity. Hydraulic conductivity is a measure of the ability of an aquifer to transmit water. It is a crucial parameter for understanding groundwater flow. At a macroscopic scale, horizontal Ks values derived from field pumping tests are usually an order of magnitude greater than the vertical Ks values measured on core samples in laboratory conditions. This is due to the fact that pumping tests create horizontal fluxes, while laboratory tests are done imposing a vertical flux inside the samples

Tracer tests involve introducing a known quantity of a tracer substance into the aquifer and monitoring how it moves through the subsurface. This test can provide information about flow velocities, pathways, and dispersion within the aquifer, which are essential for assessing

effective porosity. Effective porosity is crucial for understanding how much of the aquifer's pore space is available for fluid flow.

Pumping and tracer tests have been conducted at two sites, BH5 and BH4, as depicted in Figure 5.35. Figure 5.36 illustrates the well structure and the placement of sensors, which were installed to monitor the pressure and electrical conductivity of water in the reservoir.

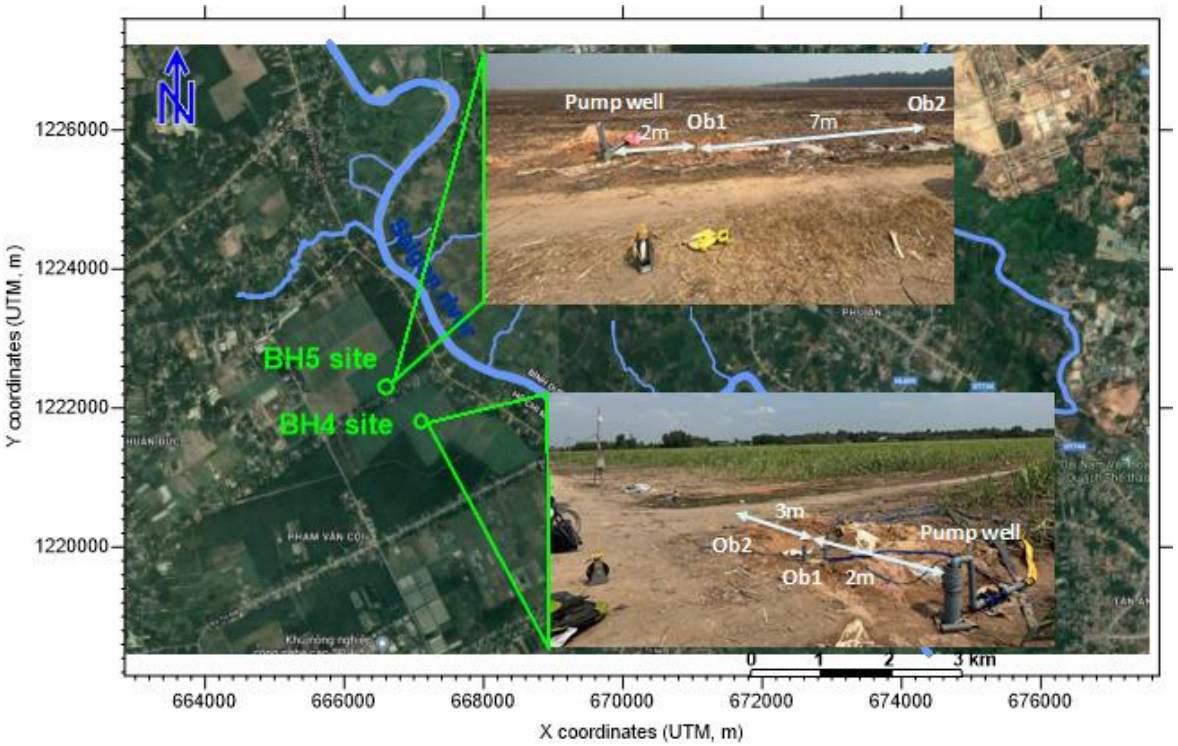

Figure 5.36 Location of pumping and tracer tests.

At the Bh5 site, the spacing between the pumping well and observation well 1 is 2 meters, and for observation well 2, it is 9 meters. Meanwhile, at the Bh4 site, the spacing between the pumping well and observation well 1 is 2 meters, and for observation well 2, it is 5 meters

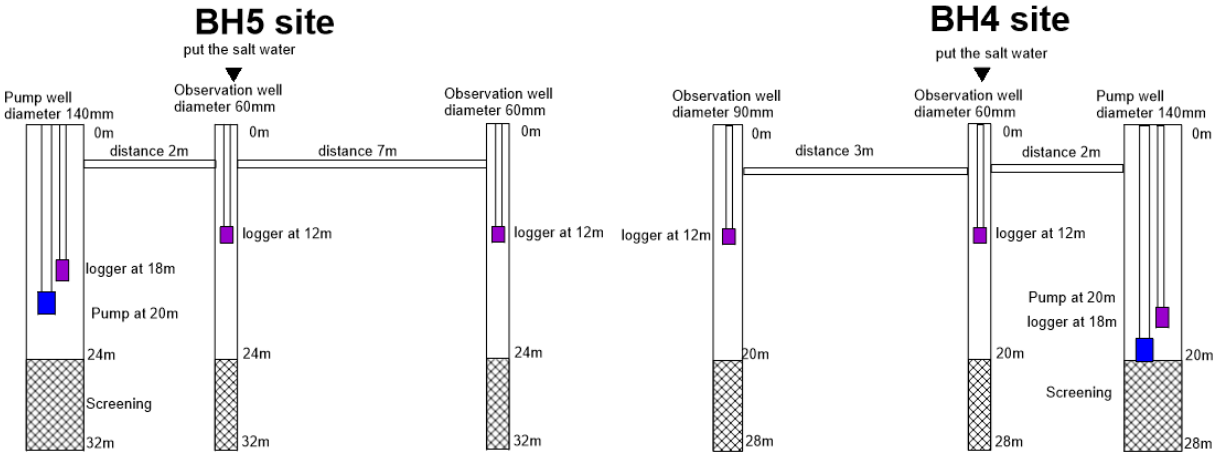

Figure 5.37 Well structure for pumping and tracer tests.

In the pumping well, the pumping setup is at a depth of 20 meters, while loggers in observation wells 1 and 2 are set up at a depth of 12 meters.

Pumping test results

The pump test spanned a total of 72 hours, concluding when the water levels in both the pumping and monitoring wells achieved a stable state. During this test, the flow rate at the pumping well was maintained at 18 cubic meters per hour. Upon completing the draw-down phase, a recovery test was initiated by ceasing the operation of the pump well. This allowed for the observation of the water level recovery process in the pumping and observation wells. Monitoring continued until the water levels in these wells returned to their original levels before the start of the pumping test.

Utilizing the data gathered from the drawdown test, which includes measurements of water level reductions in the wells, and the data from the recovery test, the Theis and Jacob method is applied to calculate the hydraulic conductivity and storativity coefficients of the aquifer at the BH4 and BH5 sites. The results are presented in Figure 5.38 and Table 5.4.

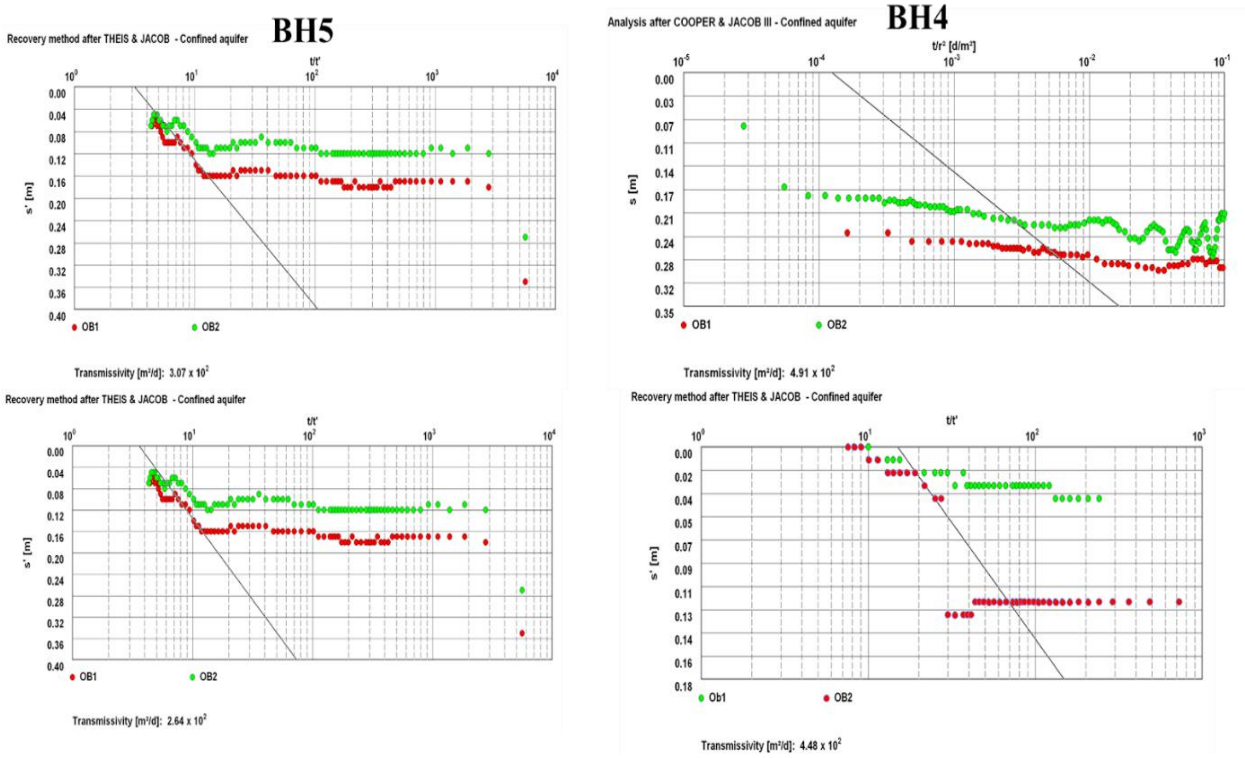

Figure 5.38 Results of the interpretation of pumping test data at BH4 and BH5 sites.

The graph illustrates the interpretation results in pumping test data for BH4 and BH5 sites. Monitoring well No. 1, depicted in red, is situated near the pumping well, while monitoring well No. 2, shown in blue, is located farther away. Notably, the pressure drops in monitoring well No. 1 surpasses that observed in monitoring well No. 2.

Table 5.4 presents the outcomes of the pumping test document interpretation, revealing that the permeability value (Ks) at site BH4 ranges from 22.4 to 24.6 m/day, twice as high as the Ks value at site BH5, which falls within the range of 10 to 11.6 m/day. This discrepancy suggests that the aquifer in the BH4 area possesses a superior exploitation capacity compared to BH5. This observation is further supported by the storativity value at BH4, which is 14%, three times higher than the value observed at BH5 (4%).

Table 5.4 Results of pumping test interpretation

	BH5 Site		BH4 Site	
	Drawdown Copper-Jacob	Recovery Theis -Jacob	Drawdown Copper-Jacob	Recovery Theis -Jacob
Transmissivity (m^2/d)	307	264	491	448
Thickness of aquifer (m)	26.5	26.5	20	20
Ks Hydraulic conductivity (m/d)	11.6	10	24.6	22.4
Storativity %	4		14	
Ks value in the previous study (m/day)	4.4-27.9m/day (Long, et al., 2017) 12.8m/day (Thoang, et al., 2015)			

The results of the pumping test in the study area align well with findings from prior studies on aquifers in Ho Chi Minh City and the Mekong Delta region. The permeability values in this region have been reported to range from 4.4 to 27.9 m/day, as indicated by research conducted by (Long, et al., 2017) and (Thoang, et al., 2015).

The findings from the hydraulic conductivity and storativity coefficient calculations display the same trend as (higher at the BH4 site and lower at BH5) the results obtained from the NMR water content measurements of core samples. Indeed, NMR measurements also indicate that the water content at the BH5 site is lower than that at the BH4 site. However, it is noteworthy that the water content values derived from NMR measurements are lower than the actual water content values determined through pumping experiments 1 and 6 % vs 4% and 16% respectively.

Table 5.4 extracted from the literature to categorize the aquifer according to the Ks results obtained at the scale of the pumping test site, it is evident that the study area's reservoir is characterized as a fine sand type.

Table 5.5 Typical values of saturated hydraulic conductivity for soils Coduto, D.P. (1999). Geotechnical Engineering Principles and Practices, Prentice-Hall, Englewood Cliffs, NJ.

Soil Description	**Hydraulic Conductivity *k* (m/day)**
Clean gravel	10^3 - 10^5
Sand-gravel mixtures	10^1 – 10^4
Clean coarse sand	10^1 – 10^3
Fine sand	1 – 10^2
Silty sand	1 – 10
Clayey sand	10^{-1} – 10
Silt	10^{-5} – 10^{-1}
Clay	10^{-7} – 10^{-3}

Tracer test result

The tracer test carried out at BH4 and BH5 involved injecting water mixed with salt with an electrical conductivity of 78 000 µS/cm into the monitoring wells and then creating a horizontal flux by pumping at the pumping wells at a rate of 18 cubic meters per hour. The test focused on monitoring the time taken for the salt concentration diffusion from the observation well to the pumping wells. Figure 5.38 illustrates the results of the water electrical conductivity monitoring with time at the pumping wells.

At BH4, represented by the orange curve in the figure, the highest recorded conductivity was 800 micro-Siemens per centimeter, and the time for the brine to diffuse from the monitoring well to the pumping well was 70 minutes. Conversely, at BH5, indicated by the blue curve, the peak conductivity reached 1380 micro-Siemens per centimeter, with a diffusion time of 150 minutes from the monitoring well to the pump.

These observations suggest that the spread rate of the salt water at BH4 is faster than at BH5. This is in agreement with the results of the pumping test, which indicated that the permeability at BH4 is 20 meters per day, twice that of BH5, which has a permeability of about 10 meters per day. Additionally, the peak conductivity at BH4 is lower than that at BH5, indicating that the effective porosity at BH4 is greater than that at BH5.

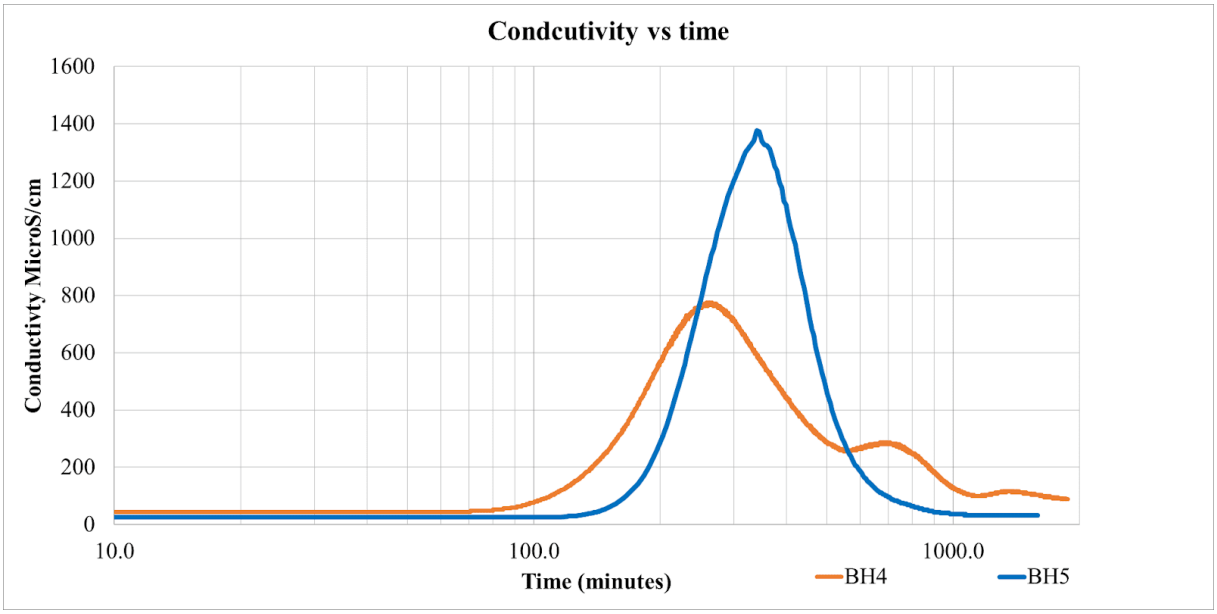

Figure 5.39 Electrical conductivity monitoring of water in the pumping wells.

The horizontal axis of the graph represents time values in minutes, while the vertical axis depicts the observed water conductivity values in µS/cm. The orange line corresponds to the water conductivity at location BH4, and the blue line represents the water conductivity at location BH5.

The interpretation of the tracer test results indicates that the effective porosity value at site BH4 is 37%, higher than that at site BH5, which is calculated at 33%. Consequently, it can be inferred that the aquifer quality at BH4 surpasses that of BH5, suggesting improved exploitation potential with similar initial reserves. Those values are under the specific yield values proposed by Johnson's triangle for the BH4 data at least. It should be noted that the

effective porosity of the aquifer calculated with the tracer test is higher than the storativity measured with the data of the pumping test.

Comparison with NMR results

To summarize, the highest NMR water contents obtained at the core scale (close to 5% for BH 4 and CC03 boreholes aquifer layers) are significantly less than the effective porosity obtained using the tracer test experiment at a larger scale (33-37%) and also less than the storativity obtained using the pumping test (3.9 to 14%). Again here, it is difficult to conclude if this discrepancy could be explained by a scale effect or rather by our experimental procedures, either for the NMR measurements for our saturation/drainage experiment, or both. In particular, some effects due to the coil heating when NMR measured could have occurred. Some attempts to attenuate this possible effect and correct the NMR measurements (not described in this manuscript) have been taken into account.

Regarding the NMR measurements, we can conclude that despite our efforts to select high signal-to-noise ratio core measurements by comparing the FID2-mean, FID2-moment, SE, and their equivalent noise signals, the obtained signals were often weak, making it difficult to fit the model and accurately determine the T1 and E_{fid} values. The figure depicting the data shows a large error range for certain acquisitions, primarily resulting from low signal core measurements. Despite reducing the noise as much as possible by increasing the stacking number, there was limited improvement in the signal measurement.

Overall, these challenges in interpreting the preprocessed data and obtaining accurate T1 and E_{fid} values highlight the difficulties associated with the water measurements taken after core measurements and emphasize the need for further investigation and refinement of the measurement techniques to overcome these issues.

At last, it is worth noting that the MRS method at the field scale, despite our difficulty due to small loops and the proximity of high-power lines, deserves to be tested in other parts on the Mekong Delta and Saigon-Dong Nai rivers using longer stacking procedures for example.

CONCLUSION AND PERSPECTIVES

Main conclusions on aquifer characterization

The TDEM method was used as the first main geophysical tool to elucidate the aquifer system's structure in the study area, with a depth of investigation from the surface down to a depth of 150 meters by utilizing resistivity maps distributed by depth and resistivity cross-section. The first set of conclusions deduced regarding the aquifer and aquitard characterization are of primary importance for assessing aquifer vulnerability.

For shallow aquifers, two situations have been evidenced:

First, in all the surveyed areas, except for the left bank of the river, shallow aquifers are not protected by a superficial clayey layer (ranging usually from 5 to 40 Ω.m). Notably, this absence of a clay layer on the surface in the study area was deduced through TDEM, but also for the shallower EM34 and ERT methods. This finding was corroborated by the Methylene Blue method made on shallow cores from 4 boreholes, confirming the lack of clay minerals in the surface layer, although the sediments close to the surface are classified with a high granulometric "clay-size" content. The absence of a surface true mineralogical clay points out the study area as a possible groundwater recharge zone. This is new information in addition to previous studies in the area conducted by Vuong (2016). In addition, this situation will create a risk that pollutants can spread into the aquifer through human activities in the area such as fertilizers, and pesticides in agricultural activities, industry, waste from livestock areas, and household activities.

Second, at the surface in the floodplain of the left bank of the river, the presence of clayey layers (usually below the paddy fields) is evidenced. They could prevent deep infiltration, but also favor lateral fluxes -i.e. runoff or temporary floodings - in monsoon season, thus transferring laterally pollutants spread at the surface by farmers, directly to the river.

At depth, the results from TDEM resistivity cross sections also show the discontinuity of the deep clay layers to separate the shallow and deep aquifers, thus giving the risk of spreading pollutants from the surface but also between compartments in the deeper aquifers below. In particular, this process can be increased through groundwater exploitation in the area to serve agricultural, industrial, and domestic activities, to create localized lower water level paths. This process is particularly concerning as it establishes conditions conducive to the infiltration of surface pollutants.

The second geophysical tool used in the Ph.D. is the novel MRS (Magnetic Resonance Sounding) method, which may bring additional valuable information on the aquifer hydrogeological parameters. When attempting to use MRS in the field, we were faced with high electromagnetic noise conditions. Thus, Nuclear Magnetic Resonance has been considered at the core scale using cores extracted from test boreholes. Several methodological procedures were found difficult to apply or incomplete to ascertain reliable conclusions. However, both NMR and MRS tests, as well as the hydrological parameter study at the scale of the cores and in the field, revealed an aquifer that is "poor", showing significant heterogeneity within the aquifer system in the study area. The "NMR water content" parameter values in core samples from various well locations illustrate substantial variations within each well. Core from borehole BH4 displays NMR water content values ranging from 0.6 to 4.5%, core from

borehole BH5 exhibits values between 0.5 and 2.5%. When using literature-specific yield determination using grain size analysis, the “theoretical” specific yield values are much higher and also indicate heterogeneity. BH4, for example, shows specific yield values fluctuating between 30-45%, whereas BH5, CC01, and CC03 exhibit a broader range of 10-30%.

Several more reliable data obtained with classical geotechnical tests (Ks) on core and large-scale pumping and tracer tests reveal that the average hydraulic conductivity of the aquifer is 15 m/day ranging from 10 to 20 m/day. These values are in accordance with previous scarce studies in the area. Our pumping test results further underscore the heterogeneity, with location BH4 displaying a conductivity value of 20 m/day, twice the conductivity value observed at location BH5 (10 m/day). Correspondingly, the storativity value at BH4 is 14%, compared to 4% at BH5. Given the pronounced heterogeneity, establishing characteristic parameters for this aquifer becomes crucial, and resistivity values stand out as a key parameter.

This convergence of results from the NMR method and permeability measurements substantiates the characterization of the aquifer in the study area as fine-grained. Such insights are pivotal for a comprehensive understanding of the aquifer's properties, contributing valuable information for water resource exploitation and related applications in the region.

In addition, the tracer test results show that the effective porosity value in the study area is quite large, up to 33% at BH5 and 37% at BH4, and much larger than the water content value determined by the NMR method. Therefore, to widely deploy and use this method, more research is needed to measure and re-evaluate the results of NMR water content compared with other methods.

At last, the question of aquifer-river interactions remains open, due to the lack of data beneath the river (too difficult to survey). Close to the river ERT cross-sections are delineating the boundary between the aquifer and the Saigon River clayey banks. While this sheds light on the aquifer's continuity and interaction with the river, the specifics of this interaction remain unanswered. The absence of TDEM measurement points and ERT survey across the Saigon River limits for now our understanding of how the aquifer and the river interact, pointing towards a crucial question for further investigation and clarification in future research.

Advantages and limitations of the geophysical methods

The TDEM method exhibits high sensitivity to sediments characterized by low resistivity, facilitating the identification of clay layers (with resistivity values below 70 Ω.m) in the research area. This reliability of TDEM (controlled in a few boreholes) has been obtained only when using an adapted interpretation procedure that involves a well-defined starting model built with known data. TDEM proves to be a valuable method for ascertaining the existence and thickness of clay layers within the study area. In the frame of the study, this method is cost-effective and easily applicable, resulting in time savings. The depth of investigation has been found between 100 and 150 m deep with a limited loop of 50x50m², rendering this method a must for shallow aquifer investigation and associated aquitards in this geological context. For TDEM however, the main challenge arises from its poor sensitivity to resistive terranes, making it difficult to clearly interpret resistivity for the aquifer's characteristics using Archie's law for example.

The effectiveness of Electrical Resistivity Tomography (ERT) in delineating the shallower part of the aquifer characteristics is notable, particularly when dealing with sediment layers exhibiting high resistivity values (above 300 Ω.m). Especially for determining the boundary between aquifers and riverine sediments, ERT proves to be an effective tool to clarify this issue when it has quite a detailed horizontal resolution. However, a significant drawback lies in its limited survey depth investigation (30 to 50 m with our equipment). Direct Current resistivity use in boreholes (logging) is a must to provide data for modeling and calibration.

The FEM (EM34) method excels in identifying the existence of conductive layers at the surface, if any. However, its utility is constrained by a restricted survey depth, and a limited quantitative interpretation to 2 or 3 layers makes it unsuitable for the examination of deep aquifers. Additionally, the method is susceptible to environmental noise, which can significantly impact its accuracy and reliability in detecting subsurface conductivity.

The current application of Magnetic Resonance Sounding (MRS) faces challenges in the research area due to elevated levels of noise, hindering the extraction of a sufficiently clear signal for accurate determination of water content in the formation and reservoir depth. In the context of Vietnam, additional measurements are imperative to validate the method's effectiveness under these specific environmental conditions. Assessing and addressing the impact of noise will be crucial in ensuring the reliability and applicability of MRS in this region for accurate water content determination and reservoir depth assessment.

In total, our approach, involving a combination of laboratory experiments and field studies, contributes to the accurate characterization. The successful deployment of this panel of tools may lay the groundwork for broader applications, particularly in the study of sedimentary sediments in the southern region of Vietnam. Furthermore, there is a call for additional research to assess the effectiveness of these methods when applied to other hydrogeological objects. This expansion of the study scope will not only enhance the understanding of different geological settings but also contribute to the overall knowledge base in the field of hydrogeology and sedimentary reservoir characterization in Vietnam.

Towards a new conceptual model of the aquifer

A major outcome from the Ph.D. work is provided by the examination of resistivity maps at different depths has proven instrumental in reconstructing the historical dynamics and positioning of the Saigon River, spanning from ancient times to the present. Currently, the Saigon River's flood plain is situated on the northeast side of the study area. However, there was a significant period in the past when the influential basin of the Saigon River was positioned on the southwest side of the research area. Incorporating resistivity cross-section research, sediment morphology analysis at outcrop points, and leveraging previous studies on sedimentation processes in the southern region of Vietnam and the Mekong Delta basin, our work has established that low-resistivity sediments distributed in the study area are probably associated with transgression-regression activity. This conclusion is drawn from morphological similarities to sediment models in previous studies, verified by actual images at outcrop points. To further reinforce this finding, additional studies focusing on pollen particles are deemed necessary to confirm the depositional environment of the low-resistivity sediments in the study area as identified through resistivity analysis. The aquifer itself, as tentatively characterized by the new Nuclear Magnetic Resonance (NMR) method, is typified by a fine-grained structure,

with T1 values concentrated in a range of about 20-250ms. This determination aligns with the permeability values derived from pumping experiments in the area, which fall within the 10 to 20m/day range. According to established classifications, these permeability values categorize the aquifer as a fine-grained aquifer.

Perspectives

In summary, the successful application of resistivity methods in the study area not only aids in understanding aquifer structures but also has broader implications for predicting subsidence, monitoring saltwater intrusion, and assessing the impact of soil layers on water and soil quality. This highlights the versatility and importance of geophysical methods in addressing various environmental and geological challenges in similar regions. The research results demonstrate the efficacy of resistivity methods, specifically Time-Domain Electromagnetic (TDEM), EM34, and Electrical Resistivity Tomography (ERT), in delineating the structural morphology of aquifers. This success suggests the potential for the widespread application of these geophysical methods in regions sharing similar geological structures, particularly those resembling the Mekong Delta. In addition to the application of determining the morphology of aquifer structure, this system of geophysical methods also helps determine the presence of a surface clay layer in the study area, which acts as a natural barrier layer protecting the aquifer from human impacts. In regions characterized by intricate topography or complex human environments (roads, fences, houses, etc.), conducting traditional surface surveys can be challenging or even impossible due to complex terrain. To overcome these obstacles and enhance survey efficiency, the Airborne Time-Domain Electromagnetic (TDEM) method emerges as an optimal solution. In addition, the advantage of airborne TDEM is that it can survey large areas and shorten survey time, this could be particularly important for surveying the Mekong Delta, characterized by its extensive sediment layers reaching depths of over 300 meters. It poses a unique challenge in understanding aquifer structures. The significant thickness of sediment layers requires electromagnetic signals to penetrate to greater depths. Larger TDEM loop size surveys facilitate this deeper exploration, allowing for a more comprehensive investigation of subsurface structures, including aquifers and geological formations buried beneath extensive sediments.

In the frame of our work, the results obtained from the pumping experiment have allowed for the determination of crucial parameters such as the conductivity value of the reservoir and the effective porosity value. Moving forward, it is imperative to conduct research aimed at establishing the optimal pumping flow. This is crucial not only to ensure the safe and sustainable exploitation of groundwater in the area but also to safeguard the aquifer from potential pollution intrusion from the surface. Currently, the TDEM maps are the base for building a 3D hydrogeological model. In addition to this perspective for modeling, we started the work using the outcomes of saturated permeability experiments conducted in a shallow layer that were initially utilized to simulate the groundwater recharge process from rainwater. Those results were not presented in this manuscript because they are for now preliminary. Some simulations aiming to assess the impact of crops above ground on the recharge process were performed using the Hydrus software. Without any influence from vegetation, the rainfall contribution to groundwater replenishment can reach up to 40%. Conversely, if cassava is planted above, the additional water amount is diminished to 15%, and it can drop to below 5%

when sugarcane is the cultivated plant. Those values of calculated recharge have to be compared to the isotope's recent studies of the team, which calculate a value close to 5% to 14% pointing also out the local variability that can be encountered.

To gain deeper insights into the interaction dynamics between aquifers and adjacent rivers, a comprehensive approach involving TDEM surveys along the riverbanks, coupled with Electrical Resistivity Tomography (ERT) surveys across the river, becomes imperative. This combined methodology facilitates precise determination of the aquifer-sediment boundary beneath the riverbed. This however requires a tricky layout.

Considering the results obtained in the frame of this work, and the perspectives it brings to the future research fields, we confirm the interest in combining hydrogeophysical tools with classical hydrogeological methods to enhance our understanding of the valuable and vulnerable groundwater resources in the sedimentary context of the South of Vietnam, soon submitted to severe hydrological changes in the near future.

REFERENCE

1. Anh, L., Loc, H., Irvine, K., Thanh, T., & Tuong, L. (2021, 5). The waterscape of groundwater exploitation for domestic uses in District 12, Ho Chi Minh City, Vietnam. *Environment, Development and Sustainability, 23*(5), 7652-7669. doi:https://doi.org/10.1007/s10668-020-00938-0

2. Arab, P., Araújo, T., & Pejon, O. (2015, 9). Identification of clay minerals in mixtures subjected to differential thermal and thermogravimetry analyses and methylene blue adsorption tests. *Applied Clay Science, 114*, 133-140. doi:https://doi.org/10.1016/j.clay.2015.05.020

3. Archie, G. (1942). The Electrical Resistivity Log as an Aid in Determining Some Reservoir Characteristics. *SPE-942054-G*, 146 (01): 54–62. doi:https://doi.org/10.2118/942054-G

4. Asian Development Bank. (2010). *Ho Chi Minh City Adaptation to Climate Change.* Retrieved from https://www.adb.org/publications/ho-chi-minh-city-adaptation-climate-change-summary-report

5. Auken, E., & Christiansen, A. (2004). Layered and laterally constrained 2D inversion of resistivity data. *Geophysics, 69*(3), 752-761. doi:https://doi.org/10.1190/1.1759461

6. Babut, M., Mourier, B., Desmet, M., Simonnet-Laprade, C., Labadie, P., Budzinski, H., De Alencastro, L., Tu, T., Strady, E., Gratiot, N. (2019, 2). Where has the pollution gone? A survey of organic contaminants in Ho Chi Minh city / Saigon River (Vietnam) bed sediments. *Chemosphere, 217*, 261-269. doi:https://doi.org/10.1016/j.chemosphere.2018.11.008

7. Behroozmand, A., Keating, K., & Auken, E. (2015, 1). A Review of the Principles and Applications of the NMR Technique for Near-Surface Characterization. *Surveys in Geophysics, 36*(1), 27-85. doi:10.1007/s10712-014-9304-0

8. Bergqvist, A., Eitrem Holmgren, K., & Rylander, P. (2012*). Impacts of Saline Water Intrusion on the Daily Lives in the Mekong Delta Viet Nam*. Department of Soil and Environment. Swedish University of Agricultural Sciences. Retrieved from https://core.ac.uk/download/pdf/11988509.pdf

9. Bernard, J., & Legchenko, A. (2003). Groundwater exploration with the Magnetic Resonance Sounding method. *ASEG Extended Abstracts*, 2003, 1 - 5. doi:https://doi.org/10.1071/ASEG2003ab013

10. Bording, T., Christiansen, A., Auken, E., & Gunnink, J. (2017). Groundbased TEM Survey in the Subsiding Mekong Delta 2017. *23rd European Meeting of Environmental and Engineering Geophysics*. European Association of Geoscientists & Engineers. doi:DOI:10.3997/2214-4609.201701991

11. Boretti, A. (2020, 6). Implications on food production of the changing water cycle in the Vietnamese Mekong Delta. *Global Ecology and Conservation, 22*. doi:https://doi.org/10.1016/j.gecco.2020.e00989

12. Braja, M., & Khaled, S. (2016). *Principles of Geotechnical Engineering* (Ninth Edition ed.). Cengage Learning.

13. Braun, G., Braun, M., Kruse, J., Amelung, W., Renaud, F., Khoi, C., Duong, M., Sebesvari, Z. (2019, 6). Pesticides and antibiotics in permanent rice, alternating rice-shrimp and permanent shrimp systems of the coastal Mekong Delta, Vietnam. *Environment International*, 127, 442-451. doi:https://doi.org/10.1016/j.envint.2019.03.038

14. Caracciolo, R., Escher, B., Lai, F., Nguyen, T., Le, T., Schlichting, R., Troger, R., Nesmeesmeery, J., Wiberg, K., Nguyen, Dan., Baduel, C. (2023). Impact of a megacity on the water quality of a tropical estuary assessed by a combination of chemical analysis and in-vitro bioassays. *Science of The Total Environment*, 877, 162525. doi:https://doi.org/10.1016/j.scitotenv.2023.162525

15. Chau, N., Sebesvari, Z., Amelung, W., & Renaud, F. (2015, 6). Pesticide pollution of multiple drinking water sources in the Mekong Delta, Vietnam: evidence from two provinces. *Environmental Science and Pollution Research*, 22(12), 9042-9058. doi:https://doi.org/10.1007/s11356-014-4034-x

16. Chiappone, A., Marello, S., Scavia, C., & Setti, M. (2004, 12). Clay mineral characterization through the methylene blue test: Comparison with other experimental techniques and applications of the method. *Canadian Geotechnical Journal*, 41(6), 1168-1178. doi:https://doi.org/10.1139/t04-060

17. Corwin, D., & Lesch, S. (2005). Apparent soil electrical conductivity measurements in agriculture. *Computers and Electronics in Agriculture*, 46(1-3 SPEC. ISS.), 11-43. doi:https://doi.org/10.1016/j.compag.2004.10.005

18. Costabel, S., Siemon, B., Houben, G., & Günther, T. (2017, 1). Geophysical investigation of a freshwater lens on the island of Langeoog, Germany – Insights from combined HEM, TEM and MRS data. *Journal of Applied Geophysics*, 136, 231-245. doi:https://doi.org/10.1016/j.jappgeo.2016.11.007

19. D. Chapellier. (2000). *Prospection electrique de surface*. Université de Lausanne - Institut Franqais du Pétrole. Cours de géophysique. Retrieved from https://www-ig.unil.ch/pdf/doc_pro/pro_f.pdf

20. Dahlin, T. (2001, 11). *The development of DC resistivity imaging techniques* (Vol. 27).

21. Dahlin, T., & Zhou, B. (2004, 9). *A numerical comparison of 2D resistivity imaging with 10 electrode arrays* (Vol. 52).

22. Dahlin, T., Bernstone, C., & Loke, M. (2002). *A 3-D resistivity investigation of a contaminated site at Lernacken, Sweden* (Vol. 67). Society of Exploration Geophysicists.

23. Dahm, R., Diermanse, F., & Long Phi, H. (2013). On the flood and inundation management of ho chi minh city, Viet nam. *International Conference on Flood Resilience*-Uinited Kingdom.

24. Descloitres, M., Ruiz, L., Sekhar, M., Legchenko, A., Braun, J., Mohan Kumar, M., & Subramanian, S. (2008, 1). Characterization of seasonal local recharge using electrical resistivity tomography and magnetic resonance sounding. *Hydrological Processes*, 22(3), 384-394.

25. Dinh, H., Le, V., & Thuy, L. (2015, 7). Mapping ground subsidence phenomena in Ho Chi Minh City through the radar interferometry technique using ALOS PALSAR data. *Remote Sensing*, 7(7), 8543-8562. doi:https://doi.org/10.3390/rs70708543

26. DNRE. (2022). *Create a list of maps delineating zones with restricted groundwater exploitation in Ho Chi Minh City.* Internal document of Department of Natural Resources and Environment, Ho Chi Minh City

27. Dobrin, M., & Mather, P. (1988). *Introduction to Geophysical Prospecting*. New York: McGraw-Hill.

28. Duy, P., Chapman, L., Tight, M., Linh, P., & Thuong, L. (2018, 1). Increasing vulnerability to floods in new development areas: evidence from Ho Chi Minh City. *International Journal of Climate Change Strategies and Management*, 10(1), 197-212. Retrieved from https://www.emerald.com/insight/content/doi/10.1108/IJCCSM-12-2016-0169/full/pdf

29. El-Kaliouby, H., & Abdalla, O. (2015, 4). Application of time-domain electromagnetic method in mapping saltwater intrusion of a coastal alluvial aquifer, North Oman. *Journal of Applied Geophysics*, 115, 59-64. doi:https://doi.org/10.1016/j.jappgeo.2015.02.003

30. Erban, L., Gorelick, S., & Zebker, H. (2014, 8). Groundwater extraction, land subsidence, and sea-level rise in the Mekong Delta, *Vietnam. Environmental Research Letters*, 9(8). doi:DOI 10.1088/1748-9326/9/8/084010

31. Fitterman, D., & Stewart. J, M. (1986). Transient electromagnetic sounding for groundwater. *Geophysics*, 51(4), 995-1005. Retrieved from https://digitalcommons.usf.edu/cgi/viewcontent.cgi?article=1018&context=gly_facpub

32. General statistics office. (2021). *Statistical yearbook of Viet Nam 2021*. Vietnam. Retrieved from https://www.gso.gov.vn/du-lieu-va-so-lieu-thong-ke/2022/08/nien-giam-thong-ke-2021-2/

33. Ghazi, S., & Mountney, N. (2009, 11). Facies and architectural element analysis of a meandering fluvial succession: The Permian Warchha Sandstone, Salt Range, Pakistan. *Sedimentary Geology*, 221(1-4), 99-126. doi:https://doi.org/10.1016/j.sedgeo.2009.08.002

34. Giang, N., Nam, T., & Bano, M. (2012, 2). Groundwater investigation on sand dunes area in southern part of Vietnam by magnetic resonance sounding. *Acta Geophysica*, 60(1), 157-172. doi:https://doi.org/10.2478/s11600-011-0040-2

35. Giang, N., Quang, C., Long, D., Ky, P., Vu, N., & Tran, D. (2022, 1). Statistical and Hydrological Evaluations of Water Dynamics in the Lower Sai Gon-Dong Nai River, Vietnam. *Water (Switzerland)*, 14(1). doi:https://doi.org/10.3390/w14010130

36. Government Office (2023), *The report on Water Resources Planning for Cuu Long River Basin in the Period 2022–2030 with Vision to 2050*, Ha Noi

37. Grombacher, D., Maurya, P., Lind, J., Lane, J., & Auken, E. (2022, 1). Rapid Mapping of Hydrological Systems in Tanzania Using a Towed Transient Electromagnetic System. *Groundwater*, 60(1), 35-46. doi:https://doi.org/10.1111/gwat.13130

38. Guérin, R., Descloitres, M., Coudrain, A., Talbi, A., & Gallaire, R. (2001, 12). Geophysical surveys for identifying saline groundwater in the semi-arid region of the central Altiplano, Bolivia. *Hydrological Processes*, 15(17), 3287-3301. doi: https://doi.org/10.1002/hyp.284

39. Gürses, A., Karaca, S., Doğar, Ç., Bayrak, R., Açikyildiz, M., & Yalçin, M. (2004, 1). Determination of adsorptive properties of clay/water system: Methylene blue sorption. *Journal of Colloid and Interface Science*, 269(2), 310-314. doi:https://doi.org/10.1016/j.jcis.2003.09.004

40. Ha, Q., Kim, K., Phan, N., Phung, T., Lee, J., Nguyen, V., & Phan, C. (2019, 12). A hydrogeological and geochemical review of groundwater issues in southern Vietnam. *Geosciences Journal*, 23(6), 1005-1023. doi:https://doi.org/10.1007/s12303-019-0021-z

41. Ha, Q., Tran Ngoc, T., Le Vo, P., Nguyen, H., & Dang, D. (2022, 2). Groundwater in Southern Vietnam: Understanding geochemical processes to better preserve the critical water

resource. *Science of The Total Environment*, 807(2), 151345. doi:https://doi.org/10.1016/j.scitotenv.2021.151345.

42. Johnson, A. (1967). *Specific Yield Compilation of Specific Yields for Various Materials*. United States Government Printing Office, Washington. doi:https://pubs.usgs.gov/wsp/1662d/report.pdf

43. Kahr, G., & Madsen, F. (1995). Determination of the cation exchange capacity and the surface area of bentonite, illite and kaolinite by methylene blue adsorption. *Applied Clay Science*, 9(5), 327-336. doi:https://doi.org/10.1016/0169-1317(94)00028-O.

44. Kaufman , A. (1983). *Frequency and Transient Soundings*. Amsterdam: Elsevier.

45. Kearey, P., Brooks, M., & Hill, I. (2002). *An Introduction to Geophysical Exploration*. John Wiley & Sons.

46. Kemgang Dongmo, T., Boucher, M., Mvondo, V. Y., Guillaume, F., Ngounou Ngatcha, B., Yalo, N., Baba, G, I., Legchenko, A. (2019, 11). Contribution of time domain electromagnetic and magnetic resonance soundings to groundwater assessment at the margin of lake chad basin, cameroon. *Journal of Applied Geophysics*, 170. doi:https://doi.org/10.1016/j.jappgeo.2019.103840

47. Khuc, V. (2000). *Lexicon of geological unit of Vietnam*. Department of Geology and Mineral of Việt Nam. doi:http://www.idm.gov.vn/Nguon_luc/Xuat_ban/Anpham/Tracuu_PVDC/Mucluc.htm

48. Kruseman, G., Ridder, N. (1990). *Analysis and evaluation of pumping test data.* International Institute for Land Reclamation and Improvement. Retrieved from https://www.hydrology.nl/images/docs/dutch/key/Kruseman_and_De_Ridder_2000.pdf

49. Kunetz, G. (1966, 10). *Principles of Direct Current - Resistivity Prospecting*. Stuttgart, Germany: Schweizerbart Science Publishers. Retrieved from http://www.schweizerbart.de//publications/detail/isbn/9783443130015/Kunetz_Principles_Geoex_Monogr_S_1

50. Legchenko, A. (2013). *Magnetic resonance imaging for groundwater*. John Wiley. doi:10.1002/9781118649459

51. Legchenko, A. (2022). *Processing laboratory measurements in soil samples Getting started*. Internal document of IGE laboratory , Grenoble-Alpes University, available upon demand with the author

52. Legchenko, A., & Valla, P. (2002). A review of the basic principles for proton magnetic resonance sounding measurements. *Journal of Applied Geophysics*, 50(1-2). doi:https://doi.org/10.1016/S0926-9851(02)00127-1

53. Legchenko, A., Baltassat, J.-M., Bobachev, A., Martin, C., Robain, H., & Vouillamoz, J.-M. (2004). Magnetic Resonance Soundings Applied to Aquifers Characterization. *Groundwater*, 42(3), 363-373. doi:DOI: 10.1111/j.1745-6584.2004.tb02684.x

54. Legchenko, A., Descloitres, M., Bost, A., Ruiz, L., Reddy, M., Girard, J., Sekhar, M., Kumar, MS.M., Braun, J. (2006, 7). Resolution of MRS applied to the characterization of hard-rock aquifers. *Groundwater*, 44(4), 547-554. doi:DOI: 10.1111/j.1745-6584.2006.00198.x

55. Loke, M. H., & Barker, R. D. (1996, 1). Rapid least-squares inversion of apparent resistivity pseudosections by a quasi-Newton methodl. *Geophysical Prospecting*, 44(1), 131-152. doi:https://doi.org/10.1111/j.1365-2478.1996.tb00142.x

56. Loke, M., Chambers, J., Rucker, D., Kuras, O., & Wilkinson, P. (2013, 8). Recent developments in the direct-current geoelectrical imaging method. *Journal of Applied Geophysics*, 95, 135-156. doi:https://doi.org/10.1016/j.jappgeo.2013.02.017

57. Long , T., & Koontanakulvong, S. (2019). Deep Percolation Charactertistics Via Soil Moisture Sensor Approach in Saigon River Basin. *Article in International Journal of Civil Engineering and Technology*, 10(3), 403-412. Retrieved from http://www.iaeme.com/IJCIET/index.asp403http://www.iaeme.com/ijmet/issues.asp?JType=IJCIET&VType=10&IType=3http://www.iaeme.com/IJCIET/issues.asp?JType=IJCIET&VType=10&IType=3

58. Long, T., & Koontanakulvong, S. (2017). Groundwater balance and river interaction analysis in Pleistocene aquifer of the Saigon River basin, South of Vietnam by stable isotope analysis and groundwater modeling. *International Conference on Water Management and Climate Change Towards Asia's Water-Energy-Food Nexus*, (pp. 25-27). Bangkok.

59. Long, T., & Koontanakulvong, S. (2020). Groundwater and river interaction impact to aquifer system in saigon river basin, vietnam. *Engineering Journal*, 24(5), 1-10. doi:DOI: https://doi.org/10.4186/ej.2020.24.5.15

60. Long, T., Koontanakulvong, S., & Aye, P. (2017). *Examination of land recharges using soil moisture approach: Case study in Thailand. Internet Journal of Society for Social Management Systems*, 11(1). Retrieved from https://ssms.jp/img/files/2019/04/sms17_2187.pdf

61. Lubczynski, M., & Roy, J. (2003). Hydrogeological interpretation and potential of the new magnetic resonance sounding (MRS) method. *Journal of Hydrology*, 283(1-4), 19-40. doi:https://doi.org/10.1016/S0022-1694(03)00170-7

62. Lubczynski, M., & Roy, J. (2004). Magnetic Resonance Sounding: New Method for Ground Water Assessment. *Groundwater*, 42(2), 291-309. doi:DOI: 10.1111/j.1745-6584.2004.tb02675.x

63. Martin, T., Günther, T., Orozco, A., & Dahlin, T. (2020, 9). Evaluation of spectral induced polarization field measurements in time and frequency domain. *Journal of Applied Geophysics*, 180. doi:https://doi.org/10.1016/j.jappgeo.2020.104141

64. McNeill, J. (1980). *Electrical Conductivity of Soils and Rocks*. Geonics limited. Retrieved from https://geonics.com/pdfs/technicalnotes/tn5.pdf

65. McNeill, J. (1980). *Electromagnetic terrain conductivity measurement at low induction numbers*. Geonics limited. Retrieved from https://geonics.com/pdfs/technicalnotes/tn6.pdf

66. McNeill, J. (1994). *Principles and Application of Time Domain Electromagnetic Techniques for Resistivity Sounding*. Technical Note TN-27. Geonics limited. Retrieved from https://geonics.com/pdfs/technicalnotes/tn27.pdf

67. Milsom, J. (2003). *Field Geophysics*. Wiley Online Library. doi:DOI:10.1002/9780470972311

68. Minderhoud, P., Coumou, L., Erban, L., Middelkoop, H., Stouthamer, E., & Addink, E. (2018, 9). The relation between land use and subsidence in the Vietnamese Mekong delta. *Science of the Total Environment*, 634, 715-726. doi:https://doi.org/10.1016/j.scitotenv.2018.03.372

69. Minderhoud, P., Erkens, G., Pham, V., Bui, V., Erban, L., Kooi, H., & Stouthamer, E. (2017, 6). Impacts of 25 years of groundwater extraction on subsidence in the Mekong delta, Vietnam. *Environmental Research Letters*, 12(6). doi:DOI 10.1088/1748-9326/aa7146

70. Minderhoud, P., Middelkoop, H., Erkens, G., & Stouthamer, E. (2020). Groundwater extraction may drown mega-delta: Projections of extraction-induced subsidence and elevation of the mekong delta for the 21st century. *Environmental Research Communications*, 2(1). doi:DOI 10.1088/2515-7620/ab5e21

71. Minh, N., Minh, T., Iwata, H., Kajiwara, N., Kunisue, T., Takahashi, S., Viet, P., Tuyen, B., Tanabe, S. (2007, 5). Persistent organic pollutants in sediments from Sai Gon-Dong Nai River basin, Vietnam: Levels and temporal trends. *Archives of Environmental Contamination and Toxicology*, 52(4), 458-465. doi:https://doi.org/10.1007/s00244-006-0157-5

72. Mitchell, J., & Soga, K. (2005). *Fundamentals Of Soil Behavior*. Wiley.

73. Müller-Petke, M. (2020, 6). Non-remote reference noise cancellation - using reference data in the presence of surface-NMR signals. *Journal of Applied Geophysics*, 177. doi:https://doi.org/10.1016/j.jappgeo.2020.104040

74. Nabighian, M., & Macnae, J. (1991). Time domain electromagnetic prospecting methods. *Electromagnetic Methods in Applied Geophysics*, 2(Application, Parts A and B). doi:https://doi.org/10.1190/1.9781560802686.ch6

75. Nabighian, M., Grauch, V., Hansen, R., LaFehr, T., Li, Y., Peirce, J., Phillips, J., Ruder, M. (2005). The historical development of the magnetic method in exploration. *Geophysics*, 70(6). doi:https://doi.org/10.1190/1.2133784

76. NAWAPI. (2022). Notification, *forecast and warning newsletter underground water resources in Ho Chi Minh City*. Internal document of Center for Water Resources Warning and Forecast - National Center for Water Resources Planning and Investigation.

77. Nghi, T., Quang Toan, N., Thi Van Thanh, D., Dinh Minh, N., & Van Vuong, N. (1991). Quaternary sedimentation of the principal deltas of Vietnam. *Journal of Southeast Asian Earth Sciences*, 6(2), 103-113. doi:https://doi.org/10.1016/0743-9547(91)90101-3

78. Nguyen , V. (2010). Geophysical investigations for groundwater augmenting in sand dunes area, BinhThuan, Vietnam. *International Association of Hydrogeologists*, 1481-1487. Retrieved from https://home.agh.edu.pl/~iah2010/extab/ext-abstract/324-iah2010_nguyen_van_giang.pdf

79. Nguyen, A. H., Tat, V.M.H., Vo, P.L., 2023. Vulnerability Assessment of the Upper-Middle Pleistocene (qp2-3) Aquifer in Ho Chi Minh City, Vietnam Using GIS and Expanded DRASTIC Methods. *Potential for Exploitation and Development of Coastal Zone in Vietnam. IOP Conf. Series: Earth and Environmental Science*, 1247 (2023) 012006, IOP Publishing, doi:10.1088/1755-1315/1247/1/012006).

80. Nguyen, B., Nguyen, T., & Bach, Q. (2020, 6). Assessment of groundwater quality based on principal component analysis and pollution source-based examination: a case study in Ho Chi Minh City, Vietnam. *Environmental Monitoring and Assessment*, 192(6). doi:DOI: 10.1007/s10661-020-08331-0

81. Nguyen, K., Le , D., Nguyen, V., Huynh , L., & Tran, B. (2009). *Studying the contamination status and the sources of nitrogen compounds in groundwater in Ho Chi Minh city area using the isotope hydrology techniques*. Center for Nuclear Techniques, Vietnam

Atomic Energy Institute. Retrieved from https://inis.iaea.org/collection/NCLCollectionStore/_Public/45/058/45058909.pdf

82. Nguyen, L., Gassara, S., Bui, M., Zaviska, F., Sistat, P., & Deratani, A. (2019, 11). Desalination and removal of pesticides from surface water in Mekong Delta by coupling electrodialysis and nanofiltration. *Environmental Science and Pollution Research*, 26(32), 32687-32697. doi:https://doi.org/10.1007/s11356-018-3918-6

83. Nguyen, N. A. (2017). Historic drought and salinity intrusion in the Mekong Delta in 2016: lessons learned and response solutions. *Vietnam Journal of Science, Technology and Engineering*, 59(1). doi:https://doi.org/10.31276/VJSTE.59(1).93

84. Nguyen, V., & Le, T. (2013). Manganese pollution in ground water of Pleistocene aquifers in Ho Chi Minh City area. *Viet Nam Journal of Earth Sicence*, 35(1), 81-87. doi:DOI: https://doi.org/10.15625/0866-7187/35/1/3043

85. Palacky, G. (1987). Resistivity Characteristics of Geologic Targets (Vol. 1). *Electromagnetic Methods in Applied Geophysics*. doi:https://doi.org/10.1190/1.9781560802631.ch3

86. Parasnis. D. S. (2012). *Principles of Applied Geophysics*. Springer Dordrecht. doi:https://doi.org/10.1007/978-94-009-5814-2

87. Pham, A., & Nguyen, T. (2018, 11). Temporal and spatial water quality assessment of Thay Cai - An Ha canal system, Vietnam. *IOP Conference Series: Earth and Environmental Science*, 191(1). doi:DOI 10.1088/1755-1315/191/1/012023

88. Pham, N., Boyer, D., Nguyen, T., & Nguyen , V. (1994, 7). Deep Ground-Water Investigation by Combined VES/MTS Methods Near Ho Chi Minh City, Viet Nam. *Groundwater*, 32(4), 675-682. Retrieved from https://onlinelibrary.wiley.com/doi/10.1111/j.1745-6584.1994.tb00904.x

89. Pham, N., Cabaltica, A., & Pham, H. (2021, 5). Feasibility of low impact development measures to mitigate inundation in tidal – impacted urban area: A case in Ho Chi Minh City, Vietnam. *IOP Conference Series: Materials Science and Engineering*, 1153(1), 012005. doi:DOI 10.1088/1757-899X/1153/1/012005

90. Pham, V., Boyer, D., Le Mouël, J.-L., & Nguyen , T. (2002). Hydrogeological investigation in the Mekong Delta around Ho-Chi-Minh City (South Vietnam) by electric tomography. *Comptes Rendus Geoscience*, 334(10), 733-740. doi:https://doi.org/10.1016/S1631-0713(02)01816-3

91. Pham, V., Sebesvari, Z., Bläsing, M., Rosendahl, I., & Renaud, F. (2013). Pesticide use and management in the Mekong delta and their residues in surface and drinking water. *Science of The Total Environment*, 452–453, 28-39. doi:https://doi.org/10.1016/j.scitotenv.2013.02.026

92. Phan, D., Nguyen, T., Vladimír, L., & Tran, C. (2019). Overview of the activities of industrial parks and impacts on surface water quality in Ho Chi Minh City, Vietnam. *Inzynieria Mineralna Journal of The Polish Mineral Engineering Society*, 2019(2), 81-86. doi:https://doi.org/10.29227/IM-2019-02-13.

93. Phuoc Van, N., & Moens, E. (2013). *HCMC towards the Sea City Moving Towards the Sea with Climate Change Adaptation*. Asian Development Bank. doi:https://www.adb.org/sites/default/files/publication/27505/hcmc-climate-change-summary.pdf

94. Prakash Maurya, S., Singh, N., & Tiwari, A. (2019). 1D Inversion of Large Loop Transient Electromagnetic Data Acquired Using Offset Loop Configuration Over Multi-layer Earth Models. *Earth Sciences*, 8(5), 285-293. doi:DOI: 10.11648/j.earth.20190805.14

95. Reynolds, J. (2011). *An Introduction to Applied and Environmental Geophysics*. Wiley-Blackwell. Retrieved from www.wiley.com/go/reynolds/introduction2e

96. Samouëlian, A., Cousin, I., Tabbagh, A., Bruand, A., & Richard, G. (2005, 9). Electrical resistivity survey in soil science: A review. *Soil and Tillage Research*, 83(2), 173-193. doi:https://doi.org/10.1016/j.still.2004.10.004

97. Scussolini, P., Tran, T., Koks, E., Diaz-Loaiza, A., Ho, P., & Lasage, R. (2017, 12). Adaptation to Sea Level Rise: A Multidisciplinary Analysis for Ho Chi Minh City, Vietnam. *Water Resources Research*, 53(12), 10841-10857. doi:https://doi.org/10.1002/2017WR021344

98. Sengpiel, K.-P., & Siemon, B. (2000). Advanced inversion methods for airborne electromagnetic exploration. *Geophysics*, 65(6). doi:https://doi.org/10.1190/1.1444882

99. Singha, K., & Gorelick, S. (2006, 6). Hydrogeophysical tracking of three-dimensional tracer migration: The concept and application of apparent petrophysical relations. *Water Resources Research*, 42(6). doi:https://doi.org/10.1029/2005WR004568

100. Spies, B., & Frischknecht, F. (1991). Electromagnetic sounding (Vol. Volume 2). *Electromagnetic Methods in Applied Geophysics*. doi:https://doi.org/10.1190/1.9781560802686.ch5

101. Telford, W. (1990, 10). *Applied Geophysics*. Cambridge University Press. Retrieved from https://www.cambridge.org/core/product/identifier/CBO9781139167932A072/type/book_part

102. Thanh, N., Cuong, D., Stattegger, K., Dung, B., Yang, S., Chi, N., Tung, N., Tinh, N., Nga, N. (2021, 2). Depositional sequences of the Mekong river delta and adjacent shelf over the past 140 kyr, southern Vietnam. *Journal of Asian Earth Sciences*, 206. doi:https://doi.org/10.1016/j.jseaes.2020.104634

103. Thoang, T., & Giao, P. (2015, 12). Subsurface characterization and prediction of land subsidence for HCM City, *Vietnam. Engineering Geology*, 199, 107-124.

104. Tran, L.T., Larsen, F., Pham, N. Q., Christiansen, A. V., Tran, N., Vu, H.V., Tran, L.V., Hoang, H.V., Hinsby, K., 2012. Origin and extent of fresh groundwater, salty paleowaters and recent saltwater intrusions in Red River flood plain aquifers, Vietnam. *Hydrogeology Journal* (2012) 20: 1295–1313, DOI: 10.1007/s10040-012-0874-y

105. Tran, O., Tran, D., Do, C., & Ho, T. (2016, 3). Current status and risks of underground water for house holds in Cu Chi District - Ho Chi Minh City. *Science and Technology Development Journal*, 19(1), 122-130. Retrieved from http://stdj.scienceandtechnology.com.vn/index.php/stdj/article/view/512

106. Truong , Q., Nguyen , T., Nguyen, T., Tran, L., Le , H., Pham , T., & Descloitres, M. (2021). Synthetic modeling of EM34 in detecting the shallow clayey layer in aquifer system. *Vietnam Journal of Construction.* Retrieved from https://tailieu.vn/readpdf/tailieu/2021/20211023/vivacation2711/43_1017.pdf?rand=521112

107. Tu, T., & Nitivattananon, V. (2011, 3). Adaptation to flood risks in Ho Chi Minh City, Vietnam. *International Journal of Climate Change Strategies and Management*, 3(1), 61-73.

108. Tu, T., Tweed, S., Dan, N., Descloitres, M., Quang, K., Nemery, J., Nemery, J., Nguyen, A., Baduel, C. (2022, 11). Localized recharge processes in the NE Mekong Delta and

implications for groundwater quality. *Science of The Total Environment*, 845, 157118. doi:https://doi.org/10.1016/j.scitotenv.2022.157118

109. Vachaud, G., Quertamp, F., Phan, T., Tran Ngoc, T., Nguyen, T., Luu, X., Nguyen, T., Gratiot, N. (2019, 6). Flood-related risks in Ho Chi Minh City and ways of mitigation. *Journal of Hydrology*, 573, 1021-1027. doi:https://doi.org/10.1016/j.jhydrol.2018.02.044

110. Van Hong, N., & Phuong Dong, N. (2022, 3). Study to assess the impact of saltwater intrusion in Ho Chi Minh City under climate change conditions. *Vietnam Journal of Hydrometeorology*, 10(1), 11-23. Retrieved from https://vjol.info.vn/index.php/TCtongcuckhituongthuyvan/article/view/67384

111. Van Leeuwen, C. J., Dan, N. P., & Dieperink, C. (2016, 4). The challenges of water governance in Ho Chi Minh City. *Integrated Environmental Assessment and Management*, 12(2), 345-352. doi:DOI: 10.1002/ieam.1664

112. Van, T., & Koontanakulvong, S. (2018, 1). Groundwater and river interaction parameter estimation in saigon river, Vietnam. *Engineering Journal*, 22(1), 257-267. doi:DOI:10.4186/ej.2018.22.1.257

113. Vest Christiansen, A., & Auken, E. (2012). A global measure for depth of investigation. *Geophysics*, 77(4). doi:https://doi.org/10.1190/geo2011-0393.1

114. Vouillamoz, J., Lawson, F., Yalo, N., & Descloitres, M. (2014). The use of magnetic resonance sounding for quantifying specific yield and transmissivity in hard rock aquifers The example of Benin. *Journal of Applied Geophysics*, 107, 16-24. doi:https://doi.org/10.1016/j.jappgeo.2014.05.012

115. Vouillamoz, J., Sophoeun, P., Bruyere, O., & Arnout, L. (2014). Estimating storage properties of aquifer with magnetic resonance sounding: A field verification in northern Cambodia of the gravitational water apparent cutoff time concept. *Near Surface Geophysics*, 12(2), 211-216. doi:https://doi.org/10.3997/1873-0604.2013038

116. Vuong, B., Long, P., & Nam, L. (2016). Groundwater Environment in Ho Chi Minh City, Vietnam. *Groundwater Environment in Asian Cities*, 287-315. doi:https://doi.org/10.1016/B978-0-12-803166-7.00013-1

117. Wagner, F., Tran, V., & Renaud, F. (2012). Groundwater Resources in the Mekong Delta: Availability, *Utilization and Risks.* Springer, Dordrecht. doi:https://doi.org/10.1007/978-94-007-3962-8_7

118. Wait, J.. (1982). *Geo-Electromagnetism*. New York, USA: Academic Press. doi:https://doi.org/10.1016/B978-0-12-730880-7.X5001-7

119. Ward, S. (1990). Resistivity and Induced Polarization Methods. *Geotechnical and Environmental Geophysics*, 1(Review and Tutorial). doi:https://doi.org/10.1190/1.9781560802785.ch6

120. Ward, S., & Hohmann, G. (1988, 1). Electromagnetic Theory for Geophysical Applications. *Electromagnetic Methods in Applied Geophysics*: Volume 1, Theory, 130-311. doi:https://doi.org/10.1190/1.9781560802631.ch4

121. Widodo, W., Zamani, M., Patimah, S., & Agustiana, E. (2022). Aquatic Sedimentation Assessment Using Electromagnetic Data in the Scheme of Flood Hazard Mitigation. *Journal of Engineering and Technological Sciences*, 55(3). doi:https://doi.org/10.20944/preprints202209.0107.v1

122. Wilbers, G., Becker, M., Nga, L., Sebesvari, Z., & Renaud, F. (2014, 7). Spatial and temporal variability of surface water pollution in the Mekong Delta, Vietnam. *Science of the Total Environment*, 485-486(1), 653-665. doi:https://doi.org/10.1016/j.scitotenv.2014.03.049

123. Woessner, W., & Poeter, E. (2020). *Hydrogeologic Properties of Earth Materials and Principles of Groundwater Flow*. The Groundwater Project. Retrieved from https://www.un-igrac.org/sites/default/files/resources/files/hydrogeologic-properties-of-earth-materials-and-principles-of-groundwater-flow.pdf

124. Wu, C., Chen, S., Cheng, C., & Trac, L. (2021, 8). Climate justice planning in global south: Applying a coupled nature-human flood risk assessment framework in a case for ho chi minh city, Vietnam. *Water (Switzerland)*, 13(15). doi:https://doi.org/10.3390/w13152021

125. Yaramanci, U., Lange, G., & Hertrich, M. (2002). Aquifer characterisation using Surface NMR jointly with other geophysical techniques at the Nauen/Berlin test site. *Journal of Applied Geophysics*, 50(1-2), 47-65. doi:https://doi.org/10.1016/S0926-9851(02)00129-5

126. Yogi, I., & Widodo. (2017, 4). Central Loop Time Domain Electromagnetic Inversion Based on Born Approximation and Levenberg-Marquardt Algorithm. *IOP Conference Series: Earth and Environmental Science*, 62(1). doi:DOI 10.1088/1755-1315/62/1/012029

127. Yukselen, Y., & Kaya, A. (2008, 11). Suitability of the methylene blue test for surface area, cation exchange capacity and swell potential determination of clayey soils. *Engineering Geology*, 102(1-2), 38-45. doi:https://doi.org/10.1016/j.enggeo.2008.07.002

128. Zohdy, A., Eaton, G., & Mabey Book, D. (1974). *Application of surface geophysics to ground-water investigations*. U.S. Dept. of the Interior, Geological Survey : U.S. Govt. Print. Off. doi:https://doi.org/10.3133/twri02D1

APPENDIX 1 SYNTHETIC DATA FOR EM MODELING

Table 1 42 Synthetic Data + Noise of different thickness and depth of clay models

Name Sounding	Synthetic Model of Clayey Layer		Apparent Conductivity (mS/m)					
			HMD Spacing (m) (Height = 0.5)			VMD Spacing (m) (Height = 0)		
	Depth of top Clay (m)	Thickness of Clay (m)	10	20	40	10	20	40
SD01	0	0.5	8.12	6.46	5.62	4.56	4.43	4.78
SD02	0	1	11.39	8.65	6.82	5.07	4.6	4.81
SD03	0	3	21.01	15.34	10.66	10.64	6.17	5.42
SD04	0	5	26.94	20.33	13.66	16.82	8.61	6.31
SD05	0	10	33.23	28.3	21.07	26.3	16.87	8.96
SD06	0	15	35.77	33.37	25.48	30.96	21.63	13.9
SD07	0	20	36.57	35.14	29.55	32.53	26.75	17.97
SD08	3	0.5	6.11	5.92	5.82	6.17	5.01	4.9
SD09	3	1	7.72	7.4	6.48	7.73	5.64	5.21
SD10	3	3	12.11	12.09	9.76	13.98	8.78	6.27
SD11	3	5	14.95	15.27	12.99	18.17	12.02	7.44
SD12	3	10	18.06	20.77	17.83	23.63	19.6	11.64

SD13	3	15	19.43	23.94	21.71	25.87	24.17	16.01
SD14	3	20	20.84	26.07	25.53	28.05	26.88	19.92
SD15	10	0.5	4.44	5.07	5.15	5.29	5	5.35
SD16	10	1	5.03	5.72	5.86	5.92	5.9	5.81
SD17	10	3	6.04	7.31	7.87	8.03	8.44	7.41
SD18	10	5	7.03	8.93	9.82	9.45	10.76	9.11
SD19	10	10	8.11	11.58	13.2	11.5	15.07	13.57
SD20	10	15	8.49	13.91	15.4	12.88	17.82	16.94
SD21	10	20	8.73	13.92	17.5	13.23	19.39	19.83
SD22	20	0.5	4.27	4.76	4.93	4.59	4.75	5.12
SD23	20	1	4.5	4.76	5.15	4.65	5.17	5.41
SD24	20	3	4.77	5.58	6.49	5.62	6.34	6.92
SD25	20	5	4.96	6.19	7.28	5.71	7.37	8.47
SD26	20	10	5.13	7.39	9.52	6.6	9.71	11.81
SD27	20	15	5.5	8.26	10.73	6.81	11.12	13.99
SD28	20	20	5.4	8.3	11.84	6.7	11.54	16.61
SD29	30	0.5	4.25	4.55	4.76	4.4	4.57	5.24
SD30	30	1	4.29	4.52	5.03	4.54	4.8	5.38
SD31	30	3	4.36	5.13	5.56	4.92	5.43	6.37
SD32	30	5	4.63	5.44	6.29	5.04	6.13	7.32

SD33	30	10	4.57	5.81	7.16	5.3	7.17	9.92
SD34	30	15	4.63	6.15	8.26	5.08	7.64	11.47
SD35	30	20	4.68	6.22	8.91	5.23	8.29	13.15
SD36	50	0.5	4.11	4.44	4.6	4.46	4.55	5.13
SD37	50	1	4.34	4.36	4.76	4.37	4.54	5.07
SD38	50	3	4.19	4.67	4.94	4.6	4.65	5.49
SD39	50	5	4.31	4.71	5.16	4.68	5.11	6.05
SD40	50	10	4.32	5.06	5.75	4.47	5.45	7.16
SD41	50	15	4.27	5.06	6.3	4.49	5.67	8.45
SD42	50	20	4.16	4.93	6.67	4.48	5.85	8.93

Table 2 Interpreted models from 42 synthetic data consist of electrical conductivities and thicknesses in three-layer solution

Name of interpreted model	**Interpreted 3-Layer Model**					
	EC1 (mS/m)	**Thickness 1 (m)**	**EC2 (mS/m)**	**T2 (m)**	**electrical conductivity of layer 3 (mS/m)**	**RMS 3rd**
IM01	21.43	1.97	2.92	10.10	5.84	1.34
IM02	39.27	1.52	3.54	10.64	5.85	0.97
IM03	47.28	3.30	4.05	13.71	6.09	1.43
IM04	50.41	3.94	18.95	3.36	5.43	3.97
IM05	49.57	2.23	47.87	8.13	5.31	0.83

IM06	42.40	1.69	58.47	8.46	11.28	1.43
IM07	45.76	2.24	53.89	13.16	12.54	1.43
IM08	5.58	1.82	12.00	2.90	5.37	2.19
IM09	4.56	1.76	19.93	2.84	5.47	1.96
IM10	3.62	2.57	42.72	3.56	5.63	1.51
IM11	4.52	2.77	47.07	5.09	6.01	1.02
IM12	6.83	3.37	49.27	9.91	6.11	1.53
IM13	7.42	3.55	51.70	12.92	8.68	1.9
IM14	5.47	3.04	52.76	14.08	15.28	1.16
IM15	3.92	2.23	6.39	6.27	5.95	2.74
IM16	4.67	3.66	8.19	6.99	6.51	1.03
IM17	4.32	5.60	15.83	9.33	7.20	0.93
IM18	5.26	7.69	23.87	10.91	7.01	0.98
IM19	5.36	8.78	34.66	14.75	8.27	1.2
IM20	4.96	8.19	37.72	19.48	9.71	3.17
IM21	4.60	8.30	40.10	20.72	15.69	1.73
IM22	5.08	9.08	4.93	9.31	6.25	1.26
IM23	5.05	11.73	6.17	9.18	6.56	1.8
IM24	4.91	7.36	8.00	10.15	8.55	0.95
IM25	5.18	17.56	18.81	14.29	8.21	0.97
IM26	4.69	15.50	26.76	17.03	10.99	1.09

IM27	5.08	18.19	38.63	19.18	8.71	1.86
IM28	5.01	18.97	40.70	20.86	18.34	2.19
IM29	5.17	9.21	3.42	10.64	7.01	1.68
IM30	5.02	9.68	4.31	10.00	7.03	1.45
IM31	5.01	9.71	5.65	10.73	8.46	2.1
IM32	5.10	14.98	8.72	10.54	10.26	1.15
IM33	4.77	15.27	10.55	10.23	16.06	3.68
IM34	4.83	20.15	16.66	10.82	21.87	2.52
IM35	4.69	19.47	18.24	11.11	26.61	3.56
IM36	4.88	9.87	4.21	9.96	6.46	2.67
IM37	5.26	7.93	3.40	9.86	6.59	1.97
IM38	5.11	11.37	3.87	11.95	7.63	2.43
IM39	4.97	10.12	4.49	10.36	8.20	2.66
IM40	5.03	10.54	3.32	12.09	11.61	2.25
IM41	4.92	12.44	3.16	15.51	17.08	2.3
IM42	4.65	17.11	4.55	14.77	19.95	1.9

APPENDIX 2 TDEM RESISTIVITY MAPS

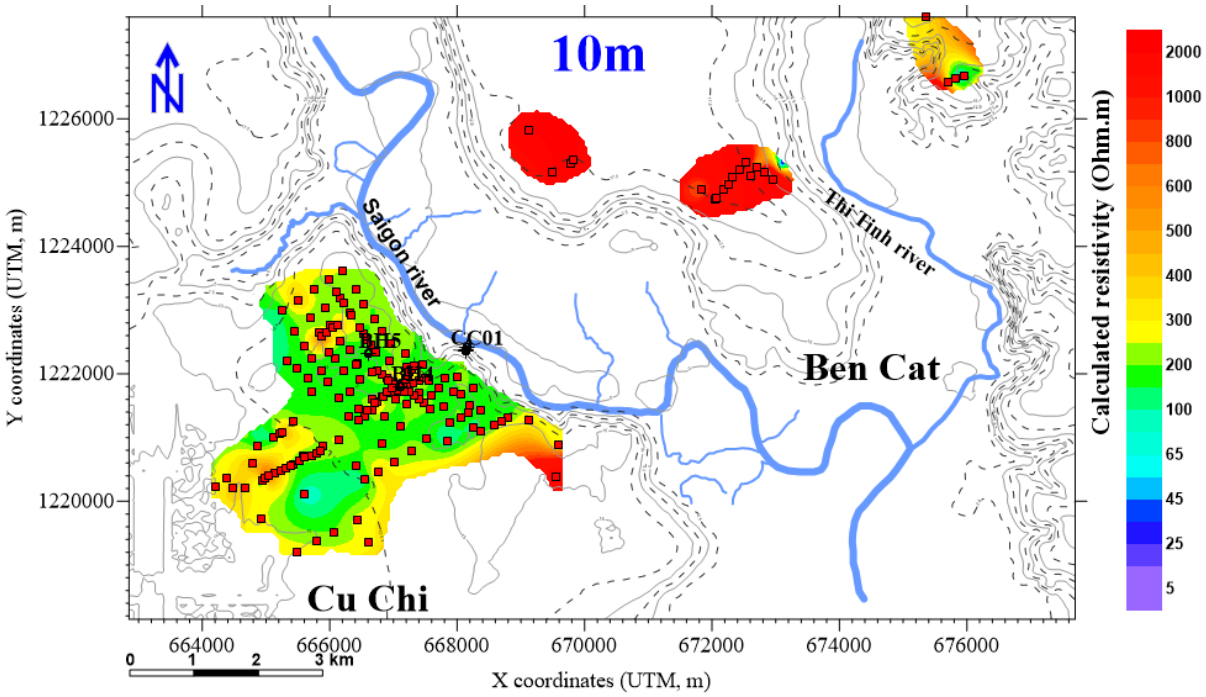

Figure 1 TDEM resistivity contour map at elevation +10m above sea level

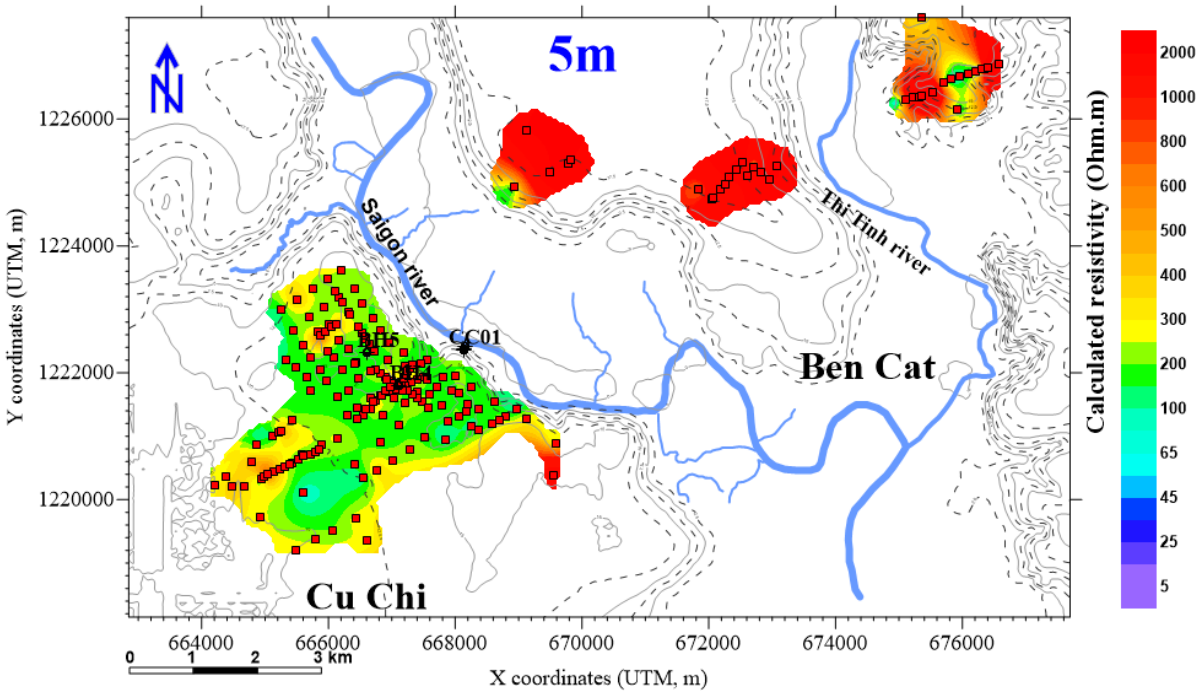

Figure 2 TDEM resistivity contour map at elevation +5m above sea level

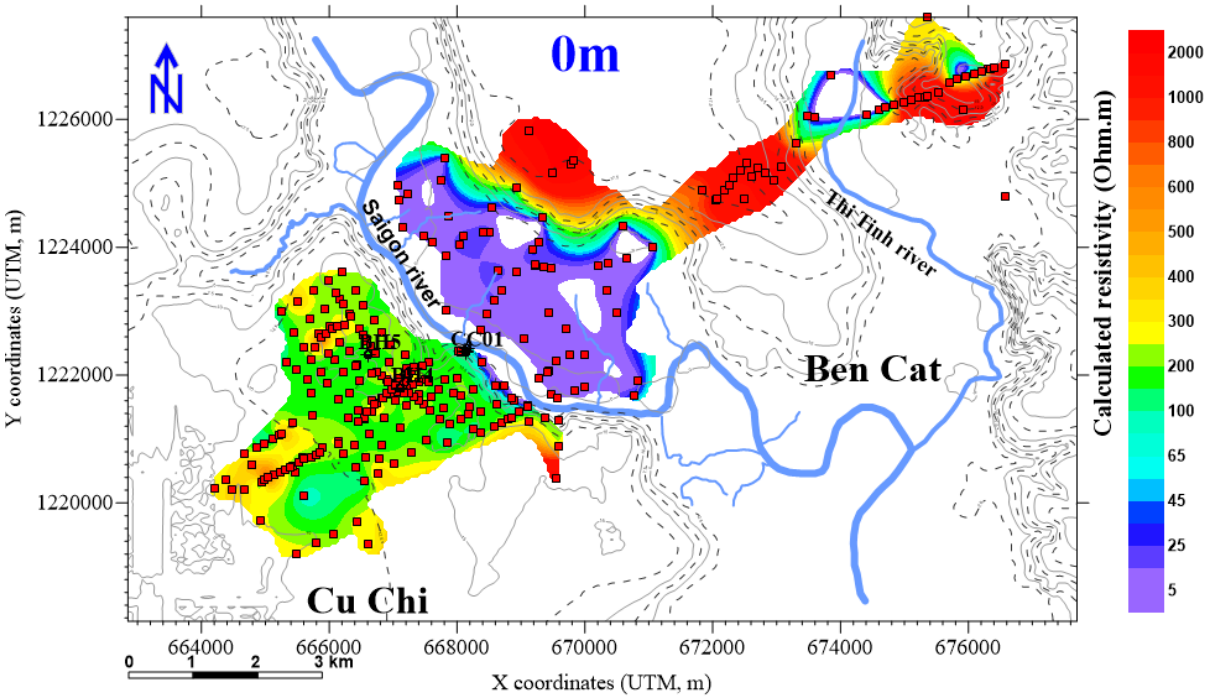

Figure 3 TDEM resistivity contour map at elevation 0m above sea level

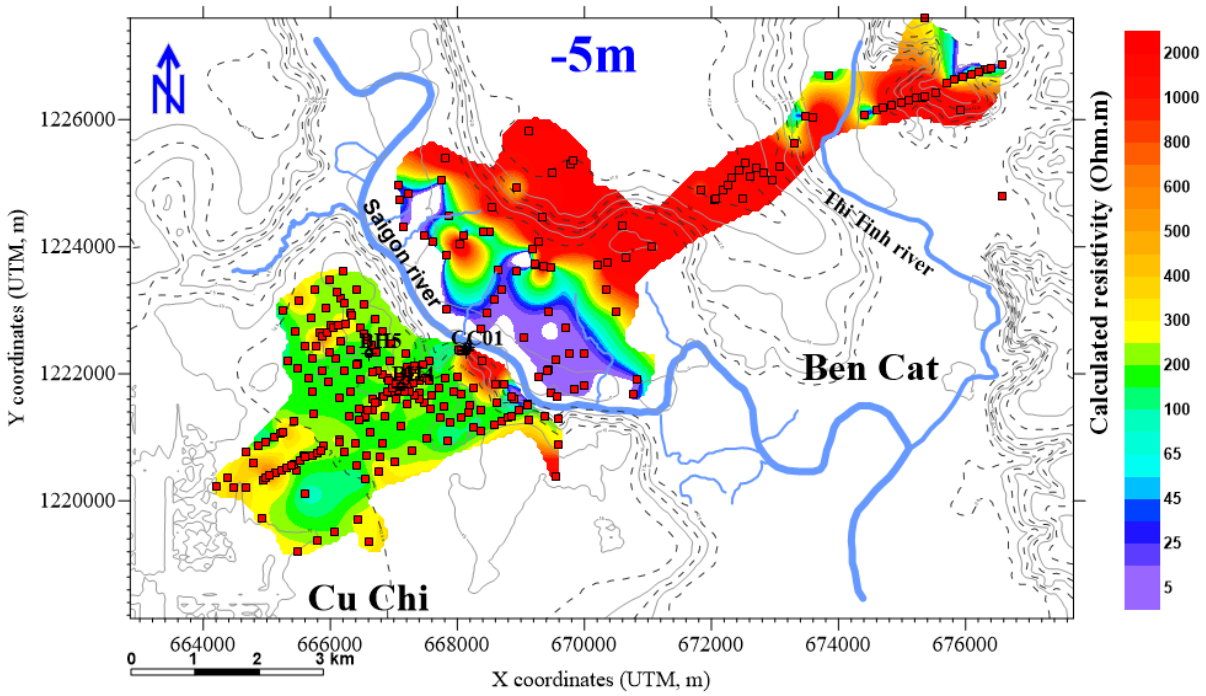

Figure 4 TDEM resistivity contour map at elevation -5m above sea level

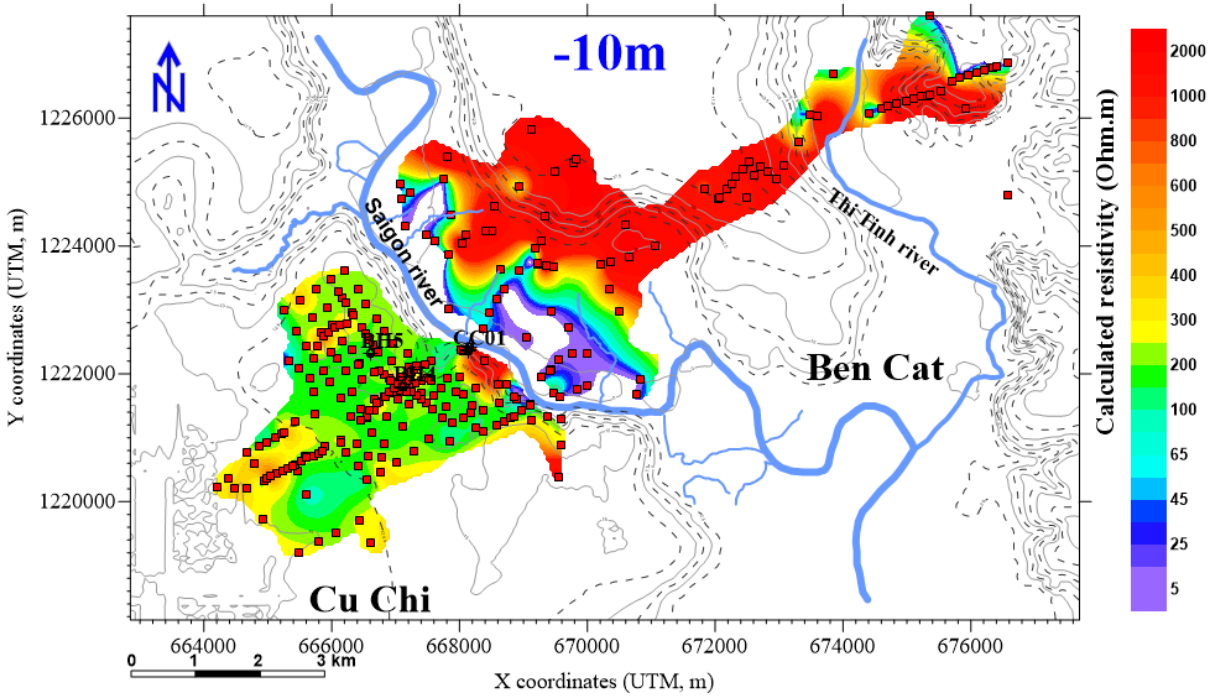

Figure 5 TDEM resistivity contour map at elevation -10m above sea level

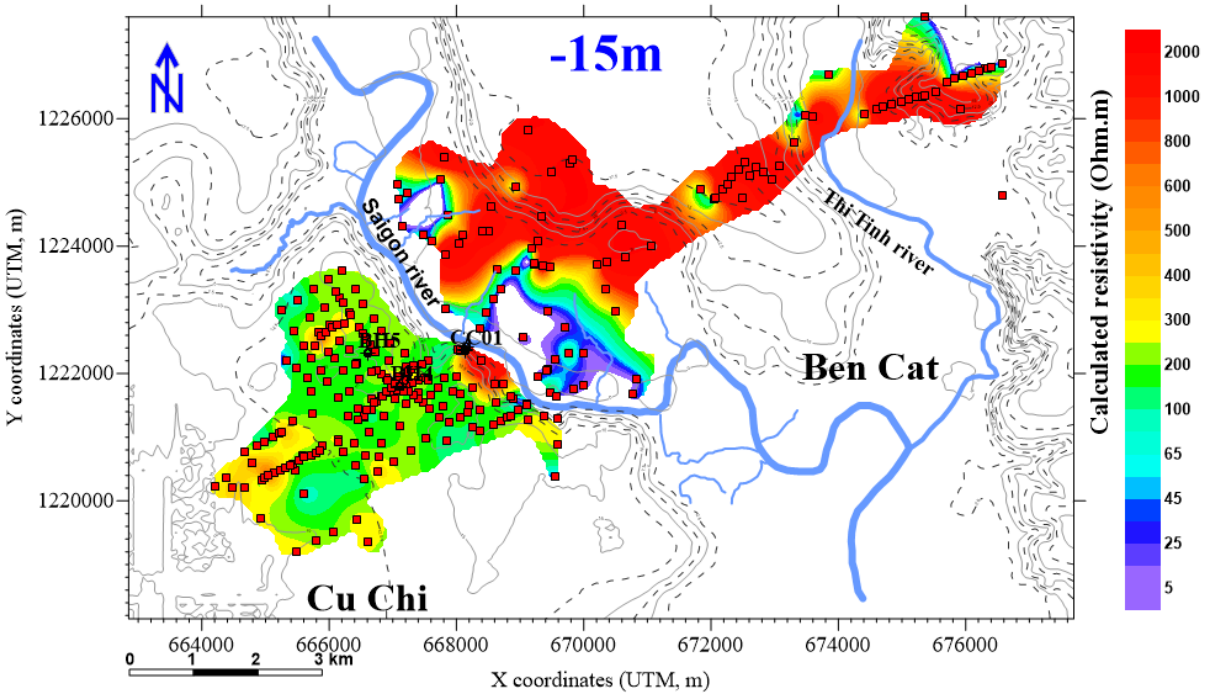

Figure 6 TDEM resistivity contour map at elevation -15m above sea level

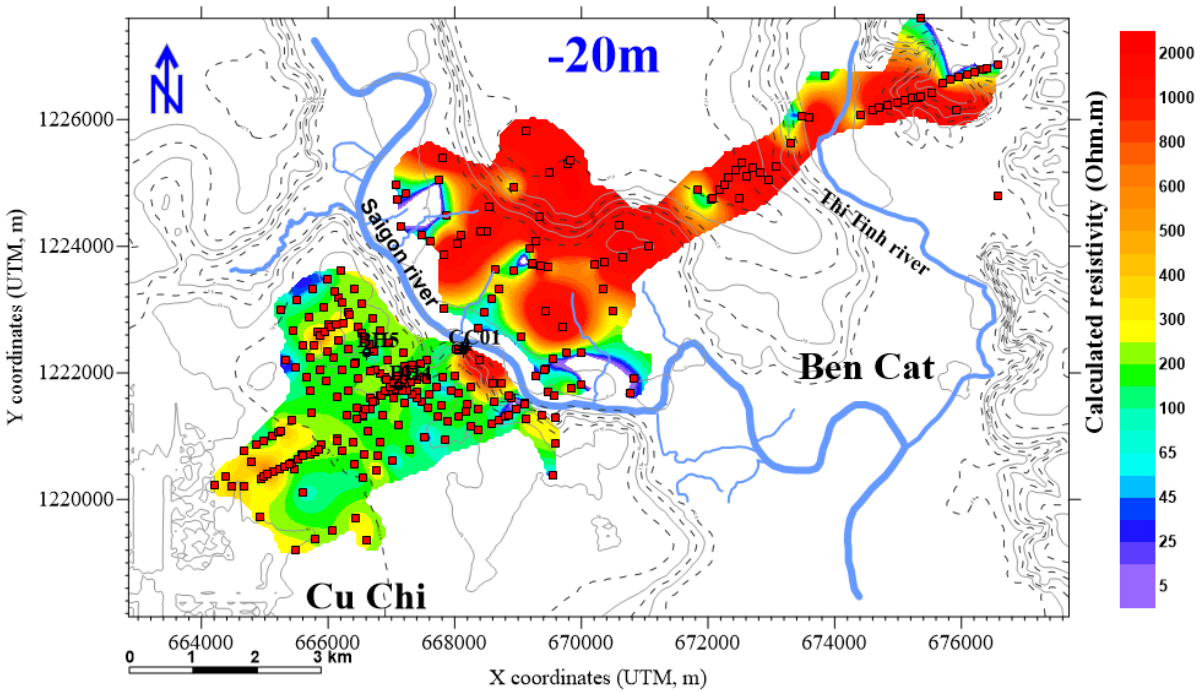

Figure 7 TDEM resistivity contour map at elevation -20m above sea level

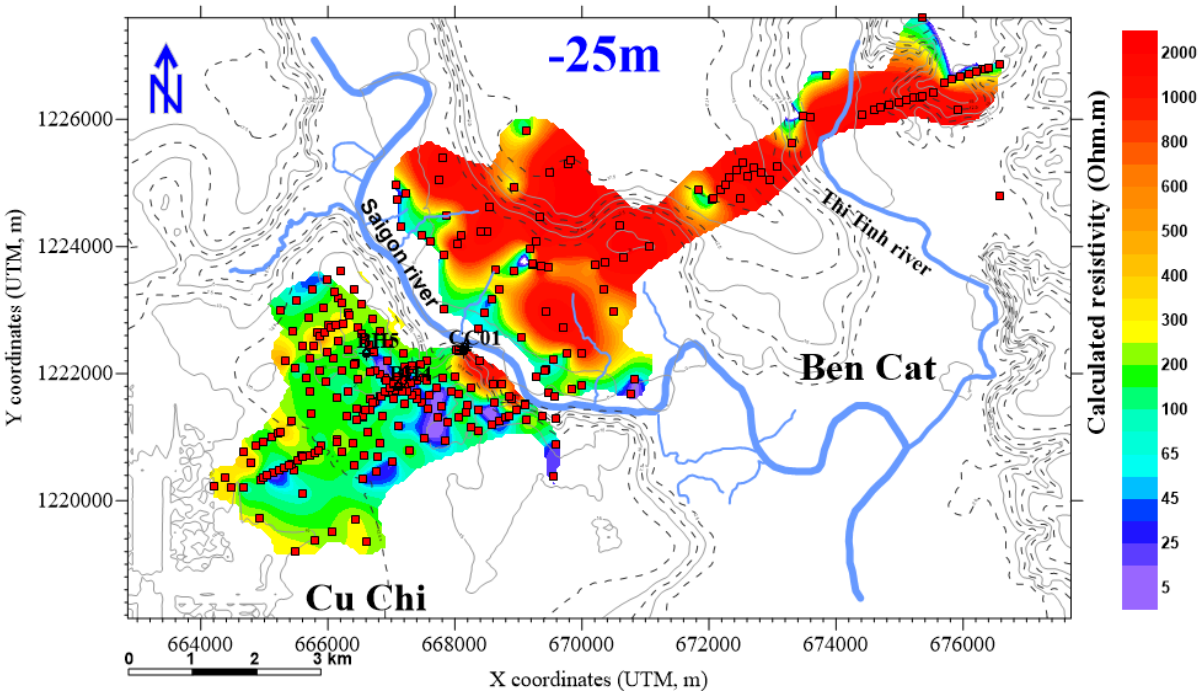

Figure 8 TDEM resistivity contour map at elevation -25m above sea level

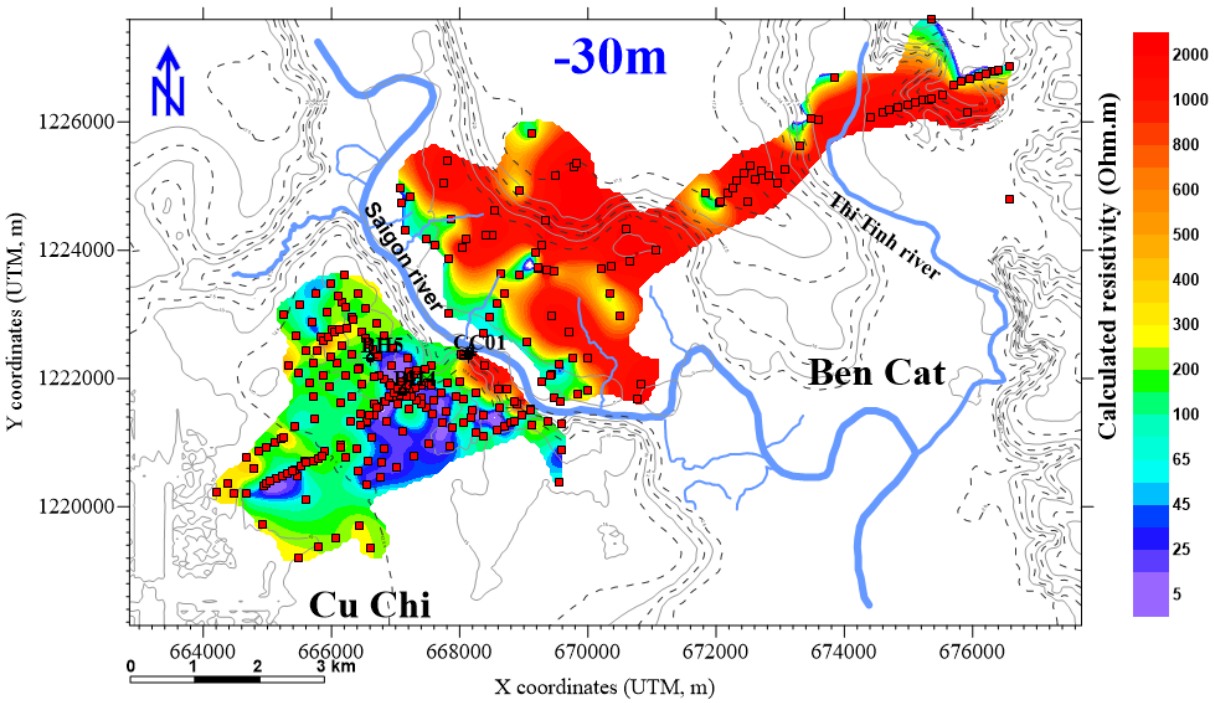

Figure 9 TDEM resistivity contour map at elevation -30m above sea level

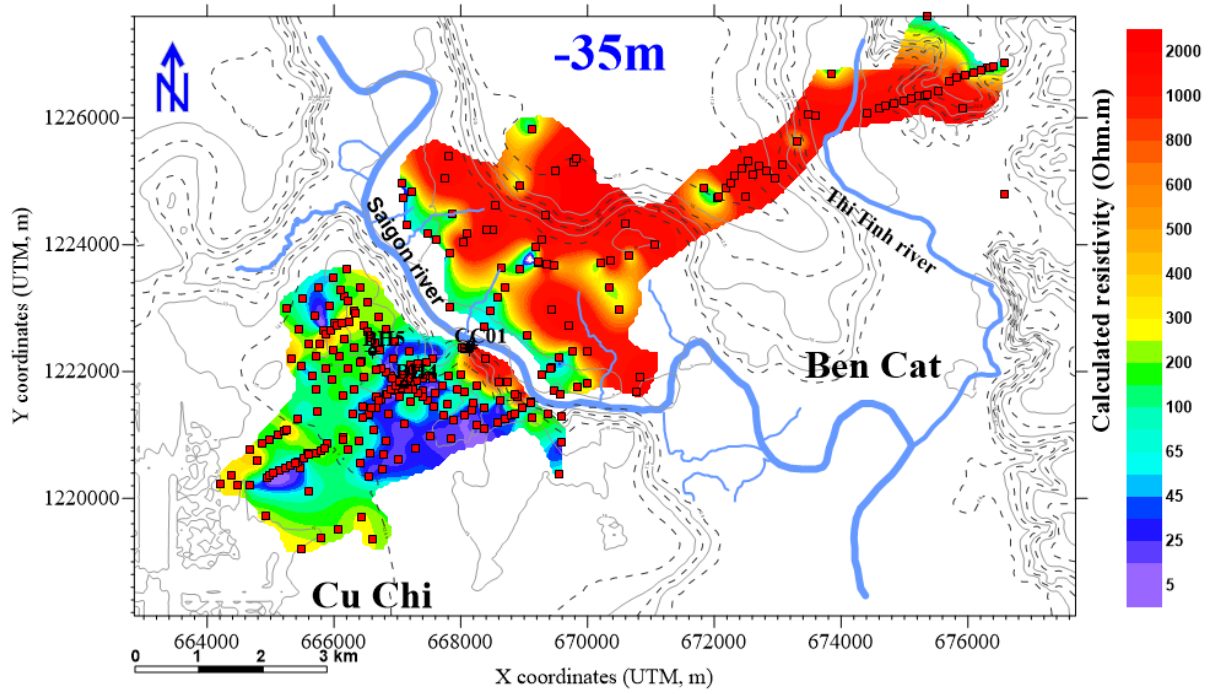

Figure 10 TDEM resistivity contour map at elevation -35m above sea level

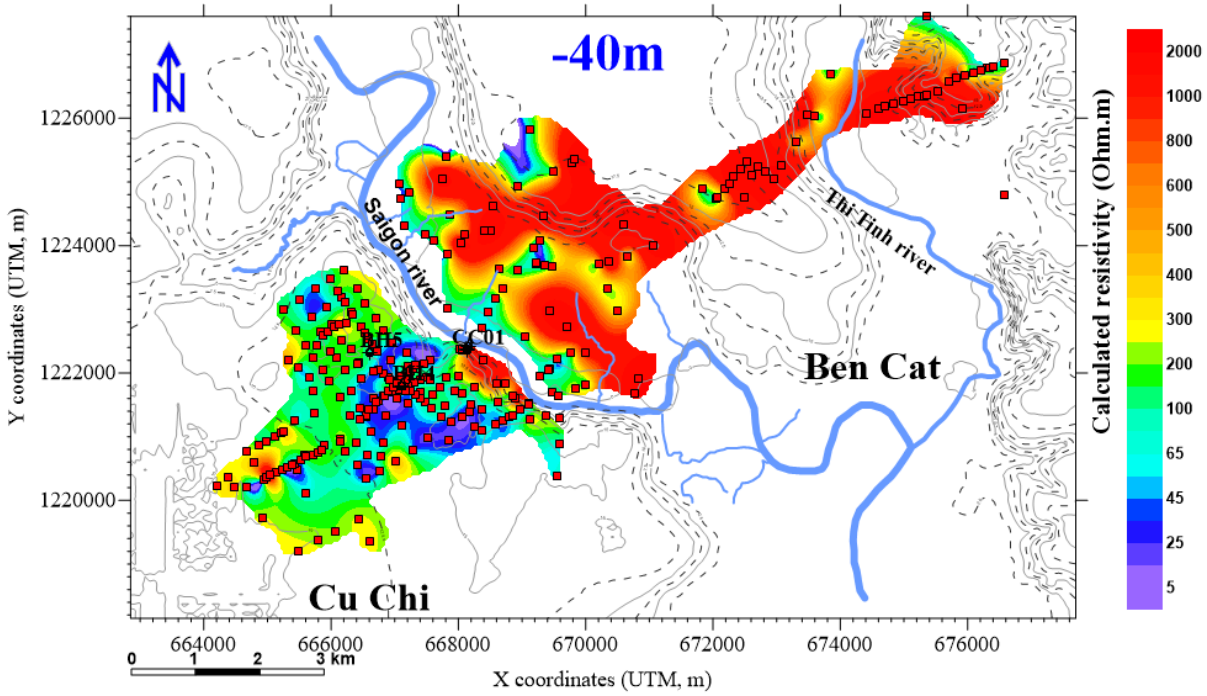

Figure 11 TDEM resistivity contour map at elevation -40m above sea level

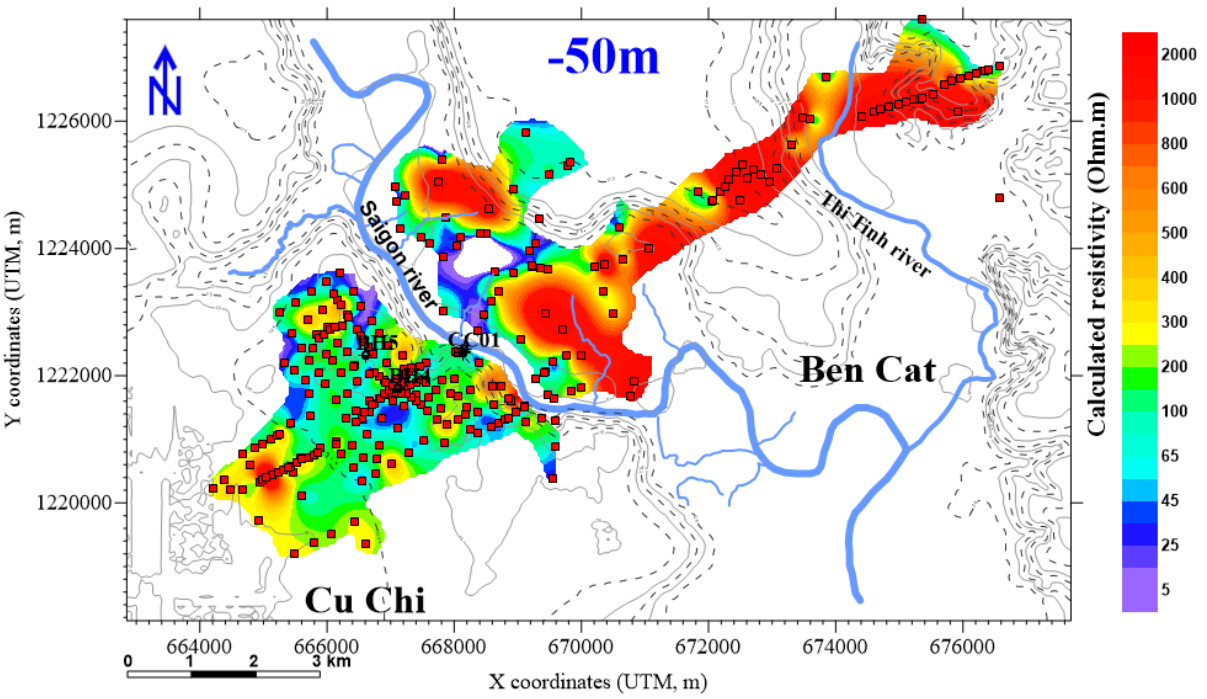

Figure 12 TDEM resistivity contour map at elevation -50m above sea level

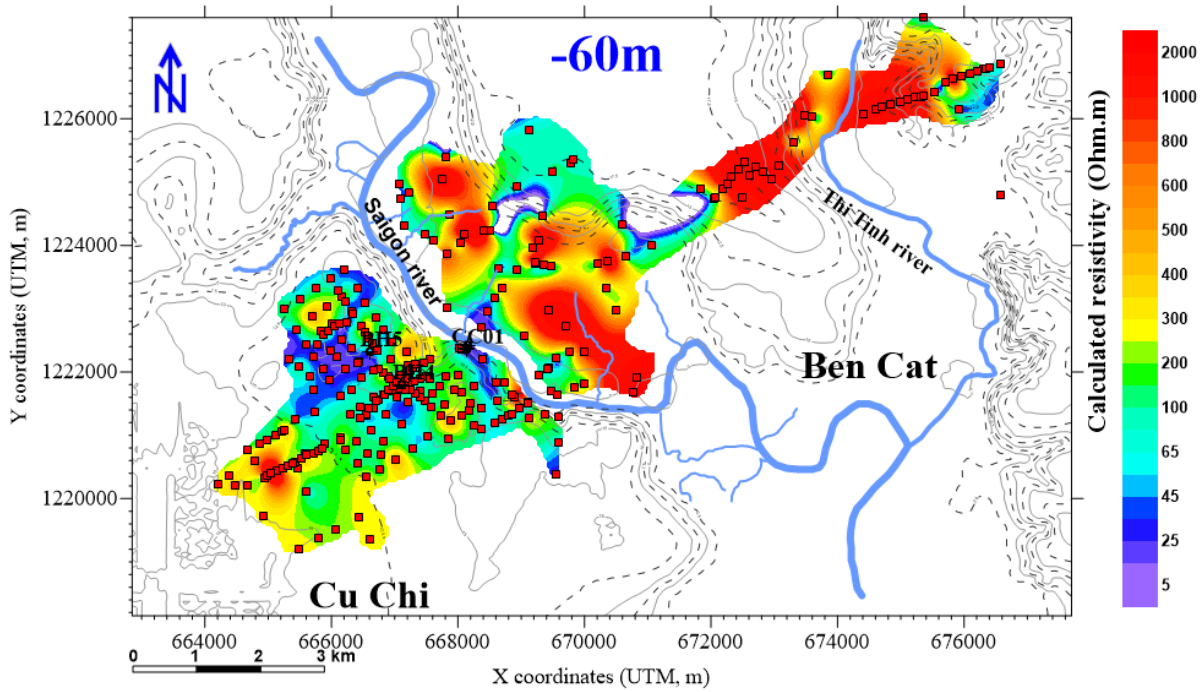

Figure 13 TDEM resistivity contour map at elevation -60m above sea level

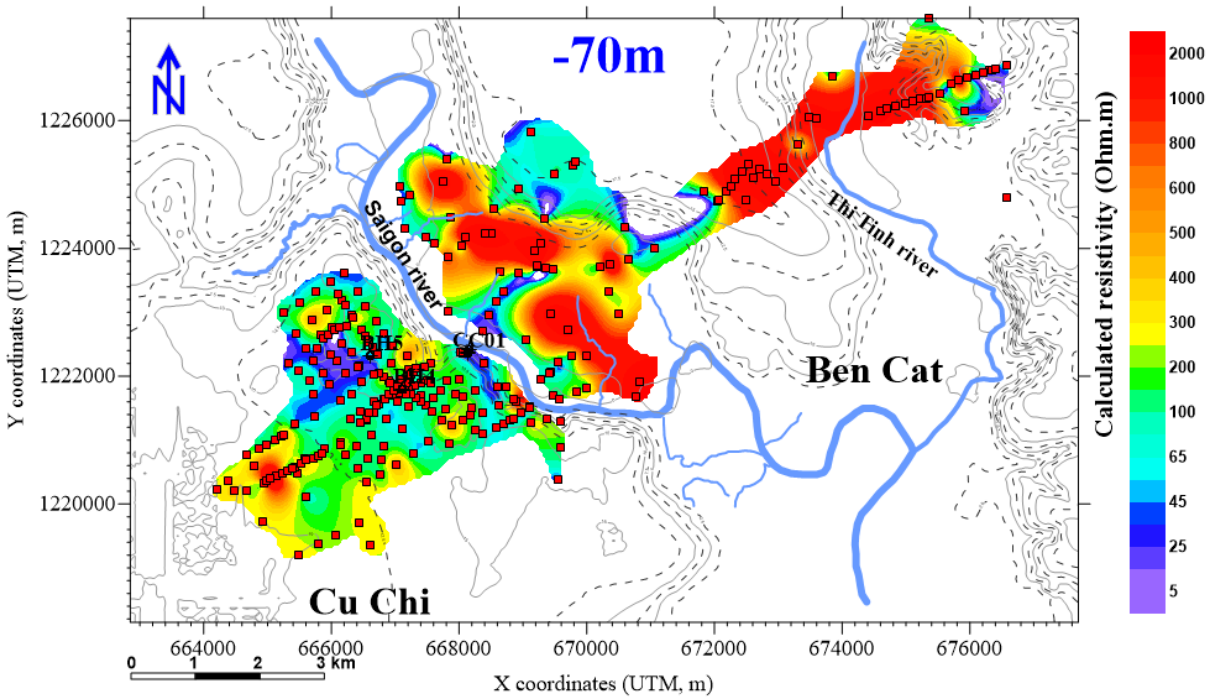

Figure 14 TDEM resistivity contour map at elevation -70m above sea level

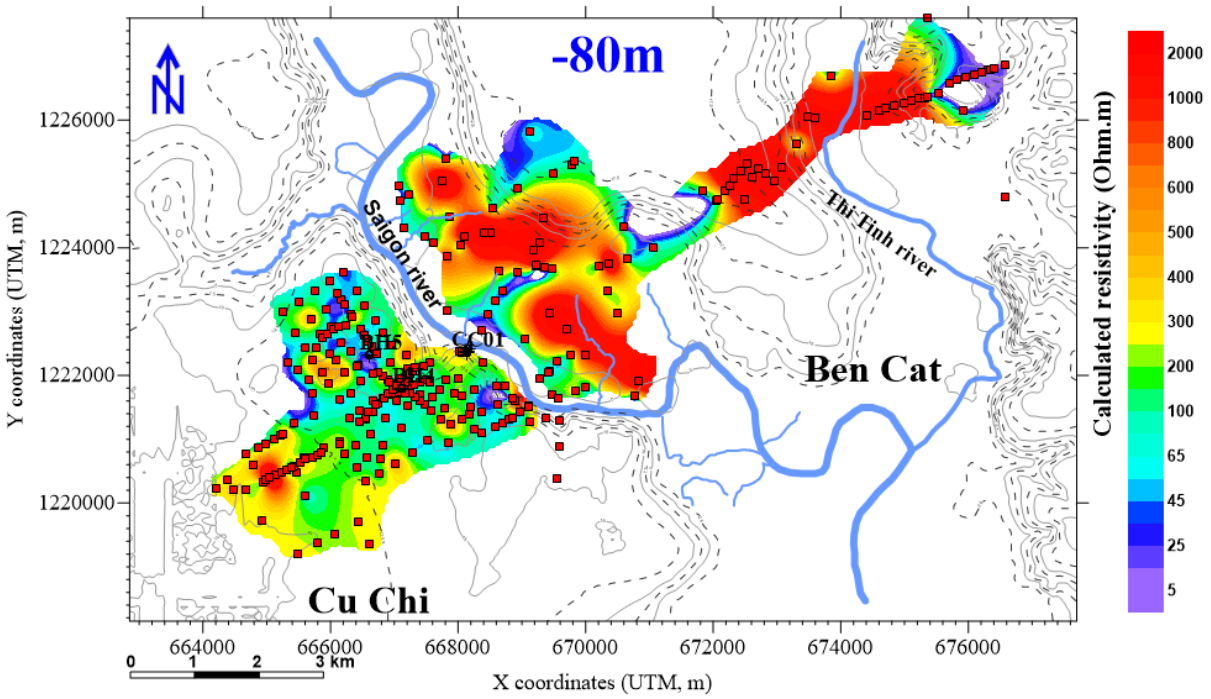

Figure 15 TDEM resistivity contour map at elevation -80m above sea level

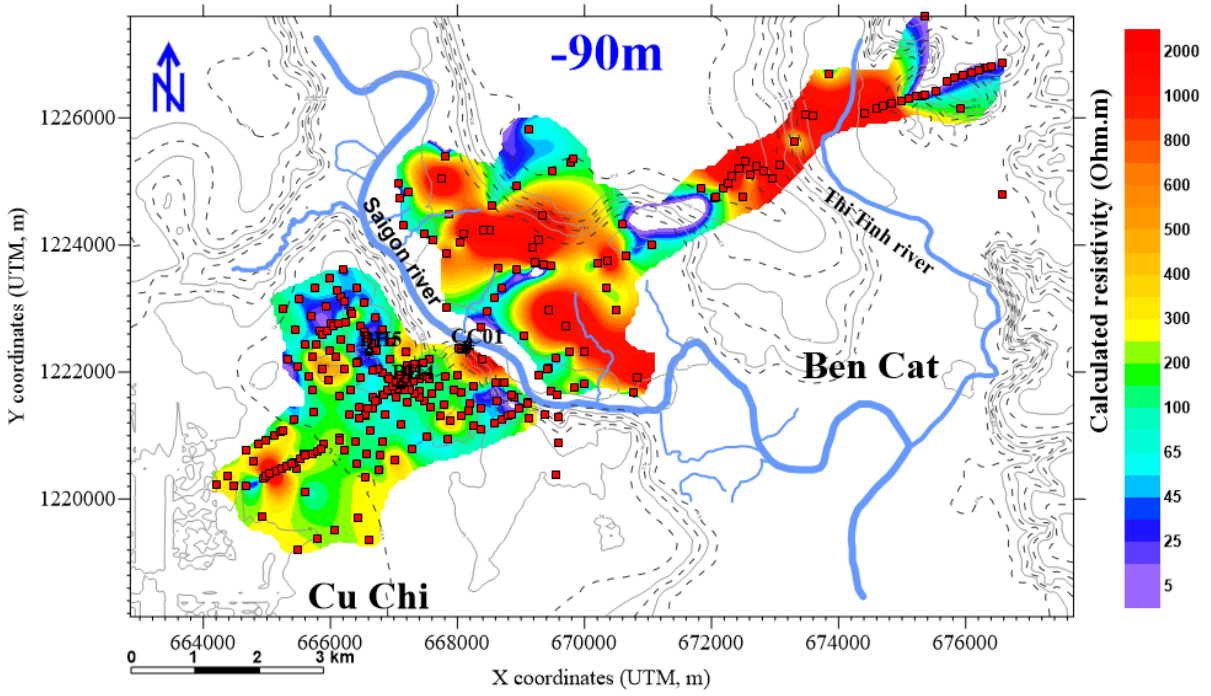

Figure 16 TDEM resistivity contour map at elevation -90m above sea level

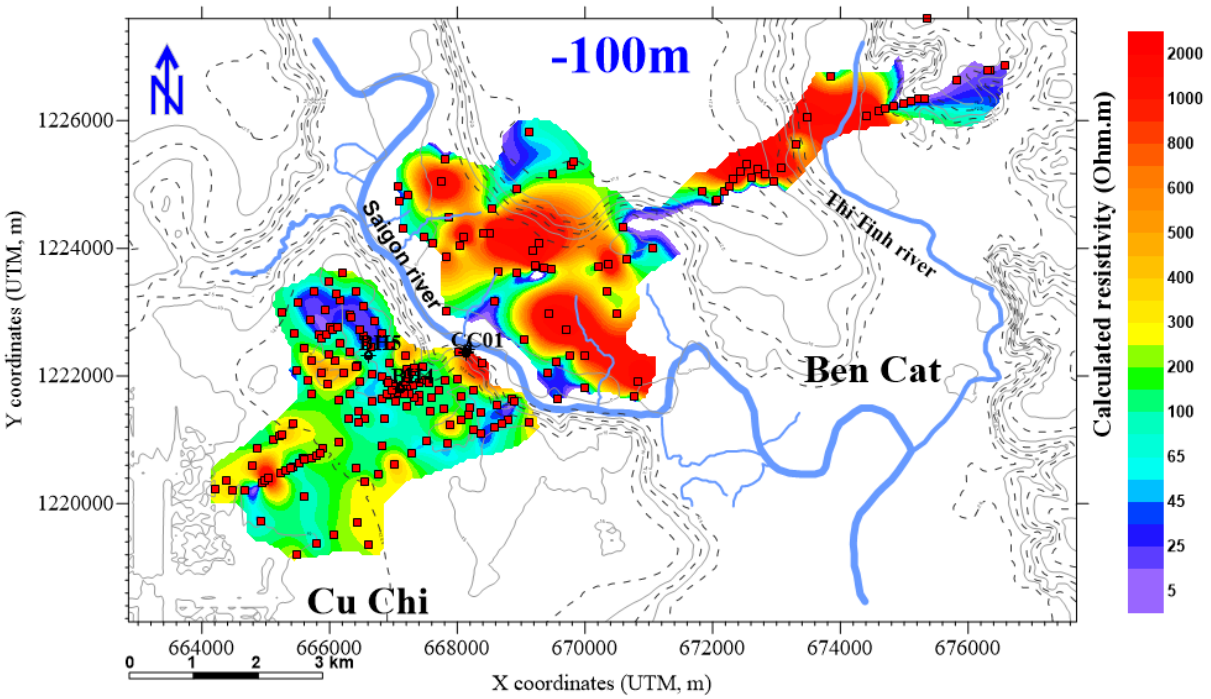

Figure 17 TDEM resistivity contour map at elevation -100m above sea level

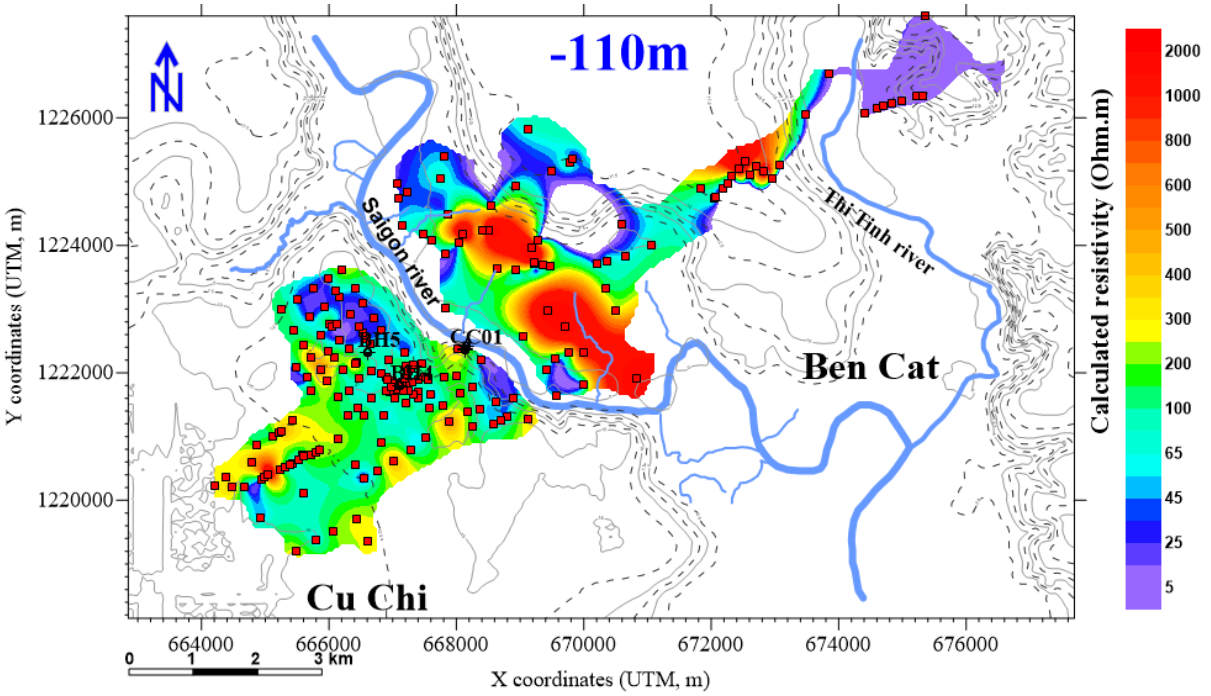

Figure 18TDEM resistivity contour map at elevation -110m above sea level

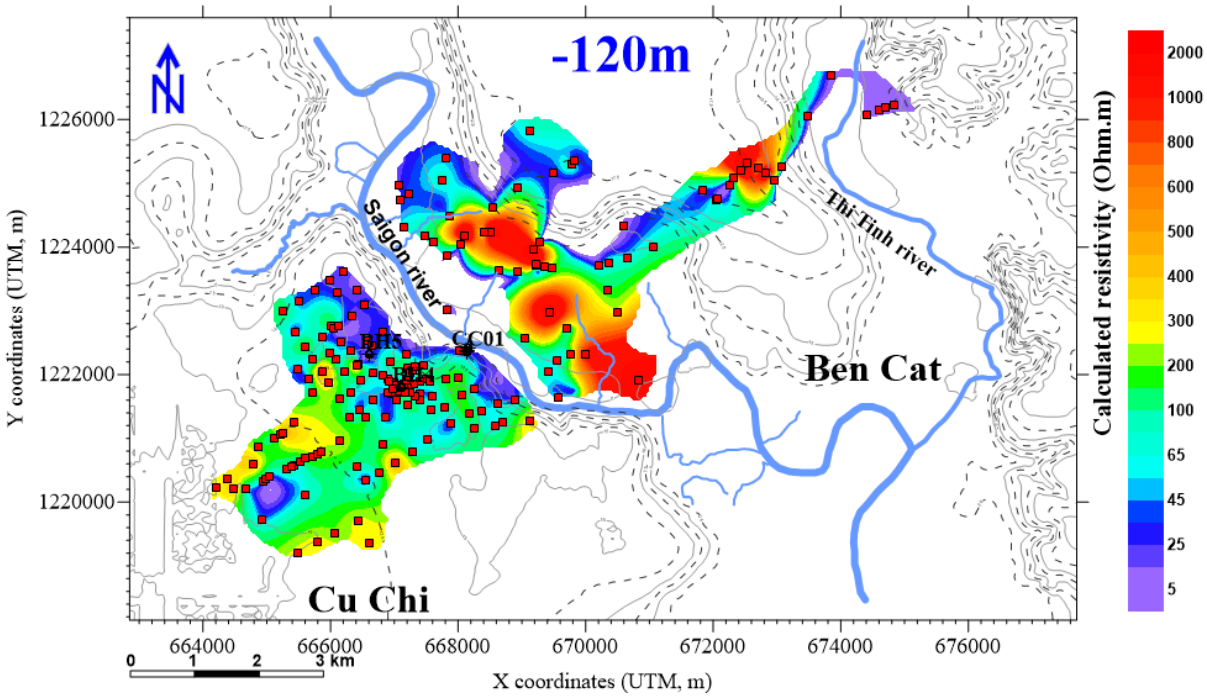

Figure 19 TDEM resistivity contour map at elevation -120m above sea level

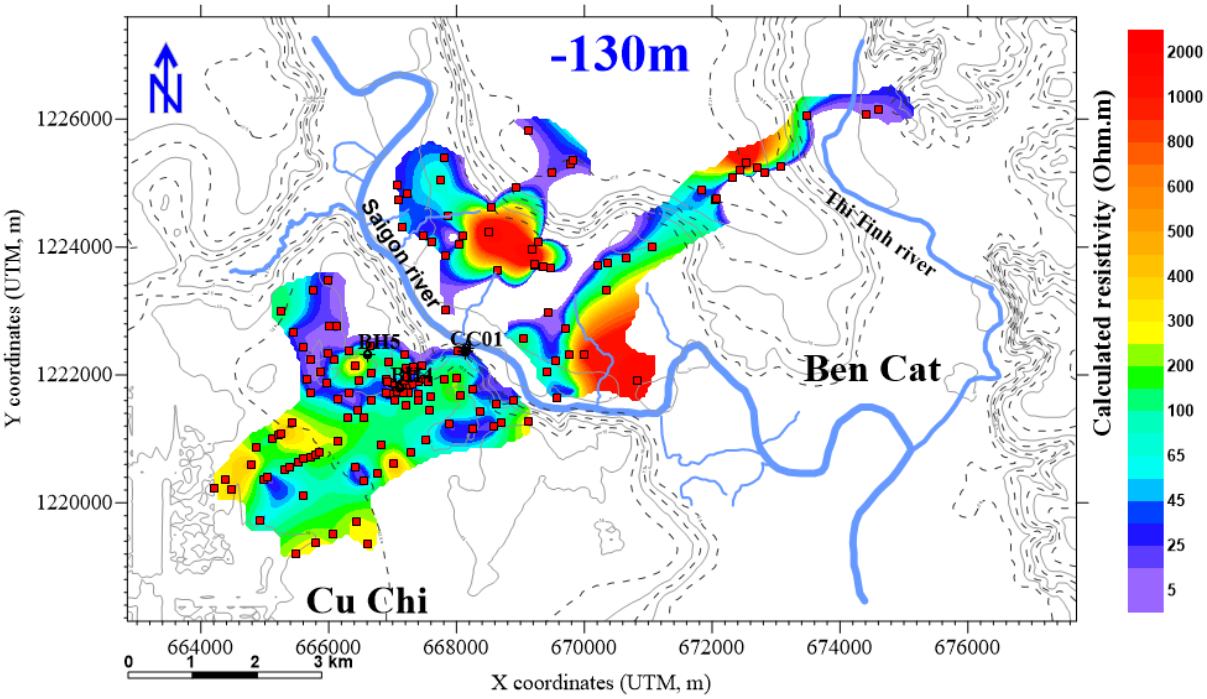

Figure 20 TDEM resistivity contour map at elevation -130m above sea level

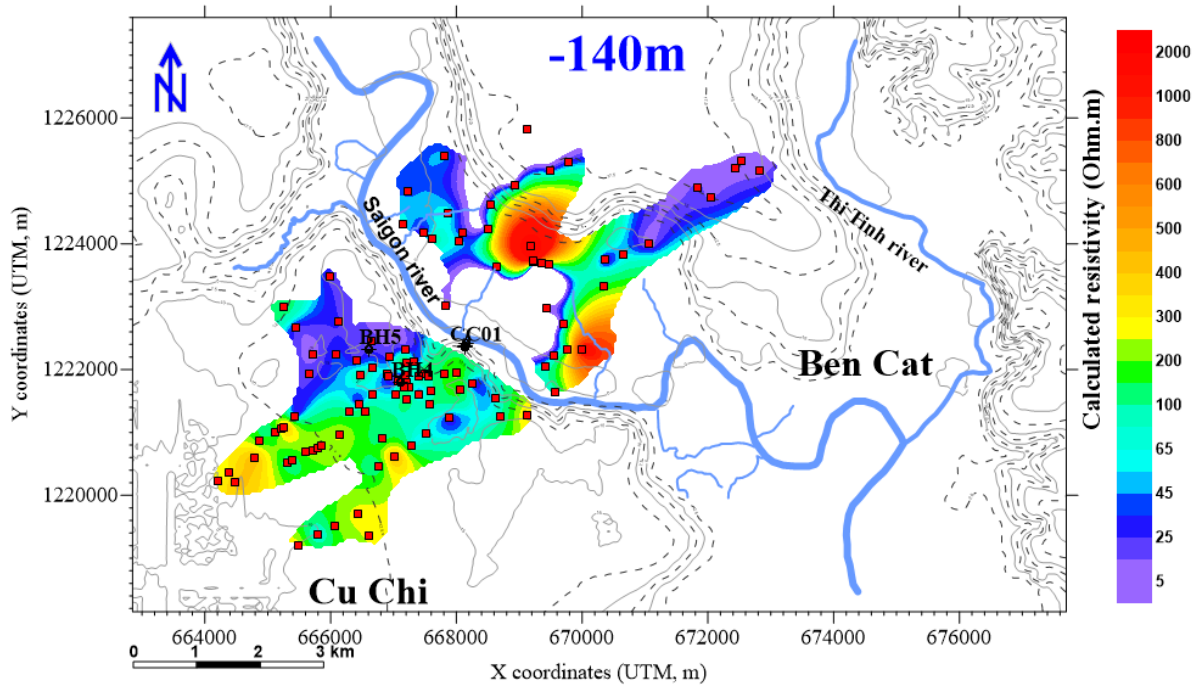

Figure 21 TDEM resistivity contour map at elevation -140m above sea level

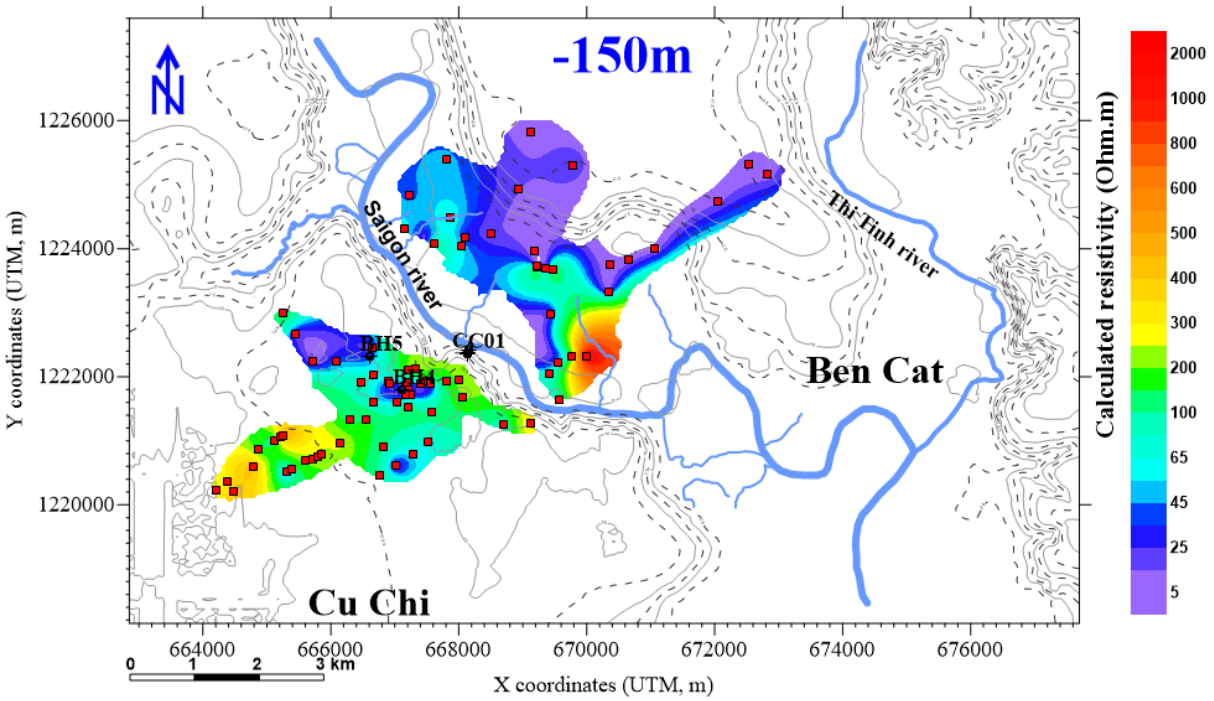

Figure 22 TDEM resistivity contour map at elevation -150m above sea level

APPENDIX 3 TDEM RESISTIVITY CROSS-SECTIONS

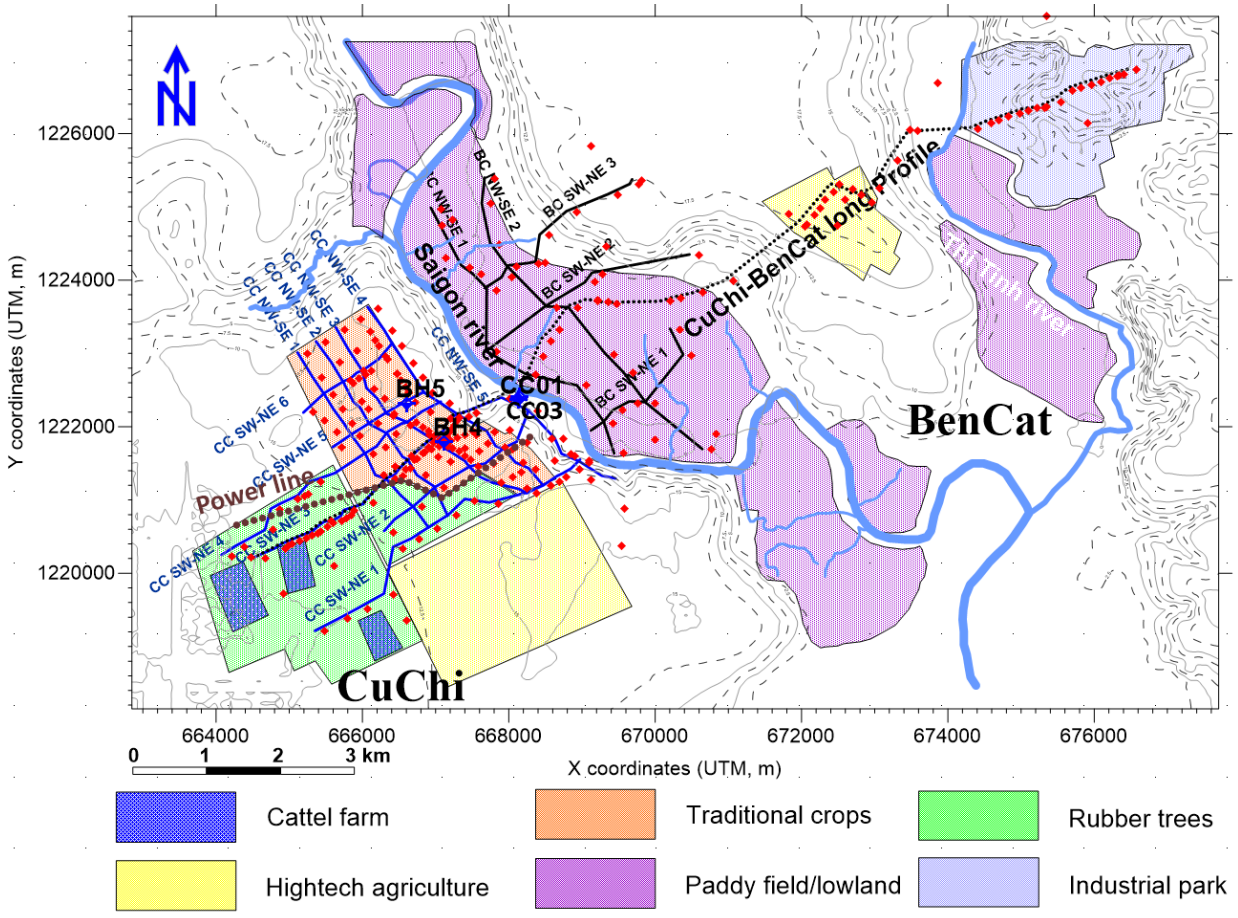

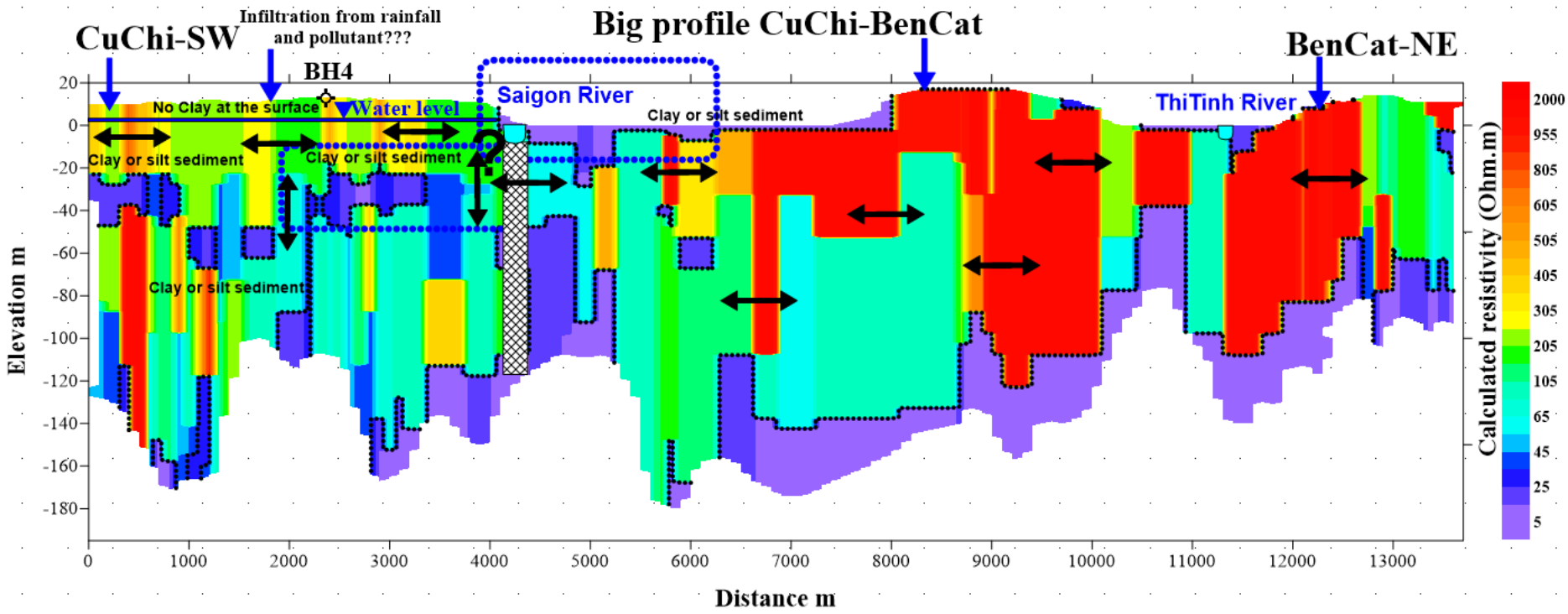

Figure 1 TDEM resistivity long profile

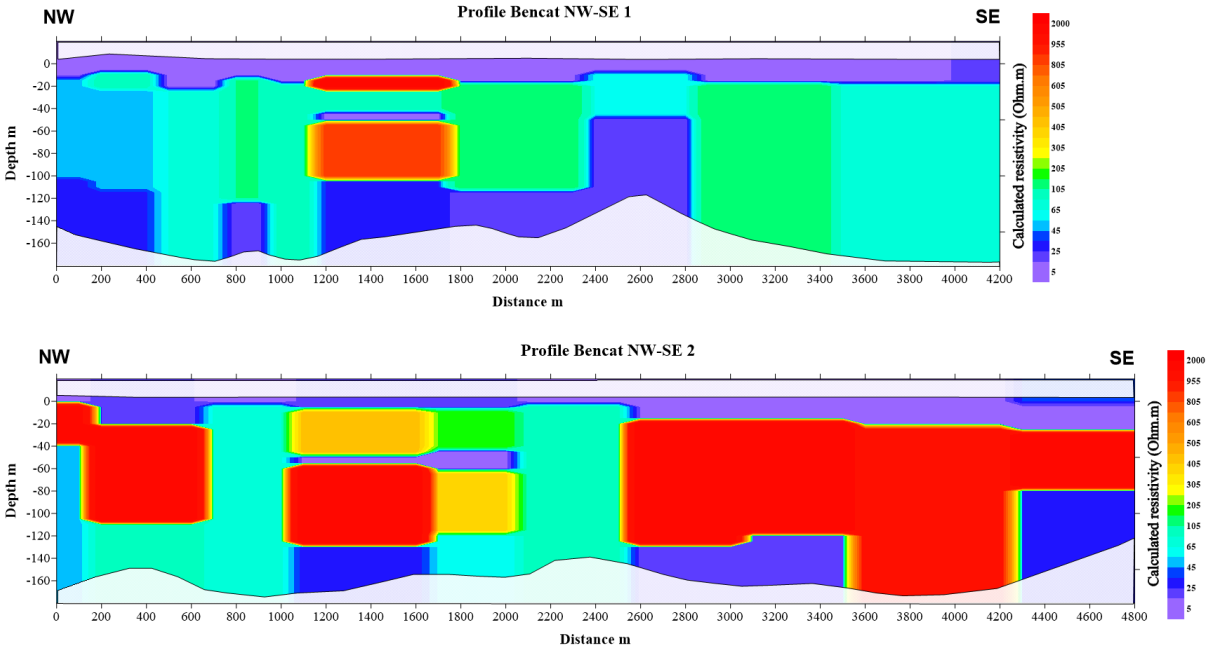

Figure 2 TDEM resistivity cross-section Ben Cat NW-SE1 and NW-SE2

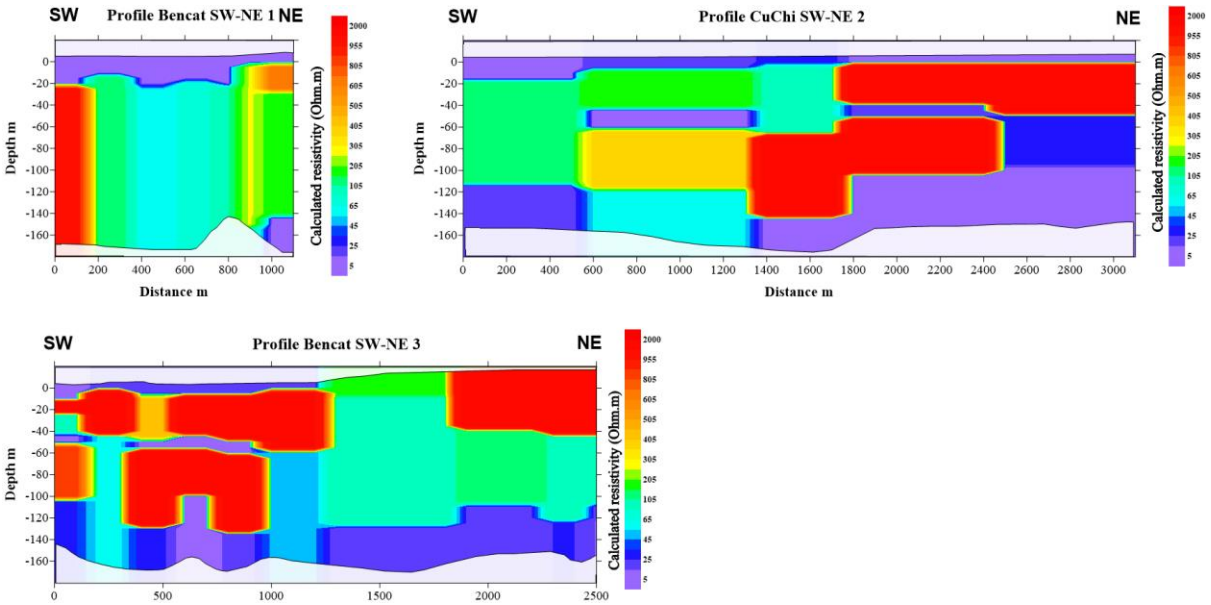

Figure 3 TDEM resistivity cross-section Ben Cat SW-NE1, SW-NE2, and SW-NE3

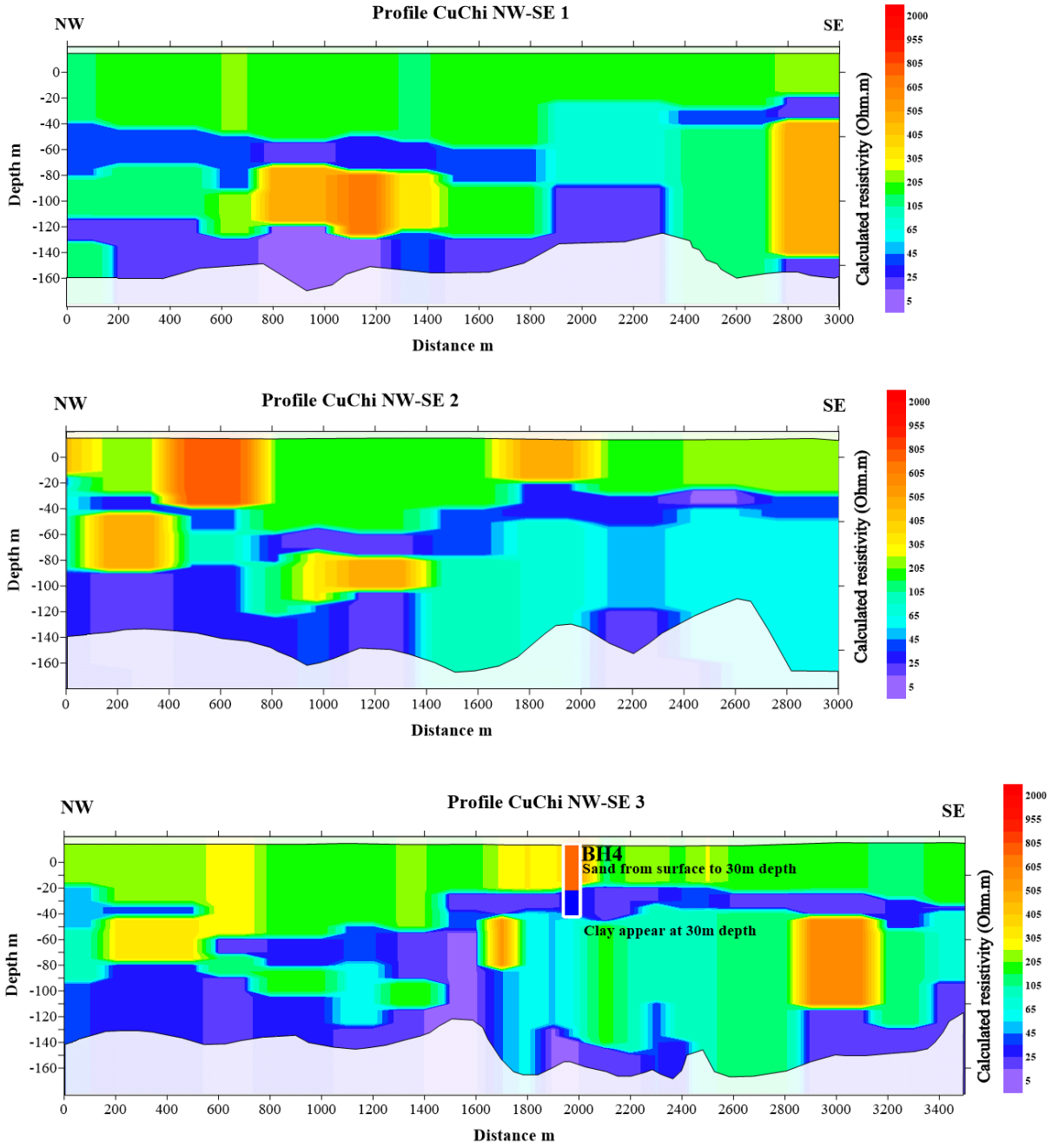

Figure 4 TDEM resistivity cross-section Cu Chi NW-SE1, NW-SE2 and NW-SE3

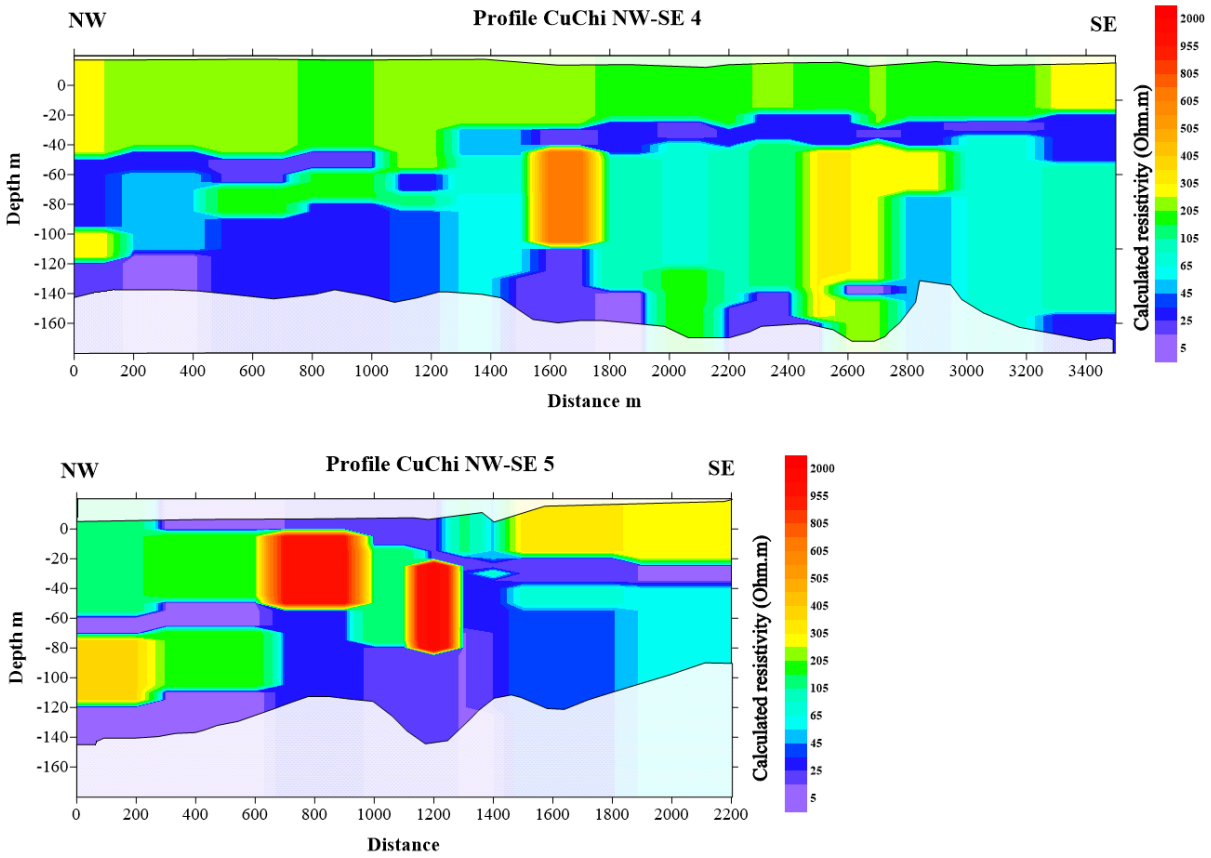

Figure 5 TDEM resistivity cross-section Cu Chi NW-SE4 and NW-SE5

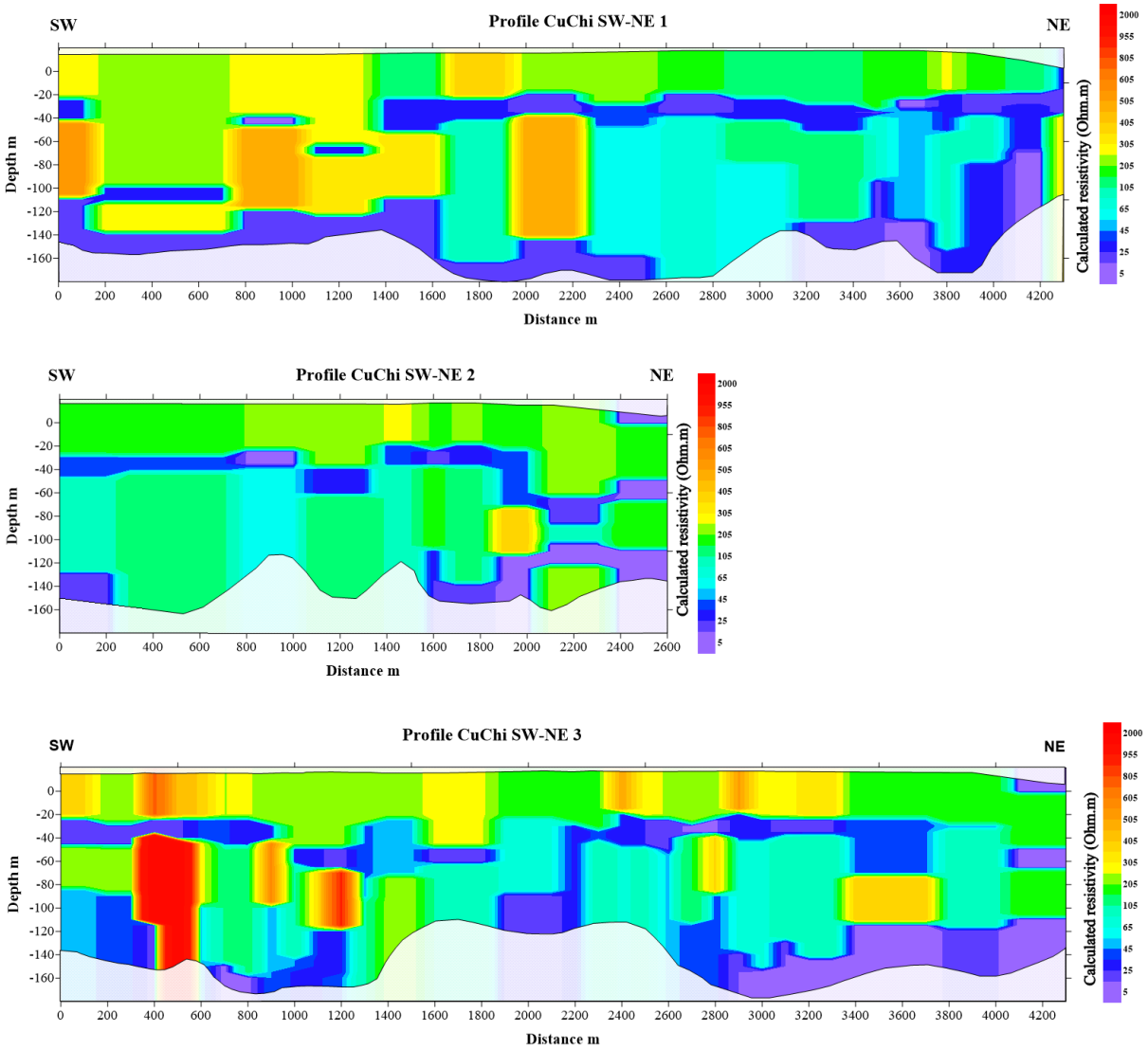

Figure 6 TDEM resistivity cross-section Cu Chi SW-NE1, SW-NE2 and SW-NE3

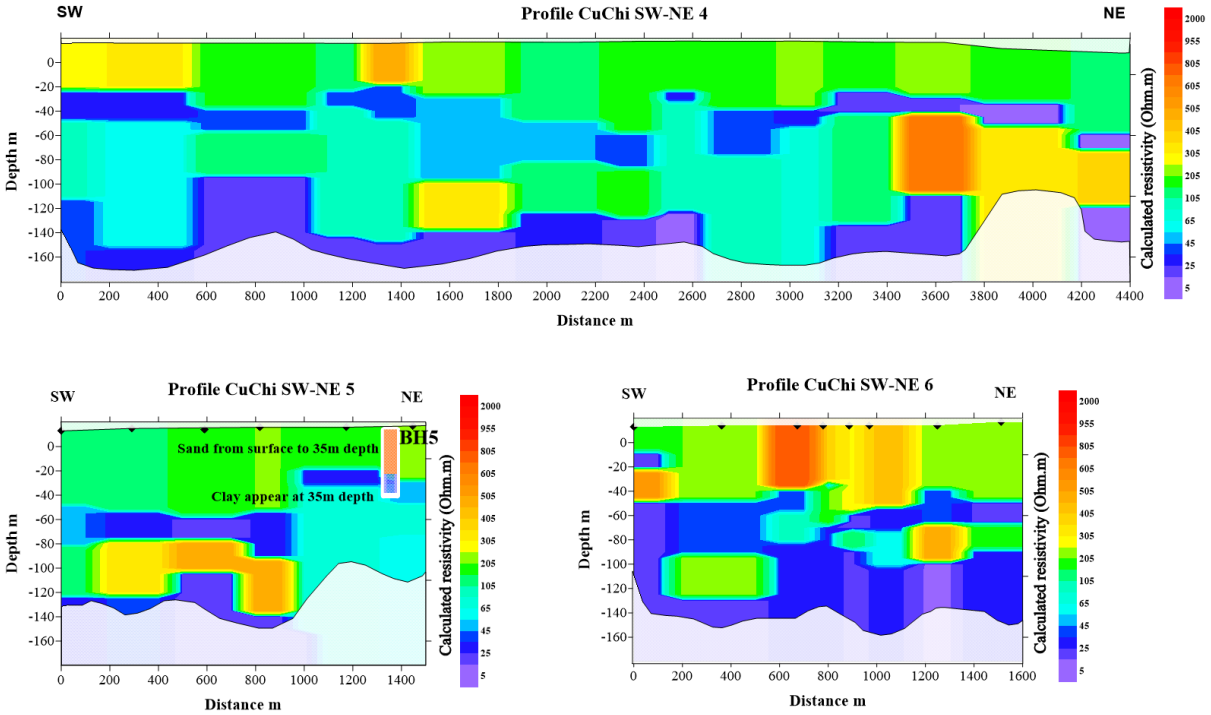

Figure 7 TDEM resistivity cross-section Cu Chi SW-NE4, SW-NE5 and SW-NE6

APPENDIX 4 ERT results

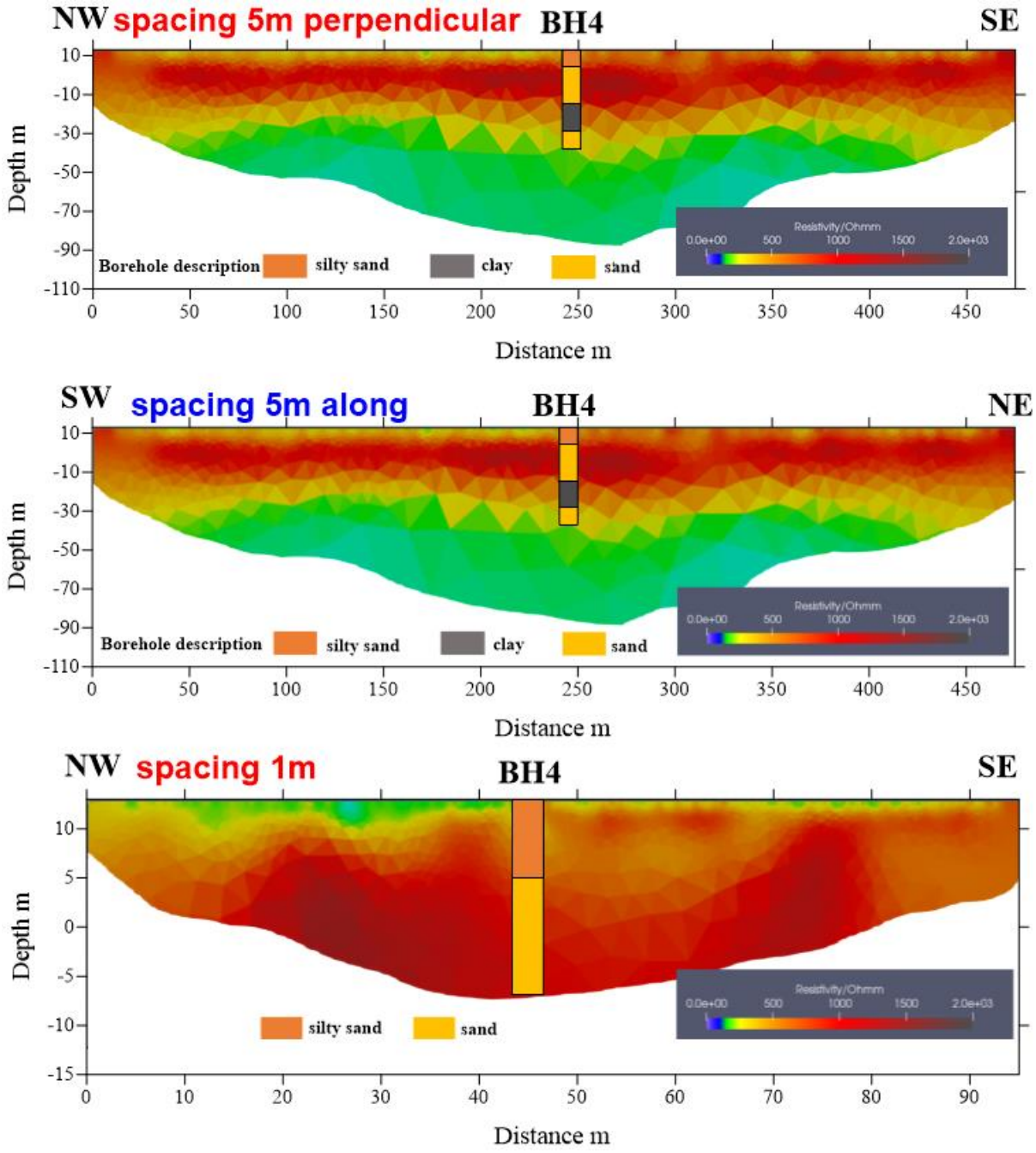

Figure 1 ERT profile at BH4 with 5m and 1m spacing

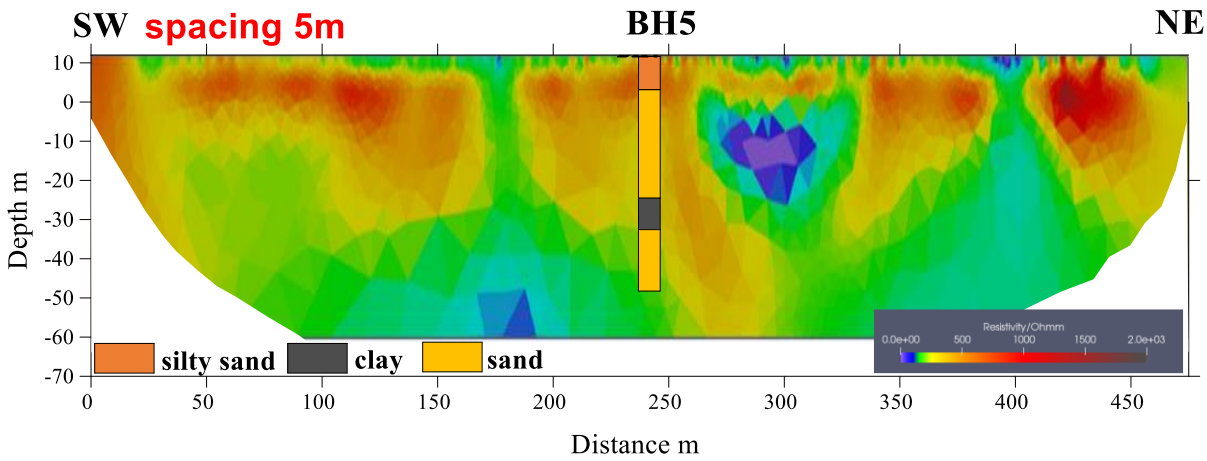

Figure 2 ERT profile at BH5 with 5m spacing

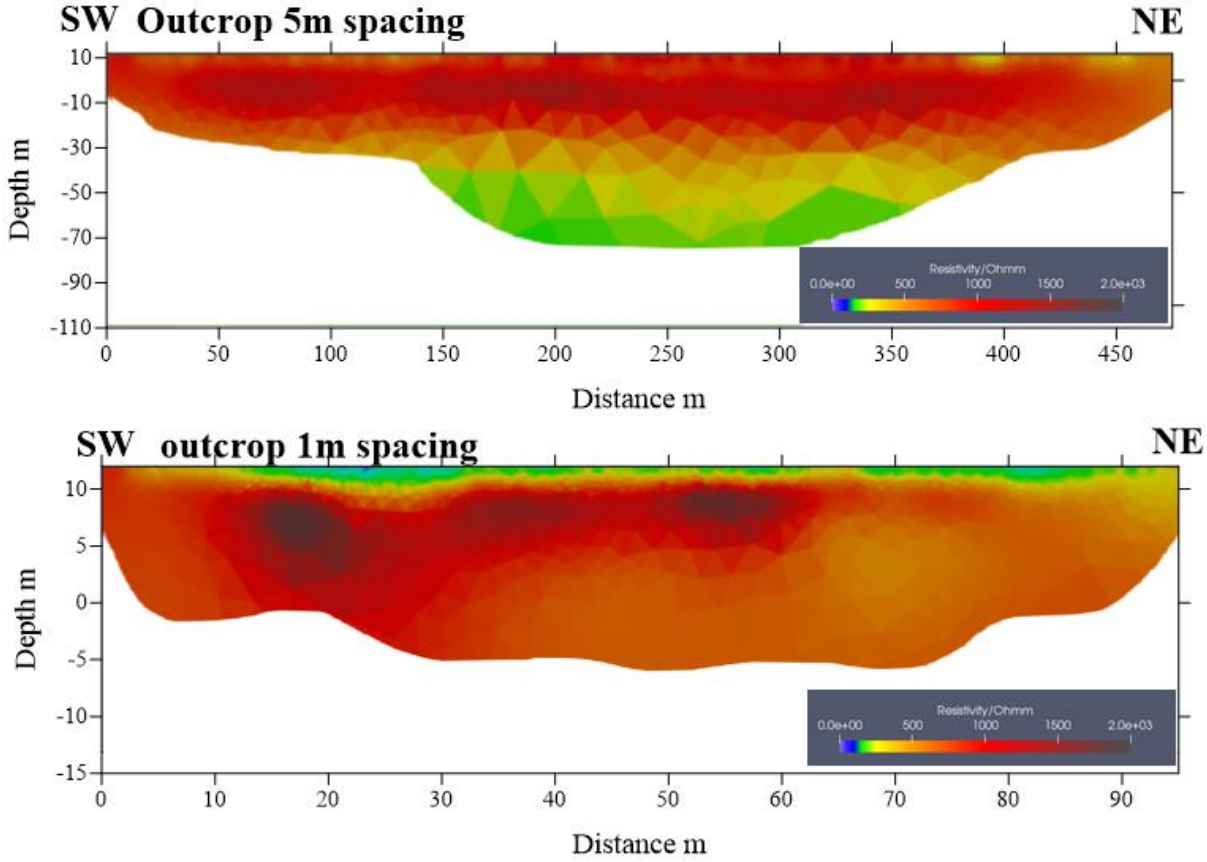

Figure 3 ERT profile at BH5 with 5m and 1m spacing

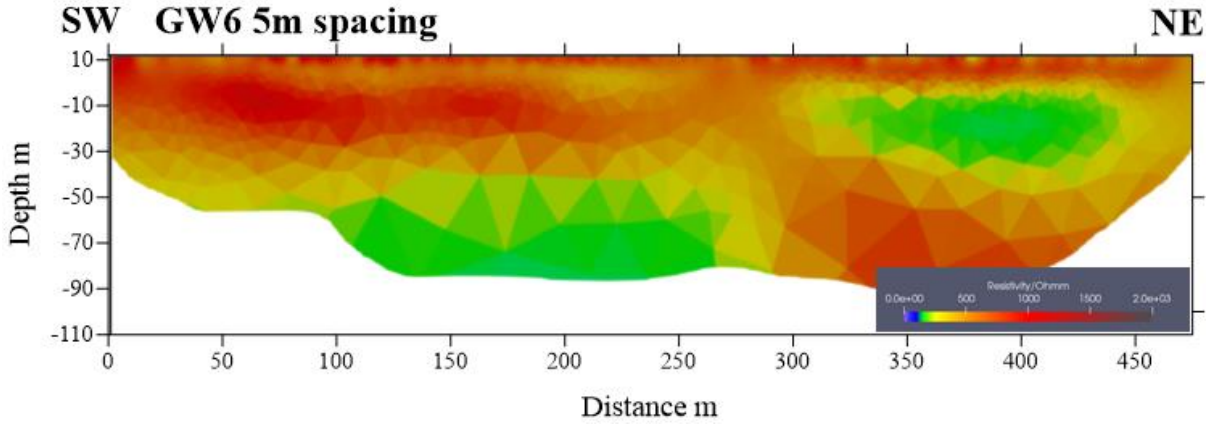

Figure 4 ERT profile at GW6 with 5m spacing

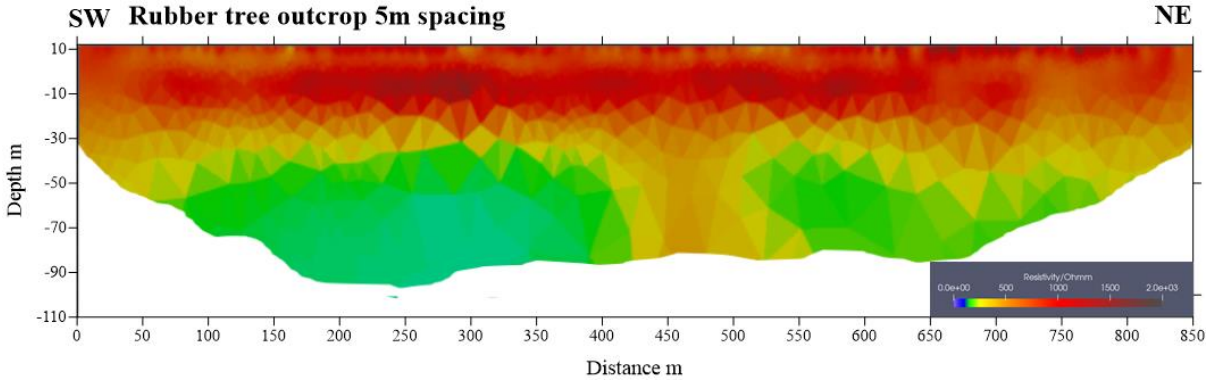

Figure 5 ERT profile at rubber tree outcrop with 5m spacing

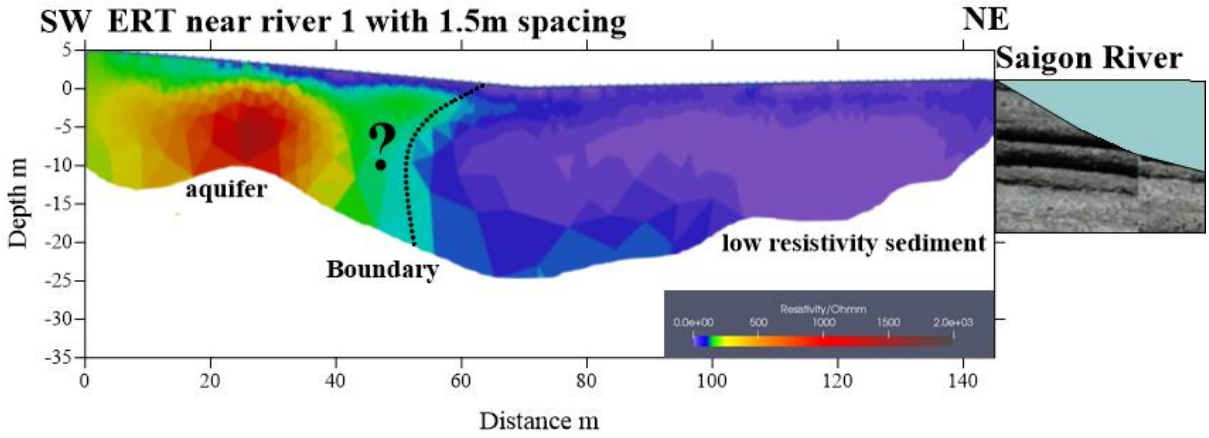

Figure 6 ERT profile at near River 1

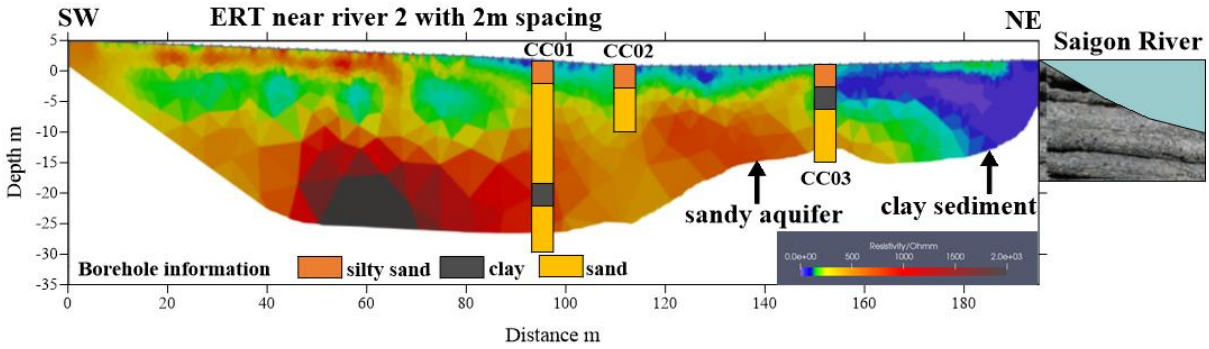

Figure 7 ERT profile near river 2